UNIVERSIDAD COMPLUTENSE DE MADRID

FACULTAD DE CIENCIAS GEOLÓGICAS

Departamento de Geodinámica

TESIS DOCTORAL

Glacial geomorphology of the flank of the Hecates Tholus Volcano, Mars
Geomorfología glaciar del flanco noroeste del volcán Hectes Tholus, Marte

MEMORIA PARA OPTAR AL GRADO DE DOCTOR

PRESENTADA POR

Miguel Ángel de Pablo Hernández

Director

Juan de Dios Centeno Carrillo

Madrid, 2016

UNIVERSIDAD COMPLUTENSE DE MADRID

FACULTAD DE CIENCIAS GEOLÓGICAS

Departamento de Geodinámica

DISSERTATION

GLACIAL GEOMORPHOLOGY OF THE NW FLANK OF THE HECATES THOLUS VOLCANO, MARS

Geomorfología glaciar del flanco Noroeste del volcán Hecates Tholus, Marte

by

Miguel Ángel de Pablo Hernández

Submitted to the Program of Geology and Geological Engineering of the

Faculty of Geological Sciences of the Complutense University

in partial fulfillment of the requirements for the award of the degree of

DOCTOR

Supervised by

Dr. Juan de Dios Centeno Carrillo

Madrid, 2015

This dissertation is lovingly dedicated to my parents, sister and brothers
for their endless love, support and encouragement.

“Always something new. I made up my mind when I came here last year I wouldn't expect nothing, nor ask nothing, nor be surprised at nothing. We've got to forget Earth and how things were. We've got to look at what we're in here, and how different it is. I'm not surprised at anything anymore.

I'm just looking. I'm just experiencing. If you can't take Mars for what she is, you might as well go back to Earth. Everything's crazy up here, the soil, the air, the canals (…).”

Ray Bradbury. *Martian Chronicles* (1950)

CONTENTS

LIST OF FIGURES

LIST OF TABLES

LIST OF ACRONYMS AND SYMBOLS

Acronyms

A	Albedo
ASCII	American Standard Code for Information Interchange
ASTER	Advanced Spaceborne Thermal Emission and Reflection Radiometer
ASU	Arizona State University
ATI	Apparent Thermal Inertia
BT	Brightness Temperature
BTR	Brightness Temperature Record
CRISM	Compact Reconnaissance Imaging Spectrometer for Mars
CSFD	Crater-size frequency distribution
CTX	ConTeXt camera
DCS	De-Correlation Stretch
DEM	Digital Elevation Model
DTM	Digital Terrain Model
ESA	European Space Agency
FUB	Free University of Berlin
GIS	Geographic Information System
GRS	Gamma Ray Spectrometer
HiRISE	High Resolution Imaging System Experiment
HRSC	High Resolution Stereo Camera
IR	Infrared
MARSIS	Mars Advanced Radar for Subsurface and Ionosphere Sounding
MC	Mars quadrant
MCD	Mars Climate Database
MEX	Mars Express
MGS	Mars Global Surveyor
MO	Mars Odyssey
MOC	Mars Orbiter Camera
MOLA	Mars Orbiter Laser Altimeter
MRO	Mars Reconnaissance Orbiter
MSFF	Mars Space Flight Facility
MSSS	Malin Space Science System

Na	Narrow angle
NASA	National Aeronautics and Space Administration
ODE	Orbital Data Explorer
OMEGA	Observatoire pour la Minéralogie, l'Eau, les Glaces et l'Activité
PDS	Planetary Data System
PSA	Planetary Science Archive
RGB	Red Green Blue
SFD	Size Frequency Distribution
SHARAD	SHAllow RADar experiment
Tday	Daytime temperature
TES	Thermal Emmision System
THEMIS	Thermal Emission Imaging System
THMPROC	THEMIS PROCcesing tool
TI	Thermal Inertia
Tnight	Nighttime temperature
Vis	Visible
Wa	Wide angle

Symbols

º	Degree (coordinates/orientation)
°	Degree (temperature)
K	Kelvin
C	Celsius
m	Meters
Km	Kilometers
J	Joules
Ga	Giga years, Thousands of millions of years
Ma	Millions of years
Ka	Thousands of years
s	Seconds

PREFACE

"*What we call the beginning is often the end.*
And to make an end is to make a beginning.
The end is where we start from"
T. S. Eliot

In June 2009, when I completed my first PhD Thesis, some topics that already captured my attention in the Elysium region of Mars were still not well studied in detail. An example is the area with possible glacial landforms at the western flank of Hecates Tholus volcano on Mars. Although some authors proposed along the time the existence of glacial features in the area, there was still not detailed and systematical works to describe, characterize, date, and to interpret them, partially due to the absence of extremely high resolution satellite images that this detailed work required.

On a very different work, my first fieldtrip in Antarctica in January-February 2009 made me possible to study Deception Island: an incredible and beautiful site on the white continent. It is an active volcano partially covered by glaciers, some of them covered by ash deposits from the last eruptions in the late 1960's. Ice, fire, cold climate conditions… Then, when I completed that first Thesis, my curiosity pointed to me to continue studding Mars focused on a small area (ok, not so small) using the first extremely high resolution images of the Mars Reconnaissance Mission of NASA in which you could distinguish individual blocks on the surface! Then, why not to start a new PhD Thesis focused on the possible ancient glaciers on the flank of that Martian volcano, trying to reveal as much as possible of their origin and evolution with the help of my experience on studding Mars, and glaciated volcanoes in Antarctica?

Although he told me I was crazy, my advisor, Dr. Juan D. Centeno (Complutense University in Madrid), who spent an important part of his scientific life as geomorphologist studding glacial landforms, was quickly captured by the images from Mars and its landforms (he insists on calling them "marsforms"). Thankfuly, he enrolled in this Martian adventure and I could start and develop this PhD Thesis. His patience and enthusiasm (that I really appreciate), and his terrestrial point of view, allowed multiple and productive discussions about the interpretation of the martian reliefs I was mapping and describing.

This research work has not been directly supported by any research project or institution, but I would like to thanks to PERMAPLANET (CTM2009-10165), ANTARPERMA (CTM2011-15565-E), PERMANTAR-2 (PTDC/AAC-CLI/098885/2008), HOLOANTAR (PTDC/CTE-GIX/119582/20109), and PERMATHERMAL projects, because, although they were focused on the study of permafrost and climate change on Earth, they made possible my participation in seven Antarctic fieldtrips between 2009 and 2015. I had time there to discover and to study Deception Island and its clear analogues to the debris covered glaciers I was studding on Mars. Really inspirational fieldtrips!

In any case, this research was possible thanks to the NASA and ESA space agencies and their politics of public and free access to the planetary data. Their database systems as well as the databases from the different instrument teams, made me possible to download and use all the different type of data and images I used in this research. Especially thanks to HiRISE, CTX, THEMIS and HRSC instrument teams from University of Arizona, Malin Space Science System, Arizona State University, Jet Propulsion Laboratory and Free University of Berlin and German Aerospace Agency for the use of their data and products.

I used this data for the past five years (not fulltime. In fact less than 2 years of effective work because of all my duties as an assistant lecturer at the University of Alcalá, and my other research topics about Antarctica) to study this corner of Mars. Of course, the next pages does not contains all the work I did (many issues are still incomplete and require more work), but the most important parts that provide important advances in our knowledge of glaciers on the Hecates Tholus volcano of Mars. I also included some speculative discussions. Why not to propose new hypothesis to be tested in the future with the data that are coming? I had a lot of fun developing this research. I hope the reader will be able to enjoy in the same way reading this document.

Are you ready? We hope you enjoy your trip to Mars!

Madrid (Spain) on May 20th, 2015

ABSTRACT

Hecates Tholus volcano (32.18°N, 150.28ºE; MC-7 quadrangle) is the only edifice of the Elysium volcanic province, at the lowlands of Mars, showing evidence of glacial activity, as deduced from the geomorphological study. This work completes the previous regional works with the aim of refine our knowledge about the glacial events occurred at this site of Mars. We build a detailed geomorphological mapping (1:100.000 in scale) of the lower NW flank of the edifice (31.8º-33.08ºN, 148.37º-149.38ºE), where the glacial "marsforms" concentrate, based on the use of CTX images. Moreover, we performed detailed crater size-frequency distribution, geomorphological, morphometric, compositional, and thermal analysis to finish the cartography and get the necessary evidences to model the glacial evolution of the area. Those analyses were possible thanks to the use of a wide variety of images, including HRSC, HiRISE, MOC, and THEMIS, as well as HRSC-derived topographic data, THEMIS-derived Brightness surface temperature, TES-derived thermal inertia maps, and SHARAD ground penetration radargrams, everything integrated into a Geographic Information System.

The first result is a detailed geomorphological map showing geomorphological units (volcanic, glacial, gravitational, fluvial, impact and others) and geomorphological elements (glacial, periglacial, fluvial, gravitacional, tectonic, aeolian and impact). We produced a set of ages for primary and resurfacing events allowing to establish the most detailed evolution model of the glacial events in the volcano, including events descrived but not dated by previous authors and events first-described in this work.

The geomorphological and morphometrical observations allowed to characterize and confirm the glacial origin of many units and landforms observed in the area. The observation of crevasses and bergschrunds related to glacial deposits indicate that ice masses are flowing nowadays since this type of features are produced under glacial flow tensional efforts, and they are fragile enough to disappear by sublimation or ablation under recent climate conditions. Moreover, the thermal and compositional characterization of the area made possible to define the different behavior of the material, mainly of those with glacial origin, marking the possible existence of ice lenses or ice layers (that previous authors had considered relict of the ancient extensive glaciers).

Finally, the analysis of satellite images of Deception Island, Antarctica, made possible to define this terrestrial site as an analogue to study and understand the covered glaciers on Mars.

RESUMEN EXTENDIDO

El volcán Hecates Tholus (32.18°N, 150.28ºE; cuadrante MC-7), de unos 180 km de diámetro y 5.300 metros de altura, es el único edificio de la provincia volcánica de Elysium, en las Tierras Bajas de Marte, en el que se han descrito rasgos geomorfológicos que podrían estar causados por procesos glaciares. Además, distintos autores relacionan la red radial de canales que surcan las laderas del volcán como causadas por la fusión de un antiguo casquete glaciar en la cima del edificio, siendo éste un ejemplo más de las intensas interacciones magma-agua en esta región del planeta, cercana al antiguo océano marciano y que dieron lugar a fenómenos muy interesantes, como los terrenos caóticos de Galaxias Chaos, a pocos kilómetros del volcán.

Una característica muy particular de este edificio volcánico es la presencia de dos depresiones anidadas en la base de la ladera Noroeste, de 20 y 60 km de diámetro. La menor de ellas (Depresión A), situada a mayor altitud, ha sido interpretada por algunos autores como causada por una erupción lateral del volcán hace unos 350 Ma. Sin embargo, la de mayor diámetro y situada a menor altitud (Depresión B), no tiene un origen claro, aunque se han discutido distintas hipótesis. En cualquier caso, es especialmente en el interior de estas depresiones donde se han encontrado los rasgos geomorfológicos que podrían estar causados por actividad glacial, como posibles cordones morrénicos y depósitos de till.

Anteriormente, algunos autores realizaron trabajos cartográficos de carácter regional basados en imágenes HRSC (12 m/pixel de resolución), así como dataciones mediante contaje de cráteres, que les permitió correlacionar la actividad glaciar y volcánica con los principales eventos de este tipo ocurridos en el planeta, especialmente durante la glaciación de Marte. Sin embargo, estos trabajos no pretendían realizar estudios detallados de esta zona, ni tenían a su disposición las imágenes que se comenzaron a recibir tiempo después de los instrumentos CTX y HiRISE (de 6 y 0.35 m/pixel de resolución). Por ello, en este trabajo se ha pretendido, utilizando el potencial de estas imágenes, profundizar en el estudio de la zona, centrándonos en la base del flanco Noroeste del edificio (31.8º-33.08ºN, 148.37º-149.38ºE), con el *objetivo de localizar, caracterizar, interpretar, y datar las distintas unidades y elementos geomorfológicos reconocibles en la zona, especialmente aquellos de origen glaciar, así como de determinar sus características térmicas y composicionales. Con ello se pretende establecer la historia de los eventos glaciares y las características de los mismos, y determinar la posible existencia de hielo en tiempos recientes (o en la actualidad) en la zona de estudio.*

Para ello, se ha realizado: (1) una cartografía geomorfológica a escala 1:100.00, (2) una datación de las principales unidades mediante la técnica del contaje de cráteres, todo ello basado en el uso de imágenes CTX, (3) una descripción detallada de las distintas unidades y elementos geomorfológicos, (4) un estudio morfométrico basado en datos topográficos derivados de datos HRSC, y (5) la caracterización térmica y composicional de la zona, basado en el uso datos THEMIS.

Todas estas tareas han sido desarrolladas mediante la integración de los datos en un Sistema de Información Geográfica desarrollado para tal fin, mediante el uso del programa ArcGIS 10.0, integrando otros muchos tipos de datos complementarios. Además se han aplicado distintas técnicas como el estudio de la distribución de frecuencias de los diámetros de los cráteres de impacto para realizar las dataciones, un análisis estadísticos de aleatoriedad para desestimar zonas de craterización secundaria que resulta en dataciones erróneas, el cálculo de la temperatura del brillo de imágenes infrarrojas del instrumento THEMIS, el cálculo de la inercia térmica aparente para derivar las características de los materiales superficiales mediante imágenes THEMIS y CTX, el ajuste matemático de datos topográficos derivados de datos HRSC para establecer el origen glacial o fluvial de algunos canales, el procesado de dichos datos topográficos para obtener distintos parámetros e índices morfométricos, o el análisis de radargramas de datos de radar de penetración del instrumento SHARAD con el fin de intentar establecer las posible estructura subsuperficial.

Además del Sistema de Información Geográfica, y de herramientas especialmente desarrolladas para él, como el USGS Image Toolbar, o CraterTools, se han empleado programas adicionales para el procesado de datos, como HRSC2GIS o scripts, como ISIS2World o ISIS2GIS, PowerLaw, o se han desarrollado scripts propios para agilizar las tareas de procesado de datos. También se han empleado programas informáticos específicos para la interpretación de los datos, como CraterStats2 para el contaje de cráteres y la obtención de edades. Finalmente, se han empleado herramientas informáticas para el desarrollo de gráficos (Surfer 9.0) o esquemas y diagramas (Inkscape 0.48).

El primer resultado de este trabajo ha sido una cartografía geomorfológica a escala 1:100.000 de la zona de estudio, resultando en la cartografía más detallada realizada hasta la actualidad de esta zona del planeta. En dicha cartografía se han diferenciado 18 unidades geomorfológicas de diverso origen, incluyendo volcánico, glacial, fluvial, eólico, impacto y de pendientes. Este mapa también recoge la ubicación de 18 elementos geomorfológicos, igualmente de diverso origen, incluyendo elementos glaciales (morrenas y depósitos de till,

eskers, rocas aborregadas, o surcos), periglaciales (pingos), fluviales (canales de diverso tipo), de pendientes (escarpes), tectónicos (fracturas y graben), eólicos (campos de dunas) y de impacto (cráteres de impacto).

La datación de las unidades geomorfológicas más importantes (por extensión) de la zona de estudio, se ha llevado a cabo tras seleccionar sectores lo más amplios y homogéneos posibles (evitando las zonas con craterización secundaria), y realizando la medida de sus diámetros. Los resultados han permitido establecer que la edad del volcán es de aproximadamente unos 3.800 Ma, y existido a lo largo del tiempo diversos eventos geológicos volcánicos y glaciares hace 980 Ma, 800 Ma, 500 Ma, 415 Ma, y 110 Ma, incluyendo una erupción hace unos 340 Ma. Entiempos más recientes, se han establecido posibles eventos glaciares hace 60 Ma, 30 Ma, 16 Ma y 6 Ma, con reactivaciones hace tan sólo 1.3 Ma, 1 Ma, and 0.44 Ma, correspondiéndose con la última edad del hielo establecida para Marte.

Los rasgos geomorfológicos cartografiados y observados en las imágenes de alta resolución confirman el origen glacial que autores previos le daban a la zona, y su análisis e interpretación han permitido establecer la altura que la masa de hielo pudo llegar a tener en el pasado durante el periodo de máxima extensión glaciar, así como los distintos episodios de avance y retroceso del hielo a lo largo de la historia geológica de la zona. El análisis morfométrico y el ajuste polinomial de los datos topográficos confirman que si bien algunos de los valles de la zona de estudio pudieron estar excavados por actividad fluvial, los glaciares los erosionaron. El estudio de los parámetros de forma de estos valles (b-FR) relacionan la actividad erosiva con un modelo de tipo patagónico-antártico como cabría esperar de estas grandes masas de hielo que parece que cubrieron la región. A la vista de los elementos geomorfológicos existentes en la zona, también es posible establecer que dichos glaciares podrían haber tenido un régimen térmico templado.

Tanto las observaciones geomorfológicas como las morfométricas podrían estar indicando la existencia de masas de hielo en el fondo de las depresiones A y B, sea en forma de lentes o en forma de capas continuas. La explicación más probable es que se trata de hielo relicto de los glaciares que existieron en el pasado, cubiertos en la actualidad por depósitos de derrubios, eólicos o de depósitos volcánicos de caída que los ocultarían y protegerían. Esto es también lo que parecen indicar los datos de temperatura de la superficie analizados. Y es que, aunque no se observan rasgos térmicos destacables más allá del distinto comportamiento de los diferentes materiales que conforman las laderas del volcán, las llanuras que lo rodean, los

materiales del fondo de las depresiones, o sus laderas, existe una pequeña anomalía térmica en el fondo de la depresión más grande, en la que el contraste térmico día-noche es distintos del que existe en la zona. Tras comprobar que tanto desde el punto de vista textural, geomorfológico, composicional, o morfométrico, la zona donde ocurre esto no es distinta del resto de las zonas del fondo de la depresión, y su inercia térmica (real y aparente) es similar a la del resto de la zona, por lo que es posible que dicha anomalía esté marcando la ubicación de una de estas lentes de hielo de mayor espesor, o recubierta por menos materiales.

En otros puntos de estas depresiones y en los valles que llegan a ellas, se han observado en las imágenes de más alta resolución, la existencia de crevasses y bergschrunds, que, sin duda, están relacionados con la presencia de hielo en la actualidad, parcialmente cubierto por depósitos finos. Pero además, su existencia es indicadora de la actividad contemporánea o muy reciente de dichas masas de hielo, pues este tipo de fracturas en el hielo se producen por las tensiones que sufre el hielo durante su desplazamiento y son formas que desaparecen con el hielo.

Si dichas lentes de hielo existen y se encuentran en movimiento en la actualidad, resulta imprescindible un gradiente del balance de masa del hielo. Si no existe acumulación de hielo, la pérdida de hielo en la zona frontal o en la base serían las únicas causas de dicho movimiento. No se puede descartar el papel de la sublimación (aunque no existen claros indicadores) pero, dado el carácter volcánico y los antecedentes de la región, es posible establecer que un incremento del flujo geotérmico asociado a las depresiones ha podido causar la fusión de la base del hielo, produciendo, por un lado la pérdida de masa, y por otro favoreciendo el movimiento por lubricación de la base.

En cualquier caso la existencia de hielo enterrado en la zona concuerda con los modelos térmicos planteados tiempo atrás por algunos autores para esta zona, y la existencia de glaciares relictos enterrados bajo depósitos sedimentarios es similar a lo observado en algunos de los glaciares de la isla Decepción, Antártida, donde las masas de hielo se encuentran cubiertas por depósitos piroclásticos. En dichas zonas, donde no se ve el hielo en la superficie, se pueden identificar rasgos geomorfológicos similares a los observados en el volcán Hecates Tholus, por lo que su estudio como análogo terrestre abriría la puerta a comprender mejor los efectos térmicos del glaciar y así, poder estudiar de forma más precisa los glaciares cubiertos de Hecates Tholus y de otros lugares de Marte.

PhD thesis

Glacial geomorphology of the NW flank of the Hecates Tholus volcano, Mars

1

Introduction

Miguel Ángel de Pablo Hernández

2015

Abstract:

The exploration of Mars has been strongly related to the search of water, from the epoch of the telescope exploration to nowadays. The analysis of the images and data obtained made possible along the time to know that liquid water and ice had played an important role on the evolution of the planet. In fact, periglacial and glacial features has been described all around the planet. In particular, the northwestern flanks of the main volcanoes of Mars show many glacial-related features formed along the history of the planet. Hecates Tholus volcano is one of these edifices with previous studies published, but without detailed geomorphological analysis. We have performed a detailed mapping and analysis of two depressions in the NW flank of the volcano. This is now possible thanks to the new high-resolution available images and data. In the next pages we show the motivation, objectives and scope of this study, as well as an explanation of the methods used. Finally, a description of the organization of this document is provided as well as the list of derived publications.

Resumen:

La exploración de Marte ha estado ligada desde el principio con la búsqueda y estudio del agua, ya desde la época de la exploración astronómica y hasta nuestros días. Las observaciones realizadas en las imágenes y datos que se han ido obteniendo a lo largo del tiempo han mostrado que el agua y el hielo han jugado un papel importante en la historia y evolución del planeta. De hecho, las formas periglaciares y glaciares se pueden encontrar en la práctica totalidad del planeta. De entre ellas, las laderas Noroeste de muchos volcanes se encuentran surcadas por rasgos que han sido interpretados como el resultado de la actividad glaciar a lo largo de la historia del planeta. Esto ocurre en el volcán Hecates Tholus de Marte, donde, si bien algunos autores han identificado y datado algunos de estos rasgos, no existe un estudio detallado de los mismos, algo que ahora puede realizarse gracias a los nuevos datos disponibles de alta resolución. En estas páginas se presentan las motivaciones, objetivos y alcance de la presente tesis doctoral, y se comentan brevemente los datos y métodos empleados. Finalmente se comenta la organización de los distintos capítulos de este trabajo, y las publicaciones de distinto tipo a las que han dado lugar.

1.1. Water on Mars

The exploration of Mars has been strongly related to water. In fact, already during the early exploration of Mars by the use of telescopes, discovery of water was one of the most important scientific events. Today we know, liquid water does not exist on the surface of the Mars, and that discovery was an incorrect interpretation of the observations of the surficial characteristics observed by telescope. On that days, astronomers made strong efforts to map the different albedo features (i.e., changes on the color of the surface), as well as to map linear structures, such as the case of the cartography made by Schiaparelli in 1888, where a number of "*canali*" were mapped. Note that "*canali*", in italian, means channel, a natural stream, but it was incorrectly translated to "canals", an artificial water conduct. This wrong translation inspired an important part of the scientific life of the astronomer Percival Lowell who made new maps of Mars by the use of the telescope, and made many publications about the life on Mars. This may look just anecdotic, but the works by Schiaparelli had serious implications- two of them do deserve to be mentioned. The first one was to father the belief of the existence of life on Mars, with the logical deduction that Mars should be a relatively adequate world to support the live. The second, and related with the first one, was to call the attention of public opinion and scientific community on the importance of the exploration of the Solar System, and specially Mars.

During the during the XX century, new astronomical observations discarded the artificial origin of the linear structures mapped by Schiaparelli and other astronomers and the search for "Martian intelligence" vanished. However, the interest about Mars increased and, it was still one of the priority targets once the first spacecraft were launched. The channels or "canali" should be related to some kind of water and, within the USA-URSS race for space conquest, Martian water was always and strategic scientific target. The first images acquired in 1964 by the Mariner 4 spacecraft revealed Mars had a dry and craterized surface, similar to the Moon's surface. The first deception did not avoid that during the next decade about 16 missions were sent to the planet to explore its surface.

In late 1970's, the twin Viking mission, each one formed by a lander and an orbiter, finally obtained images from the 99% of the surface of the planet, among many other data. Those images made possible to have a whole view of the planet. Many features were discovered, most of them similar to those we have on Earth: canyons, plains, volcanoes, faults,… and also channels (Carr, 1996a, 1996b, 2006). So finally, channels exist in many

different sites of the planet, but completely different than those “canali” mapped by the use of the telescope in ancient times. Evidences of ancient streams were ientified, similar to those we have on Earth caused by surface runoff, but also huge channels, probably caused by enormous episodic outflows. Moreover, most of those channels end on the lower, smooth and low cratered land on the northern hemisphere, interpreted to be the floor of an ancient ocean. On the contrary, the higher, rough and densely cratered terrains of the martian highlands, interpreted to be the “continental” sector of the planet. Then, the idea of Mars like a dry planet completely changed during the late 1970’s and early 1980’s, because important water quantities must have flowed on the planet surface on the past to excavate those channels and to fill the ancient ocean.

In 1997, after a long gap of 20 years without missions sent to Mars, started a new exploration epoch of Mars, characterized by smaller, cheaper and more frequent missions, but full of instruments to study the planet. Mars Pathfinder mission opened this epoch with a small vehicle capable to drive on the surface taking images and different scientific data. From that moment other 16 missions have been sent to Mars until 2011 when Mars Science Laboratory (Curiosity rover) was sent there. Each mission included more, more precise, robust and varied type of instruments to analyze the atmosphere, the water, the surface and the soils, not only with the objective of to know the geology and the evolution of the planet, but also to locate water on it. And water is there. Many direct and indirect evidences of water existence have been reported thanks to the analyses carried out by the hundreds of instruments on board those missions.

Nowadays, the complete scientific community agrees with the idea that water existed on Mars in the past forming oceans, lakes and rivers, and also in the atmosphere, allowing precipitation like rain and snow (Carr, 1996a, 1996b, 2006; Carr and Head, 2010). We also have a solid model of the evolution of the planet and its climate, and also of its hydrosphere. In fact, we know water had an important role in the evolution of the planet. All this knowledge was possible thanks to all those missions sent to Mars to locate, and study water, or its influence on the geology and climate on present and past history of the planet.

1.2. The invisible ice

The different missions sent to Mars, not only observed landform related to liquid water such as channels, deltas or coastlines, but many other evidences of frozen water existence. In fact, the most important evidence is the two polar caps, formed by layers of ice

and dust that is the unique ice deposits ever observed on Mars. However, although no more ice has been directly observed on the planet, these ice deposits are not the unique evidences or ice existence on past and present times on Mars. Polygonal terrains, protalus, thermokarsts, or pingos, are examples of features what point to the ice existence on past and present on Mars (e.g., Müller, 1962; Carr and Schaber, 1977; McKay, 1979, 1998; Luccchita, 1981, Greeley, 1985; French, 1993; Costard and Kargel, 1995; De Hon, 1997; Gurney, 1998; Tanaka et al., 2000; Soare et al., 2005; Lefort et al., 2006; Page and Murray, 2006; Page, 2007; de Pablo and Komatsu, 2008)

In spite of those evidences of ice-related geological processes, images do not allow to observe clean ice on the surface of the planet outside the polar caps. However, ice is stable under the surface temperature (10ºC and -120ºC) and pressure (6.1 mBar) conditions. These values are below the triple point of the water and given the low water vapor concentration on the atmosphere, if water exists on Mars surface, it should be in solid state.

Surficial ice volume on Mars today should not be huge. If the planet had many lakes (e.g., Cabrol and Grin, 2001, Irwin and Howard, 2002; Irwin et al., 2002) and an ocean covered a third of the surface, as deduced from the geomorphological, topographical and compositional evidences (e.g., Baker et al., 1991, 2000, 2001; Fairén et al., 2003 and references there in), the ice contained in the polar caps represent only a small portion of that water. Although the small size of the planet could explain the lost of water vapor (and other gases) to the space due to the relative small gravity (e.g., Melosh and Vickery, 1989; Carr, 1996; Chassefière and Leblanc, 2004) still an important quantity of water should remain in the planet outside the polar caps. Viking landers took pictures where frost accumulated on the rocks and soils early in the morning was visible before sublimate to form again on the next day.

Moreover, presence of ice on present time outside the polar caps, was confirmed by Phoenix mission in 2008 after excavate few centimeters on the regolith discovering a white material that freezes-sublimates from day to day. That mission confirmed the presence of ice under the surface, something that it has been proposed many times to exist on the basis of the observation of different landforms and surficial features at a wide range of latitudes in the planet. Basketball terrains, polygonal terrains, thermokarsts, and also gullies and outflow channels on Mars could be caused by ground ice sublimation or melting. The most recent missions made possible, thank to their high resolution cameras, to study in details all those features, as well as their wide distribution on the planet, confirming the important role of the

cryosphere with a frozen ground that could be some kilometers thick (e.g., Clifford, 1993; Schorghofer and Forget, 2012). Spectrometrical data made also possible to know the wide distribution and concentration of hydrogen on the surface of Mars, which was interpreted as water concentration, practically global, supporting the idea of a thick permafrost layer almost all around the planet. Consequently, although not ice has been observed on present day outside the polar caps on the images from any mission sent to Mars until present day, there are many geomorphological and spectrometrical evidences of ice existence below the surface, just only at few centimeters below the surface such as confirmed by Phoenix mission at high latitudes, and with a pretty wide distribution all around the planet, supported by the present cold climate conditions.

1.3. Glaciers and ice ages on Mars

The list of evidences of former ice and glaciers on Mars is huge. Subglacial volcanoes in Martian lowlands, as Elysium and Utopia planitiae areas, points toward the existence of an iced ocean at the time of the eruptions; and this ideas has found further support in recent works (e.g., Chapman, 1993; Wilson, 2003; Woodworth-Lynas and Guigné, 2004; Howard and Moore, 2004; Murray et al., 2005; Kossacki et al., 2006).

Different images from many different sites of Mars show features interpreted like caused as glacial reliefs in spite of present lack of ice on the surface outside the polar caps. Lobated debris aprons and lineated valley fill deposits has been interpreted as different types of till deposits, such as frontal or central moraines (e.g., Richardson and Wilson, 2002; Head et al., 2003, 2005; Head and Marchant, 2003; Mischna et al., 2003; Fastook et al., 2005; Shean et al., 2005; Levy et al., 2007; Kress and Head, 2008; Morgan et al., 2009; Baker et al., 2010). Furthermore, these features are found at all latitudes. With the identification and mapping of these features, several authors have founds glacial tongues, piedmont glacier and ice caps. Moreover, possible eskers and drumlins fields have been also described in many different sites of Mars (e.g., Kargel, 1995; Banks et al., 2008). This is just a sample of the huge list of evidences that supports the extensive distribution and importance of glacial dynamics on the geological history of Mars (e.g., Carr, 1996, 2006; Clifford and Parker, 2001; Carr and Head, 2010).

The last studies about the Martian climate and its relation with many different ice-related “marsforms” all around the planet helped to draw a full history of glaciations and recent ice ages (e.g., Head et al., 2003, 2005; Schorghofer, 2007; Carr and Head, 2010) in which

the orbital variations could play an important role (e.g., Mustard et al., 2001; Laskar et al., 2004; Aharonson and Schorghofer, 2006; Schorghofer, 2007, 2010; Byrne et al., 2009; Schon et al., 2009; Schorghofer and Forget, 2012).

The interesting issue about glaciers on Mars is that no ice, appart of regolith-interstitial ice and polar caps, has been found related to any of the glacial landforms above described. Therefore, there are two clear options: either all glacial forms are relicts and ancient glaciers o all remnant glacial ice, still modeling the planet surface, is hidden by debris deposits. Both possibilities are feasible but, at present time, evidences to discern which one is the real case do not exist, although some thermophysical models propose that the existence of buried ice at selected sites is feasible (e.g., Mellon and Jakosky, 1995; Helbert et al., 2005).

1.4. Glaciers on Hecates Tholus

Many of the glacial marsforms are located at the flanks of the main volcanoes of the Tharsis volcanic province. Arsia Mons, Ascraeus Mons, Pavonis Mons or Olympus Mons, show lineated valley fills and lobated debris aprons at their northwestern flanks. This aspect-restricted distribution of the glacial landforms has been interpreted as caused by local weather conditions. The main predominant wind direction favors the snow accumulation on that flanks and the formation of glaciers (e.g., Richardson and Wilson, 2002; Head et al., 2003; Head and Marchant, 2003; Mischna et al., 2003; Fastook et al., 2005; Shean et al., 2005; Baker et al., 2010).

The Elysium volcanic province includes the Elysium Mons, Hecates Tholus and Albor Tholus volcanoes but, in contrast with Tharsis province, only Hecates Tholus shows any glacial relief (Neukum et al., 2004; Hauber et al., 2005), may be related to the predominant wind direction in the area (e.g., Neakrase et al., 2005). In this volcano, although lineated valley fills and lobated debris aprons are the main evidences of glacial activity, other landforms such as a radial channels network has been also related to an ancient ice cap on the volcano summit (e.g., Mouginis-Mark et al., 1981, 1982; Gulick and Baker, 1989, 1990; Gulick et al., 1997; Zent, 1999; Gulick, 2001; Carr and Head, 2003; Fassett and Head, 2006, 2007, 2008). The glacial origin of these channels by melting of a possible ice-cap or snowpacks has a terrestrial analog at the Antarctic Dry Valleys (e.g., Head and Marchant, 2003), and it is in agreement with the important role of magma-water interaction in the area (Mouginis-Mark et al., 1981, 1982, 1984; Mouginis-Mark, 1984, 1985). On the other hand, the existence of possible glaciers on Hecates Tholus NW flank and ice caps on the volcano summit agrees with recent glacial activity

on Mars during the last ice ages (e.g., Head et al., 2003, 2005; Neukum et al., 2004; Hauber et al., 2005).

Focussing on the lineated valley fill and lobated debris aprons features on the NW flank of Hecates Tholus, most of them are located inside the 2 nested depressions. One of them is at higher altitude and it has been interpreted as a peripheral caldera resulting from of an explosive eruption ~350 Ma ago (Neukum et al., 2004; Hauber et al., 2005; Werner, 2009). The other one, at lower elevation, is more extensive and not indisputable origin has been proposed (see de Pablo, 2009 for a brief discussion about different hypothesis about the origin). Both depressions are filled by materials showing lineated valley fill and lobated debris aprons, and their walls dissected by narrow and deep valleys, what marks the glacial activity had an important role on the volcano flank sculpting.

1.5. Motivation, objectives and scope

Although general geological mapping and dating is already published (Greeley and Guest, 1987; Tanaka et al., 1992, 2005; Neukum et al., 2004; Hauber et al., 2005; Werner, 2009), not detailed geomorphological studies about NW Hecates Tholus volcano flank, and particularly on glacial forms, are still available. This is mainly due to the lack of high resolution images with extensive coverage of the area. The recent images acquired by Context (CTX) and High Resolution Imaging Science Experiment (HiRISE) instruments, of about 6 and 0.35 m/pixel in resolution(respectively) make now possible to answer further questions about the glacial processes on the lower NW flank of the Hecates Tholus (31.8ºN-33.08ºN, 148.37ºE-149.38ºE): what are the glacial-related features existing in the area? How is their distribution? When they formed? How many events were required to form them? In which climatic conditions they formed? How was their evolution? Is there still any ice there?

The aim of this study is to provide an answer to these and other questions in to refine our knowledge about the glacial events occurred at the lower NW flank of the Hecates Tholus volcano because the big picture of the history of water, climate and geology of Mars starts with very detailed studies such as this one. This target that can be expressed in the following objectives:

1.- Geomorphological cartography (scale 1:100.000)

2.- Description of the geomorphological units and landforms.

3.- Age determination for the different geomorphological units and events.

4.- Develop of an evolution model for the glacial episodes occurred in the area.

5.- Surface temperature characterization and ice-related thermal anomalies location.

6.- Analysis of Earth-Mars analogues on volcanic and glaciated areas.

A few details make this work different to any previous study on the subjects of glacial forms, and about Hecates Tholus: (a) the detailed view of the glacial forms thanks to the use of medium and very high-resolution resolution images recently available of the area. This study includes the analysis of high and very high resolution images to produce the first detailed (1:100.000) geomorphological map of the glaciated area, what is more detailed than any other cartography previously made on Elysium volcanic region; (b) the detailed crater size frequency distribution analysis to develop, most detailed and extensive crater counting made in the area, thanks to the use of the medium-resolution images, but also because it is based on our own geomorphological cartography; (c) the combination of geomorphological analysis and cartography, and crater counting, to propose a model of the evolution of the glaciers in the study area in a detail not previously reached; (d) the use of thermal analysis techniques that provides evidences to locate possible buried ice bodies in the area, relict of the past glacial activity, or still flowing; and (e) the comparative analysis of a terrestrial analogue what support the existence of buried ice. All the information about the site to be included into the international databases of Mars-Earth analogues is provided.

1.6. Data and methods

To successfully achieve the objectives previously described, a wide variety of data and methods has been used, connected with the different objectives. Due to the wide variety of methods, we do not describe them here in detail, and provide only an overview of the used data, their properties, and cite the methods we used to achieve each objective. The detailed and focused description of each corresponding data and methods is contained in the shown in each chapter. However, the development of the present research was based on the use of a Geographic Information System (GIS) supported by the use of ArcGIS software (by ESRI), following the guidelines from the USGS Astrogeology section (e.g., Hare and Tanaka, 2000; Hare et al., 2005, 2007; Dobinson et al., 2006).

Because this research if focused on the study of a relative small area, and trying to observed small features and landforms, our base map is based on two images acquired by the High Resolution Stereo Camera (HRSC) instrument on board of Mars Express (MEx) mission from the European Space Agency (ESA). The resolution of these images is 12 m/pixel.

Together with the images, we used an HRSC-derived digital elevation model (DTM), that does not cover the complete study area (about 80%), but its 50 m/pixel in resolution is higher than the globally available Mars Orbiter Laser Altimeter (MOLA) DTM, which resolution is about 463 m/pixel.

We have used images acquired by the Context (CTX) instrument (Malin et al., 2007) on board of Mars Reconnaissance Orbiter (MRO) from the National Aeronautics and Space Administration (NASA) to carry out the geomorphological study of the area,. They were co-registered by the use of the HRSC base images. The resolution of the images is about 6 m/pixel. The use of these images was fundamental for the development of the present research, because they were not used previously to study glacial landforms on this region of Mars. This was also the case of the images acquired by the High Resolution Imaging Science Experiment (HiRISE) instrument on board of MRO spacecraft (McEween et al., 2002, 2003). The resolution of these images is about 0.35 m/pixel. They were included into the GIS and only position corrections to adjust them to the base HRSC and CTX images were required. These images were also fundamental to the study of the glacial landforms in the area. The very high resolution provided a new point of view, and many details were identified on them. Although the global coverage of each HiRISE image is not small, only ten images of the area are available at the time of the study. For that reason, other images were also used, such as the images acquired by the Mars Orbiter Camera (MOC) instrument (Malin et al., 1991) on board of the Mars Global Surveyor (MGS) mission, already finished. Although their resolution is about 2 m/pixel, they have a smaller footprint than HiRISE images, and their coverage of the study area is not complete.

Additionally, in order to carry multiple-scale analysis of landforms and provide a correct interpretation and to avoid incorrect interpretations (Chamberlain, 1897; Zimbelman, 2001), we also used images acquired by the Thermal Emission Imaging System (THEMIS) instrument (Christensen et al., 2004; Saunders et al., 2004), on board of the, still in active, Mars Odyssey (MO) mission of NASA. Images acquired in the visible (VIS) range of the spectrum, have about 19 m/pixel in resolution, meanwhile infrared (IR) images have about 100 m/pixel. They were processes by the use of ISIS software (by the United States Geological Survey). Those IR images were also used to derive surface brightness temperature and decorrelation stretch images by the use of THMPROC on-line tool by the Arizona State University. These products were used on the regional thermal and mineral composition characterizations of the study area.

Finally, ground penetration radar data acquired by the Shallow Radar (SHARAD) instrument (Seu et al., 2007) on board of MRO mission were used to study the radargrams in order to study the subsurface structure and support interpretations of geomorphological features.

All those data were obtained through the official databases of NASA and ESA agencies, but also throught the databases of the research teams of each instrument, as it will be described below. Except MGS mission, all the missions that provided the used data are still active while we write this lines. Databases were regularly checked in order to detect new available data of the study area. When this occurred, the data were processed and added to the GIS. However, the research was conducted only with the available images at the begins of this work.

On the other hand, appart of those data here presented, other type of data could be used (such as those acquired by CRISM, GRS, OMEGA, MARSIS, or TES instruments, among others). However, a balance between their resolution, coverage and applications to the research topics make us to discard their use. Other data and products were discarded because they require resources to process them that were not available for us, such as the very high resolution DTM derived from HiRISE instrument data, or the spectrometrical analysis of CRISM data due.

All these data were included into the GIS, and manipulated in different ways, depending of each particular research topic. Consequently, the exact methods used to reach each objective are explained in detail in each section of this thesis. As a general advance, spatial analysis tools were used to produce topographic profiles, shadow relief models, as well as aspect, slope, ruggedness, or insulation maps. Maps algebra was also used, for example, to derive Apparent Thermal Inertia, or analyze day/night thermal variations, or to sample tens of surface temperature images. Special tools were also used to develop the impact crater counting, such as Crater Tools 2 toolbar for ArcGIS, or the USGS image tools to help in image manipulation.

Other computer tools and software used along the development of this research included different scripts to process the data outside the GIS, such as PDS2GIS or ISIS2WORLD perl scripts, and HRSC2GIS tool for image processing, CraterStats2 for crater size-frequency distribution analysis and age derivation, Grapher 9 (by Golden Software) for plots production, or Inkscape 0.48 to draw the models and figures presented in this document.

1.7. About the thesis

Then, this work is structured into different chapters what include the results of each research topic about the study area:

- Chapter 2: Geomorphological cartography (1:100.000). This chapter briefly describes the data (fundamentally CTX images) and methods use to develop the geomorphological mapping of the study area. This short technical chapter does not include other results except the proper geomorphological map (included at full scale in Appendix A.3)

- Chapter 3: Age and evolution. In this chapter the results from the impact crater counting technique, crater size-frequency distribution, as mapped on CTX images, applied to the main geomorphological units mapped in the study area are shown. A detailed evolutive interpretation, including final resurfacing processes, follows the obtained absolute ages, elevation and geomorphological observations. A model about the evolution of the glacial processes in the study area along the last 3.5 Ga completes this chapter.

- Chapter 4: Geomorphology and morphometry. A detailed description of each geomorphological unit and elements mapped in the area, as well as other landforms observed on MOC, HIRISE, CTX, and THEMIS (Vis and IR) is described here. On the other hand, a morphometrical analysis of the topographic data and landforms is described, as well as the implications of all the observations combined to discuss different implications in the glaciers evolution in the study area.

- Chapter 5: Thermal characterization. This chapter contains the description and analysis of surface temperature data, mainly derived from THEMIS-IR daytime and nighttime images, of the study area. A thermal characterization of the different sectors of the study area is discussed, as well as a description and interpretation of the day/night and seasonal thermal behavior. The relation with topography, elevation, thermal inertia and general mineral composition completes the characterization. Finally, thermal anomalies in the area are described and a model to explain them discussed.

- Chapter 6: Mars-Earth analogues. The glacial-related landforms observed in satellite images of the study area that were described on previous chapters characterize posible debris-covered glaciers on Mars. Here, the hypothesis of the glacial origin of

the described landforms is supported by the analysis of glacial-related features at the pyroclastic deposits-covered glaciers on Deception Island (Antarctica), on the Earth. After a detailed comparative description of the analogues, we discuss the implications for the glaciers on Hecates Tholus, and provide all the required data to include Deception Island in the international database of planetary analogues.

- Chapter 7: Discussion. This chapter contains a global discussion of the observations, results and models to provide a general view of the glacial history of the volcano and the posible state, on present time, of the debris-covered glaciers what could exist in the area. Additional observations of glacial-related landforms are used to support the discussion.

- Chapter 9: Conclusions. The last chapter summarizes the most important conclusions derived from the different researches focused on the study of the lower NW flank of the Hecates Tholus volcano of Mars.

Complementarily, we include the complete list of all the references cited in the text. Finally, a number of appendixes (CD-Rom) include other important data used in this research as the resulting files of the crater counting, or power law fitting, our own script for THEMIS-IR images processing, and all the related publications derived from this research.

Note that each chapter works like an independent research paper. For that reason, each chapter contains its own introduction to focus on its own research topic and providing the necessary background and state of the art for the selected topic. Research area and data and methods description is also presented in each chapter. This could seems reiterative but, because the main topic of each chapter is different, variations on data usage and analysis methods exist and they are detailed explained in the corresponding chapter to help to the reader to follow the specific data processing and analysis. Only, the list of references has been joined into a final section of the document to avoid excessive repetitions.

1.8. Related publications

A number of papers and abstracts have been published (or are under review) to show the preliminary of final results of each research topic of this thesis. An outreach paper has been also published showing the objectives and interest of the present research.

Papers:

- de Pablo, M.A. and Centeno, J.D. 2012. Geomorphological map of the lower NW flank of the Hecates Tholus volcano, Mars. *Journal of Maps*, 8(3). 208-214.
- de Pablo, M.A., Michael, G.G., and Centeno, J.D. 2013. Age and evolution of the lower NW flank of the Hecates Tholus volcano, Mars, based on crater size frequency distribution on CTX images. *Icarus*, 226(1). 455-469.
- de Pablo, M.A. and Centeno, J.D. 2015. Analogues of possible glaciers on the lower NW flank of the Hecates Tholus volcano (Mars) and Deception Island (Antarctica). *Icarus*, (under review by authors after first review by referees).
- de Pablo, M.A. and Centeno, J.D. 2015. Thermal characterization of the lower NW flank of the Hecates Tholus volcano, Mars: is there buried ice there? *Icarus*, (in preparation)

Abstracts:

- de Pablo, M.A. and Centeno, J.D. 2011. New observations of glacial features on the lower NW flank of Hecates Tholus volcano (Mars) based on CTX and HiRISE images. *Lunar and Planetary Science Conference*, 42. Abstract #1030.
- Centeno, J.D. and de Pablo, M.A. 2011. Possible evidences of ice dynamics in the putative glaciers at the lower NW flank of Hecates Tholus volcano, Mars. *Lunar and Planetary Science Conference*, 42. Abstract #1031.
- de Pablo, M.A. and Centeno, J.D. 2011. Relieves glaciares en el flanco Noroeste del volcán Hecates Tholus, Marte. Análisis y cartografía de imágenes CTX y HiRISE. *II Encuentro de Exploración del Sistema Solar*, 122-123.
- Centeno, J.D. and de Pablo, M.A. 2012. Preliminary Analysis of Surface Temperature in the Depression at the Lower NW Flank of Hecates Tholus Volcano, Mars. *Lunar and Planetary Science Conference*, 43. Abstract #1097.
- de Pablo, M.A. and Centeno, J.D. 2012. Geomorphological Map of the Lower NW Flank of Hecates Tholus Volcano, Mars. *Lunar and Planetary Science Conference*, 43. Abstract #1098.

- Centeno, J.D., de Pablo, M.A., Molina, A., and Ramos, M. 2013. Glaciers on Decepction Island, Antartica: Analogue of the debris-covered glaciers on the Hecates Tholus volcano of Mars. *Lunar and Planetary Science Conference*, 44. Abstract #1495.

- de Pablo, M.A. and Centeno, J.D. 2013. Qualitative Analysis of THEMIS-Derived Brightness Temperature of the Lower NW Flank of the Hecates Tholus Volcano, Mars. *Lunar and Planetary Science Conference*, 44. Abstract #1589.

- de Pablo, M.A., Michael, G.G., and Centeno, J.D. 2013. Glaciarismo en la ladera Noroeste del volcán Hecates Tholus de Marte: datación y evolución. *III Encuentro de Exploración del Sistema Solar*, 5-6.

- de Pablo, M.A., Orosei, R., and Centeno, J.D. 2014. Looking for buried ice relict of glacial activity at the lower NW flank of the Hecates Tholus volcano on Mars by SHARAD Data. *Lunar and Planetary Science Conference*, 45. Abstract #1151.

- de Pablo, M.A. 2015. Morphometry of glacial valleys at the lower NW flank of the Hecates Tholus volcano, Mars. *Lunar and Planetary Science Conference*, 46. Abstract #1268.

<u>Outreach papers:</u>

- de Pablo, M.A. and Centeno, J.D. 2012. Glaciers on Mars: looking for the ice. Science in School, 28. 12-17.

PhD thesis

Glacial geomorphology of the NW flank of the Hecates Tholus volcano, Mars

2

Geomorphological map

Miguel Ángel de Pablo Hernández

2015

Abstract:

Hecates Tholus (centered at 32.18ºN 150.28ºE), is a shield volcano in the Elysium volcanic province, located in the Martian lowlands in the northern hemisphere. Images of this volcano acquired by the Context Camera (CTX) instrument on board NASA's Mars Reconnaissance Orbiter spacecraft show many glacial landforms that have gone unnoticed by previous authors. We present a geomorphological map of the lower northwestern flank of the Hecates Tholus volcano, at 1:100,000 scale, based on the use and analysis of CTX images with a resolution of 6 meters/pixel. The map is organized into a series of geomorphological units (surface cover) and elements (located at a point, along a line or distributed over an area) in order to provide a clearer understanding of the extent of glacial processes and the main dynamic element of this Martian glacial complex.

Resumen:

Hecates Tholus (centrado en 32.18ºN 150.28ºE), es un volcán en escudo de la provincial volcanic de Elysium, en las Tierras Bajas de Marte, en el hemispherio norte del planeta. Las imágenes recientemente adquiridas por el intrumento Context (CTX) embarcado en la misión de la agencia NASA Mars Reconnaissance Orbiter muestra una gran diversidad de formas glaciares que no han sido previamente descritas. En este trabajo se presenta un mapa geomorfológico (escala 1:100.000) de sector inferior del flanco Noroeste del volcán Hecates Tholus realizado a partir de las mencionadas imágenes CTX cuya resolución es de 6 m/píxel. El mapa muestra tanto en una serie de unidades geomorfológicas en función de las texturas superficiales observadas, como de elementos geomorfológicos (puntuale, lineales y areales) con el fin de facilitar una visión clara de los extensos procesos glaciares que han afectado a la este complejo glaciar de Marte.

Related publications:

de Pablo, M. A., Centeno, J. 2011. New observations of glacial features on the lower NW flank of Hecates Tholus volcano (Mars) based on CTX and HiRISE images. Lunar and Planetary Science Conference, 42. Abstract #1030.

Centeno, J.D., and de Pablo, M.A. 2011. Possible evidences of Ice Dynamics in the Putative Glaciers at the Lower NW Flank of Hecates Tholus Volcano, Mars. Lunar and Planetary Science Conference, 42. Abstract #1031.

de Pablo, M.A., and Centeno, J.D., 2012. Geomorphological Map of the Lower NW Flank of Hecates Tholus Volcano, Mars. Lunar and Planetary Science Conference, 43. Abstract #1098.

de Pablo, M.A. and Centeno, J.D. 2012. Geomorphological map of the lower NW flank of the Hecates Tholus volcano, Mars. (scale 1:100,000). Journal of Maps, 8(3). 208-2014.

2.1. Introduction

Hecates Tholus is the only large volcano outside the Tharsis region for which various authors have found evidence of glacial activity – past or present. In addition, Hecates Tholus has received less attention from the glacio-geomorphological perspective than the other large volcanoes on Mars. Most of the main volcanic edifices on Mars show several features that have been described as being produced by glacial processes (e.g., Williams, 1978; Lucchita, 1981; Zimbelman and Edgett, 1992; Head and Marchant, 2003; Shean et al., 2005; Milkovichet al., 2006; Shean et al., 2007; Kadish et al., 2008). Olympus Mons, Arsia Mons, Ascraeus Mons or Pavonis Mons are some examples of Martian volcanoes showing putative glacial features on their flanks or in the nearby surrounding plains. However, all of these are located in the Tharsis volcanic region. Some of the other large volcanoes on Mars, Elysium Mons, Hecates Tholus and Albor Tholus, are located in the Elysium volcanic province (Figure 2.1), in the Martian lowlands in the northern hemisphere. Of these three volcanoes, glaciers have been described only on Hecates Tholus (e.g., Neukum et al., 2004; Hauber et al., 2005; Helbert et al., 2005; Fassett and Head, 2006, 2007), while relief possibly related to the interaction of magma, water and ice (such as sub-glacial volcanoes, mobergs, or chaotic terrains, among others) have been widely described in the Elysium volcanic province and the surrounding area (e.g., Chapman, 2003; Jaumman and Head, 2003; Nussbaumer, et al., 2004; Carr, 2006; Levy et al., 2009; Soare et al, 2009; Head et al., 2010; among others), marking the important role of water (probably also of ice) in this region of Mars.

Identification and mapping of glaciers on Mars is more difficult (than on Earth) because in all cases they are covered with glacial debris (dirty-ice) and the research is always dependent on the observation of images. This led to a decades-long discussion about the existence of glaciers on Mars (e.g., Zimbelman and Edgett, 1992; Shean et al., 2005; Carr, 2006). However, this discussion has been settled and glaciers have been identified. Head et al. (2010) published a geomorphological guide to identifying landforms on Mars in high-resolution images and many authors now accept the existence of glaciers throughout the history of the planet, including in times as recent as 2.1–0.4 Ma during the Late Amazonian (e.g., Head et al., 2003; Carr and Head, 2010; Fassett et al., 2010).

On the other hand, models of the evolution of glaciers (and especially changes in ice thickness) have been built on the basis of geomorphological observations of the tropical volcanoes on Mars, as well as on observations of ice deposits at different latitudes (e.g., Head

et al., 2006a, 2006b, 2010). A wide variety of causes have been considered to explain the location, spatial distribution and ice thickness of the geomorphological features on the flanks and bases of the Martian volcanoes, including orbital, climatic and volcanic processes (e.g., Laskar et al., 2002; Laskar et al., 2004; Fastook et al., 2008; Wilson and Head, 2008).

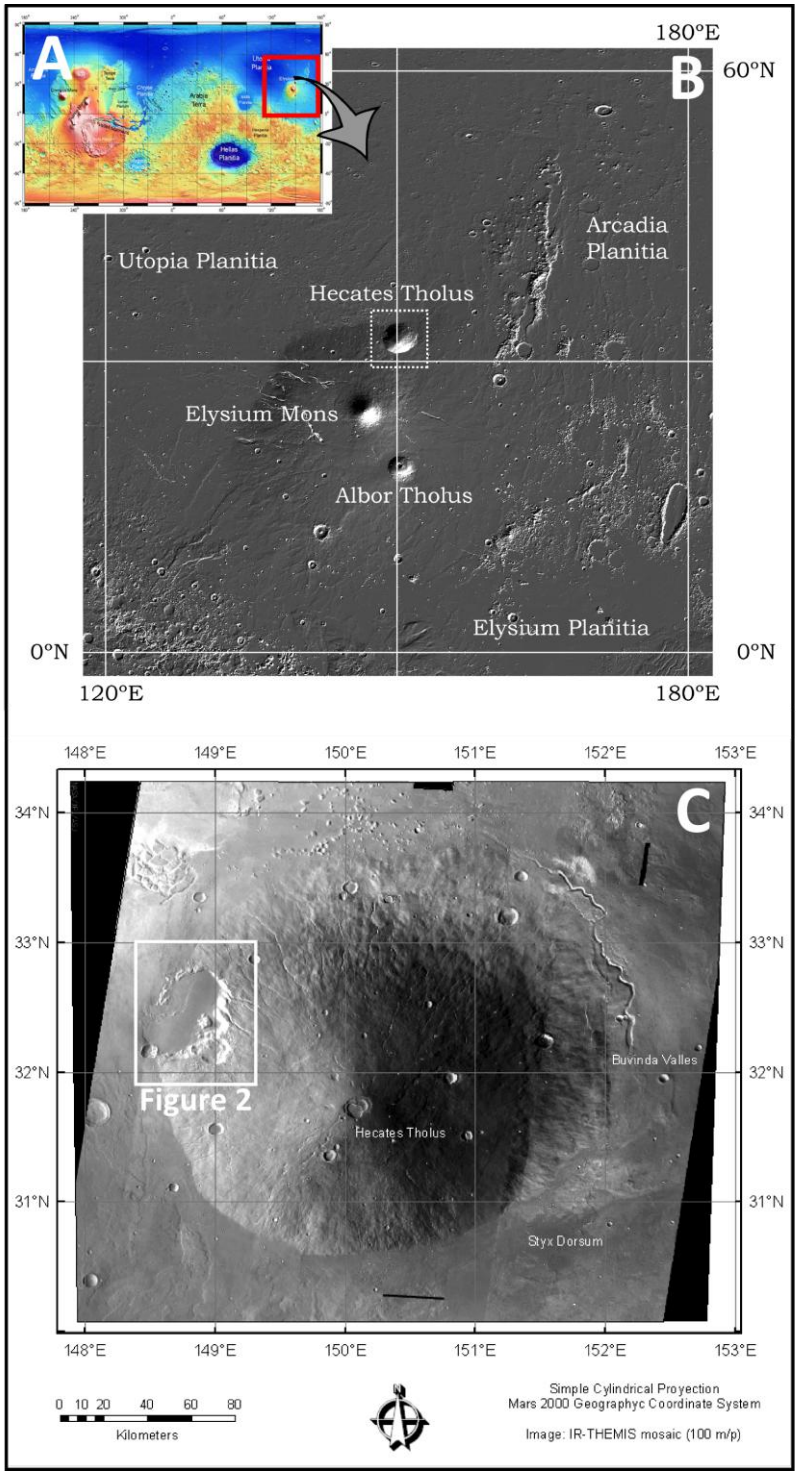

Fig. 2.1: (A) MOLA-derived topographic map of Mars showing the location of the Elysium volcanic province (EVP); (B) MOLA-derived shaded relief map of EVP and the location of Hecates Tholus shield volcano; and (C) Mosaic of THEMIS-IR daytime images of Hecates Tholus volcano and the location of the mapped area (shown in Figure 2.2).

Hecates Tholus (Figure 2.1) is a shield volcano located at 32.18ºN 150.28ºE (MC-7 quadrangle), in the Elysium volcanic province of Mars, in the Martian lowlands in the northern hemisphere. The edifice is about 8000 meters high above the surrounding plains (summit located at about 4600 meters above the Martian Datum). It is slightly elliptic, being 170 × 190 kilometers in diameter at the base, although the lower southern flanks appear to be covered by lava flows from the Elysium Mons volcano (e.g., de Pablo, 2009). Its most recent volcanic episode seems to have occurred between 1000 and 100 Ma (Neukum et al., 2004; Hauber et al., 2005), although it has had a long history of magmatic, tectonic and water-related interactions (e.g., Mouginis-Mark et al., 1982, 1984; Gulick and Baker, 1989, 1990; Hauber et al., 2005; Fassett and Head, 2006, 2007; Kangi, 2007; and others summarized in de Pablo, 2009).

As mentioned above, glacial features have been described previously on the flanks of Hecates Tholus. Although a possible ice cap covering the highest part of the edifice has been proposed (Fassett and Head, 2006, 2007), most of the glacial features are located on the NW flank of the edifice (e.g., Neukum et al., 2004; Hauber et al., 2005; Helbert et al., 2005;), and mostly on the lower part, related to a nested depression. The main area with glacial elements are, first, an elliptical depression at the base of the volcano (40 × 30 km, SW-NE oriented), and, second, a smaller depression (15 km in diameter) on the middle part of the flank. Following the recent terminology proposed by Head et al. (2010), Lineated Valley Fill and Lobate Debris Aprons have been observed in THEMIS-Vis (18 m/pixel), HRSC (12 m/pixel) and MOC (2 m/pixel) images, as described and mapped previously (e.g., Hauber et al., 2005). However, the newly available high-resolution images from CTX and HiRISE instruments on board the NASA's Mars Reconnaissance Orbiter (MRO) now provide sufficient resolution (6 m/pixel and 0.25 m/pixel, respectively) to produce a detailed geomorphological map of those glacial features that could help to understand the glacial and geological history of this area.

The main target of our research was to produce a detailed (1:100,000 scale) geomorphological map of a selected area (Figure 2.2) of the Hecates Tholus volcanic edifice where glacial features are particularly abundant, the lower NW flank (31.8-33.08ºN, 148.37-149.38ºE), using CTX images as the base map, since these provide sufficient spatial coverage and resolution to enhance the study reported here. This map adds new information to the previous regional thematic maps of Mars which include this volcano (e.g., Tanaka et al., 1992, 2005; Hauber et al., 2005). This map also provides a basis for future detailed geological and geomorphological studies focused on understanding the geological and climatic history of this

region of the planet and the possible relief related to magma, water and ice interactions, with the aim of expanding on the results of previous extensive studies (e.g., Mouginis-Mark et al., 1982, 1984; Mouginis-Mark, 1985; Mustard et al., 2001; Mustard, 2003; Carr and Head, 2010, among others).

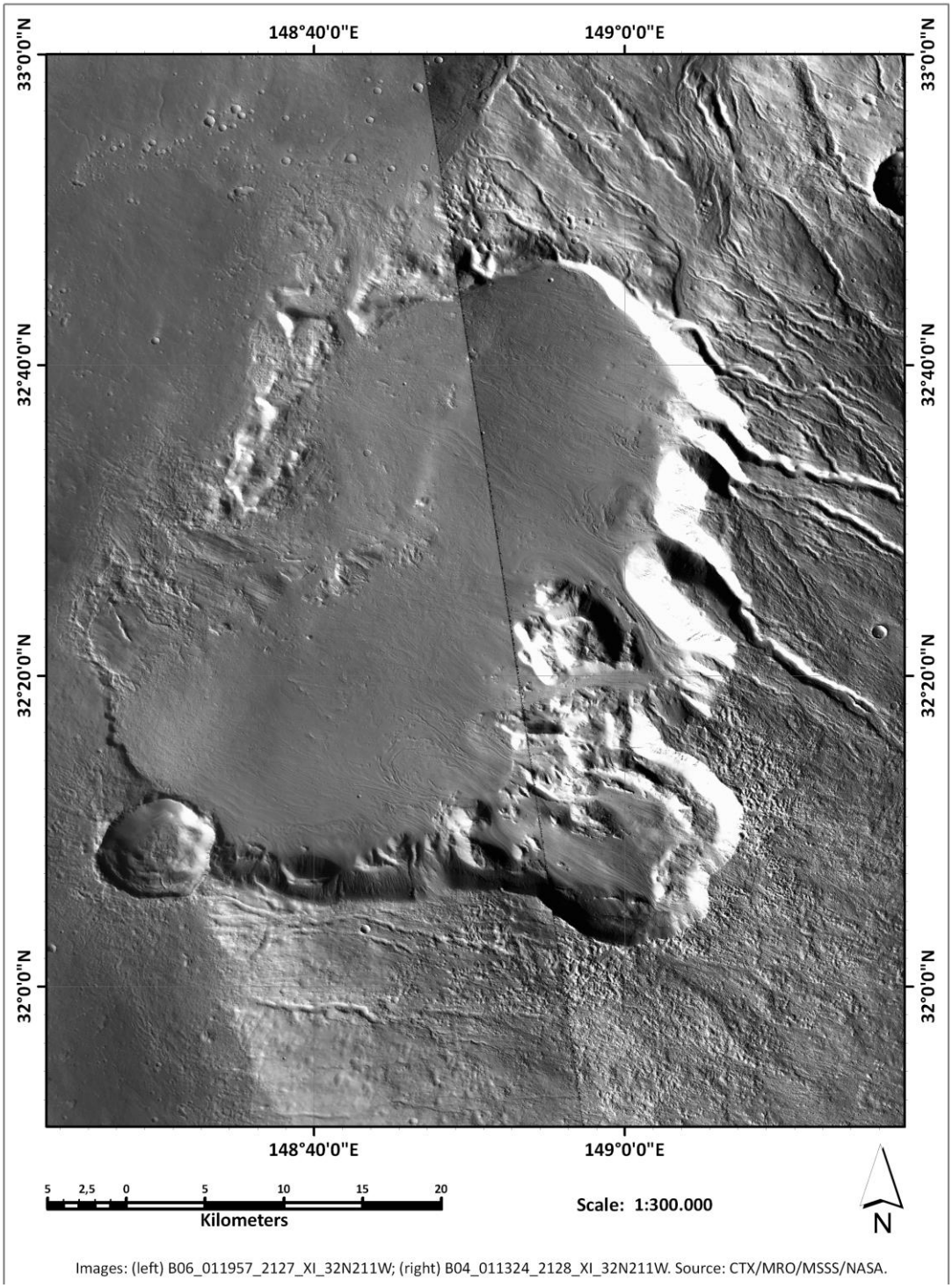

Fig. 2.2: Composition of CTX images of the study area used here to develop the geomorphological cartography.

2.2. Data, methods and software

Mapping the geomorphological features of the lower NW flank of the Hecates Tholus volcano of Mars was made possible through the analysis of high-resolution images from the CTX instrument on board the MRO spacecraft (NASA: 2006–present). These images were acquired in the visible to near infrared spectrum range (0.5–0.8 mm), with a resolution of about 6 meters per pixel. We used a mosaic of two CTX images: B06_011957_2127_XI_32N211W and B04_011324_2128_XI_32N211W. Although other CTX images covering the study area are available we selected these two because of their high quality (without errors or gaps). These images were obtained through the NASA Planetary Data System (PDS: http://pds.nasa.gov/) and the Mars Space Flight Facility of Arizona State University (ASU-MSFF: http://www.mars.asu.edu/).

During the mapping process, we also used other accessory data to improve our understanding of the geological and geomorphological processes which have affected the volcano. First, a nadir image acquired by the High- Resolution Stereo Camera (HRSC) instrument on board the Mars Express (MEX) spacecraft (ESA: 2003 – present) was used as the basis for co-registration of the CTX images, with a spatial error of 6 meters. Image H2907_0008 (50 m/pixel) was not used for mapping due to its lower spatial resolution compared to the CTX images. We also used an HRSC – derived Digital Elevation Model (DEM), which provides topographic information at 50 m/pixel in resolution (H1262_da4), although it does not cover all of the study area. All these data were obtained through the ESA Planetary Science Archive (ESA-PSA: http://www.rssd.esa.int) and the HRSC Team at the Free University of Berlin (HRSC/FUB: http://hrscview.fu-berlin.de).

The base HRSC image (PDS-IMG in format) was processed using the ESA Mars Express HRSC data to GIS converter (HRSC2GIS tool), developed by J. Oosthoek from the Geological Survey of the Netherlands. Topographic data derived from the HRSC images were also processed using the same tool. Then, the resulting projected HRSC image and HRSC-derived DEM data were incorporated into a Geographic Information System developed for the study area through the use of ArcGIS 9.3 (manufactured by ESRI company).We used this software to derive shaded relief, slope and aspect maps, as well as a contour line map (equidistance of 100 m), useful both in the mapping process, and in the interpretation of the different mapped geomorphological features.

With the GIS, we used the Geographic Coordinate System Mars 2000 spheroid (Semi-major axis: 3396190.0 m; Semi-minor axis: 3376200.0 m; Inverse flattening: 169.894) and the Equidistant Cylindrical projection system with central meridian at 1808. Once the coordinate and projection systems had been established, we included our selected data: the HRSC image, HRSC-derived DEM, and CTX images. The HRSC image was used to manually co-register the CTX image (JPG2000 in format) through the use of ArcGIS 9.3 tools, by including more than 400 control points for co-registration of both images.

2.3. Geomorphological elements and units

The geomorphological map (elements and units) of the lower NW flank of the Hecates Tholus volcanic edifice is based on texture and relief, using terrestrial analogue sites, and previous geomorphological maps of glacial areas (e.g., Hattestrand and Stroeven, 2002; Smith et al, 2006; Kjaer et al., 2008; Evans et al., 2009). In addition, some of the geomorphological features (such as impact craters, ridges, faults or channels, among others) have already been included in the geological maps of Mars at different scales (e.g., Tanaka et al., 1992; de Hon et al., 1999). In recent times, more detailed studies have been conducted of the Martian surface using the high-resolution images provided by the last missions to Mars.

These studies have made it possible to identify and define more features, especially those related to glaciers (e.g., Neukum et al., 2004; Hauber et al., 2005; Helbert et al., 2005; Pacifici et al., 2009), and also to define and establish their possible origin (Head and Marchant, 2003; Head et al., 2003, 2006a, 2006b, 2010). Consequently, our geomorphological map is based on previous common practices for geomorphologic mapping of Mars, the most recent geomorphological criteria for glacial features, and terrestrial analogues.

We identified 18 geomorphological elements and 18 geomorphological units (Table 2.1), named in agreement with our interpretation (eskers, moraines, pingos, etc.) and classified according to their origin (glacial, fluvial, impact, etc.). In other words, the geomorphological units mapped here were classified and named according to their origin and main texture (e.g., smooth lava flows, rough slopes, etc.). These units represent terrain sectors characterized by an association of geomorphological elements related to common genetic processes. Units are marked on the map in different colors, with an acronym to identity them clearly on the map.

The map map also shows the relationship between units and elements according to their origin (Table 2.1). However, some elements are only related to specific units with a similar origin (e.g., crevasse element to glacier unit), meanwhile some other elements are

widely distributed throughout all of the geomorphological units (e.g., impact crater or channel elements).

The resulting geomorphological map (Figure 2.3.; Appendix A.3) of the lower NW flank of the Hecates Tholus volcano (1:100,000 scale) contains a brief description of each unit, its spatial distribution and geological/geomorphological interpretation, as well as an image of the study area of each unit.

Table 2.1: Mapped geomorphological units and elements, and their interpreted origin.

Origin	Units	Elements
Volcanic	Smooth outcrop Smooth lava flow Dissected lava flow Rough lava flow Patterned lava flow	
Slope	Slope deposit Creep deposit Rocky slope Rough slope Smooth slope	Scarp Slope base ridge
Fluvial	Badland Gulley sedimentary deposit	Channel Shallow channel Terrace scarp
Periglacial		Pingo
Glacial	Roche moutonée Glaciar deposit	Serac Flute Esker Arête Morraine Glacier erratic
Aeolian		Dune field
Tectonics		Graben Alignment Ridge
Impact	Ejecta deposit Crater material	Crater Impact crater
Other	Knobby terrain Rugged terrain	

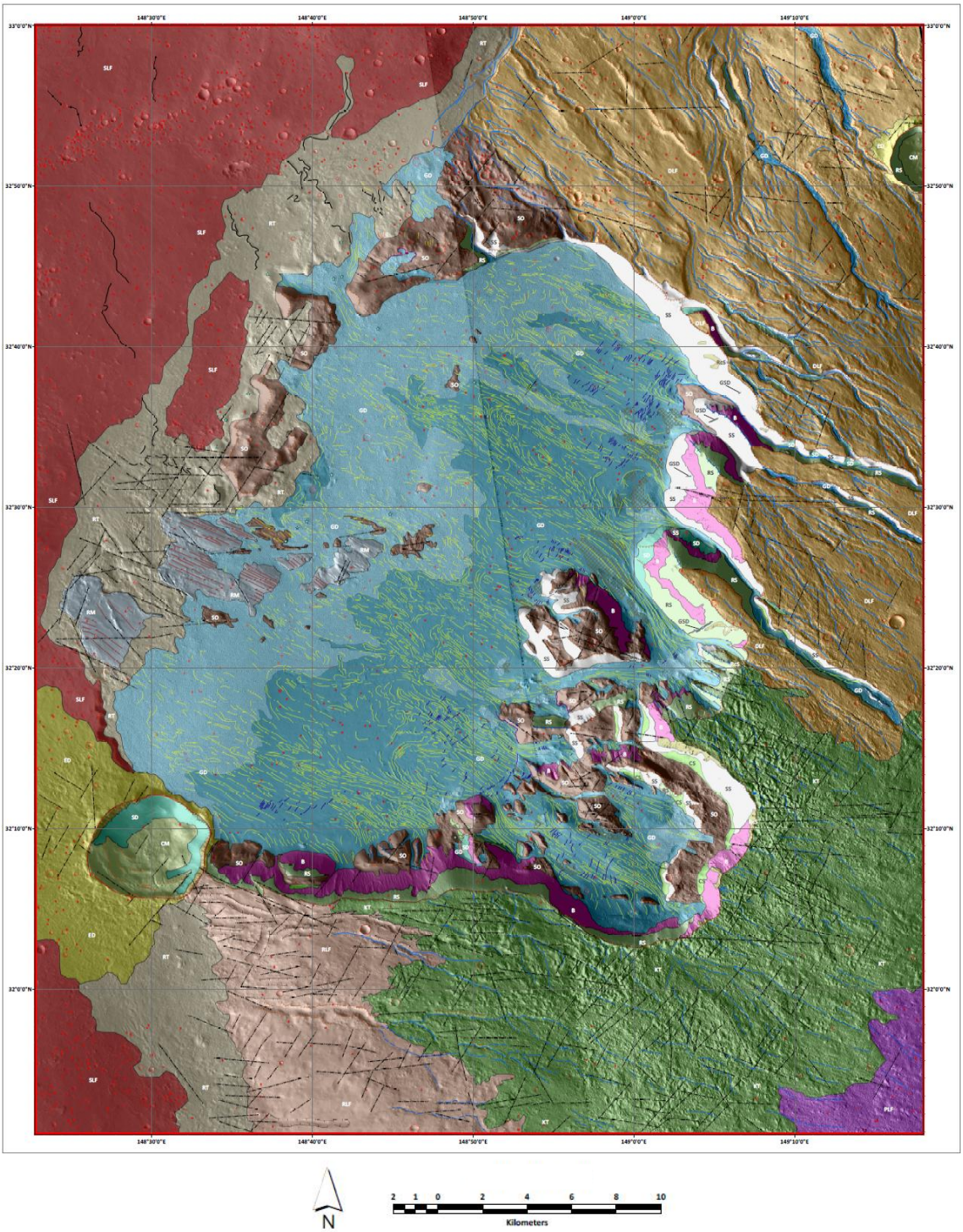

Figure 2.3: Geomorphological map of the lower NW flank of the Hecates Tholus volcano and map explanation (next page).

MAP EXPLANATION

Location of geomorphological units (3 km boxes) and elements (1.5 km boxes) samples are show on the satellite image.

Geomorphological units:

Volcanic

Unit name: SMOOTH OUTCROP
Description: Smooth, undivided and unfeatured rock outcrops.
Distribution: Inside and forming some edges of the main depression on the lower NW flank of the Hecates Tholus volcano.
Interpretation: Ancient volcanic materials forming the lower part of Hecates Tholus volcano, later modeled by putative glacial flows.

Unit name: SMOOTH LAVA FLOWS
Description: Regular surface with abundant lobated scarps, with rugged texture near the edges.
Distribution: Plains surrounding the western base of Hecates Tholus.
Interpretation: Distal lava flows from Elysium Mons volcano, flowed surrounding Hecates Tholus volcano, with different spatial erosion rates caused by fluvial and impact processes.

Unit name: DISSECTED LAVA FLOW
Description: Irregular, heavily dissected terrain with smooth steps.
Distribution: NW flank of the Hecates Tholus volcano.
Interpretation: Lava flows forming the flank of Hecates Tholus, later dissected by fluvial, glacial and tectonic features.

Unit name: ROUGH LAVA FLOW
Description: Rough terrain on the lower western slope of the volcano, partially covered by smooth materials.
Distribution: Lower western flank of Hecates Tholus volcano.
Interpretation: Distal lava flows from Hecates Tholus volcano, later modified by tectonic, impact and fluvial processes.

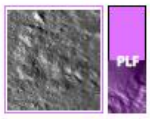

Unit name: PATTERNED LAVA FLOW
Description: Irregular terrain on the middle part of the western slope of the volcano, partially covered by smooth materials oriented with a SW-NE pattern.
Distribution: Lower western flank of Hecates Tholus volcano.
Interpretation: Distal lava flows from Hecates Tholus volcano, later modified by tectonic, impact and fluvial processes.

Slope

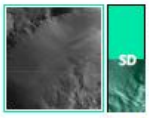

Unit name: SLOPE DEPOSIT
Description: Irregular smooth terrain on high slopes, locally forming clear cone-shaped deposits.
Distribution: Few scarps on the eastern edge of the main depression on the lower NW flank of the Hecates Tholus volcano.
Interpretation: Sedimentary deposits formed by mass-wasting and other slope movements clearly related to high slopes.

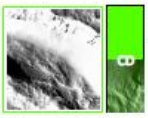

Unit name: CREEP DEPOSIT
Description: Smooth and wavy terrain on the lower part of high slopes.
Distribution: Eastern edge of the depressions on the lower NW flank of Hecates Tholus volcano, always on west- and south-facing high slopes.
Interpretation: Sedimentary deposits accumulated by creep processes on high slopes.

Unit name: ROCKY SLOPES
Description: Printine rough terrain on the upper part of high slopes and scarps.
Distribution: Upper part of some scarps on the eastern edge of the nested depressions on Hecates Tholus.
Interpretation: Rock outcrops on upper part of scarps and high slopes inside the depression, and also in some craters.

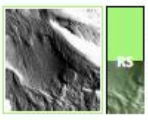

Unit name: ROUGH SLOPE
Description: Unfeatured rough surface on high slopes and scarps generally unfeatured.
Distribution: Upper part and head of the main scarps of the main valleys and depressions on the lower NW flank of Hecates Tholus.
Interpretation: Rock outcrops heavily eroded by different processes, and locally covered by sediments.

Unit name: SMOOTH SLOPES
Description: Unfeatured smooth surface on high slopes.
Distribution: East- and south-facing slopes of the main valleys and depressions on the lower NW flank of Hecates Tholus.
Interpretation: Undivided slope deposits.

Fluvial

Unit name: BADLANDS
Description: Rough surface forming narrow valleys on upper part of slopes.
Distribution: Typically on the middle part of the slopes of the main depression on the lower NW flank of the volcano.
Interpretation: Erosion by diffuse superficial runoff on the slopes.

Unit name: GULLIE DEPOSIT
Description: Downslope elongated unfeatured dark deposit.
Distribution: South-east-facing slopes of the main depression on the lower NW flank of Hecates Tholus.
Interpretation: Water-rich sediments from gullies.

Glacial

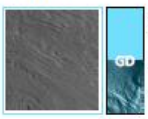

Unit name: GLACIER DEPOSITS
Description: Smooth terrain with elongated scarps and lobate structures.
Distribution: Inside the main valleys on the western flank of the volcano, and most of the floor of the depressions on this flank.
Interpretation: Dust-covered glacial and/or rocky glacial flowing inside the main valleys toward the depressions, and also inside them.

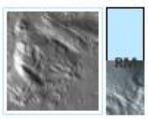

Unit name: ROCHES MOUTONÉES
Description: Smooth terrain with gentle slope and asymmetrical edges, and clearly dissected by elongated, straight valleys.
Distribution: Near the edge, on the western inner part inside the main depression on the lower NW flank of the volcano.
Interpretation: Rock outcrops heavily eroded by the action of an ancient glacial tongue.

Impact

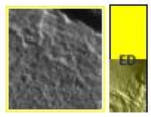

Unit name: EJECTA DEPOSIT
Description: Surface of variable texture (rough to smooth) around impact craters, locally with radial pattern.
Distribution: Surrounding impact craters at different sites throughout the area.
Interpretation: Ejecta deposits from the impact craters.

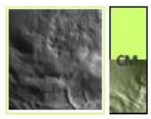

Unit name: CRATER MATERIAL
Description: Rough materials filling impact crater slopes.
Distribution: Inside the rounded depression of impact craters.
Interpretation: Undefined material of different origin, including sedimentary, slope, fluvial, and volcanic, among others.

Other

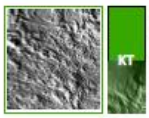

Unit name: KNOBBY TERRAIN
Description: Regular surface with abundant irregular hills and mounds without clear orientation or patterns.
Distribution: Upslope and surrounding the secondary depression on the lower NW flank of the Hecates Tholus volcano.
Interpretation: Materials of undefined origin, including impact ejecta and volcanic fall materials among other possible origins.

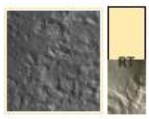

Unit name: RUGGED TERRAIN
Description: Rough surface with very irregular reliefs from hills to mounds, locally clearly oriented, and with chaotic patterns.
Distribution: Nearest plains surrounding the western flank of the volcano.
Interpretation: Strongly rugged terrain formed by different materials of different (including volcanic, fluvial, glacial, etc.) later dissected by fluvial and tectonic processes.

Geomorphological elements:

Glacial

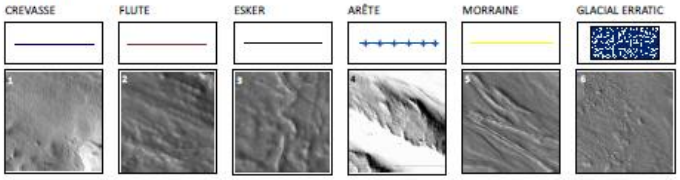

Slope

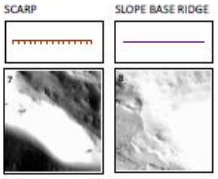

Aeolian

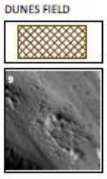

Fluvial

Tectonic

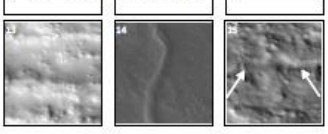

Impact

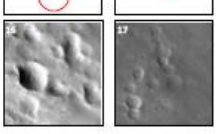

Periglacial

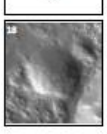

2.4. Conclusions

The 1:100,000 scale geomorphological map of the lower NW flank of the Hecates Tholus, based on CTX images, shows that the studied area is rich in possible glacial features (landforms, deposits, etc.), including moraines, covered glacial tongues (or possibly, rocky glaciers), lineated deposits, eskers, drumlins, etc. It also reveals the existence of other interesting relief related to several processes, including: tectonics (ridges, faults and graben, or morphological alignments), fluvial and water-related (gullies, channels, or terraces), periglacial (pingos), gravitational (mass wasting deposits or creeping slopes) and impact-related (impact craters or ejecta deposits) forms.

All those features suggest a complex hydrological, climatic and geological history for this volcano in very recent times, perhaps as recent as 0.4 Ma (Hauber et al., 2005). A detailed analysis of each feature and its distribution will help to understand the geological evolution of this area and the possible important role of climate, or how changes in climatic conditions may have been responsible for the present surface characteristics.

This map provides a substantial amount of information about the existence and spatial distribution of features not described in previous studies of this area, based on THEMIS-Vis, HRSC (due to their lower resolution), or MOC (due to their low spatial coverage) images. We hope this geomorphological map will inspire other thematic cartographies of the Martian surface using CTX and HiRISE images, due to their high quality and usefulness for understanding the geological evolution of the Red Planet.

PhD thesis

Glacial geomorphology of the NW flank of the Hecates Tholus volcano, Mars

3

Age and evolution

Miguel Ángel de Pablo Hernández

2015

Abstract:

We present results of crater size–frequency distribution (SFD) analysis of the main 10 geomorfological units of the lower NW flank of the Hecates Tholus using images of the Context instrument (CTX) of Mars Reconnaissance Orbiter mission. We derived absolute model ages for the origin and the end of resurfacing events. Our results establish the origin of the Hecates Tholus volcano at 3.8 Ga, with possible volcanic eruptions occurring at least until 335 Ma. Glacial events could begin at 1.4 Ga, with glaciations dated at 90, 30 16, and 6 Ma, as well as events related to the recent ice ages of Mars, between 2 and 0.4 Ma. The resulting ages, our observations on CTX images and the geomorphological map imply that glacial-related processes played an important role in sculpting this flank of the volcano. In addition, we provide a reconstruction of the ice surface elevation of the glacial sheet in the main depression of this flank, with altitudes ranging between ~2035 m and ~2490 m, in agreement with the presence of smooth outcrops and roche moutonnées in the area. Finally, this chapter includes a discussion on the evolution of this region of the Hecates Tholus, establishing the sequence of the most important geological events which occurred in the area.

Resumen:

Mediante el uso de imágenes el instrumento Context (CTX) de la mission Mars Reconnaissance Orbiter se ha realizado un análisis de la distribución de frecuencias del diámetro de los cráteres de impacto de las 10 principales unidades geomorfológicas de la base del flanco Noroeste del Volcán Hecates Tholus de Marte, obteniéndose edades absolutas para el origen de dichas unidades así como del final de los procesos de rejuvenecimiento que los afectó. Los resultados permites establecer el origen del volcán en 3.800 Ma, aunque ha podido tener erupciones hasta hace 350 Ma. Los eventos glaciares pudieron comenzar hace 1.400 Ma y han sido identificados y datados en 90, 30, 16, y 6 Ma, así como en 2 y 0.4 Ma, relacionados con las últimas edades del hielo. Estas dataciones y las observaciones geomorfológicas permiten afirmar que el modelado glaciar jugó un papel importante en el modelado de este sector del volcán, siendo posible incluso determinar la presencia de una masa glaciar cuya altitud en el borde oeste de la depresión que caracteriza este sector osciló entre ~2035 m y ~2490 m. Con todo ello, aquí se propone una posible evolución para este sector del volcán Hecates Tholus en la que se ubican los eventos más importantes de su historia geológica y de los eventos glaciares.

Related publications:

de Pablo, M.A., Michael, G.G., and Centeno, J.D. 2013. Age and evolution of the lower NW flank of the Hecates Tholus volcano, Mars, based on crater size-frequency distribution on CTX images. Icarus, 226. 455-469.

3.1. Introduction

Hecates Tholus (32.12ºN, 150.24ºE) is a shield volcano of the Elysium volcanic province of Mars, at tropical latitude (Figure 3.1). This volcano shows a complex evolution with spatial interaction of tectonic, magmatic and water-related activity (e.g., Mouginis-Mark et al., 1982; Neukum et al., 2004; Hauber et al., 2005; Williams et al., 2005; Fassett and Head, 2006, 2007; Kangi, 2007). The age of Hecates Tholus volcanism ranges between 3800 and 100 Ma, which implies this volcano was active in some way for 80% of the history of Mars (Tanaka, 1986; Neukum et al., 2004; Hauber et al., 2005; Werner, 2009; Platz and Michael, 2011; Robbins et al., 2011). The different stages of the volcano growth on this long-lasting system must therefore have developed within different climatic and regional tectonic settings during the planet's history that could have influenced its evolution (e.g., Baker et al., 1991, 2000 among others).

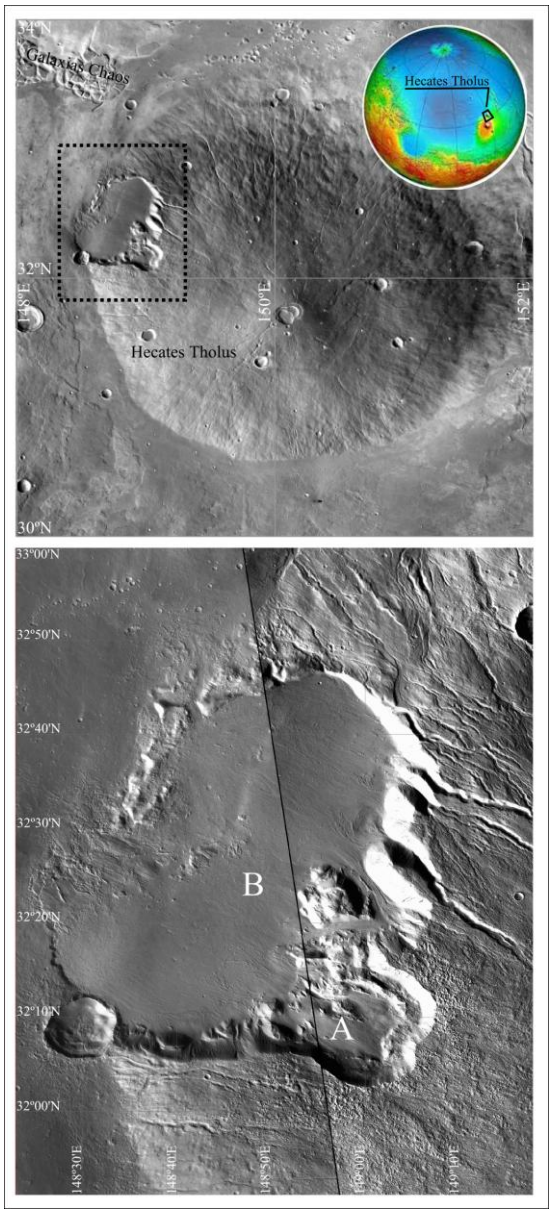

Fig. 3.1: THEMIS-IR daytime mosaic of the Hecates Tholus volcano of Mars (above), and CTX mosaic of the study area (bottom), the lower NW flank of the edifice. A and B indicate the two depressions which characterize this flank.

In fact, water had an important role in the evolution of this edifice, indicated, for example, by the clear radial channel network on the flanks of the volcano (Mouginis-Mark, et al., 1981, 1982), probably relatively young (Gulick and Baker, 1989, 1990; Fassett and Head, 2006, 2007, 2008), and the magma–water interactions that characterize this region of Mars (e.g., Mouginis-Mark et al., 1981, 1982, 1984; Mouginis-Mark, 1984, 1985). Although some authors have suggested different origins for these channels (e.g. volcanic origin proposed by Williams et al. (2005)), the fluvial origin seems to be the most feasible for most of them, and different possibilities for the origin of the water have been proposed: (1)

changes in martian obliquity and redistribution of water equatorward, as revealed by the evidence of glacial landforms located near the martian equator (e.g., Jakosky and Carr, 1985; Jakosky and Haberle, 1992; James et al., 1992; Carr, 1996, 2006; Richardson and Wilson, 2002; Head et al., 2003, 2005; Head and Marchant, 2003; Mischna et al., 2003; Shean et al., 2005); (2) geothermal melting of snow cap on the volcano (Gulick et al., 1997; Zent, 1999; Gulick, 2001; Carr and Head, 2003); (3) remobilization of volatiles during a degassing stage of this volcano (Scott and Wilson, 1999); and (4) basal melting of snowpacks located on the flanks of the volcano (Carr and Head, 2003; Fassett and Head, 2006, 2007,2008).

The glacial origin of these channels by melting of a possible icecap or snowpacks has a terrestrial analog at the Antarctic Dry Valleys (e.g., Head and Marchant, 2003). On the other hand, the existence of possible glaciers on Hecates Tholus NW flank and the evidence for glacial retreat to be explained below is consistent with recent glacial activity on Mars (e.g., Neukum et al., 2004; Hauber et al., 2005).

This NW flank of the volcano (Figure 3.1) is characterized by a complex structure of nested depressions, one of them at higher altitude that has been interpreted as a peripheral caldera resulting from an explosive eruption ~350 Ma ago (Neukum et al., 2004; Hauber et al., 2005; Werner, 2009). Images acquired by the different cameras on board the Mars Global Surveyor, Mars Odyssey, and Mars Express missions, made it possible to recognize possible glacial features inside those complex depressions (e.g., Neukum et al., 2004; Hauber et al., 2005; Werner, 2009), and to confirm the important role of water and ice in the geological and volcanic evolution of this volcano (e.g., Mouginis-Mark et al., 1982; Mouginis-Mark and Christensen, 2005). For that reason, to conduct detailed studies about the glacial features observed on the volcano, it becomes necessary to refine our knowledge about its glacial and volcanic history, especially when new data are available thanks to the instruments on board the Mars Reconnaissance Orbiter such as the Context (CTX) instrument, which provides images at 6 m per pixel in resolution with a wider spatial coverage than the Mars Orbiter Camera (MOC) and High Resolution Imaging System Experiment (HiRISE) images.

This region was geologically mapped in the global (Greeley and Guest, 1987) and regional (Tanaka et al., 1992, 2005) geological maps of Mars. Recent works also include a more detailed regional mapping (Neukum et al., 2004; Hauber et al., 2005) as well as a 1:100,000 scale geomorphological map (de Pablo and Centeno, 2012) of the western flank of Hecates Tholus. This geomorphological map, based on CTX images and an HRSC-derived digital

elevation model, shows a wide variety of glacial-related landforms and features concentrated inside the complex depressions on the lower NW flank, as well as in the surrounding area.

However, to establish a geological, geomorphological and climatic history of this volcano from this map requires dating the different terrains of the area, including those possible glacial deposits. For that reason, the objective of this research is to make a crater-size frequency distribution (from here SFD) analysis of the geomorphological units of the lower NW flank of the Hecates Tholus volcano (on CTX images of the area), and to use the results to derive their absolute ages. This work, the most extensive and detailed ever made in this area due to the coverage and resolution of the used data, will complete the first dating works from Neukum et al. (2004), Hauber et al. (2005), and Werner (2009), and provide the necessary information to complete our knowledge about the possible volcanic, glacial, and fluvial evolution of this martian volcano, and about the role played by water ice.

3.2. Methods

This study is based on the geomorphological map of the lower NW flank of the Hecates Tholus volcano (de Pablo and Centeno, 2012), and we used the mapped geomorphological units to carry out impact crater counts (e.g. Hartmann, 1973, 1984, 2005; Neukum and Hiller, 1981; Neukum, 1983; Neukum and Ivanov, 1994; Hartmann and Neukum, 2001; Ivanov, 2001; Werner and Tanaka, 2011) in order to date those units, using the results to establish the possible evolution of the geological processes that formed and modeled the region. The counts consisted of diameter measurements of all the impact craters observed on two Context (CTX) images from Mars Reconnaissance Orbiter: B04_011324_2128 and B06_011957_2127 (both of them about 6 m/pixel in resolution), the same images used for the geomorphological mapping of the area (de Pablo and Centeno, 2012), carried out within a Geographic Information System environment (using the ArcGIS software from ESRI). We selected CTX images because they cover the whole study area rather than small sectors, in spite of their slightly lower resolution than HiRISE or MOC images. The study area was the same as that contained in the geomorphological map, and extends from 31.85ºN to 33.0ºN and from 148.3ºE to 149.3ºE (Figure 3.1).

From all the mapped units, we used only a selection of them in this analysis (Table 3.1), discarding those units related to high slopes, low areas, or both. Then, only the most representative and important geomorphological units were selected for this work: smooth outcrops (SO), smooth lava flows (SLF), dissected lava flows (DLF), rough lava flows (RLF),

patterned lava flows (PLF), ejecta deposits (ED), glacier deposits (GD), roche moutonnée terrains (RM), knobby terrains (KT), and rugged terrains (RT), following the nomenclature used in de Pablo and Centeno (2012).

Table 3.1: Main geomorphological units of the lower NW flank of the Hecates Tholus volcano (from de Pablo and Centeno (2012)) considered for the analysis of the crater size–frequency distribution (SFD) analysis.

Unit	Name	Description/interpretation
SO	Smooth outcrop	Smooth, undivided and unfeatured rock outcrops Ancient volcanic materials forming the lower part of Hecates Tholus volcano, later modeled by putative glacial flows
DLF	Dissected lava flow	Irregular, heavily dissected terrain with smooth steps Lava flows forming the flank of Hecates Tholus, later dissected by fluvial, glacial and tectonic features
RLF	Rough lava flow	Rough terrain on the lower western slope of the volcano, partially covered by smooth materials Distal lava flows from Hecates Tholus volcano, later modified by tectonic, impact and fluvial processes
PLF	Patterned lava flow	Irregular terrain on the middle part of the western slope of the volcano, partially covered by smooth materials oriented with a SW–NE pattern Distal lava flows from Hecates Tholus volcano, later modified by tectonic, impact and fluvial processes
SLF	Smooth lava flows	Regular surface with abundant lobated scarps, with rugged texture near the edges Distal lava flows from Elysium Mons volcano, flowed surrounding Hecates Tholus volcano, with different spatial erosion rates caused by fluvial and impact processes
ED	Ejecta deposits	Surface of variable texture (rough to smooth) around impact craters, locally with radial pattern Ejecta deposits from the impact craters
GM	Glacier deposits	Smooth terrain with elongated scarps and lobate structures Dust-covered glacial and/or rocky glacial flowing inside the main valleys toward the depressions, and also inside them
RM	Roches moutonées	Smooth terrain with gentle slope and asymmetrical edges, and clearly dissected by elongated, straight valleys Rock outcrops heavily eroded by the action of an ancient glacial tongue
KT	Knobby terrain	Regular surface with abundant irregular hills and mounds without clear orientation or patterns Materials of undefined origin, including impact ejecta and volcanic fall materials among other possible origins
RT	Rugged terrain	Rough surface with very irregular reliefs from hills to mounds, locally clearly oriented, and with chaotic patterns Strongly rugged terrain formed by different materials of different (including volcanic, fluvial, glacial, etc.) later dissected by fluvial and tectonic processes

We used the 3-point method of the CraterTools software (Kneissl et al., 2011) for ArcGIS to measure the diameter of each impact crater observed in the CTX images, and to export the results to an ASCII file. We used the CraterStats2 software (Michael and Neukum, 2010) to plot and analyze the results.

In order to avoid artifacts as well as erroneous results in the SFD and the derived ages, on the first hand, we measured only those circular structures that could be clearly interpreted to be impact craters. We studied the images at different scales to be certain about the interpretation (Zimbelman, 2001). On the other hand, we made two different clustering analyses of the spatial distributions of mapped impact craters in order to exclude areas with

possible secondary cratering. The first was a visual inspection of the CTX images to locate possible areas with clusters of craters (Figure 3.2). The second was a randomness analysis of the mapped impact craters by the use of randomness analysis tool from Michael et al. (2012), applying both standard deviation of adjacent area (SDAA) and mean closest two neighbors distance (M2CND) methods (with 300 iterations in each method). We applied this randomness analysis to all the impact craters mapped on the whole area of each geomorphological unit included in this study.

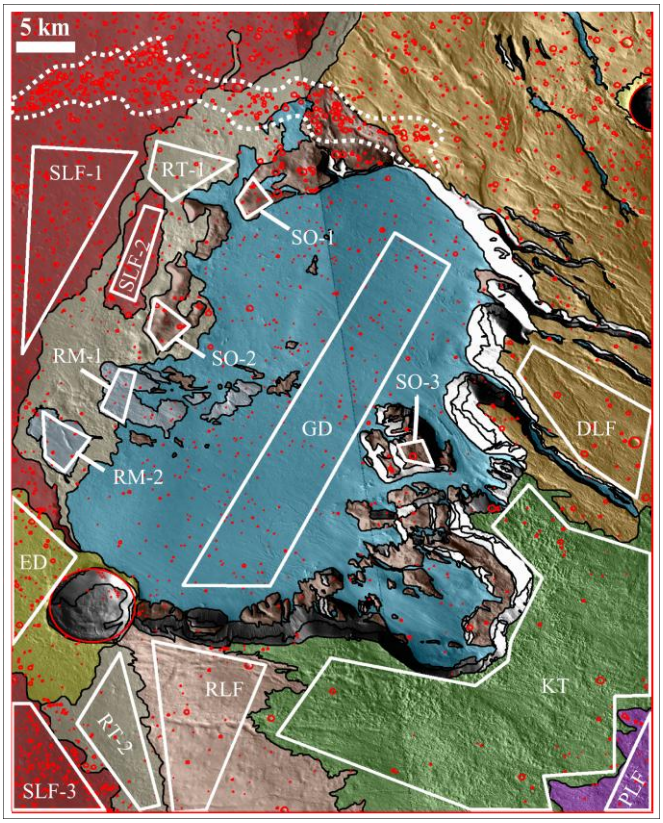

Fig. 3.2: Study area showing a possible secondary crater field in the northern part of the study area (enclosed by the white dotted line), and the sector (white empty polygons) used for each main geomorphological unit of the area. Black lines represent the limits of each geomorphological unit on the original map (modified from de Pablo and Centeno (2012)).

The results of these analyses indicated that some ranges of crater size showed a more clustered than random spatial distribution on some of the analyzed geomorphological units. We observed that in several cases the results were in agreement with our inspection of the CTX images and the visual location of possible secondary cratering (Figure 3.2). Taking into account the results of the analyses as well as our observations of the images, we selected 16 smaller arbitrary areas (as far as possible avoiding apparent clusters of impact craters) corresponding to 10 geomorphological units (Figure 3.2) from the 18 units included into the geomorphological map of this area (de Pablo and Centeno, 2012). Then, using the impact craters mapped inside each one of these 16 areas (Appendix A.1.), we made new randomness analyses to verify that the crater configurations were consistent with being random.

We finally derived both cumulative and differential SFD plots (Figure 3.3) using the CraterStats2 software. Absolute ages were calculated using the same software fitting the SFD curves on a differential frequency plot splitting the craters into 10 bins per logarithmic decade

(Figure 3.3), because this type of plot is particularly well-suited to the study of highly resurfaced units. In such a presentation, portions of the SFD which correspond to isochrons, i.e. sequences of data points which lie parallel to the production function curve, can be seen directly. This is an advantage over the cumulative presentation, where a resurfacing correction must be applied. On the down side, it can be more difficult to establish the base age for a unit because of the low number of craters per bin at the largest diameters, making these data points noisier than in a cumulative presentation. For this work, we switched between the two presentations to ensure that reasonable diameter ranges were selected for the isochron fits.

We derived the ages from the Hartmann and Neukum (2001) chronology function, the Ivanov (2001) production function, and taking into account the Hartmann (1984) equilibrium function. We fitted the age of each unit and, wherever it was possible according to the crater SFD, we calculated the age of the end of resurfacing periods affecting each unit (Michael and Neukum, 2010). Thus, in some cases we fitted more than one isochron to each SFD, corresponding to the age of origin and/or the age of the end of a resurfacing event (Table 3.2).

3.3. Results

In general, the results from the randomness analysis (Figure 3.3) showed the analyzed sectors to have populations which are not clustered, and in agreement with random distributions with the exception of a small numbers of diameter bins on some units. Those bins were excluded from any age-fitting procedure. We show these results together with their corresponding SFD cumulative and differential plots (Figure 3.3). We fitted at least one isochron to each differential plot, likely related to the age of origin with additional isochrons for any resurfacing events affecting the SFD. The results of the randomness analysis and isochron fitting are summarized in Figure 3.4.

SO unit: We analyzed three different and rather small sectors (between 4.2 and 6.5 km^2 in area each one) where we measured 23 impact craters from 33 to 465 m in diameter. Cumulative plots for each of them reveal that this unit is lightly cratered, especially at the higher diameters, where the SFD shows bigger error bars. Clear isochron segments are not distinguishable on them, except for the SO-3 area, where a short segment is recognized. The randomness analysis diagrams show that the measured impact craters on the SO sectors are randomly distributed. We use a threshold around the 3-sigma level to identify non-randomness: not in a strict yes/no sense, but in combination with a visual inspection of the spatial configuration within a diameter bin close to the threshold. This way, one can often

understand the source of the result and decide whether there is indeed a bias in the configuration caused by some geological process, or the configuration is simply 'unusual' but random. We note that visually clustered populations are often indicated at levels as high as 5- or even 10-sigma.

For sector SO-3, there were insufficient craters to develop this analysis. The low numbers are also the reason for the presence of a data point above the Equilibrium function line (Hartmann, 1984). In spite of the light impact cratering of this area, we fitted at least one age for each sector, with ages ranging between 3.8 Ga and 32.1 Ma. In the case of the SO-1 sector, we were able to fit only one isochron corresponding to 1.4 Ga. The older isochrones we fitted to sectors 2 and 3 are approximately similar at 3.4 Ga and 3.8 Ga, respectively.

DLF unit: We only analyzed one sector (about 56.5 km^2) covering a small area of this terrain inside the study region, avoiding possible clustering in the crater distribution. We measured 17 impact craters from 31 to 0.84 m in diameter. The SFD plot of this unit shows a wide range of impact crater diameters. Steps on the curve are distinguishable both on the cumulative and differential plots, which made it possible to fit four different isochrons to this curve. Those isochrons mark ages ranging between 3.6 Ga and 440 ka, with intermediate ages of 806 Ma and 107 Ma. Because of the low number statistics, it is not possible to conclude with certainty that the history of this surface was made up of four events at these times: however, the accumulation times can be interpreted to obtain an impression of when the resurfacing activity was occurring. The randomness analysis reveals that the crater distribution is consistent with being random.

RLF unit: The analyzed sector (covering an area of about 70.8 km^2) also shows a wide range of diameters of the 24 measured impact craters, from 23 to 570 m in diameter. Such as occurs on the DLF Unit, some crater diameters are less frequent, forming gaps in the SFD cumulative plot, and small steps in the curve are also visible. Those craters lie slightly towards the more ordered direction in the randomness analysis, although still within the 3-sigma range to be considered random. We fitted four isochrons to this SFD curve, returning ages from 3.4 Ga to 1.3 Ma. Intermediate fitted isochrones correspond to 415 Ma and 19.4 Ma ages.

PLF unit: The analyzed area (about 13.5 km^2) of this unit contains 10 impact craters at CTX image resolution, with diameters ranging between 56 and 177 m. The randomness analysis reveals that their spatial distribution is consistent with being random. The SFD accumulative plot shows a clear curve with small gaps and steps such as the SFD curves of previously

described RLF and DLF units. We were able to fit only one isochron to this curve, returning an age of 342 Ma. Observing the differential plot, we could not exclude other younger ages using the craters with lower diameters, but we are not confident of the possible result.

SLF unit: We analyzed three different sectors (covering areas between 12.4 and 64.5 km^2) of this geomorphological unit in which we measured a total of 246 impact craters from 22 to 354 m in diameter. SLF-1 area shows a clear curve on the SFD cumulative plot as well as smaller gaps than the previous described units. On the other hand, SLF-2 and SLF-3 sectors only show partial curves related to the higher diameters. In all the three cases, the randomness analysis returned a normal spatial distribution, neither ordered and nor clustered. We fitted at least one isochron for each sector, with ages ranging between 2.35 Ga and 8.61 Ma. On Sector 1 (SLF-1), we were able to fit two isochrons returning ages of 724 Ma, and 8.61 Ma. We could not discard the possibility of fitting two other isochrons with the available data, but we could not be completely confident of the result. On Sector 2 (SLF-2) we only fitted one isochron corresponding to 975 Ma. Finally, on Sector 3 (SLF-3) we fitted two isochrons corresponding to 2.35 Ga and 1.22 Ga.

GD unit: We analyzed one sector (of about 163 km^2 on area) corresponding to this geomorphological unit where we measured 122 impact craters from 24 to 229 m in diameter. The SFD cumulative curve shows a long and complex track with different steps and small gaps, while the randomness analysis shows a configuration consistent with being random. The differential plot made it possible to fit four isochrons to this distribution, corresponding to 61.9 Ma, 30.4 Ma, 16.2 Ma and 6.11 Ma.

RM unit: We analyzed two different sectors (with areas of about 5.81 and 9 km^2, respectively) of this geomorphological unit in which we measured a total of 15 impact craters from 24 to 190 m in diameter. The SFD cumulative plots show very different curves, mainly centered at the lower diameter bins, but without a clustered spatial distribution, such as could be interpreted from the randomness analyses. The SFD differential plots made it possible to fit isochrones for each sector corresponding to very different ages: 16.8 Ma on Sector 1 (RM-1), and 1.08 Ga and 72.8 Ma on Sector 2 (RM-2).

KT unit: The single sector analyzed (about 366.85 km^2) of this geomorphological unit contains 43 impact craters, at CTX image resolution, with diameters ranging between 38 and 521 m. They do not have clustered or ordered patterns in their spatial distribution such as were derived from the randomness analysis. The SFD cumulative plot shows a curve from which we

were able to fit, on the SFD differential plot, four isochrons corresponding to 335 Ma, 44.7 Ma, 4.96 Ma and 274 ka.

RT unit: The two analyzed sectors of this geomorphological unit (about 15.98 and 34.24 km2) show 22 impact craters from 24 to 272 m in diameter that we measured at CTX images resolution. Both sectors show clear curves with small gaps in the crater diameter bins, but not a clustered spatial distribution such as derived from the randomness analyses. The SFD differential plot made it possible to fit different isochrons corresponding to 980 Ma and 31.1 Ma on Sector 1 (RT-1), and to 54.1 Ma, and 988 ka on Sector 2 (RT-2).

ED unit: Only one sector (about 20.57 km^2), corresponding to the most extensive deposit, was analyzed of this geomorphological unit. We measured 43 impact craters with diameters ranging between 24 and 438 m, which do not show a clustered spatial distribution as revealed by the randomness analysis. The SFD cumulative plot shows a clear curve marking a complex evolution, although only we were able to fit only two isochrons on the SFD differential plot, corresponding to 3.43 Ga and 3.87 Ma.

A summary of all these results is shown in Table 3.2 and Figure 3.4 which contains the derived absolute ages of the different analyzed units. These ages ranges between 3.8 Ga and less than 1 Ma. The older terrains correspond, following the nomenclature from de Pablo and Centeno (2012) to the volcanic lava flows forming the NW flank of the Hecates Tholus volcano (units DLF, and RLF) and the outcrops at the edge and inside the complex depressions formation (unit SO), with ages ranging between 3.8 Ga and 3.4 Ga. Clearly younger are the terrains inside the complex depressions, with ages ranging between about 62 Ma and 1.5 Ma. The volcanic lava flows from the Elysium Mons volcano, which surround the Hecates Tholus volcano in all the western part of the studied area, show ages of about 2.4 Ga. We could not confirm that those ages reflect the formation age of each studied area, but the older age we could fit to the SFD by the measured impact craters. On the other hand, all the analyzed sectors (except SO-1 sector) show at least one younger age corresponding to the end of resurfacing events which modified the crater population (Michael and Neukum, 2010). In some cases, especially in the youngest, the resulting ages may be times where the processes were more intensive during a long-lasting resurfacing interval, rather than distinct events.

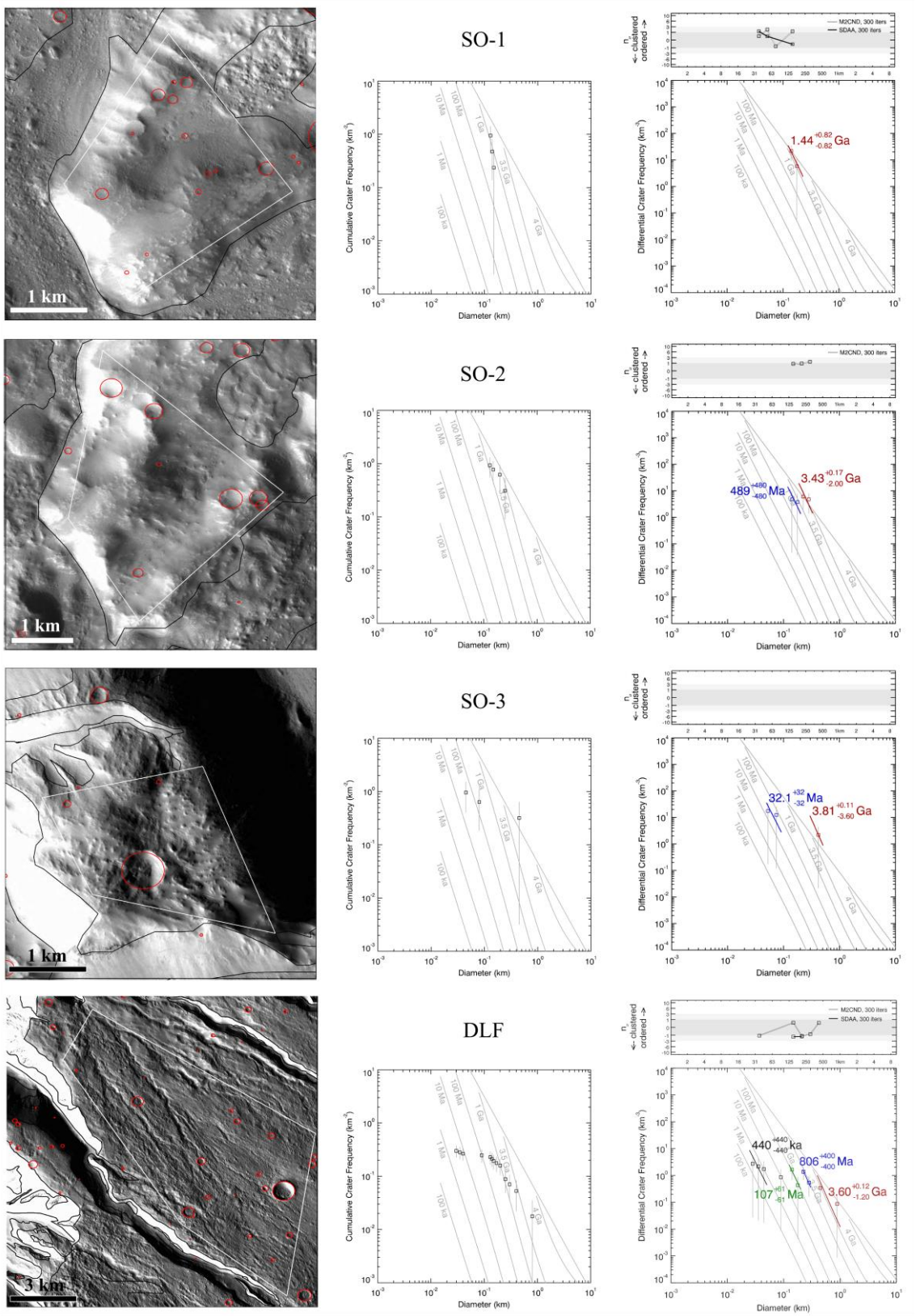

Figure 3.3: Results from randomness analysis and cumulative and differential crater size–frequency distribution (SFD) plots for selected sectors of the main geomorphological units (Table 3.1) mapped by de Pablo and Centeno (2012). [Continue…]

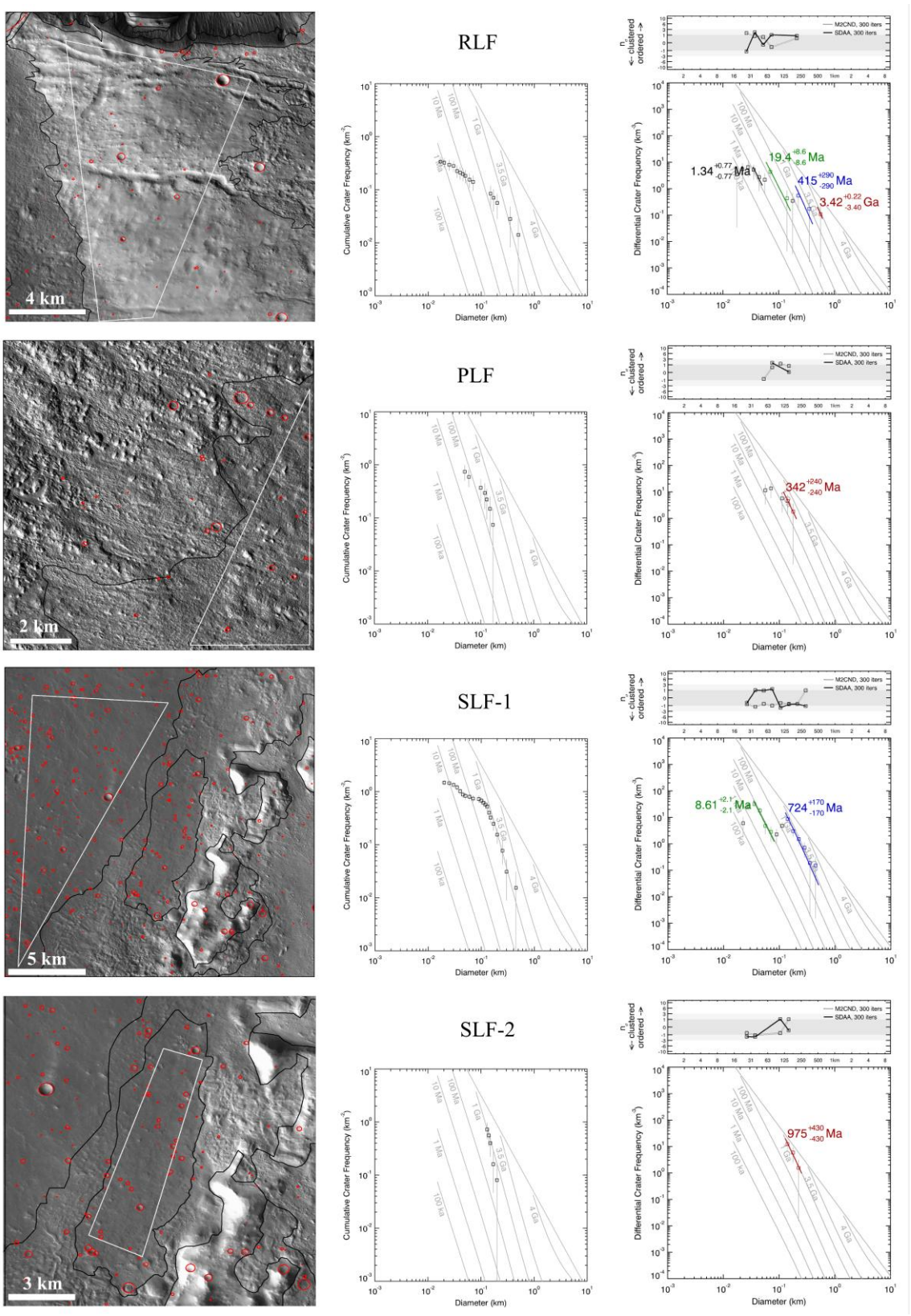

Figure 3.3: [Continue…]

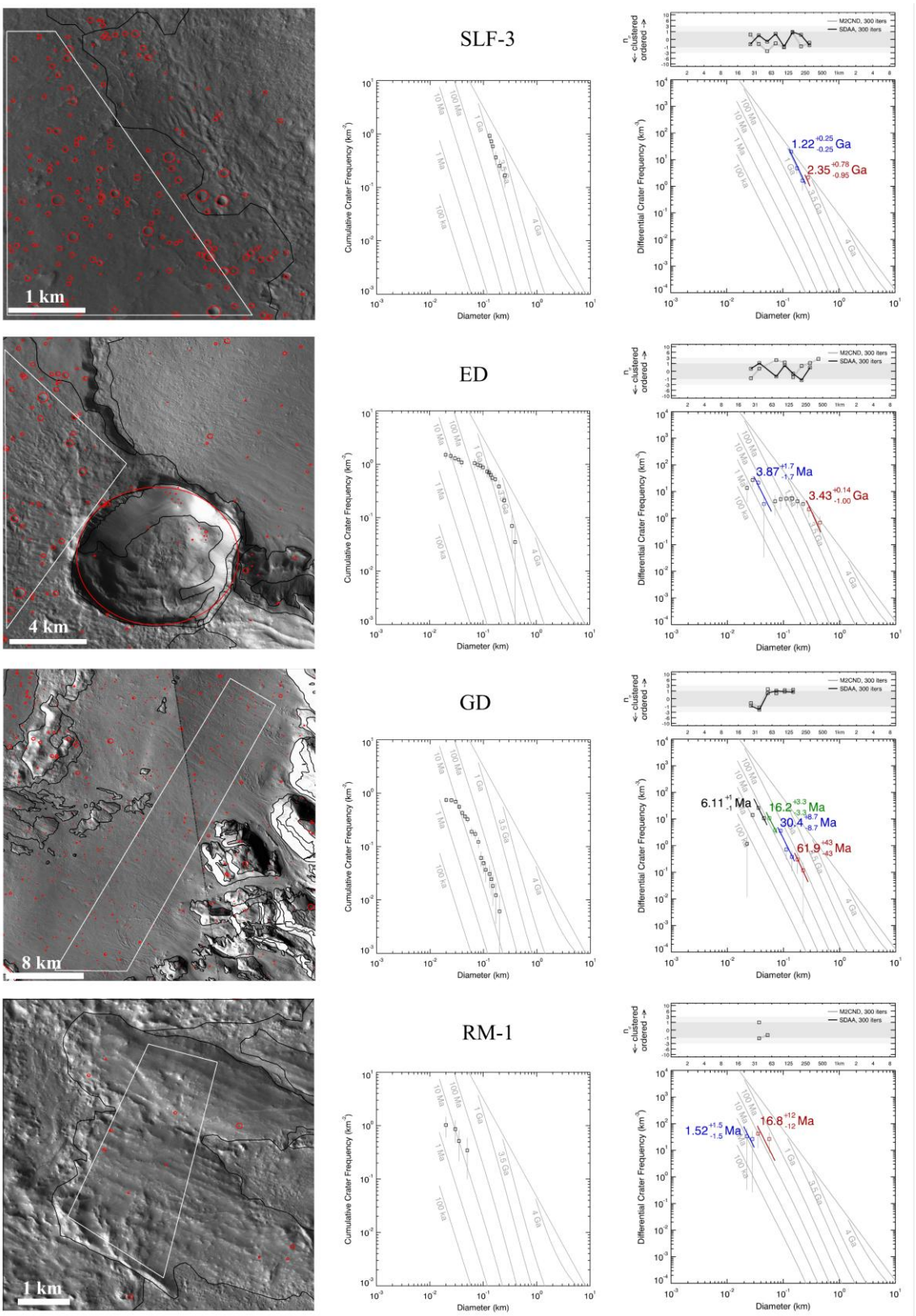

Figure 3.3: [Continue…]

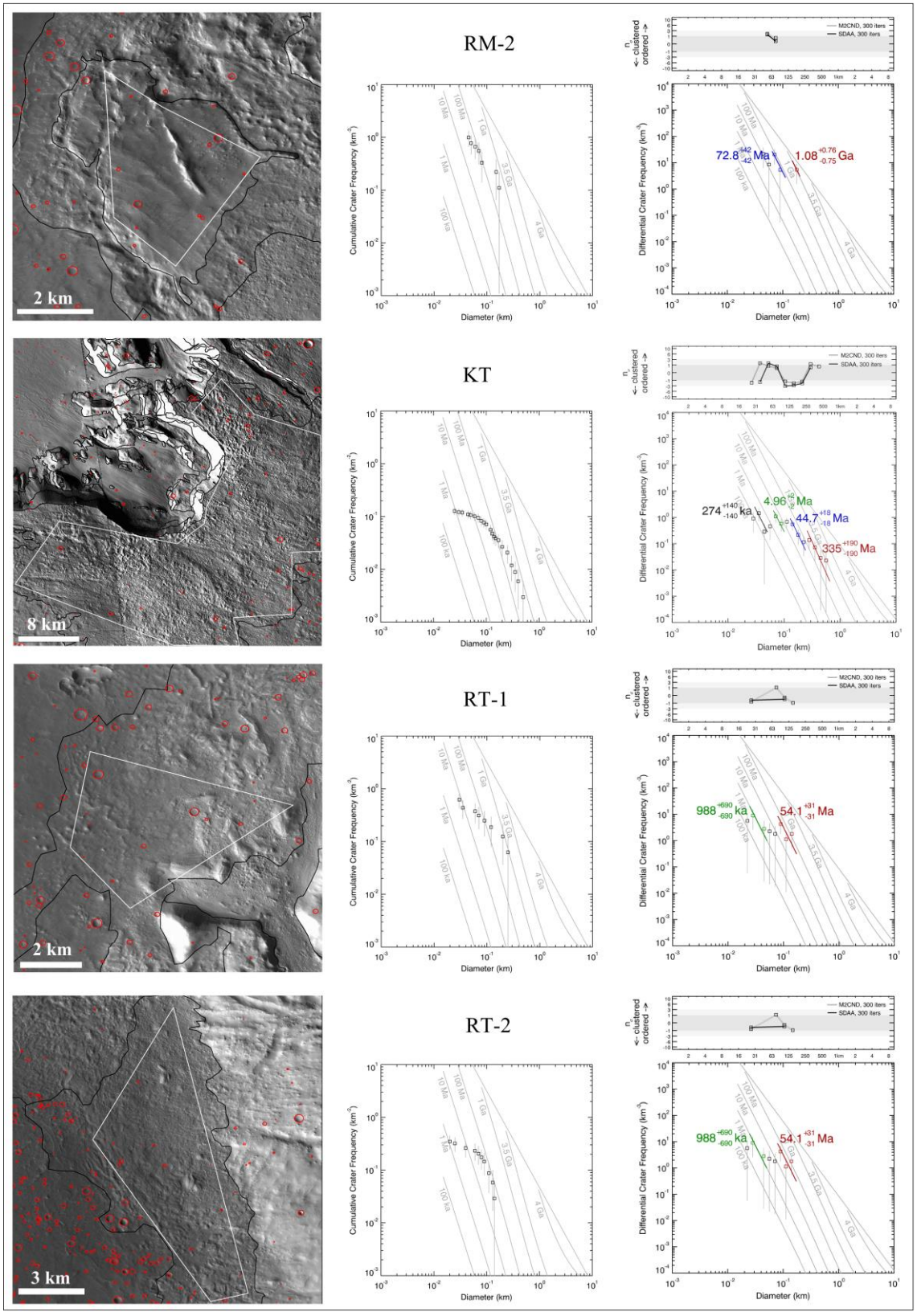

Figure 3.3: [last plate]

Table 3.2: Summary of crater counting measurements and isochrons fitted to the crater size–frequency distribution (SFD) for the different geomorphological units analyzed.

Unit	Crater counting					Crater SFD Isochrons fitting								
	Sector	Area (km^2)	Measured craters			Age (Ga)			Used craters			N(1)		
			n.	Dmin	Dmax	Age	(+)	(-)	n.	Dmin	Dmax	N(1)	(+)	(-)
SO	SO-1	4.21	13	0.033	0.166	1.44	0.82	7.03E-04	4	0.125	0.225	7.03E-04	4.02E-04	4.02E-04
	SO-2	6.45	7	0.052	0.311	3.43	0.17	2	4	0.19	0.325	2.37E-03	1.66E-03	1.66E-03
						0.489	0.48	0.48	2	0.12	0.2	2.38E-04	2.36E-04	2.36E-04
	SO-3	3.13	3	0.048	0.465	3.81	0.11	3.6	1	0.3	0.5	1.14E-02	1.13E-02	1.13E-02
						0.0321	0.032	0.032	2	0.05	0.09	1.57E-05	1.55E-05	1.55E-05
DLF	DLF	56.5	17	0.031	0.838	3.6	0.12	1.2	3	0.4	1	3.93E-03	2.75E-03	2.75E-03
						0.806	0.4	0.4	6	0.22	0.3	3.93E-04	1.95E-04	1.95E-04
						0.107	0.061	0.061	4	0.126	0.2	5.23E-05	2.99E-05	2.99E-05
						0.00044	0.00044	0.00044	3	0.025	0.05	2.14E-07	2.12E-07	2.12E-07
RLF	RLF	70.83	24	0.023	0.569	3.42	0.22	3.4	1	0.5	0.6	2.29E-03	2.26E-03	2.26E-03
						0.415	0.29	0.29	3	0.2	0.4	2.03E-04	1.42E-04	1.42E-04
						0.0194	0.0086	0.0086	6	0.06	0.16	9.44E-06	4.18E-06	4.18E-06
						0.00134	0.00077	0.00077	5	0.035	0.05	6.53E-07	3.73E-07	3.73E-07
PLF	PLF	13.46	10	0.056	0.177	0.342	0.24	0.24	3	0.12	0.2	1.67E-04	1.17E-04	1.17E-04
SLF	SLF-1	64.55	96	0.024	0.471	0.724	0.17	0.17	36	0.13	0.5	3.53E-04	8.24E-05	8.24E-05
						0.00861	0.0021	0.0021	36	0.035	0.08	4.20E-06	1.01E-06	1.01E-06
	SLF-2	12.44	23	0.022	0.17	0.975	0.43	0.43	9	0.13	0.25	4.75E-04	2.11E-04	2.11E-04
	SLF-3	35.63	127	0.027	0.354	2.35	0.78	0.95	5	0.25	0.3	1.14E-03	4.62E-04	4.62E-04
						1.22	0.25	0.25	33	0.13	0.25	5.93E-04	1.22E-04	1.22E-04
ED	ED	20.57	43	0.024	0.438	3.43	0.14	1	6	0.26	0.45	2.33E-03	1.15E-03	1.15E-03
						0.00387	0.0017	0.0017	6	0.03	0.06	1.89E-06	8.35E-07	8.35E-07
GD	GD	163.25	122	0.024	0.229	0.0619	0.043	0.043	3	0.16	0.27	3.02E-05	2.11E-05	2.11E-05
						0.0304	0.0087	0.0087	17	0.08	0.155	1.48E-05	4.23E-06	4.23E-06
						0.0162	0.0033	0.0033	33	0.05	0.075	7.90E-06	1.63E-06	1.63E-06
						0.00611	0.001	0.001	53	0.03	0.05	2.98E-06	4.99E-07	4.99E-07
RM	RM-1	5.81	6	0.024	0.058	0.0168	0.012	0.012	4	0.035	0.07	8.20E-06	5.74E-06	5.74E-06
	RM-2	9	9	0.047	0.19	1.08	0.76	0.75	2	0.15	0.2	5.26E-04	3.68E-04	3.68E-04
						0.0728	0.042	0.042	4	0.065	0.11	3.55E-05	2.03E-05	2.03E-05
KT	KT	366.85	43	0.038	0.521	0.335	0.19	0.19	7	0.26	0.65	1.63E-04	9.32E-05	9.32E-05
						0.0447	0.18	0.18	11	0.13	0.24	2.18E-05	8.81E-06	8.81E-06
						0.00496	0.02	0.02	10	0.065	0.1	2.42E-06	9.78E-07	9.78E-07
						0.000274	0.00014	0.00014	5	0.03	0.05	1.34E-07	6.62E-08	6.62E-08
RT	RT-1	15.98	10	0.031	0.272	0.98	0.97	0.97	2	0.22	0.3	4.78E-04	4.73E-04	4.73E-04
						0.0311	0.022	0.022	3	0.06	0.11	1.52E-05	1.06E-05	1.06E-05
	RT-2	34.24	12	0.024	0.143	0.0541	0.031	0.031	6	0.08	0.17	2.64E-05	1.51E-05	1.51E-05
						0.000988	0.00069	0.00069	3	0.025	0.05	4.82E-07	3.37E-07	3.37E-07

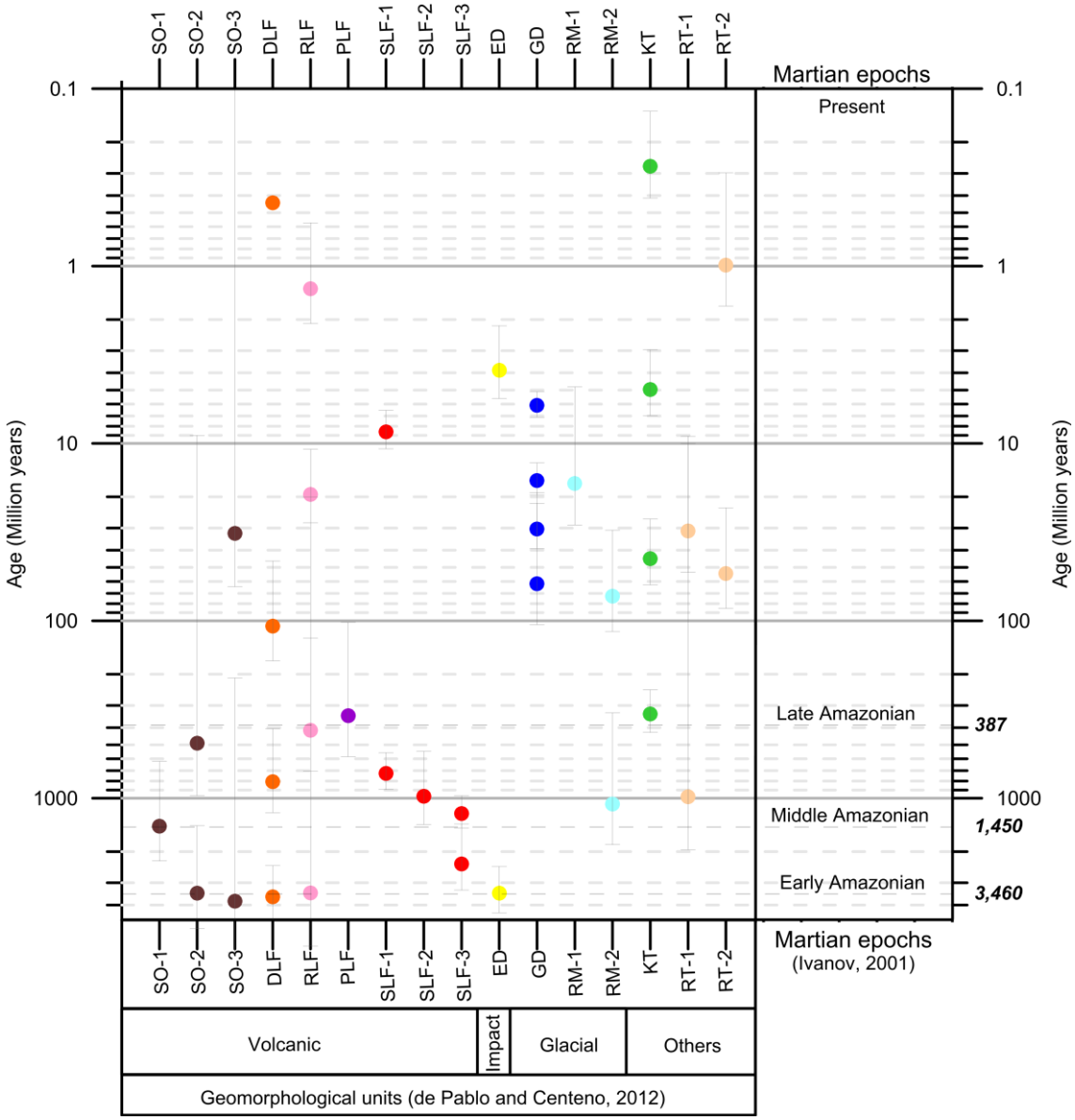

Figure 3.4: Summary of all ages obtained by the analyses of crater size–frequency distribution for the most important geomorphological units at the lower NW flank of Hecates Tholus volcano (Table 1), in the Ivanov (2001) and Hartmann and Neukum (2001) age system, as shown in Werner and Tanaka (2011) (see Figure 3.2). SO: Smooth outcrop unit; DLF: Dissected lava flow unit; RLF: Rough lava flow unit; PLF: Patterned lava flow unit; SLF: Smooth lava flow unit; ED: Ejecta deposits unit; GM: glacier deposits unit; RM: Roches moutonées unit; KT: knobby terrain unit; RT: Rough terrain unit (Table 3.1).

3.4. Discussion: volcanic and glacial evolution

3.4.1. Ages interpretation

The here derived ages for the geomorphological units forming the lower NW flank of the Hecates Tholus volcano ranges between 3.8 Ga and less than 1.0 Ma, marking a long evolution of this volcano, with at least some processes capable of flank resurfacing (Figure 3.3;

Figure 3.4). The ages we suggest are in general agreement with the ages proposed by other authors for the volcanic and glacial activity in this volcano (e.g., Neukum et al., 2004; Hauber et al., 2005; Werner, 2009; Robbins et al., 2011).

The older ages correspond to SO, DLF and RLF volcanic units, at 3.8 Ga, 3.6 Ga and 3.4 Ga respectively. These ages are in agreement with the origin of the volcanic edifice proposed by other authors and the volcanic activity in the Elysium rise (e.g., Tanaka et al., 2005; Werner, 2009; Platz and Michael, 2011; Robbins et al., 2011; Pasckert et al., 2012 and references therein) The SO unit located at the base of the volcano could represent outcrops of the older lava flows forming this volcano; meanwhile the RLF and DLF units could represent younger lava flows since they are located at the middle part of the flank. These date the origin of this volcano at least at 3.8 Ga, in Late Noachian (following the conversion of the Tanaka (1986) epoch boundaries using the Ivanov (2001) and Hartmann and Neukum (2001) chronology). The SO, DLF and RLF units also show other crater retention ages from 800 Ma to less than 1Ma (Figure 3.3; Figure 3.4), marking different events of resurfacing, which could include volcanic activity (e.g., Dohm et al., 2001; Anderson et al., 2001; Tanaka et al., 2003, 2005). The DLF area corresponds to the Fd unit mapped by Neukum et al. (2004), who obtained an age of 930 Ma, which, in our opinion, is comparable to the 800 Ma age we obtained for a resurfacing process.

Another volcanic unit in the area (in agreement with de Pablo and Centeno (2012) interpretation), the PLF unit, shows a younger age of about 340 Ma (Late Amazonian). This unit is located at the higher part of the studied volcanic flank, so the natural interpretation is to relate this unit to more recent lava flows from the volcanic caldera on the edifice summit. However, we could not exclude that this age, very different (early Late Amazonian) from the other volcanic units previously discussed (Late Noachian to Late Hesperian), could represent the end of a resurfacing process later than the time of the origin of this unit. CTX images of the surface of this mapped unit show that it is covered by fine-grained material with a complex morphology and a clear pattern, which could support this interpretation of an older origin for this unit with later resurfacing. In fact, this age is similar to the 335 Ma we obtain for the KT unit, and the age of 350 Ma obtained by Neukum et al. (2004), Hauber et al. (2005), and Werner (2009) for the same area, which they interpret to be pyroclastic material from a lateral volcanic eruption. Thus, we interpret the PLF unit to be an older unit, later covered by pyroclastic material during one or more explosive volcanic eruptions around 335–350 Ma.

On the other hand, the SLF unit, which represents the distal lava flows from the Elysium Mons volcano surrounding the base of the Hecates Tholus edifice (Tanaka et al., 1992,

2005), shows an age of about 2.3 Ga (Early Amazonian). This is slightly younger than the volcanic units forming the lower flank of the Hecates Tholus edifice (SO, DLF, and RLF units), which is in agreement with the age proposed for the volcanic activity in the Elysium Mons volcanic edifice and surrounding plains, between 3.4 Ga and 630 Ma (Dohm et al., 2001; Anderson et al., 2001, 2004; Tanaka et al., 2003, 2005; Pasckert et al., 2012 and references therein). On the other hand, the observation on the CTX images of the lava flows bordering the Hecates Tholus volcano support this relation between the ages.

In spite of this observation, the SLF unit has different ages depending on the studied sector (Table 3.2; Figure 3.3; Figure 3.4). Some sectors show younger ages of about 975 Ma (SLF-2) and 725 Ma (SLF-1), which is early to middle Middle Amazonian, but these ages are still inside the proposed limits for the volcanic activity on the Elysium Mons volcano (e.g., Werner, 2009; Pasckert et al., 2012). However, those lava flows are more distal than the older one (SLF-3). For that reason, in our opinion, these ages (on SLF-1 and SLF-2 sectors) could represent either the age of the lava flows' formation or the age of the end of resurfacing processes based on the DLF unit, which also shows an age of about 800 Ma for a resurfacing event (Table 3.2; Figure 3.3; Figure 3.4). In fact, SLF-3 also shows a resurfacing age, although somewhat older, of about 1.2 Ga, supporting the occurrence of different processes that could have modified the impact crater population on the unit over time.

Finally, the presence of possible secondary cratering (Figure 3.2) and the observed fine-grained mantle covering some parts of these plains could confirm this interpretation. The SLF unit forms the surrounding plains of the Hecates Tholus edifice but is separated from this volcano by the RT unit (Figure 3.2). The age of the RT unit ranges between 980 Ma (RT-1) and 54 Ma (RT-2). The geomorphological map of the area (de Pablo and Centeno, 2012) relates this unit to materials of different origins (including glacial, volcanic, and fluvial) later modified by different processes (fluvial, tectonics, etc.). The ages we obtained by the crater SFD analysis could support this interpretation since the age of RT-1 sector is similar to the age of the end of resurfacing event on the SLF-1 sector. Since this unit is nearest to the Hecates Tholus volcano, RT-1 and SLF-1 could be the same materials (lava flows), but later modified by different processes. Because the RT-1 sector is nearest to the base of the volcano, it could be later covered by other materials (including fluvial sediments, glacial deposits, pyroclastic materials, etc.), resulting in a younger age derived from the SFD. The age derived for SLF-2 of 975 Ma could confirm this interpretation.

A similar scenario could be applied to RT-2 sector, although its relation to the SLF-3 sector is not as clear. However, the age of 54 Ma is comparable to other resurfacing ages of other units in the area (such as the GD unit, with a resurfacing age of 62 Ma). For that reason, in our opinion, this unit only reflects ages of resurfacing events but not the formation age. In fact, sector RT-1 shows a similar resurfacing age of 31 Ma, as well as other units such as GD (62 Ma and 30 Ma), RM (72 Ma) or SO (32 Ma) units, which could support this scenario.

The last main unit on the flank of the volcano is the KT unit. Its SFD-derived age is about 335 Ma (early Late Amazonian). This age is comparable to that derived by Neukum et al. (2004), Hauber et al. (2005) and Werner (2009) by the use of HRSC and MOC images: about 300–350 Ma. Moreover, we obtained other ages of 45 Ma, 4.9 Ma and 270 ka that could be related to the end of different resurfacing events ages which could be the same processes or events that produced the resurfacing of GD unit, due to their comparable ages of 30 Ma and 6 Ma obtained in our crater SFD analyses and by Neukum et al. (2004) and Hauber et al. (2005). The geomorphological map of this area (de Pablo and Centeno, 2012) does not describe a possible origin of the KT geomorphological unit, although Hauber et al. (2005) interpret this unit such as pyroclastic material from a volcanic explosion in the NW flank of the Hecates Tholus. They favor a volcanic origin of the smaller and higher depression located in this flank of the volcano (named depression A in Hauber et al., 2005) based on geomorphological, stratigraphical and topographical evidence (Mouginis-Mark et al., 1982; Hauber et al., 2005). However, the surface of this unit is composed of complex chaotic blocks and some linear or streamlined or elongated forms, which could be caused by different processes including episodic runoff, which itself may be caused by melting of snowpacks on the volcano summit (Carr and Head, 2003; Fassett and Head, 2006, 2007, 2008). This would beconsistent with the resurfacing ages we obtained.

Depression A and the other (extensive) depression on this flank (Figure 3.1) of the volcano (named depression B in Hauber et al., 2005) are filled by the GD unit. This unit was interpreted to be different types of glacial deposits by Neukum et al. (2004), Hauber et al. (2005) and de Pablo and Centeno (2012). We obtained an age of 60 Ma for this unit. This age is comparable to the age obtained by Neukum et al. (2004) for some sectors of this depression: 50 Ma. We also obtained ages of the end of resurfacing events at 30 Ma, 16 Ma, and 6.0 Ma (early to middle Late Amazonian) (Table 3.2; Figure 3.4; Appendix A.1.). These ages are in agreement with the ages obtained by Hauber et al. (2005) based on crater counting on HRSC and MOC images: 95 Ma, 25 Ma, 15 Ma, and 5.0 Ma. The older age obtained by Hauber et al.

(2005) is comparable to that obtained by Neukum et al. (2004) for some sectors of the same materials filling the depression. These multiple ages of resurfacing are compatible with the ''multiple successive stages of advance and retreat'' during the Late Amazonian epoch proposed by Fastook et al. (2008) for the cold-related environments.

Although no hypothesis about the origin of depression B is provided, the three research teams interpret the materials filling depression A and depression B to be possible glacial deposits, including moraines, meltwater channels, drumlins, proglacial braided outwash plains, etc. (Neukum et al., 2004; Hauber et al., 2005; de Pablo and Centeno, 2012). Some of their described features are also in agreement with the morphologies recently described by different authors to be glacial features on other regions of Mars (e.g., Whalley and Azizi, 2003; Head et al., 2005, 2006a,b; Morgan et al., 2009; Pedersen and Head, 2010; Fassett et al., 2010). In fact, the RM unit was also interpreted to be a glacial-related feature (roche moutonnée) by de Pablo and Centeno (2012), and we obtained a wide range of ages for this unit. The older age we obtained, 1.0 Ga (on sector RM-2) (Middle Amazonian), could reflect the age of the origin of these materials, meanwhile the younger ages of 73 Ma (RM-2) and 17 (RM-1) (middle Late Amazonian) are in agreement with the ages we obtained for the GD unit confirming both units were affected by the same process in the same epoch. The older age could be comparable, in our opinion, with the age of other volcanic units we previously discussed, such as the SO and DLF units. The geographic location of the RM unit at the edge of depression B and the base of the volcano (Figure 3.2) allows us to interpret that those materials are the old volcanic materials forming Hecates Tholus, later sculpted by glaciers that could fill and flood over the NW edge of depression B. Glacial landforms (such as eskers) mapped on the area (de Pablo and Centeno, 2012), and the ages we obtained for sector RT-1 outside depression B of 30 Ma agree with this hypothesis and the ages we obtained for GD and RM units. Moreover, the old age of 1.0 Ga returned by sector RM-2 is also compatible with the existence of old episodes of glacial activity, as old as Late Noachian, such as proposed by Clifford and Parker (2001) to occur in equatorial latitudes of Mars.

Finally, we paid attention to one ejecta deposit (ED unit), located at the SW of the study area, because it is the most extensive ejecta deposit in the mapped area and its location at the edge of depression B could help to date the formation of this depression, which has not been done before. The ages we obtained for the ED unit are 3.4 Ga (Early Amazonian), and 3.9 Ma (Late Amazonian). Thus, the ejecta deposit is as old as the Hecates Tholus volcano, but still slightly younger than the SO, DLF and RLF units, interpreted to be the volcanic materials

forming the edifice. The ejecta deposit returns an age older than the lava flows surrounding the edifice (SLF unit), but a visual analysis of CTX images and HRSC-derived DTM did not allow us to establish clear cross-cutting relationships between them.

Assuming an age of 3.4 Ga for the ejecta deposit, and consequently, for the associated impact crater, the age of the main depression in this flank of the volcano (depression B), should be greater, because the images show how the impact crater structure cuts the southern wall of the depression (Figure 3.1). Ejecta deposits from this impact crater were not recognized on CTX images inside depression B, because, if this deposit existed, it was later modified, buried or eroded by other processes, including those forming the possible glacial deposits forming the GD unit. Thus, depression B should have formed after 3.8 Ga, which is the age of the exposed outcrops forming the SO unit inside the depression (sector SO-2), but also after 3.6 Ga, which is the age of the DLF unit that forms the NE edge of depression B, and before 3.4 Ga which is the age of the ejecta deposit forming the ED unit. If this deduced chronology is correct, depression B could have formed between 3.6 and 3.4 Ga ago, before depression A was formed. Another scenario in which both depressions formed at approximately the same time is not possible from our point of view, because in this case, the edge of both depressions should be as intricate as that of depression B, due to the fluvial and glacial processes (e.g., Mouginis-Mark et al., 1982, 1984; Neukum et al., 2004; Hauber et al., 2005; Fassett and Head, 2006). Nevertheless, Werner (2009) postulates that depression B is younger than depression A, although evidence was not provided or cited.

In any case, we cannot approach the possible origin of depression B, which could include volcanic explosive activity (e.g., Mouginis- Mark et al., 1981, 1982; Walter and Troll, 2001; Greeley et al., 2005; Hauber et al., 2005), landslides on the flank of the volcano (e.g., Dingle, 1977; Oehler et al., 2005; Vanneste et al., 2006; Neuffer and Schultz, 2006), volcano deformation and instability (e.g., Thomas et al., 1990; van Wyk de Vries et al., 2000; López and Williams, 1993; McGuire et al., 1996; van Wyk de Vries and Matela, 1998; Reid et al., 2001; Lundgren et al., 2003; Neri and Acocella, 2006), hydrothermal activity (e.g., López and Williams, 1993; Russell and Head, 2003) volcano–ice interactions (e.g., Mouginis-Mark, 1984, 1985; Smellie and Chapman, 2002; Russell and Head, 2007), etc., such as discussed by de Pablo (2009). All those scenarios in which water could have played an important role are possible taking into account the fact that this volcano grew at the coast of the Oceanus Borealis watersheet or icesheet (e.g., Parker et al., 1993; Chapman, 1994; Clifford and Parker, 2001; Fairén et al., 2003; Head and Wilson, 2007), the important role of magma–water interactions

described in the surrounding area, such as is the case for the Galaxias Chaos chaotic terrain (e.g., Mouginis-Mark, 1984, 1985; de Hon et al., 1999; Russell and Head, 2007; Pedersen and Head, 2011), among other processes related to the volcano structure, evolution and hydrothermal characteristics.

Other geomorphological features also provide key information to sequence the formation of the depressions: the valleys on the flank of the volcano (Mouginis-Mark et al., 1982, 1984; Mouginis-Mark, 1985; Gulick and Baker, 1989, 1990; Hauber et al., 2005; Fassett and Head, 2006). These channels radial to the volcano summit have ages consistent with Late Hesperian (Plescia, 2000, 2001; Fassett and Head, 2006, 2007), and different origins have been proposed for them, including: fluvial (Mouginis-Mark et al., 1992; Gulick and Baker, 1989, 1990; Hauber et al., 2005), pyroclastic flows (Mouginis-Mark et al., 1982), lava flows (Williams et al., 2005), or geothermal melting of snow packs (Gulick et al., 1997; Zent, 1999; Gulick, 2001; Shean et al., 2005; Fassett and Head, 2006). Since snow/ice could have been present at middle and equatorial latitudes as early as Late Noachian (Clifford and Parker, 2001; Head et al., 2005), and the geothermal activity could also cause the formation of channels on the flanks of the volcano in a cold and dry climate (e.g., Gulick, 1998; Carr and Head, 2003; Fassett and Head, 2006), we believe that those channels could be very old, especially if we take into account their variable engagement, probably due to the modifications on the volcano (e.g., Fassett and Head, 2006; Byrne et al., 2009a,b). In any case, the enlargement of some of those channels leading to depression B has been related to glacial processes in more recent times (Hauber et al., 2005). They also observed (1) two different valley directions, one of them (set A on Hauber et al. (2005)) related to fluvial activity prior to depression B's formation because their paths are not modified or relatively far from its edge (unmodified channels in Figure 3.5), and the other (set B on Hauber et al. (2005)) related to path modification toward this depression (modified channels in Figure 3.5); and (2) how some valleys to the east of depression B are cut by this depression (cut channels in Figure 3.5). Additionally, we also observed how some of those channels located near the northern edge of depression B do not have heads (headless channels in Fig. 4), because the valleys are cut by the depression. Finally, other channels have enlarged valleys (enlarged channels in Figure 3.5). Those observations point to depression B not forming prior to the volcano's growth, but sometime during the evolution of the edifice, such as we interpreted previously based on the ages we obtained by crater SFD analysis. Hauber et al. (2005) propose that those channels had a fluvial origin with continual activity, in contrast to the snowpack melting origin and episodic activity proposed by

Fassett and Head (2006). Then, it is not possible to date the origin of this depression by their observations, but our proposal of an age of 3.6–3.4 Ga (such as we discussed previously) is compatible with both models and their geomorphological observations.

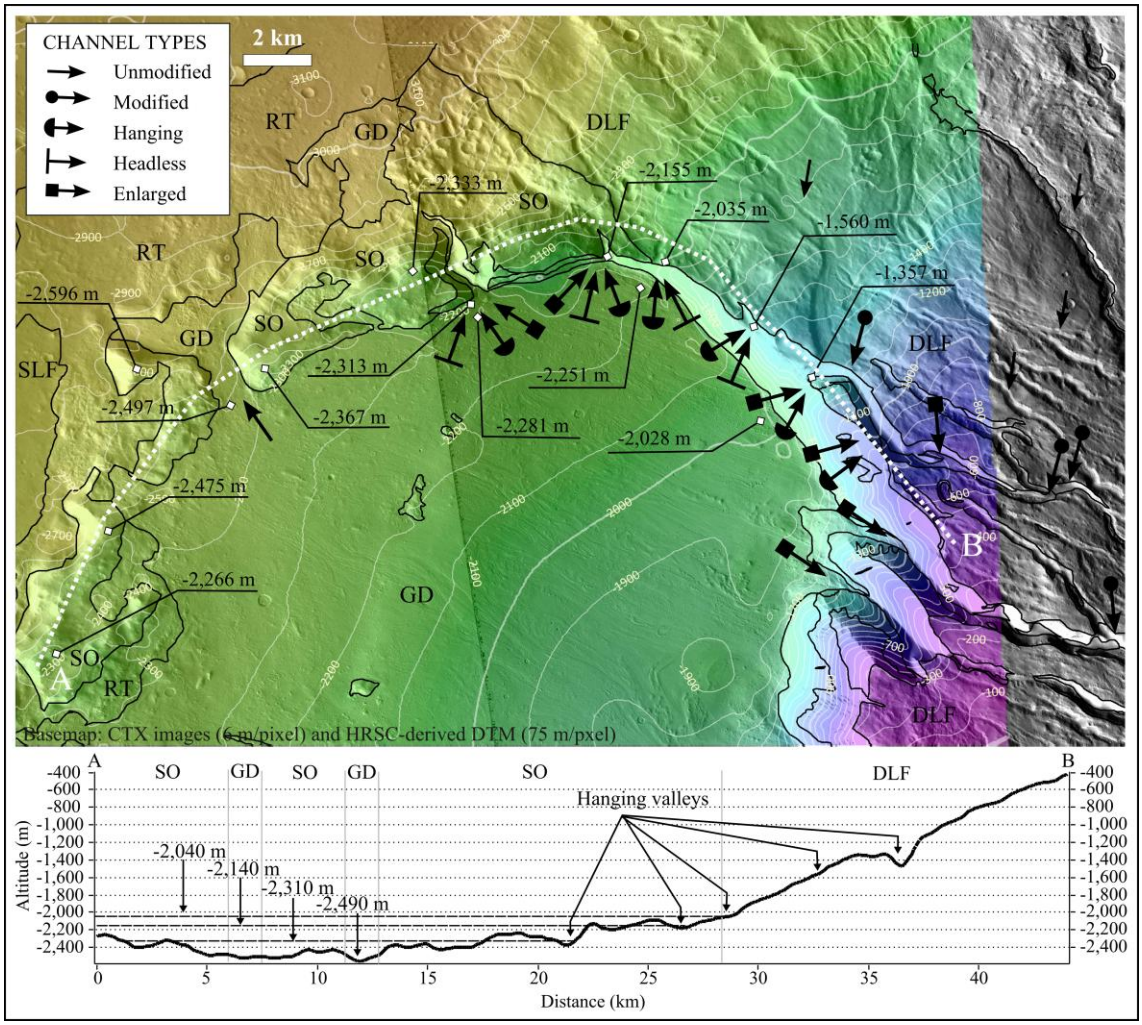

Fig. 3.5: CTX mosaic of the northern sector of the study area showing the limits of the main geomorphological units, and the HRSC-derived topographic contour lines (equidistance 100 m). Arrows marks examples of the different channels types discussed in the text: unmodified, modified, headless, enlarged and hanging. White squares mark some altitudes representative of the outcrops, valleys floors and depression B floor. A topographic profile along the edge of depression B (white dotted curve) is represented below, marking the position of the hanging valleys what marks the higher levels (~2040 m, ~2140 m, ~2310 m, and ~2490 m) of a possible ancient glacier through time, supporting the interpretation of an extensive and long-lasting glacier filling depression B, such as deduced by the ages obtained by crater SFD.

Hauber et al. (2005) proposed the glacial-related process overflood of the NW edge of depression B. The geomorphological map of the area from de Pablo and Centeno (2012) confirms it by the RT unit and the eskers they mapped in it, extending the glaciers' presence outside the depression covering the lava flows surrounding the volcanic edifice not later than 31 Ma ago, which is the resurfacing age of this area (sector RT-1). 30 Ma is also the age of one of the resurfacing events of the GD unit filling depressions A and B, and 32 Ma the resurfacing

age of some outcrops of the SO unit (sector SO-3). We could deduce from these ages that the maximum extent of the glaciers in this area filling depressions A and B started to reduce at 32 Ma, exposing to the atmosphere a 3.8 Ga old surface (sector SO-3), forming a nunatak-like relief. Related to this event, a retreat of the glacier front leaving a rugged terrain outside the depression (sector RT-1) and exposing eskers should also occur. However, this is probably not the first reduction of the ice sheet to have occurred in this area, since the RM unit formed by glacier erosion and was later exposed probably about 73 Ma ago (sector RM-2), after the glacier stabilization at about 62 Ma, the age of the GD unit. The age we obtain by SFD analysis of the KT unit of 45 Ma could also be related to glacial activity, as well as the age of about 5 Ma, similar to the resurfacing age of 6 Ma of the GD unit. On the other hand, sector RM-1 also returns an age of about 17 Ma, marking a more recent glacier retreat, in agreement with a younger age of the GD Unit of about 16 Ma. So, advances and retreats of the glaciers could be episodic or continuous, but exposing outcrops at different sites at different times.

We found other evidence of glacial evolution in the area. Those valleys at the northwestern edge of depression B are deep, similar to those proposed by Hauber et al. (2005) to have been excavated by ice-related processes on the eastern edge of the same depression. However, these valleys at the north and northeast edge do not have a head because depression B cut the valley upslope (headless channels in Figure 3.5). Moreover, they are disconnected in altitude from the floor of the depression, forming hanging valleys (Figure 3.5). Those hanging valleys increase in width, depth and altitude from the NW to W edges pointing, in our opinion, to a long-acting glacial erosion. The extreme case is the first gap between the SO unit (immediately to the southeast of sector SO-1 studied here; white arrow in Figure 3.5) showing how one of these valleys (still filled by glacial deposits forming the GD unit), cut the edge of depression B. These characteristics could only be explained, from our point of view, if the glacier surface had a higher altitude in the past, at least as high as ~2035 m (on H1262_0000 HRSC-derived DEM), which is the altitude of the floor of the northern valley of those described, meanwhile the floor of the depression in this area is about ~2150 m. This altitude is slightly higher than the altitude of some of the outcrops of the SO Unit at the northwestern edge of the depression (about ~2400 m), as well as those outcrops interpreted to be roches moutonnées (de Pablo and Centeno, 2012). The smooth surface of those SO unit outcrops, the presence of roches moutonnées, and the diminishing altitude of the possible glacial valleys allow us to interpret the existence of an extensive and deep ice deposit filling this depression, which reduced its thickness (and extent) over time. This reduction of the ice

deposit thickness (or altitude) could be the cause of the enlargement of those valleys located to the east of the depression (until their floor reached the floor of the depression), and the formation of hanging valleys at the northern edge of depression B. We believe that these hanging valleys reflect: (i) an significant glacial erosion earlier than that reflected by the GD unit age (60 Ma), and (ii) the depression formed relatively early, more recently than depression A itself. The altitude of the hanging valleys could indicate the altitude of the surface of the possible glacier filling depression B, from ~2040 m to ~2490 m (Figure 3.5) to the NW of the glacier. Roches moutonnées (RM unit) and smooth outcrops (SO unit) remain below those levels, supporting the idea of the glacier as the agent eroding and polishing these terrains.

Thus, older glacial activity seems to be the more feasible scenario. The ages of 1.4 Ga (SO-1 unit), 980 Ma, and 800 Ma (DLF unit) may be related to those earlier glacial events, which could have been as recent as 490 Ma, the younger age we obtained for the SO unit (sector SO-2). However, we do not have enough evidence of the relation between those ages and the presence of an extensive and/or thick ice deposit filling depression B and its later disappearance. We neither have evidence to decide between the existence of a thick ice deposit which disappeared over time, or a very dynamic thin ice layer which continuously excavated the depression to what is observed at the present time, removing the material from the flank of Hecates Tholus volcano toward the northern plains on Utopia Planitia. However, an approximate and speculative model of the most important events in the evolution of this flank of the volcano is summarized in Figure 3.6.

This model is consistent with the degradational processes occurring over time on the flanks of volcanoes on Iceland and in Siberia, widely used as terrestrial analogs of some martian features (e.g., Chapman and Smellie, 2007, and references therein; Komatsu et al., 2007). Tuyas, subglacial mounts or tindar (e.g., Hickson, 2000), should have steep slopes due to their origin under an ice sheet, which facilitates their degradation before the deglaciation. Failure of steep slopes, gully formation (caused by both stream runoff and debris flows), and modification by rock glaciers are some of the processes occurring when the ice sheet disappears (Chapman and Smellie, 2007; Komatsu et al., 2007). The slopes of both depressions are steep but they show different degradational states. The northwest-facing slopes are strongly dissected by valleys. Moreover, the higher regions of the slopes show gullies that could be related to both surficial runoff related to snowpack melting and groundwater seepage related to the impermeable volcanic layers of the volcano. In fact, the former could also explain the texture we previously described on the KT unit, such as a possible pyroclastic

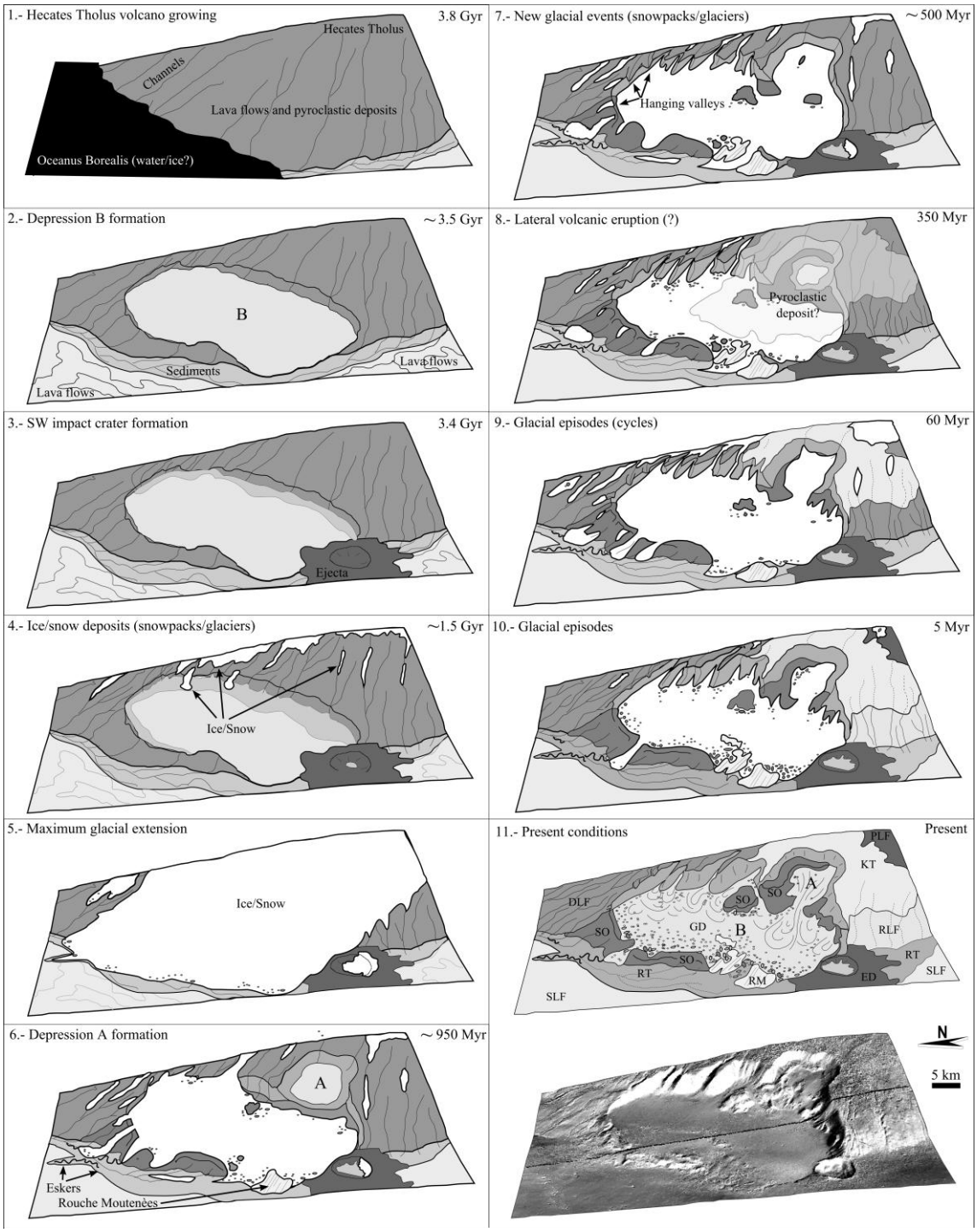

Fig. 3.6: Schematic evolutionary model of the lower NW flank of the Hecates Tholus volcano based on the ages derived from crater SFD analysis of the different geomorphological units of this area (de Pablo and Centeno, 2012). Only the most important events are shown, and the approximate ages of some of them reflected. Other multiple episodes of advance and retreat of glacier have been deduced in the text, but they are not included in this schematic model for simplicity (vertical exaggeration of the model: x2).

deposit later modified and eroded by runoff processes. However, not all the slopes of the depression are characterized by gullies, and the lower parts of the slopes are covered by fine-grained materials, possibly produced by mass wasting. These observations agree with the

different episodes of disappearance of the ice sheet filling the depression on the flank of the volcano: the more degraded slopes of the southeast are caused by longer glacier (and mass wasting) activity, while the other slopes remained under the ice sheet. When the ice sheet reduced, it exposed the slopes of the other sectors of the depressions, initiating their degradation in a similar way as was described for the different tuya in the Azas Plateau, Russia, where the longer exposed edifices show more degradation of their slopes (Komatsu et al., 2007). Our proposed model (Figure 3.6) combines the ages obtained with the crater SFD analysis, the interpreted glacial episodes along the geological history of the area, and the geomorphological observations of the images and the geomorphological map of this region of Mars (de Pablo and Centeno, 2012).

A recent ice age has been proposed to have occurred on Mars between 2.1 and 0.4 Ma (Head et al., 2003), based on stratigraphical analysis of satellite images and planetary obliquity change models, and supported by recent works (e.g., Mustard et al., 2001; Laskar et al., 2004; Aharonson and Schorghofer, 2006; Schorghofer, 2007, 2010; Byrne et al., 2009a,b; Schon et al., 2009; Schorghofer and Forget, 2012). We obtained ages in this range on the DLF unit (0.44 Ma), RT unit (1 Ma on RT-2 Sector) and RLF unit (1.3 Ma). The DLF unit is characterized by a fine grained dust-mantled surface, and the glacial deposits (GD unit) have been mapped inside some of the valleys dissecting this terrain (de Pablo and Centeno, 2012), so they could be related to this event, although detailed analysis on HiRISE images should be carried out to confirm this idea, which we are not confident to apply to RLF and RT units.

Recent volcanic activity, as recent as 100 Ma, has been also proposed on Hecates Tholus (Neukum et al., 2004; Hauber et al., 2005; Werner, 2009; Robbins et al., 2011) based on crater counting on the complex caldera. The single age we obtained around this magnitude is also present on the DLF unit (100 Ma), but we could not indisputably assign this age to the volcanic event because the DLF unit is clearly dissected by channels and not by lava flows. So the presence of fine-grained material covering the surface of this unit made it feasible to relate this deposit (and age) to the deposition of pyroclastic material covering only this flank of the volcano. We believe that only a NW oriented pyroclastic cloud could produce the sedimentation on this sector of the studied area and not in the nearer ones. However, wind direction analysis (e.g., Neakrase et al., 2005), pyroclastic cloud evolution analyses (e.g., Kerber et al., 2011, 2012) and geological studies and mapping of the whole volcano should be carried out to study and to test this scenario.

3.4.2. Volcanic and glacial evolution

After the interpretation of the SFD-derived ages of the different analyzed geomorphological units, we could derive a summarized proposed evolution of the main events that occurred on the lower flank of the volcano (Figure 3.6).

The main construction of Elysium Mons was established at least 3.6 Ga ago, but more recent activity on its flanks occurred through time until about 100 Ma ago (Hauber et al., 2005; Werner, 2009; Pasckert et al., 2012). Our SFD-derived ages allow us to determine that the construction of the Hecates Tholus volcanic edifice occurred between 3.8 and 3.4 Ga, in agreement with those authors. The volcanic activity in the Elysium Mons area produced long lava flows that bordered the Hecates Tholus volcano (SLF unit), in agreement with other authors (e.g., Mouginis-Mark et al., 1982, 1984; Mouginis-Mark, 1985; Tanaka et al., 1992, 2005; Pasckert et al., 2012). A radial channel network started to dissect the flanks of the volcano during the volcanic edifice growth (DLF unit). Although a volcanic origin could not be discarded for some channels (e.g., Williams et al., 2005), this network could have had a fluvial origin (e.g., Mouginis-Mark et al., 1982), although glacialrelated processes could have episodically contributed to the valley enlargement due to melting of ice caps or snowpacks on the volcano summit (e.g., Fassett and Head, 2006). Although in general the channels on the flanks of the volcanoes are dated as Hesperian (e.g., Gulick et al., 1997; Carr, 1996, 2006), fluvial activity on the flanks of Hecates Tholus could have occurred on the volcano from its earliest volcanic episodes, because their existence does not require a warm and wet climate (see Gulick et al., 1997; Gulick, 1998, 2001; Zent, 1999; Carr and Head, 2003; Fassett and Head, 2006, among others). In fact, snow/ice could also have been stable at low latitudes during the Late Noachian (Clifford and Parker, 2001).

Depression B on the NW flank of the edifice could have formed between 3.6 Ga and 3.4 Ga, according to the geomorphological and crater counting evidence. We cannot establish the process forming this depression, which may have included landslides or lateral explosive eruptions, among other processes we discussed previously. A detailed study is needed to complete this part of the geological history of this volcano. The location of Hecates Tholus on the northern edge of the Elysium rise, where the proposed paleoshorelines of the Oceanus Borealis (Contacts 3–5 from Fairén et al., 2003 and references therein) were also located (e.g., Chapman, 1994; Clifford and Parker, 2001; Fairén et al., 2003; Head and Wilson, 2007). In any case, we presented evidence of how this depression dissected the previously existing channels,

which produced a change of their paths as well as an increase of the erosive processes in some channels at the eastern edge of the depression resulting in their enlargement (an idea already pointed out by Hauber et al. (2005)). The process forming this depression exposed some of the old lava flows, from that moment forming outcrops (SO unit), later modified by other processes including glacial activity, such as we discussed based on geomorphological and crater counting evidence. Some of these outcrops are very smooth, possibly due to glacial abrasion at 1.4 Ga. Then, the glacial activity in the area could have extended from before 1.4 Ga to, at least, 6 Ma, such as deduced from glacial-related materials filling depression B and depression A (GD unit), and the ages of resurfacing we derived for different units in the area. We find that the GD unit had possible glacial-related events at 60 Ma, 30 Ma, 16 Ma and 6 Ma, in agreement with other authors (e.g., Hauber et al., 2005), and supported by the idea that changes in obliquity could favor the presence of snow/ice at low latitudes (e.g., Richardson and Wilson, 2002; Mischna et al., 2003; Head et al., 2005) and accumulated on the NW flanks of some volcanoes (e.g., Gulick et al., 1997; Haberle et al., 2004). Other geomorphological units in the area also reflect some of these ages, such as the RM, RT, KT, or SO units, implying that glacial processes had an important role in the area, not only for the GD unit formation, but in the resurfacing of other terrains in the area. In fact, we propose that glacial processes had an important role in the enlargement of, at least, depression B based on the analysis of resulting ages, as well as on geomorphological evidence (related to the channels dissected by the depression), although a more detailed analysis should be done to confirm and quantify it. On the other hand, these glacial-related materials (GD unit) also fill depression A. We were not able to date the origin of this smaller depression, but Neukum et al. (2004) and Hauber et al. (2005) propose an explosive volcanic eruption for the origin of the depression, forming a pyroclastic deposit surrounding it (the KT unit). The age of this putative volcanic event is 350 Ma (Neukum et al., 2004; Hauber et al., 2005), although we cannot exclude that depression A formed earlier and by a different process. No evident younger volcanic activity has been observed on the lower NW flank of Hecates Tholus after 3.4 Ga, except this possible lateral volcanic explosion, although we cannot exclude that some channels on the flank could be episodically active due to snowpack melting caused by hydrothermal activity on the volcano (Fassett and Head, 2006). However, other authors dated the Hecates Tholus caldera floors and established the occurrence of volcanic activity at 2.6 Ga, 1.0 Ga., and 200 Ma (Werner, 2009; Robbins et al., 2011). Thus, it is possible that some of the ages marking the end of resurfacing events on the DLF unit (800 Ma, and 110 Ma), RLF (415 Ma) or PLF unit (340 Ma) could be related to other pyroclastic eruptions that covered the surface of the flank.

3.4.3. Ice stability

The important role of ice in the presented evolution for this flank of the Hecates Tholus volcano, producing resurfacing and the formation of some materials, requires a transiently present but significant amount of ice.

In the present day, ice is unstable at the surface at middle latitudes. In fact, we did not observe ice (or dusty ice) on CTX images of the studied area, but glacial-related features, similar to those described by other authors in different regions of Mars, and based on terrestrial analogs (e.g., Richardson and Wilson, 2002; Head et al., 2003; Head and Marchant, 2003; Mischna et al., 2003; Shean et al., 2005). If we take into account that the surface temperature drops quickly with depth, it is possible to have stable relict ice at only a few centimeters under the surface (e.g., Mellon and Jakosky, 1995), and the presence of ice detected by different sensors on board several orbiters seems to confirm this, not only including ice emplaced by diffusion (Mellon et al., 2008) but also primary deposition of snow and ice (Head et al., 2003, 2005). Thus it is still possible that ice is present under the surface, mainly related to the glacial-related deposits (GD unit). In fact, de Pablo and Centeno (2012) mapped some pingos in depression B, evidence of the presence of ice layers inside the sediments forming the GD unit. This presence of ice under the surface of depression B in the present day has also been supported by recent thermal models based on surface properties (Helbert et al., 2005). This model reveals that the existence of residual ice from the glacial activity during the last high obliquity period of 5–10 Ma ago at 1–2 m below the surface is possible, corresponding with the ages we obtained for different geomorphological units in the flank of the Hecates Tholus volcano. Helbert et al. (2005) indicate that small increases in original ice content in the materials could result in a deeper ice table. This model confirms the analysis of the remote sensing data (e.g., Feldman et al., 2002; Mitrofanov et al., 2002), and the observations in high resolution images of the surrounding plains (Byrne et al., 2009a,b).

Thus, if these ice tables or lenses exist, they could be extensive in area, as extensive perhaps as the GD unit, probably relict from long lived glaciers existing in the area such as those revealed in our study. The post-Noachian ice evolution summarized by Carr and Head (2010) provides the key to establish the possible presence of ice in the NWflank of the Hecates Tholus volcano. The presence of ice lenses in the area is consistent with models that propose that ice is stable at latitudes of 30–55□ forming surficial ice-rich mantles (Mustard et al., 2001; Carr, 2001) in recent times (Head et al., 2003), capable of forming glaciers when they have

enough thickness (Milliken et al., 2003) or even to be the water source for gullies (Christensen, 2003). If this occurred in the present time with an ice-rich dust mantle, it is feasible, in our opinion that it also occurred in the past. The general atmospheric circulation models show the NW flanks of the martian volcanoes are a preferred site for precipitation of ice (Forget et al., 2006; Fastook et al., 2008) not only in recent high obliquity periods (Laskar et al., 2004; Head et al., 2003), but also at earlier times, as early as Late Hesperian at mid latitudes of the planet (Head et al., 2004; Morgan et al., 2009), which agrees with the ages we obtained from our crater SFD analyses and the interpretation presented here.

Thus, although an ice layer under the surface, a relict of old ice sheets and glaciers, at least filling the depressions and some valleys of the flank, could be stable, further and detailed studies based on ground penetrating radar data from Mars Express and Mars Reconnaissance Orbiter missions should be carried out to confirm the presence of a debris-covered glacier on the lower NW flank of Hecates Tholus volcano.

3.5. Conclusions

The SFD analyses here presented are the most detailed and extensive of the terrains forming the lower NW flank of Hecates Tholus volcano, and they confirm the general ages provided by the analyses previously done by other authors (Neukum et al., 2004; Hauber et al., 2005; Werner, 2009; Robbins et al., 2011).

The crater SFD-derived ages based on CTX images allowed us to derive the probable volcanic and glacial evolution of the lower NW flank of the Hecates Tholus volcano. On the one hand, volcanic activity was more important during the Late Noachian–Hesperian forming the volcanic edifice between 3.8 and 3.4 Ga, although later events could be as recent as 350 Ma in this sector of the edifice. The analysis of our results and the geomorphological analysis of the CTX images do not allow us to derive any other clear volcanic activity in the area forming new terrains (lava flows, pyroclastic deposits, etc.), although this does not exclude other volcanic-related activity (e.g., hydrothermal activity) which could mantle the study area or selected sectors.

On the other hand, glacial activity had an important role in the resurfacing of the volcano flanks at relatively early times, as far back as 1.4 Ga, and the younger events could have occurred 60 Ma, 30 Ma, 16 Ma and 6 Ma ago, although other intermediate events could not be excluded at about 980 Ma, 800 Ma, 500 Ma, 415 Ma, 340 Ma, or 110 Ma ago. We also obtained ages of resurfacing events of 1.3 Ma, 1 Ma, and 0.44 Ma which could be related to

glacial activity during the last ice age of Mars (Head et al., 2003). However, we could not determine if these glacial events occurred thanks to long-lasting glacial systems (ice sheet and glacier tongues) or episodic events of ice accumulation and flow, although we support the first scenario that is compatible with episodic snowpack melting due to hydrothermal activity on the volcano. This long-lasting glacial activity could have formed an extensive and very dynamic glacier that produced erosion and polishing of the outcrops forming smooth outcrops, roches moutonnées (de Pablo and Centeno, 2012) and hanging valleys. We deduced from the topography that the glacier level at the edge of the depression B could vary from ~2035 m to ~2490 m in altitude during its retreat. This glacier could also have produced the enlargement of some fluvial valleys (as was already pointed out by Hauber et al. (2005)), the abrasion of outcrops of old basal volcanic materials of the edifice, and the resurfacing of different terrains in the flank of the volcano as well those as bordering it. We also propose that a thick and dynamic ice sheet filled the depressions of this flank of the volcano, and the glacial-related processes caused their enlargement.

Thanks to the crater SFD analyses we were able to establish a feasible sequence of the most important geological events occurring in this flank of the Hecates Tholus volcano.

PhD thesis

Glacial geomorphology of the NW flank of the Hecates Tholus volcano, Mars

4

Geomorphology and morphometry

Miguel Ángel de Pablo Hernández

2015

Abstract:

The analysis of HiRISE, MOC, CTX and HRSC images allowed to provide a detailed description and interpretation of the 18 different geomorphological units what were mapped by de Pablo and Centeno (2012) on CTX images of the lower NW flank of the Hecates Tholus volcano, as well as to briefly describe the wide variety of geomorphological landforms they mapped, but also others visible only on HiRISE images. Different morphometrical analyses have been also conducted, in order to derive slope, aspect, curvature, rudgeness, catchment slope and area, solar anisotropical diurnal heating and protection index, based on the use of a HRSC-derived DTM. All those observation and analyses, together with topographic sections made possible to distinguish between till deposits and debris-covered glaciers, what could still remain relict with about 100 m in thickness from the original 600 m. Those glaciers could have temperate thermal regime in agreement with the different geomorphological landforms observed, with a behavior similar to the Patagonian-Antarctic model. Nowadays, some quantities of ice could still remain in the near surface mantle deposits due to the creeping landforms observed at the south-facing slopes.

Resumen:

El análisis de imágenes HiRISE, MOC, CTX y HRSC a pemitido la descripción detallada de las 18 unidades gemorfológicas que fueron definidas y cartografiadas por de Pablo y Centeno (2012). Además se describen los elementos geomorfológicos, tanto los cartografiados por estos autores en las imágenes CTX, como otros visibles en las imágenes HiRISE de la ladera Noroeste del volcán Hecates Tholus. En este trabajo también se han realizado diversos análisis morfométricos cuantificando pendientes, orientaciones, curvatura, rugosidad, pendiente y área de la red de drenaje, el calentamiento anisotrópico diurno de la superficie y el índice de protección, mediante el uso de un modelo digital de elevaciones derivados de las imágenes HRSC. Estas observaciones y análisis han permitido, junto con perfiles topográficos, distinguir entre depósitos de till y glaciares relictos cubiertos de derrubios, que podrían aún tener hasta 100 m de espesor de los 600 m aproximados en este trabajo. Estos glaciares pudieron tener un regimen térmico cálido, de acuerdo a los rasgos geomorfológicos observados, y haber evolucionado de acuerdo a un modelo Patagónico-Antártico. En la actualidad, en la zona podrían quedar además ciertas cantidades de hielo subsuperficial en los sedimentos que cubren las laderas, debido a la presencia de formas típicas de los procesos de reptación, principalmente en las laderas de orientación Sur.

Related publications:

de Pablo, M.A. and Centeno, J.D. 2011. New observations of glacial features on the lower NW flank of Hecates Tholus Volcano (Mars) based on CTX and HiRISE images. Lunar and Planetary Science Conference, 42. Abstract #1030.

4.1. Introduction

Glaciers existence on Mars led a decades-long discussion by the scientific community (e.g., Zimbelman and Edgett, 1992; Shean et al., 2005; Carr, 2006; among others), mainly due to the absence of clean, evident and visible ice deposits outside the polar caps. In spite of that, many features have been described and interpreted to be caused by glacial activity, in particular on the main volcanoes of the planet at the Tharsis volcanic province (e.g., Williams, 1978; Lucchita, 1981; Zimbelman and Edgett, 1992; Head and Marchant, 2003; Shean et al., 2005, 2007; Milkovich et al., 2006; Kadish et al., 2008).

Thanks to the use of the higher resolution images provided by the last missions sent to Mars (Mars Global Surveyor, Mars Odyssey, Mars Express, and Mars Reconnaissance Orbiter), the existence of non-polar glaciers on Mars on recent times is widely accepted, after the location all around the planet of many features related to possible glacial activity. In fact, the study of glacial features quickly evolved to the point that a guide to identify them on high resolution images has been published (Head et al., 2010) aiming to expand our knowledge about the role of ice in the history of the planet.

Their abundance on the flanks of the Martian volcanoes, as well as the existence of ice deposits at different latitudes (e.g., Head et al., 2006a, 2006b; Head et al., 2010) was the key to reconstruct the ice ages of Mars, probably caused by orbital, atmospheric and/or volcanic processes (e.g., Fastook et al., 2008; Laskar et al., 2002, 2004; Wilson and Head, 2008). In fact, these proposed glaciations of Mars could be as recent as 2.1–0.4 Ma during the Late Amazonian period (e.g., Carr and Head, 2010; Fassett, et al., 2010; Head et al., 2003). As we explained above, the glacial features have been widely studied on the flanks of the main volcanoes of Tharsis volcanic province. In the case of the Elysium volcanic region, glacial features have been only described on the flanks of Hecates Tholus shield volcano (e.g., Neukum et al., 2004; Hauber et al., 2005; Helbert et al., 2005; Fassett and Head, 2006, 2007) (Figure 4.1). Although magma, water and ice interactions have been proposed to explain many features observed in the Elysium volcanic area and surrounding plains, including sub-glacial volcanoes, mobergs, or chaotic terrains (e.g., Mouginis-Mark et al., 1982, 1984; Mouginis-Mark, 1985; Chapman, 2003; Jaumman and Hauber, 2003; Nussbaumer et al., 2004; Carr, 2006; Fassett and Head, 2006, 2007; Levy et al., 2009; Soare et al., 2009; Head et al., 2010), no evidence of glaciers has been described in Elysium Mons neither Albor Tholus.

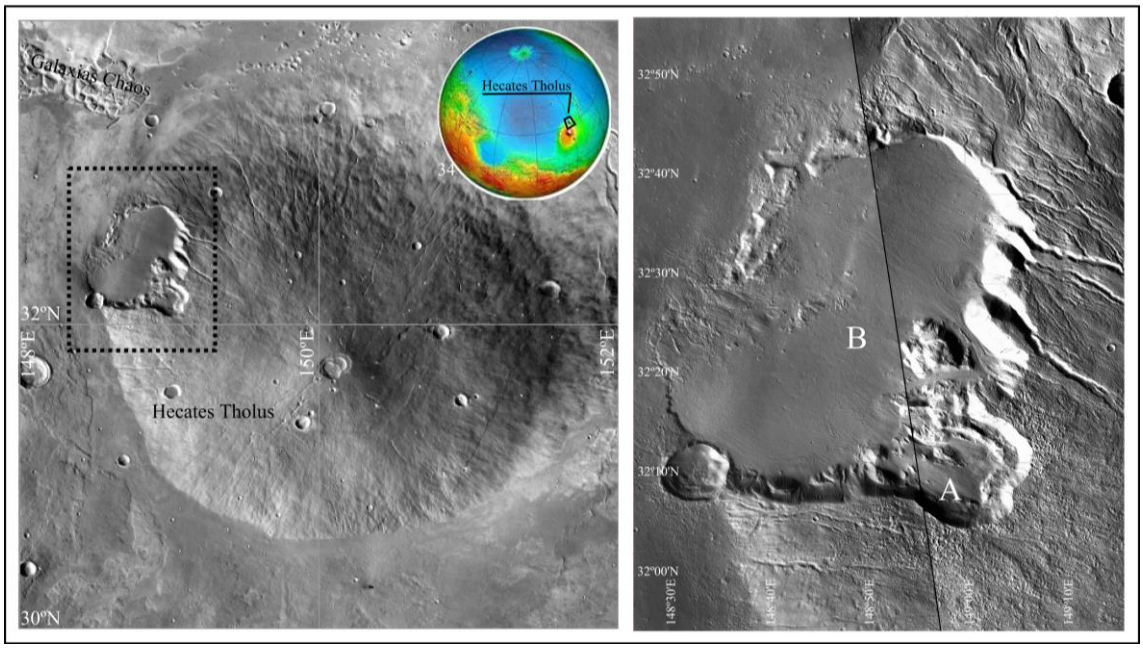

Fig. 4.1: Hecates tholus volcano on a THEMIS-IR daytime mosaic (left), and CTX mosaic of the study area (right), the lower NW flank of the edifice. A and B indicate the two depressions which characterize this flank of the volcano.

On Hecates Tholus, Fassett and Head (2006, 2007) among several authors (e.g., Gulick et al., 1997; Zent, 1999; Gulick, 2001; Carr and Head, 2003), proposed a past ice cap covering the summit of the edifice existed, and they suggested that its melting water could excavate some of the radial streams what dissect the flanks. However, most of possible glacial features in Hecates Tholus are distributed at the lower NW flank of the volcano (Neukum et al., 2004; Hauber et al., 2005; Helbert et al., 2005), as seen on Mars Orbiter Camera (MOC) and High Resolution Stereo Camera (HRSC) images. The floor of the two nested depressions (A and B on Figure 4.1) show abundant Lineated Valley Fill and Lobate Debris Aprons (terms proposed by Head et al., 2010; Hauber et al., 2005), interpreted to be sedimentary remnants of ancient glaciers. Those possible glacial features has been proposed to be the last important geological events of this volcano, which last eruption occurred between 1,000 and 100 Ma (Neukum et al., 2004; Hauber et al., 2005; Werner, 2009), although it has had a long history of magmatic, tectonic and water-related interactions (e.g., Mouginis-Mark et al., 1982, 1984; Gulick and Baker, 1989, 1990; Hauber et al., 2005; Williams et al., 2005; Fassett and Head, 2006, 2007; Kangi, 2007; among others).

Our recent study of the glacial activity in Hecates Tholus volcano resulted on a detailed geomorphological map 1:100,000 in scale (de Pablo and Centeno, 2012). The map shows the area between 31.8º-33.08ºN and 148.37º-149.38ºE, and confirms the ideas of Neukun et al. (2004) and Hauber et al. (2005) of an extensive area affected by glacial activity at the NW flank of Hecates Tholus. Our research revealed a complex glacial evolution in the area, with multiple

pulses, most of them coincident with the already proposed recent Martian ice ages (Head et al., 2003; Hauber et al., 2005), and as recent as 0.4 Ma (de Pablo et al., 2013). The information provided by the cartography as well as by the crater counting allowed to propose a general model about how was the evolution of the glacial activity in the volcano (de Pablo et al., 2013). In this chapter, we present here the description and interpretation of those mapped geomorphological units and elements, the first detailed morphometrical and morphological analysis of the glaciated area, and new evidences of events along the complex glacial evolution on the lower NW flank of the Hecates Tholus volcano.

4.2. Material and methods

Each glacial feature shows a typical range of size, at least on the Earth (e.g., Bennett and Glasser, 2009), that should be considered on the search for similar features on the surface of Mars. For that reason, each type of image, depending of their resolution, could be used to locate different types of features (Figure 4.2), at least as a reference and starting point on the search for glacial morphologies on the surface of Mars.

Taking into account this scenario, we made a wide review and analysis of all the available images, but, based on their resolution and spatial coverage, we focused, for the study of the regional context, on the analysis of images acquired by Context (CTX) instrument on board of Mars Reconnaissance Orbiter (MRO) of NASA, about 6 m/pixel in resolution. CTX images are available through the the NASA's Planetary Data System (PDS) Geosciences Node's Orbital Data Explorer (ODE) by the University of Washington in Saint Louis (http://ode.rsl.wustl.edu/; Benneth et al., 2008; Wang et al., 2009, 2010, 2011).

This was also the source of the images we used for the detailed geomorphological analysis of the study area. We analyzed both 67 Mars Orbiter Camera (MOC) narrow angle images with a resolution of 2 m/pixel, and 14 very high resolution images provided by High Resolution Imaging System (HiRISE) instrument on board of MRO spacecraft, which resolution ranges between 0.25 and 0.50 cm/pixel. We also analyzed the 4 available images acquired by Context Camera (CTX) instrument on board of MRO mission, which resolution is about 6 m/pixel. All those images were processed to be included into a Geographic Information System (GIS) developed for Mars, what was the base for the geomorphological cartography of this area (de Pablo and Centeno, 2012). We used ArcGIS 9.3 software (by ESRI) and the geographic coordinate system Mars 2000 spheroid and the Equidistant Cylindrical projection system with central meridian at 180º.

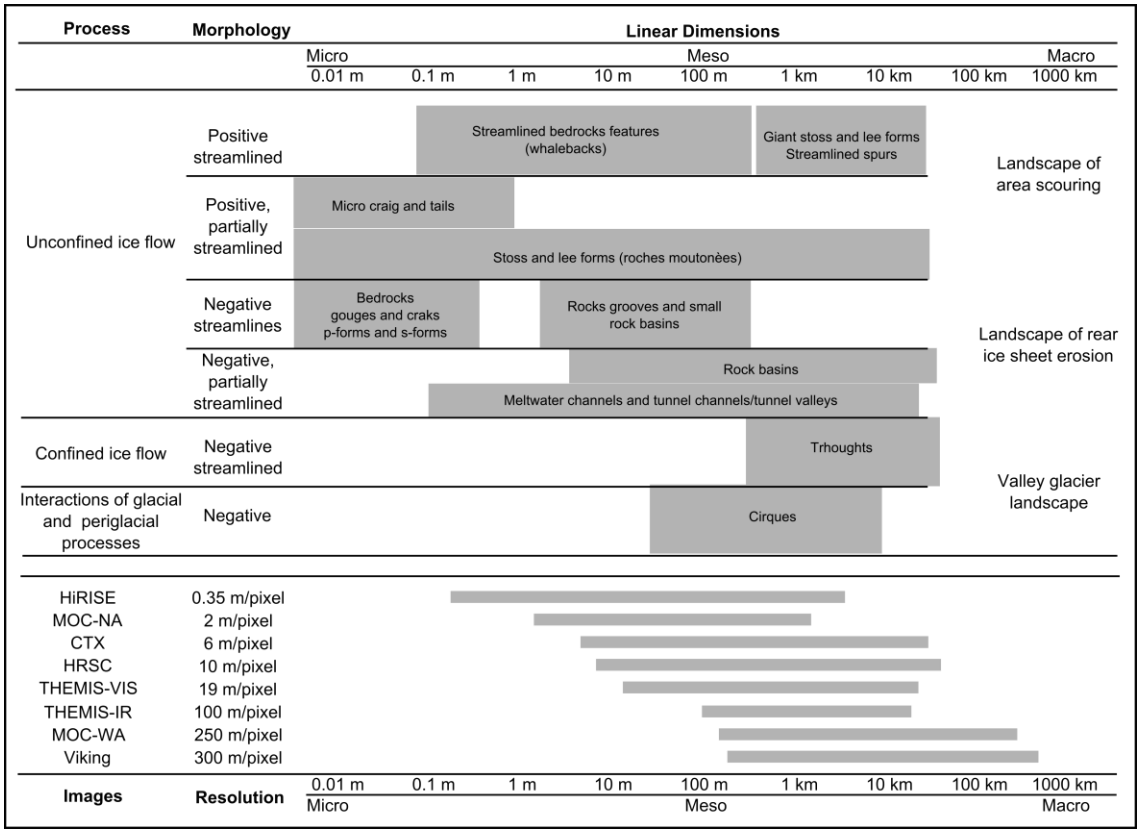

Fig. 4.2: Dimensions of the main glacial erosional landforms (top) (modified from Bennet and Glasser, 2009), and range of observation in different satellite images acquired by instruments on board on present and past missions sent to Mars, based on their spatial resolution and images swath dimensions.

We used GIS tools to derive different maps from the HRSC-derived digital elevation model including: slope, aspect, catchment area, curvature, ruggedness index (Blaszczynski, 1997; Riley et al., 1999), and anisotropical diurnal solar heating (e.g., Bhöner and Antonic, 2009), as well as to produce topographic profiles to analyze both the general topography of the area and the valleys morphology in order to correlate the morphometry and shapes observed in the topography with the geomorphologycal units and their glacial-related interpreted origin.

Moreover, we used the GIS to produce multiple topographic cross sections of the study area from a HRSC-derived DTM (H1262_0000_DA4). Detailed topographic profiles were also produced to develop a morphometrical analysis of three valleys and study their origin.

Topographic data were also used to develop a fourth-polynomial fitting (Eq. 1) in order to extract the valleys data (Schaefer, 2011). The selected data for each valley were fit by to a power law (Eq. 2) by the Pattyn and Huele (1998) method (Eq. 3) because, although the method is still under discussion by the scientific community (see Coles 2014 for a detailed review), the results provide a way to distinguish between glacial and fluvial origin of valleys.

The used equations are on the power-law fit had been:

$$Y = a + b\,x + c\,x^{2} + d\,x^{3} + e\,x^{4} \quad \text{(Eq. 1)}$$

$$y = a\,x^{b} \quad \text{(Eq. 2)}$$

$$y - y_0 = a\,|\,x - x_0\,|^{b} = a \exp\{\,b \ln |\,x - x_0\,|\,\} \quad \text{(Eq. 3)}$$

where X and Y are distance in meters from the origin of the topographic section and elevation, respectively, and a and b are considered form parameters of the resulting fitting curve. Parameter b is later considered to distinguish between fluvial and glacial origin (e.g., Pattyn and Van Huele, 1998).

The extracted topographic data of the valleys were also used to derive other parameters such as elevation of the left edge (Eld), elevation of the right edge (Erd), elevation of the valley bottom (Esd), valley width (Vw), and valley floor width (Vfw). These parameters were used to derive Valley floor height-width ratio (Vf) following the equations proposed by different authors (Bull and McFadden, 1977; Pedrera et al., 2009) (Eq. 4) as well as the Form Ratio (FR) (Eq. 5) (Graf, 1970), in order to analyze the b-FR correlation (Hirano and Aniya, 1988) what has been widely discussed, but here is used like a qualitative parameter to help on the valley's origin interpretation.

$$Vf = 2Vfw / [(Eld - Esc) + (Erd - Esc)] \quad \text{(Eq. 4)}$$

$$FR = D / Vw \quad \text{(Eq. 5)}$$

where D is the depth of the valley. In our case, we calculated for both sides left (Eq. 6) and right (Eq. 7).

$$D\_left = Eld - Esd \quad \text{(Eq. 6)}$$

$$D\_right = Erd - Esd \quad \text{(Eq. 7)}$$

4.3. Geomorphological units and elements

4.3.1. General geomorphology

The lower NW flank of the Hecates Tholus volcano is marked by a relative restricted variety of units and elements. Volcanic, slope, fluvial, glacial and periglacial, tectonics, impact and aeolian geomorphological units and/or elements has been observed and mapped (de

Pablo and Centeno, 2012). Some of those geomorphological units have been also dated by the use of the crater counting technique (de Pablo et al., 2013). The area is characterized by 18 geomorphological units (Figure 4.3; Table 4.1).

The volcanic units are distributed through all the study area, including the flanks of the Hecates Tholus volcano, as well as the surrounding plains, at the NW sector of the study area. This group of geomorphological units includes Smooth Outcrops (SO), Smooth Lava Flows (SLF), Dissected Lava Flows (DLF), Rough Lava Flows (RLF), Patterned Lava Flows (PLF), and Knobby Terrain (KT) units. Geomorphological elements with volcanic origin had not been identified and mapped (de Pablo and Centeno, 2012).

Table 4.1: Mapped geomorphological units and their interpreted origin.

Origin	Geomorphological units	Code
Volcanic	Smooth outcrop	SO
	Smooth lava flow	SLF
	Dissected lava flow	DLF
	Rough lava flow	RLF
	Patterned lava flow	PLF
Slope	Slope deposit	SD
	Creep deposit	CD
	Rocky slope	RcS
	Rough slope	RS
	Smooth slope	SS
Fluvial	Badland	B
	Gulley sedimentary deposit	GSD
Glacial	Roche moutonée	RM
	Glaciar deposit	GD
Impact	Ejecta deposit	ED
	Crater material	CM
Other	Knobby terrain	KT
	Rugged terrain	RT

The depressions on the lower part of this flank of the volcano (Figure 4.1) is the area where glacial geomorphological units has been widely identified, although only two units have been distinguished: Glacier Deposits (GD) and Roches Moutonèes (RM), but many geomorphological elements with a possible glacial origin: crevasses, flute, esker, arêtes, moraines and glacial erratic fields. A periglacial element, pingos, has been also observed related to the glacial units already cited.

There are other geomorphological units and elements related to liquid water activity and with smaller extension: Badlands (B), Gullie Sedimentary Deposits (GSD), and Rugged Terrain (RT) unit. In addition, channels, shallow channels and terraces are identified elements. All those units and elements are located in the flank of the volcano or its base, dissecting the lava flows of the Hecates Tholus volcano, but not inside the main depressions on this flank.

Slope units and elements are also restricted in extension inside the study area, mainly located in the walls of the channels dissecting the flank of the volcano as well as to the walls of the depressions. Slope Deposits (SD), Creep Deposits (CD), Rocky Slopes (RcS), Rough Slopes (RS) and Smooth slopes (SS) units and scarps and slope base ridges are the slope elements we observed in the study area.

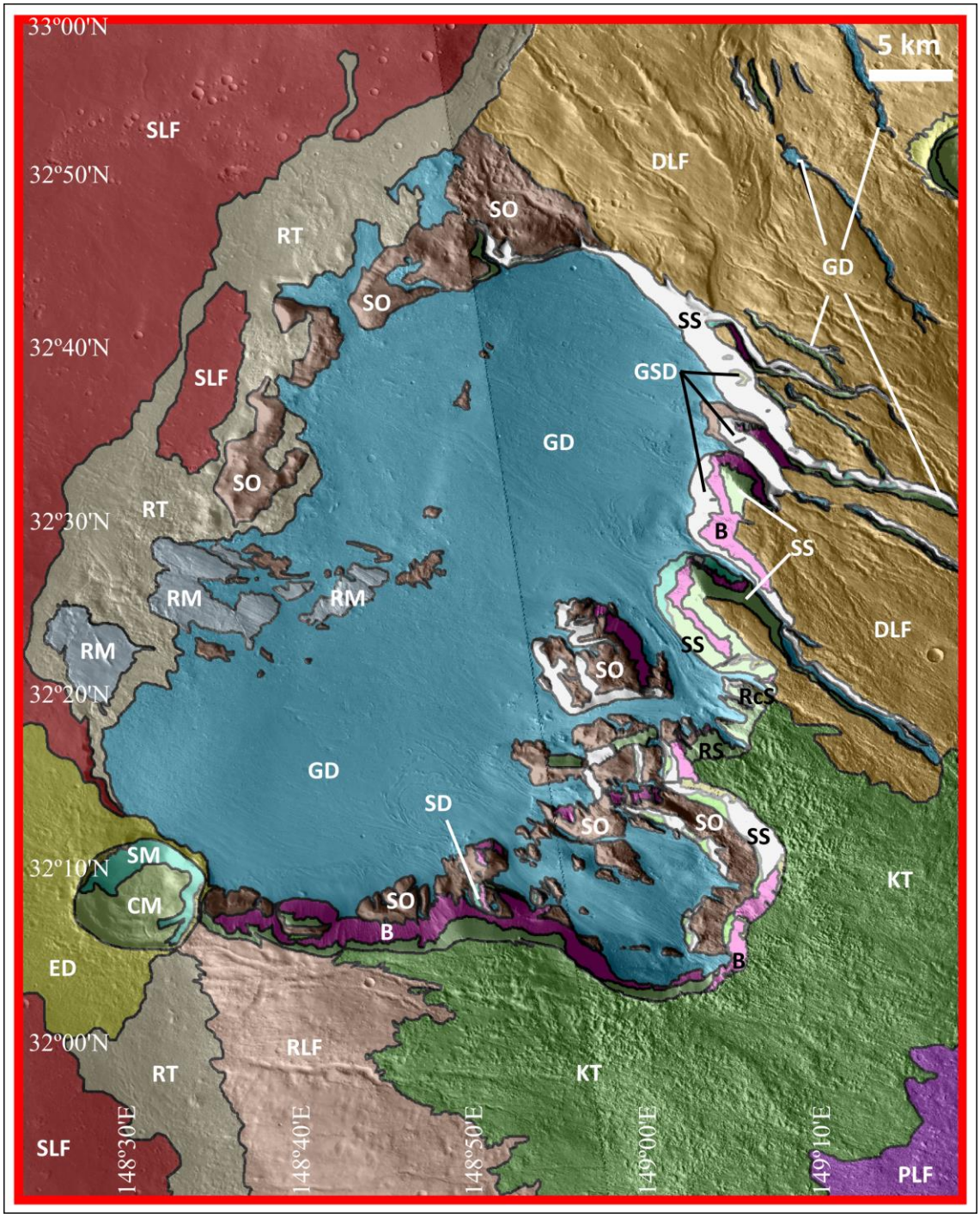

Fig. 4.3: CTX images mosaic showing the geomorphological units of the lower NW flank of the Hecates Tholus volcano (modified from de Pablo and Centeno, 2012). Unit codes in the text and Table 4.1.

The two main impact craters existing in the area are related to other mapped units: Ejecta Deposits (ED), and Crater Materials (CM). The high resolution images used in this research made possible to observe and to map smaller impact crater and their rims. Those elements are distributed by all the study area, although they are less common in the main depressions at the flank of the volcano (Figure 4.3).

Other geomorphological elements have been also mapped such as fields of Aeolian deposits and different tectonic features like graben, ridges or morphological alignments, what are related to the flanks of the volcano, but not to the materials inside the depression in that flank, or the surrounding volcanic plains.

In the next sections we describe in detail each one of these geomorphological units (Figure 4.4) and elements (Figure 4.5; Figure 4.6), as well as showing their assigned ages (based on de Pablo et al., 2013), when available.

4.3.2. Geomorphological units

A) Volcanic units:

Smooth lava flows (SLF) unit is characterized by a regular surface with abundant lobated scarps, with rugged texture near the edges. It is located in plains surrounding the western base of Hecates Tholus. Based on its regional distribution, this unit could be interpreted to be distal lava flows from Elysium Mons volcano, that flowed around Hecates Tholus volcano, with different spatial erosion rates caused by fluvial and impact processes. This unit has been dated on 2.35 Ga, although younger ages has been also derived from crater counting, including 1.22 Ga, 975, 724, and 8.61 Ma, showing a long history of resurfacing processes (de Pablo, 2009). However, we interpret that those processes do not include glacial activity, or if they existed, they were not effective enough to completely change the texture of the terrain and therefore, or leave a distinct glacial relief. This allows to map the lava flows surrounding the volcano such as an independent geomorphological unit: Rugged Terrain (RT) unit.

Smooth outcrops (SO) unit is undivided and unfeatured rock outcrop, characterized by its smooth morphology, located inside and forming some edges of the main depression on the lower NW flank of the Hecates Tholus volcano. We interpret this unit such as ancient volcanic materials forming the lower part of Hecates Tholus volcanic edifice, dated on 3.8 Ga at the transition between Late Hesperian and Early Amazonian. Younger ages (3.6 Ga, 3.4 Ga, 1.4 Ga and 32.1 Ma) support the interpretation of resurfacing processes in this unit. The rounded and smooth morphology, their location on the front of the glacial unit (GD units) mainly forming the edge of the depression in which it is contained, and the glacial setting of the area allow to deduce the glaciers were the main responsible of the smoothing of these outcrops.

Dissected lava flows (DLF) unit is an irregular terrain, heavily dissected by fluvial valleys, with smooth steps at the NW flank of the Hecates Tholus volcano. This unit could be interpreted to be lava flows forming the flank of this volcano, later dissected by fluvial features. Many

channels have been observed in the area (e.g., Gulick et al., 1997; Zent, 1999; Gulick, 2001; Carr and Head, 2003, Fasset and Head, 2006, 2007, 2008). Such as we will see later, some of those valleys are also filled by glacial materials, what could be also the responsible of the smooth texture of the surface hiding and eroding the fronts of the lava flows what should exist in the area. Crater counting of DLF unit returned an age of 3.6 Ga, what support the hypothesis about this unit represent old lava flows of the volcanic edifice, but younger than SO unit. Resurfacing ages are 806 Ma, 107 Ma, and 440 ka.

Rough lava flows (RLF) unit is characterized by its rough surface on the lower western slope of the volcano, partially covered by smooth materials. It is located at the lower western flank of Hecates Tholus volcano, and could be interpreted to be distal lava flows of the volcanic edifice, later modified by tectonic, impact and fluvial processes. This unit could be the same materials than DLF unit, but less dissected by fluvial channels and fractures, as well as covered by a fine-grained mantle material. The crater counting returned and age of 3.4 Ga for this unit, as well as ages for the end of resurfacing events at 415 Ma, 19.4 Ma, and 1.34 Ma.

Patterned lava flows (PLF) unit is an irregular terrain on the middle part of the western slope of the volcano, partially covered by smooth materials oriented with a SW-NE pattern. This unit is only located at the lower westernmost sector of the flank of Hecates Tholus volcano in the study area. Due to its location on the flank of the volcano, may be it could be interpreted like tuff or lapilli deposits on top of the lava flows of the volcanic edifice (the same forming DLF and RTF units), later modified by fluvial and/or glacial processes eroding them and resulting on this patterned texture. The crater counting returned an age of 342 Ma for their origin.

Knobby terrain (KT) unit shows a irregular surface with abundant hills and mounds without clear orientation or patterns. This unit is spatially restricted to upslope and surrounding the depression A. Different authors interpreted this unit such as pyroclastic deposits from a lateral eruption on Hecates Tholus volcano, this one forming the upper and smaller depression on the flank of the edifice (Neukum et al., 2004; Hauber et al., 2005; Werner, 2009). We do not have enough evidences to support or reject this hypothesis, but we agree that this unit occurred latter than the DLF and RLF units, and its distribution surrounding the rounded depression on the flank of the volcano could point toward this origin, although we do not discard other possible origins like an impact to produce this deposit or landslide (see de Pablo, 2009 for a discussion about its origin). Crater counting (Neukum et al., 2004; Hauber et al., 2005; Werner, 2009; de Pablo et al., 2013) returned ages of about 350 Ma and 335 Ma (respectively). Other

younger ages could be related to the end of resurfacing event at around 44.7 Ma, 4.9 Ma, and 274 Ka.

B) Glacial units:

Glacier deposits (GD) unit is a smooth terrain, convex-upward surface, that occupies most of the bottoms of depressions A and B. It shows elongated and lobated lineaments similar to the lobate debris aprons (LDA) and lineated valley fill (LVF) that Head et al. (2010) describe as evidences of glacial events on Mars. This unit is located inside the main valleys on the western flank of the volcano at the DLF unit, and most of the floor of the depressions on this flank. We interpret the GD unit as dust- or debris-covered glaciers, or rocky glaciers flowing inside the main valleys toward the depressions, and also inside them. The crater counting returned ages of 61.9 Ma, 30.4 Ma, 16.2 Ma, and 6.1 Ma. These ages agree with other crater counting made by other authors (Neukum et al., 2004; Hauber et al., 2005), that also related the materials forming this unit to glacial events.

We observed two sectors on this unit. The first one, located and filling the eastern sector of the depressions A and B, is more similar to LDA described in the literature (e.g., Head et al., 2010). However, its western limit is marked by a topographic step, visible on images, but nicely observable on topography sections the depression from SW to NE. However, at the western sector, LFV features are less abundant, they are less abundant than on the eastern sector, and the surface is more rough and knobby. We interpret those sectors as 1) debris-covered glacier in the east, with a front marked by the topographic step, and 2) glacial drift deposits from an ancient debris-covered glacier in the west. However, we do not discard that the hummocky, rough and knobby texture of this western sector could still hide some relict ice below the surface, what is the only explanation for the abundance of LVF structures.

Roches Moutonèes (RM) unit is characterized by a smooth terrain with gentle slope and asymmetrical edges, and clearly dissected by long, narrow, shallow and straight valleys. This unit is located near the edge, on the western part of depression B. Due to its topographic asymmetry, RM unit could be interpreted to be rock outcrops heavily eroded by the action of an ancient glacial tongue by abrasion and plucking processes. This unit has been dated on 1.8 Ga, with younger ages of 16.8 and 7.2 Ma. This ages agrees with the ages of the GD unit, so, moreover of the morphology, it could support the interpretation of the origin of this unit.

C) Fluvial units:

Badlands (B) unit is a rough surface forming narrow valleys typically located on the middle part of the slopes Depressions A and B, and could be caused by erosion by diffuse superficial runoff on the slopes along the time.

Gullies sedimentary deposits (GSD) unit is observable as downslope elongated unfeatured dark deposit located at the south-east-facing slopes of depression B. This unit could be formed by water-rich sediments from gullies, such as many others on Mars (e.g., Malin and Edget, 2000, 2001; Edget et al., 2003; Christensen, 2003; Heldman, 2004; Heldmann and Mellon, 2004; Dickson et al., 2007; Dundas et al., 2012; Harrison et al., 2015).

Rugged Terrain (RT) unit is the most extended water-related unit. It is characterized by a rough surface with very irregular reliefs from hills to mounds, either with chaotic or patterns. It is located at the plains surrounding the western flank of the volcano. We interpret this rugged terrain as accumulation of materials of different sources (mainly fluvial and glacial) that seems to cover the lava flows of the SLF unit. Its texture, the spatial distribution at the northwestern edge of the depression, filled by glacial materials (GD unit), and its connection to channels at the base of the volcano support this interpretation. The crater counting returned ages of 980 Ma, 54.1Ma, 31.1 Ma, and 988 ka. These ages support the idea of an origin later than the formation of GD and RM units..

D) Slope units:

Slope deposits (SD) unit is an irregular smooth terrain on at the base of step slopes, locally forming clear cone-shaped deposits. It is located at few scarps on the eastern edge of the depression B. This unit could represent sedimentary deposits formed by mass-wasting and other slope movements clearly related to high slopes.

Creep deposits (CD) unit is also characterized by wavy terrain, smooth in texture, located on the lower part of step slopes at the eastern edge of the depressions on the lower NW flank of Hecates Tholus volcano, always on west- and south-facing high slopes. This unit could be interpreted as sedimentary deposits accumulated by creep processes on high slopes.

Rocky slopes (RcS) unit is a pristine rough terrain on the upper part of high slopes and scarps on the eastern edge of the nested depressions on Hecates Tholus. This unit could be interpreted to be rock outcrops on upper part of scarps inside the depression, and also in the inner walls of some craters.

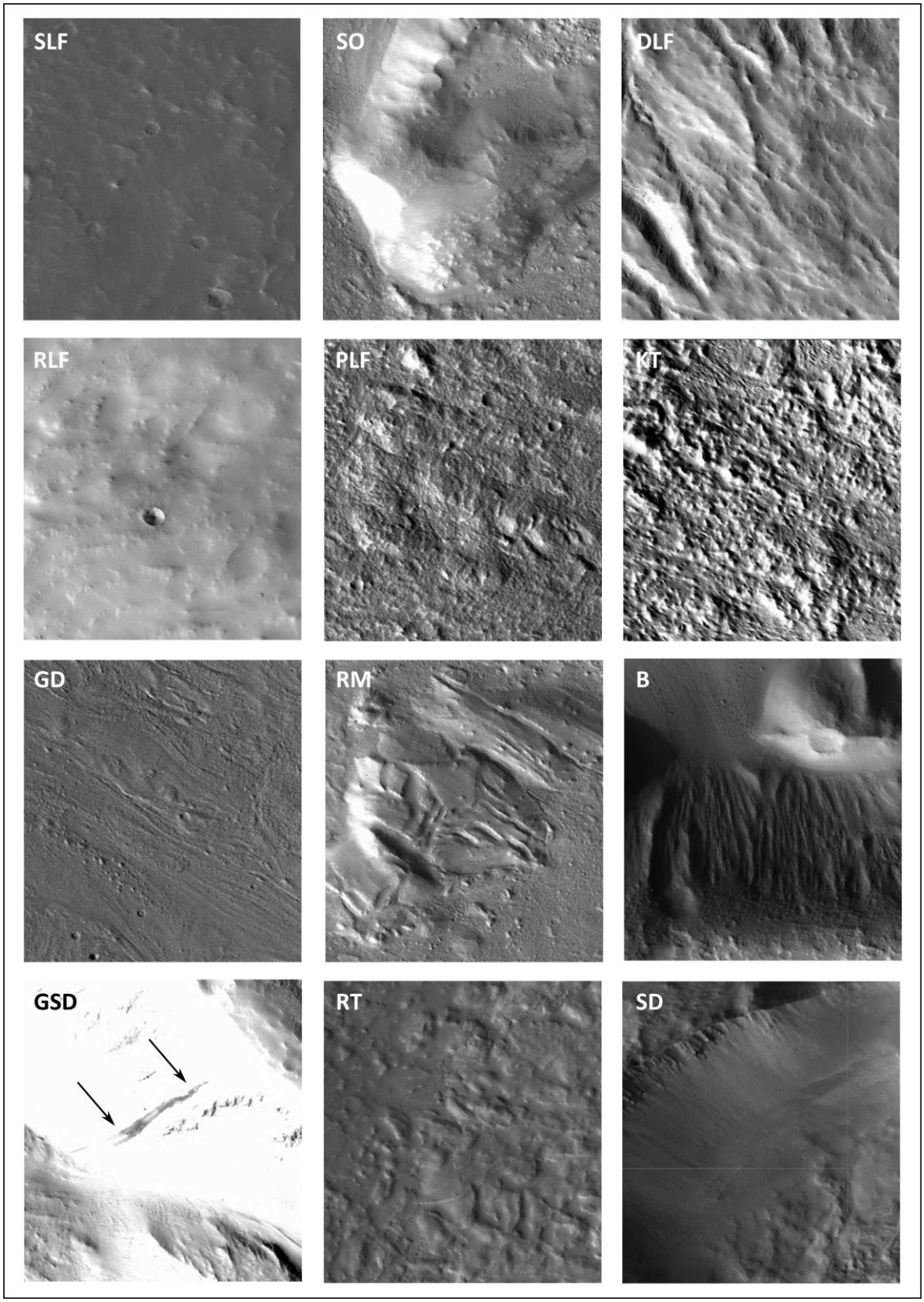

Fig. 4.4: Frames of CTX images showing examples of the different geomophological units identified at the lower NW flank of the Hecates Tholus volcano. Each image frame is 3 km wide, and North to the top (Continue on the next plate).

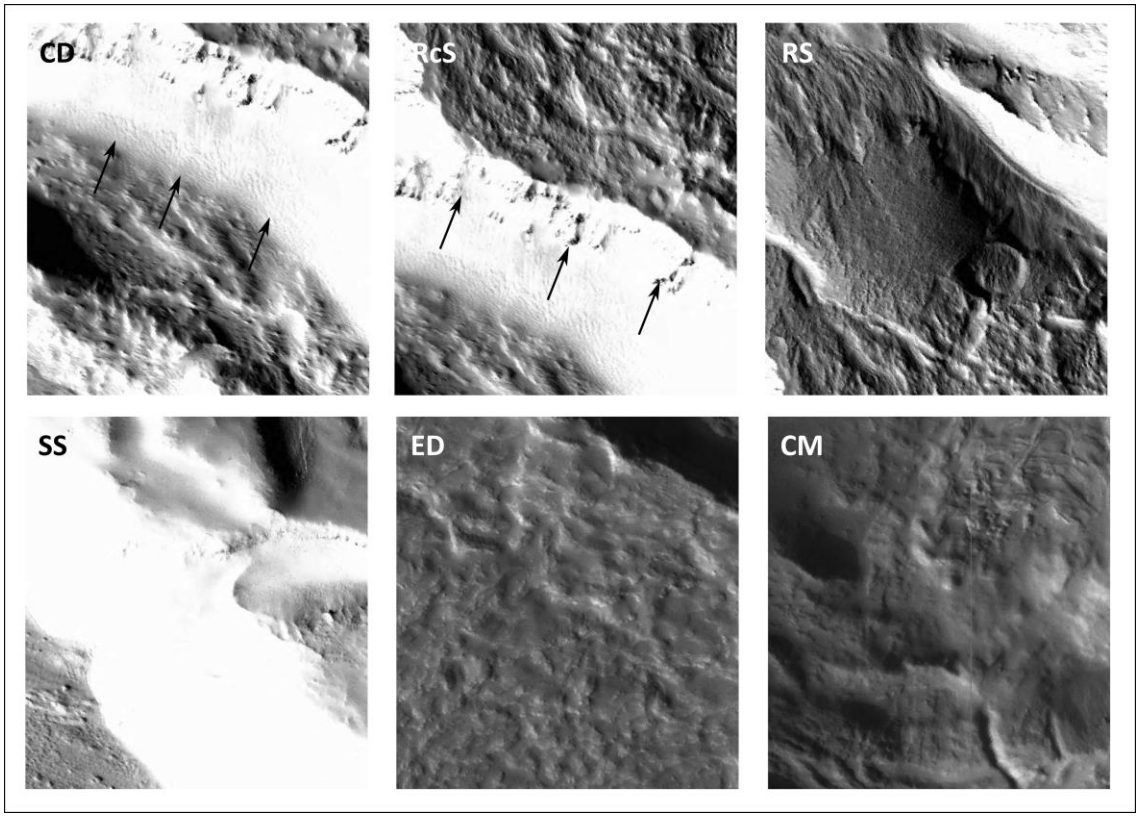

Fig. 4.4: (Continue from previous page).

Rough slopes (RS) unit shows an unfeatured rough surface on high slopes and scarps. This unit is restricted to the upper part and head of the main scarps of the main valleys and depressions on the lower NW flank of Hecates Tholus. It could represent rock outcrops heavily eroded by different processes, and locally covered by sediments.

Smooth slopes (SS) unit is also an unfeatured terrain, but hi one shows a smooth surface on step slopes at the east- and south-facing slopes of the main valleys and depression on the flank of the volcano. Due to its unfeatured character and its smooth texture, we interpret it like undivided slope deposits.

E) Impact units:

Ejecta deposits (ED) unit that shows a surface of variable texture (rough to smooth) around impact craters, locally with radial pattern. It is located around impact craters at different sites throughout the area, and it is interpreted to be ejecta deposits from the impacts, a very common unit in all the planet.

Crater materials (CM) unit is a terrain formed by rough materials filling impact crater slopes formed by undefined material of different origin, including sedimentary, slope, fluvial, and volcanic, among others.

4.3.3. Geomorphological elements

CTX, MOC and HiRISE instruments provide enough high resolution images to allow distinguish a wide variety of geomorphological elements with many different origins in the study area, including: slope, fluvial, periglacial, glacial, aeolian, tectonics and impact, most of them mapped by de Pablo and Centeno, 2012 (Figure 4.5; Figure 4.6).

A) Slope elements:

The slope-related geomorphological elements are mainly the scarps around depressions A and B and in many deep channels dissecting the slope, mainly at the northern and northwestern flank of the volcano. In two cases, we found ridges parallel to the base of scarps, but related to So unit in the SW-facing slopes of depression B.

B) Periglacial elements:

Although periglacial features has not been previously described in the area, we observed the presence of possible pingos. We observed 16 mound-like features, most of them at the westernmost area of depression B related to GD unit, abut also outside the depression related to RT unit. Based on interpretation of CTX images and HRSC-derived DTM, these pingos are about 240 m in diameter and reach 5 m in height. They are characterized by a pit on the summit and about circular morphology ad dome in shape. In some cases, they have small fractures crossing the relief. It is because of their morphological and size similarities with pingos described on Mars in general, and in the nearest Elysium and Utopia Planitiae regions in particular (e.g., Burr et al., 2005; Soare et al., 2005, 2009; de Pablo and Komatsu, 2008; Dundas et al., 2008), as well as taking into account the glacial setting of the study area, that we interpret those reliefs to be pingos.

C) Glacial elements:

We observed many glacial-related geomorphological elements, including sedimentary and erosive elements. Respect the glacial drift, the most abundant features are moraine deposits: elongated, arcuate, undulate and lobated positive reliefs (ridges) only related to the GD unit, similar to those named as lineated valley fills (LVF) in the literature (e.g., Head et al.,

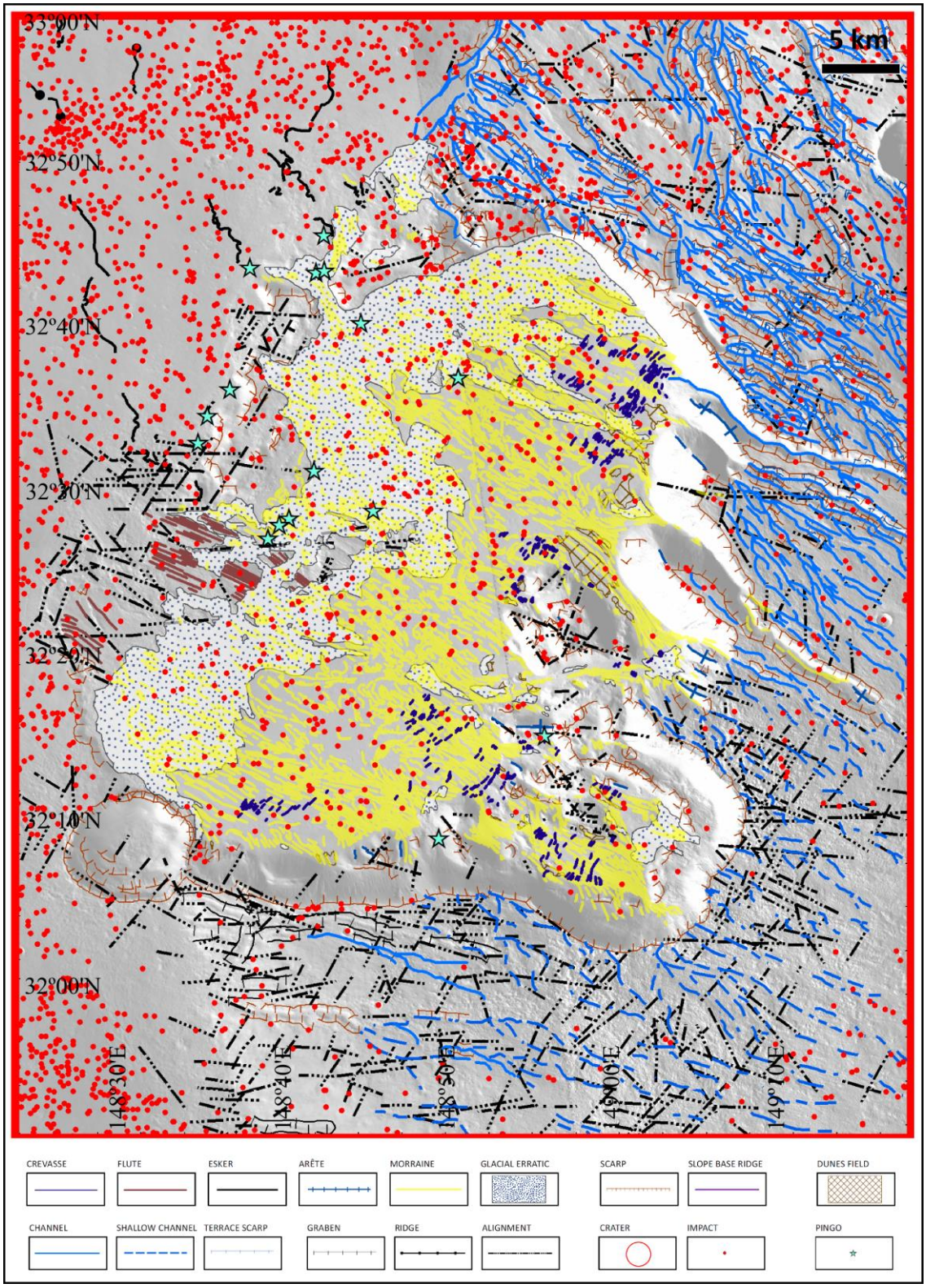

Fig. 4.5: CTX images mosaic showing the main geomorphological landforms of the lower NW flank of the Hecates Tholus volcano (modified from de Pablo and Centeno, 2012).

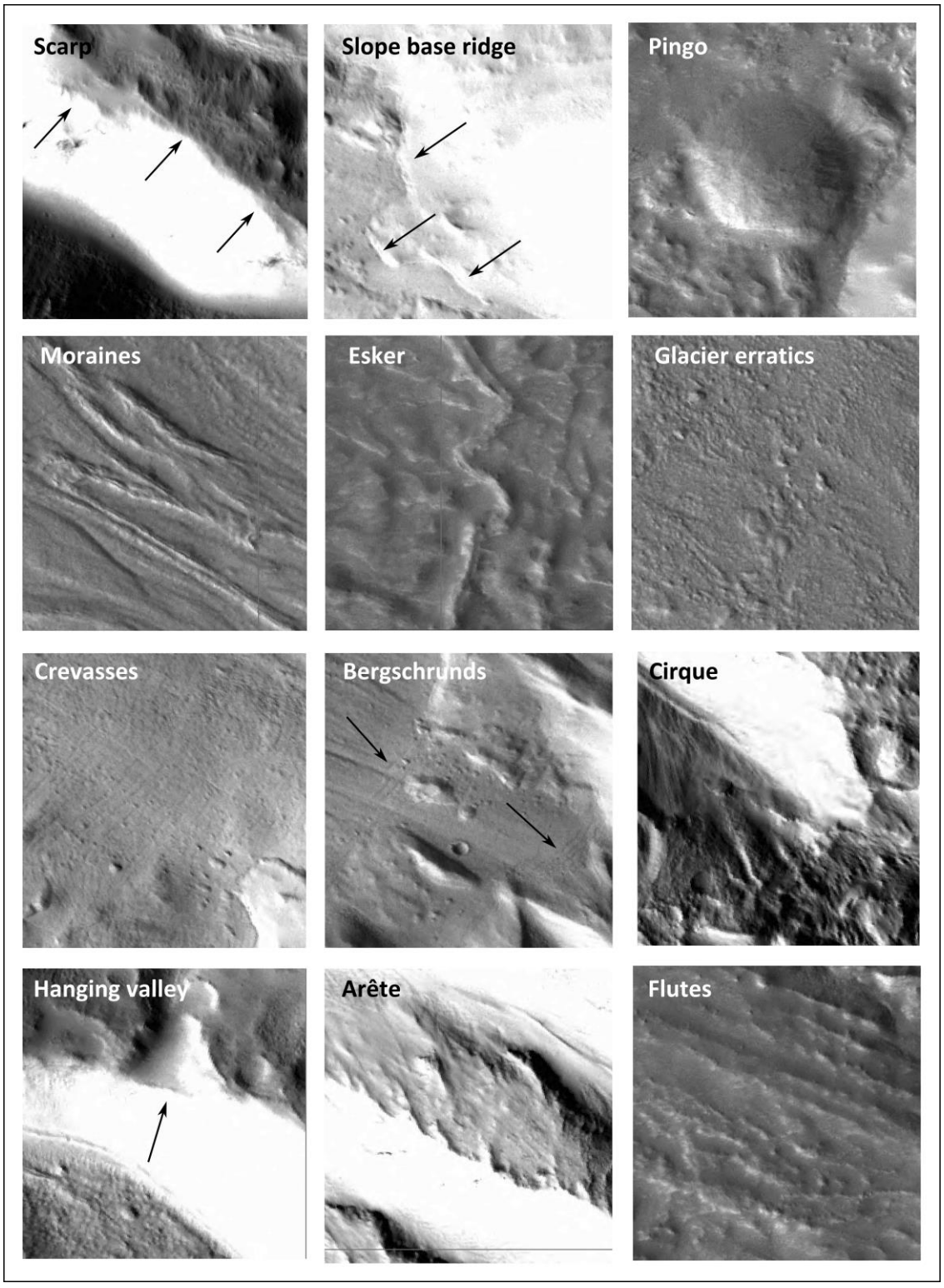

Fig. 4.6: Frames of CTX images showing examples of the different geomophological landforms identified at the lower NW flank of the Hecates Tholus volcano. Each image frame is 1.5 km wide, and North to the top (Continue on the next plate).

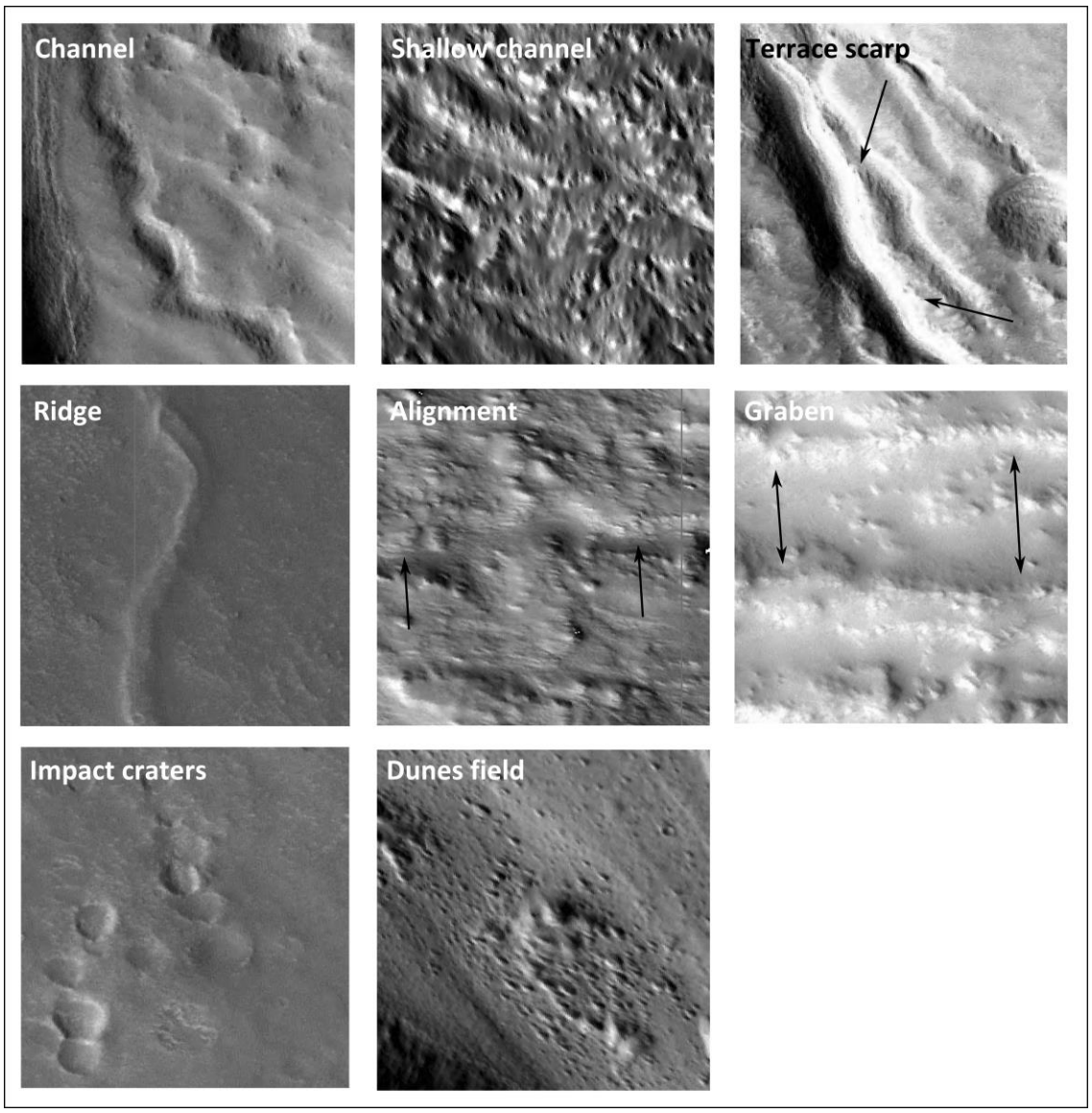

Fig. 4.6: (Continue from previous page).

2006, 2010). Merging, both simple and complex lobate and chevron, horseshoe-like or lineations have been observed on those ridges, supporting the idea of the deformation of debris deposits, such as occurs on the moraines on Earth and those proposed to exist on Mars described as LVF on debris-covered glaciers (e.g., Head et al., 2010 and references therein).

We also identify eskers in the CTX images (de Pablo and Centeno, 2012). They are single, positive, elongated and sinuous features, with vertical flanks and a flat top when they are not eroded, increasing in thickness from east to west. Those features are located outside the depression, but still near its edge, related to the RT unit. Although some of them are ghosty because of their degradation, and their null effect on the HRSC-derived DTM, they show meander-like morphologies, and also some division and merging, as well as a possible alluvial

fan at the end of one of them. All those features, and their similarities with terrestrial eskers, made possible to interpret them such as eskers resulting of the existence of a huge glacier filling the depression and overflowing its limits covering the surrounding plains (de Pablo et al., 2013).

Areas where LDA structures dominate on the Glacial Deposit unit (GD unit) are also characterized by the presence of many linear to curved features that we think are crevasses. These are groups of fractures organized as glacial crevasses organize on Earth glaciers. We observed four main types of crevasses depending of their location and their morphology and distribution: chevron, transverse, radial, and bergschrunds (Figure 4.7).

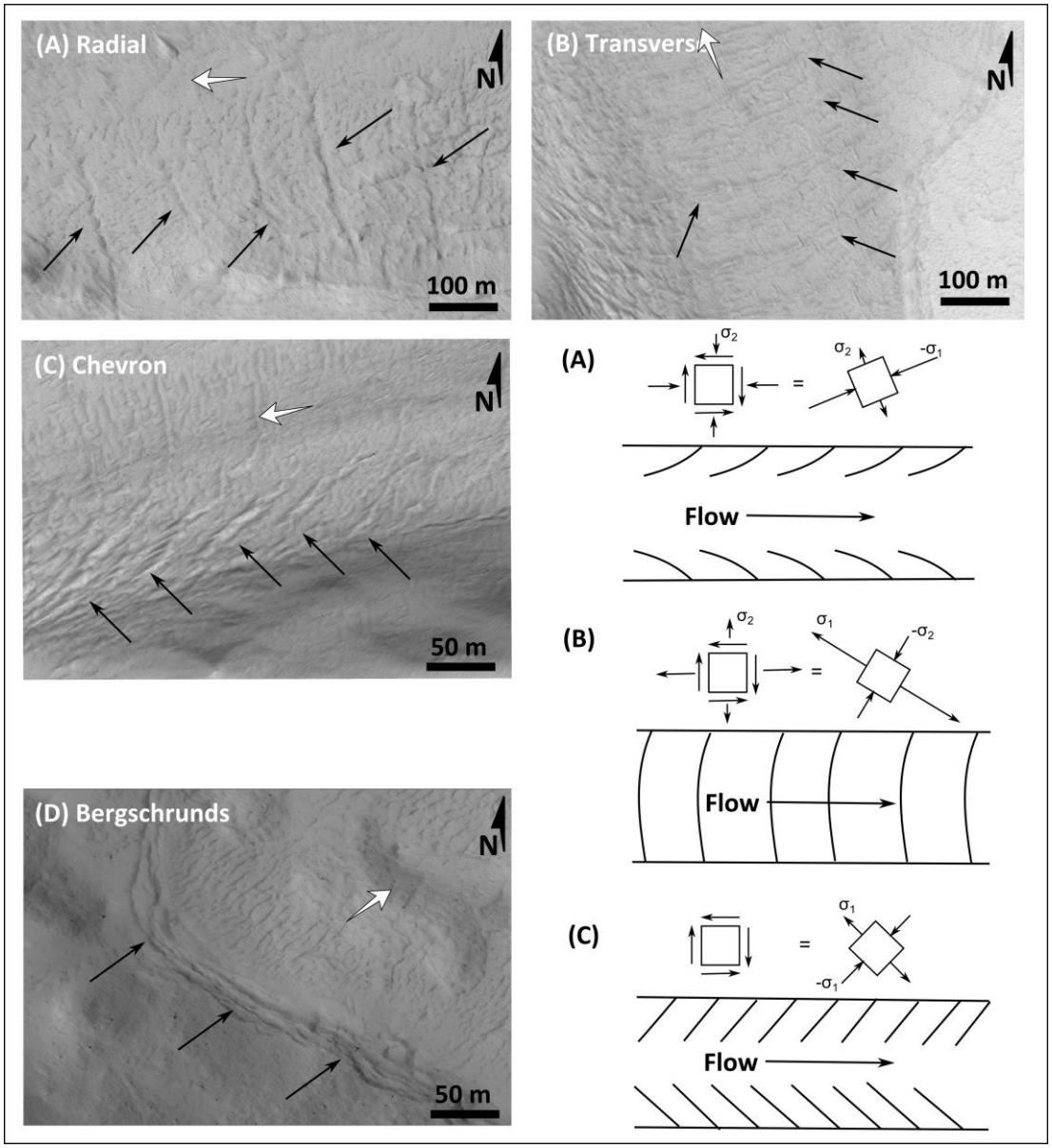

Fig. 4.7: Example of the different types of possible crevasses and bergschrunds (black arrows) as seen on HiRISE images. White arrows mark the possible glacier flow direction. Sketches shows the efforts diagrams causing the different types of crevasses (modified from Paterson, 1981, after Nye, 1952).

The radial and chevron types are about curved and straight (respectively) fractures, cents of meters in length, normally forming groups oblique to edge of the GD unit, pointing upslope. The transverse type is longer and usually cross the entire valley when it is narrow, or extend for long. In general they are slightly curved and they are more frequent than radial and chevron types in the study area. This kind of features does not appear only on the valleys raising the main depression, but at the eastern half part of depression B. These possible crevasses remark the downslope flow of and ice mass under normal expansion (transverse and radial), and tensional (chevron) conditions.

The last type of crevasses is similar in morphology to the transverse type of crevasses but it is only located on limit between the wall of the depression and valleys, and GD unit deposits. We interpret them to be a special case of crevasses: bergschrunds. These bergschrunds appear in groups, forming parallel swarms and extending in relays for more than 1 kilometer.

On Earth, glacial crevasses are elements clearly associate to active glaciers as they form developed already on flowing ice. Even a thin cover of sediments reduces the possibilities of these crevasses being visible in vertical aerial and satellite images. Ice ablation implies a fast destruction of crevasses as they can only survive as “inprints” on the thin sediment cover.

HiRISE images show individual blocks in the floor of depression B as well as at the bottom of valleys. These boulders are dark colored and, although they could be (we do not discard this origin for some of them at selected locations) debris materials from the walls of the valleys, the main origin of most of the boulders observed in the images could be glacial erratic, because they concentrate on the floor of the valley (i.e., GD unit), but not on the slope deposits and valley slopes, (i.e. the different slope units previously described).

Glacial erosive features have been also observed in the area. In fact, considering all the valley flowing into depression B, we can distinguish the following kinds: a) Hanging valleys with glacial origin; b) leveled valleys (with their bottom leveled with the bottom of depression B), with U-shaped sections and glacial origin; c) leveled valleys with V-shaped sections and not evient glacial origin what could result of glaciers that left a sedimentary filling in the bottom (GD unit) or have a complex fluvial-glacial origin.

Glacial cirques are rather scarce, but e suspect there are some at the eastern wall of the depression B. The almost circular shape of the indentations in depression B walls,

containing possible glacial materials (GD unit), made us classify those reliefs such as cirques. We think the glacial processes were the responsible of the resurfacing of the edge and the morphology of the wall of this depression. In addition, the presence of sharp summits of elongated spurs remnants of the volcano flanks, that we interpret to be arêtes, also supports the identification of cirques in the area.

Flutes appear on the satellite images related to rochees moutonèes (RM unit) at the western edge of the main depression. They are ESE-WNW oriented and they could reach more than one kilometer in length and tens of meters in width. Their orientation is in agreement with the general slope in the main depression, and, therefore, with the possible flow direction that could be deduced from the distribution of the moraines. We do not observe this streamlined features in any other geomorphological unit, such as smooth outcrops (SO unit), at the western edge of the depression. We interpret them such as caused by the erosion (abrasion) caused by debris material at the base of the glaciers what covered this area in the past, such as proposed in de Pablo et al. (2013).

D) Fluvial elements:

The fluvial processes excavated many narrow and shallow channels due to the flow of water from the summit of the volcanic edifice. They were already mapped and interpreted such as fluvial channels related to surficial runoff due to hydrothermal activity, precipitation or snow-packs melting on the summit of the edifice (e.g., Gulick, 1997, 2001; Zent, 1999; Carr and Head, 2003, Fasset and Head, 2006, 2007). These channels show evident dendritic to parallel patterns, probably depending on differences in the flank slope.

Deeper valleys show a “V”-shaped cross section with steep slopes. Most of them reach the edge of the depression in the flank of the volcano dissecting it. In some cases, they show narrow flat steeps on their slopes, that we interpreted to be terraces. In general the floors of those valleys reach the floor of the main depression, but in some cases they form the hanging valleys we already described above. However, a detailed morphometrical analysis has been done in order to confirm the origin of the main valleys, as we show below.

Other valleys are shallower and discontinuous. These shallow valleys are related to PLF and KT units, this one showing patterned and knobby surfaces. They are less clearly visible in the images, probably because they were ancient channels latter covered by the materials forming KT and PLF units, or because of the friable character of the materials of those units, they excavated a less clear and depth valleys network.

E) Aeolian elements:

Wind processes also had some role on the modification of the landscape. Wind marks and wind streaks formed by accumulation of materials next to blocks and boulders, erratic described above mainly at the floor of valleys, such as observed in detail in HiRISE images. They show the typical drop-shape, as long as 200 meters, marking the wind direction which mainly flow downslope along the valleys. However, near the mouth of the valleys in the main depression, the direction of the wind is more variable blowing even cross the valley. In some places, Aeolian sediments accumulate to form extensive dune fields, mapped by de Pablo and Centeno (2012). Further analysis of HiRISE images shows they are not typical dunes but huge wind streak deposits. The source for these deposits can be quite diverse: fine grained volcanic pyroclastic materials coming from the eruptions on Hecates Tholus volcano, dusty material from the glacial drift deposits, fine materials from depressions walls, and finer particles from debris deposits forming the GD unit.

F) Tectonic elements:

The tectonic processes are also the responsible of some of the geomorphological elements we observed in the study area. Most of them are morphological alignments with W-E, SW-NE and NW-SE as main directions. Scarps, alignment of hills and knobs, or straight channels and valleys, are some of the examples of morphology marking the alignments. Those alignments are more frequent at the southern part of the study area, in the flank of the volcano surrounding the two nested depressions. More evident are other tectonic elements such as graben, mainly at the lower eastern flank of the volcanic edifice, also with W-E trend, or ridges, at the northwestern sector of the study area and related to SLF unit.

G) Impact elements:

Finally, such as in any other region of mars, impact craters are also widely distributed across the study area, although only 2 of them are bigger than 5 km in diameter. In genera,l all craters are clearly identifiable, conserving their rims but, only in few cases, the ejecta deposits. For the smaller craters, they only conserve the bowl shape due to later erosion of the ejecta and rim. Secondary impact crater were not clearly identifiable, except a possible field at the northern sector of the study area, showing a W-E distribution affecting to SLF, RT, SO and DLF units (Figure 3.2). In general, the impact craters density is higher at the geomorphlogical unit related to the lava flows that surround the Hecates Tholus volcano (i.e. SLF unit).

Geomorphological units distributed on the flank of the volcano (i.e., DLF, RLF, KT and PLF) show lower impact crater densities. The lower density of impact craters is also recognizable on the GD unit filling the two nested depressions (Figure 4.5).

4.4. Morphometry

4.4.1. Elevation

The study area, at the flank of a volcano, shows a wide range of elevations from about -3.500 m to 3.000 m (Figure 4.8). Due to the primary volcanic origin of the relief and materials of the area, there is a general gradient from SE (+2000 m) towards the NNW (-3000 m). Volcanic units show a wide altitudinal range and an altitudinal distribution (Figure 4.9), increasing from SLF to PLF unit. Only PLF unit seem to be restricted to a narrow altitudinal range, but this in an artifact due to the limited available topographic data. On the other hand, the main glacial unit (GD unit) also have a wide altitudinal distribution, since glacial materials has been observed all along the flank of the edifice although concentrate in the depression of the flank. However, RM unit is strongly restricted to the floor of the depression.

Fluvial-related units seem to have a higher mean elevation since they are related to the higher part of the walls of the depression, except RT unit, relate to the accumulation of material at the base of the volcano from the fluvial activity on the flank of the edifice (e.g., Gulick, 1997, 2001). Slope-related units have also a wide altitudinal distribution, although they are slightly organized from the higher elevations (CD unit) to the lower ones (SD unit). Finally, impact-related units seems to have a narrow altitudinal distribution, but this represent only the two main impact craters of the area that could be drawn at the map scale (de Pablo and Centeno, 2012).

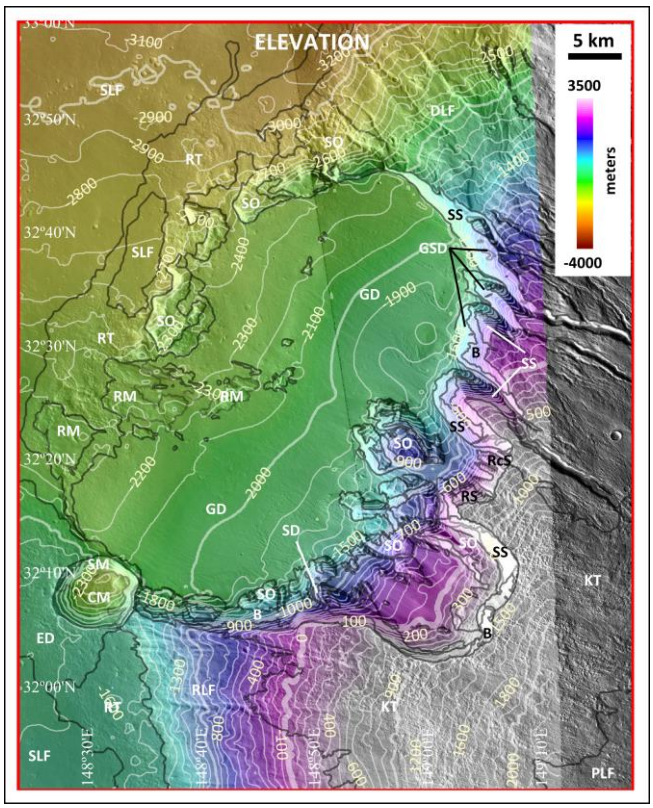

Fig. 4.8: HRSC-derived DTM on top a CTX images mosaic showing the elevations distribution of the lower NW flank of the Hecates Tholus volcano, Mars. Limits of the geomorphological units and their codes are shown.

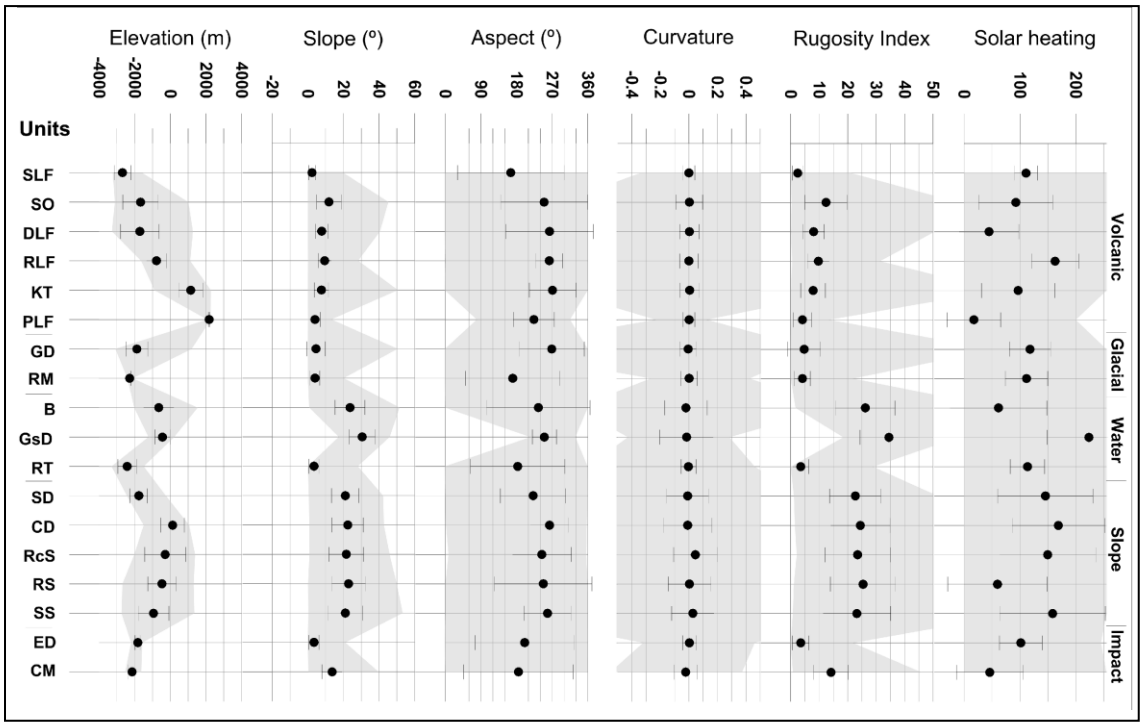

Fig. 4.9: Summary of terrain parameters for each geomorphological unit, showing mean values (dots), standard deviation (whispers), and maximum and minimum values (grey zones).

4.4.2. Aspect, slope, curvature and ruggedness

We analyzed the topography of the study area in order to characterize the different geomorphological units we described above. This general analysis is based on the aspect, slope, curvature and ruggedness maps (Figure 4.9; Figure 4.10).

Such as expected because we are focused on the NW flank of the volcano, the main slope orientations (aspect) on the study area are N, NW and W. However, we observed some aspect-related units depending on its variability. In fact, we are able to define different areas (sectors) with similar behaviour. Sector I is characterized by mainly NW and W aspect with mean spatial variability, related to the flank of the volcano and the units located on it: DLF, RLF, KT and PLF units. Sector II is also characterized by NW and W aspect with low spatial variability, related to the floor of the depressions on the flank of the volcano. This area is that one where GD unit is located. Sector III is characterized by multiple aspect with high spatial variability, related to the plain surrounding the volcano, i.e., SLF and RT units, as well as some other geomorphological unit at the NW edge of the depression on the flank of the volcano, i.e., SO and RM units. The last sector, Sector IV, is related to the walls on the main depression in the area and also the main impact craters, with progressive aspect variation. This sector is related to the slope geomorphological units, i.e., SD, CD, RcS, RS and SS units.

This spatial pattern on the distribution on the aspect variability is also observable on the slopes map (Figure 4.10). The Sector I is characterized by variable slopes of 5º to 15º, although with spots of lowers slopes (0º-5º). Sector II slopes are around 0º-5º, with small variability. Sector III has low slopes (0º-5º) but shows a higher variability with many spots of higher slopes (5º-15º). Sector IV is characterized by the higher slopes, ranging between 15º and 45º, but reaching values as high as 65º.

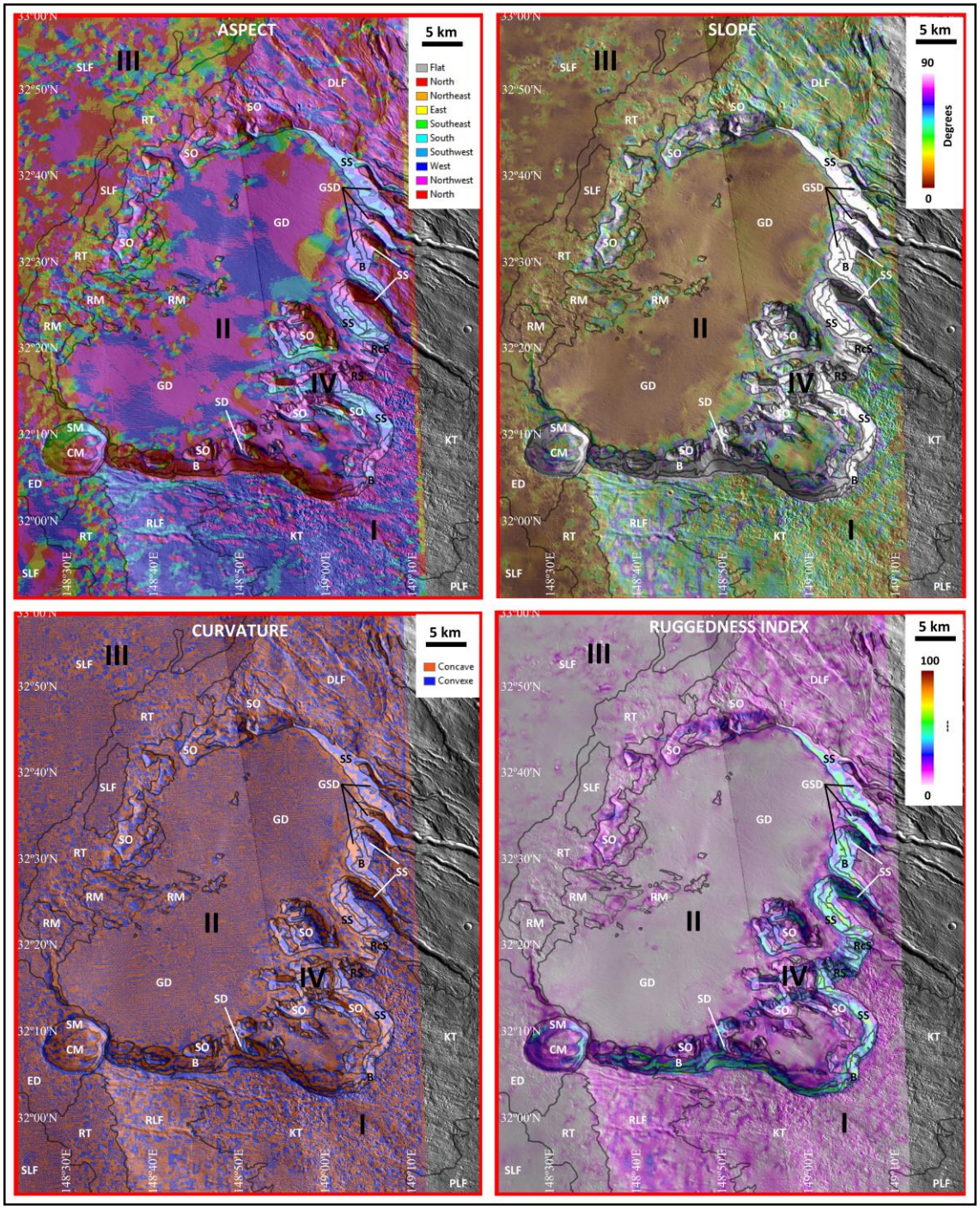

Fig. 4.10: Aspect, slope, curvature and ruggedness index maps. Sectors with similar behavior are observed: Sector I: the flank of the volcano; Sector II: the floor of the depressions on the lower part of the flank; Sector III: the plains surrounding Hecates Tholus volcano; Sector IV: the walls of the depressions and main impact craters.

The curvature map (Figure 4.10) shows that all the study area is characterized by convex terrains, with higher variability on sector I and IV, and lower on sectors II and III. In the case of Sector 2, where GD unit has been mapped related to LDA and possible moraines do not show a clear convex curvature different than the curvature we observe in other units not related to glacial activity, like SLF.

Terrain ruggedness index (TRI) map (Figure 4.10) shows a similar pattern. TRI is low for Sectors II and III, although less variable on the first one. Sector I shows mean TRI values, and Sector IV shows the higher ones. In spite of those differences, all the study area, except Sector IV, could be considered as level terrain (elevation differences lower than 80 m), meanwhile Sector IV is nearly level (80 to 116 m in difference) to slightly rugged (115 to 160 m in difference), following the terms generally used (see Riley et al., 1999).

In spite all those differences observed in the spatial distribution of each parameter, the mean values of aspect and curvature made indistinguishable the different units, although the first one shows a higher variability. Something similar occurs with aspect (due to the location and relief characteristics of the study area) (Figure 4.10). On the other hand, mean slope and rugossity values remain low for volcanic and glacial units and higher for slope units.

4.4.3. Catchment slope and area

Calculated catchment for the entire study area (Figure 4.11) shows, such as expected, a similar pattern than slope, with Sector IV, related to the wall of craters and depressions, showing the higher values. On the other extreme, sectors II and III shows lower values related to the flatter areas in the floor of the depression on the flank of the volcano, and the volcanic plains surrounding the Hecates Tholus edifice. Here the catchment slope is also more variable than in the case of Sector II. On the other hand, Sector I shows low variability and similar values than the other sectors.

Catchment slope map shows a scarcely defined pattern. At selected sites of Sector I there are alignments what correspond to graben dissecting the western flank of the volcano, related to RLF unit. In Sector II, related to GD unit where the slope is low and almost constant, elongated and radial patterns cross the bottom of the depressions, from SE to NW, from the mouth of the valleys reaching the depression, where the putative glaciers flowing from the flank of the volcano reach the inner plain of the depression.

This “radial” pattern in the catchment slope map supports the idea of a glacial origin from GD unit. A milimar pattern could also result from other processes or environments, as alluvial fan, but accumulation of glacial evidences suggest that some outwash deposits are the most likely origin of this pattern.

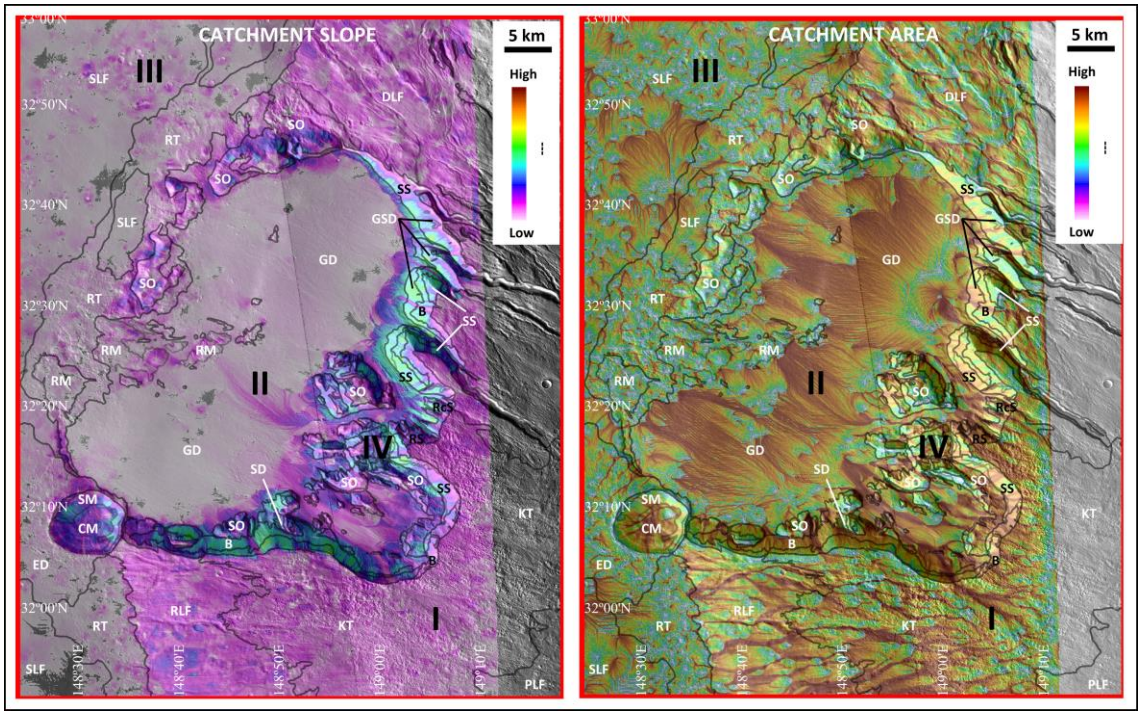

Fig. 4.11: Catchment slope and area maps of the lower NW flank of the Hecates Tholus volcano, Mars.

On the other hand, catchment area map (Figure 4.11) shows greater variability of patterns between the different sectors. Meanwhile the pattern existing on Sector III is completely random without general and defined areas of accumulation, Sector I is characterized by the presence of lineated areas of accumulation coincident with the channels dissecting the flank of the volcanic edifice, forming a dentritical network. This pattern is also visible in RLF, KT and PLF units, where de Pablo and Centeno (2012) mapped shallow and discontinuous channels based on CTX images. This pattern extends to Sector IV showing the preferential areas of accumulation of the flow, from the flank of the volcano toward the floor of the depression.

Sector II shows a completely different pattern respect the others, with an evident SE-NW distribution of the accumulation areas, in most characterized by groups of accumulation lineation with parallel to radial distribution, spreading from the mouth of the main valleys that reach the depression. Those areas of accumulation end at the western edge of the depression, in the limits of GD unit. In fact, those areas of flow accumulation are well correlated to the

morphology observed in the images, where reliefs stop or divert the flow. This behavior agrees with the interpretation of GD unit like debris-covered glaciers what flowed through the walls and floor of the depression, from east to west or northwest (Neukum et al., 2004; Hauber et al., 2005; de Pablo and Centeno, 2012).

4.4.4. Solar heating

The surface aspect and the relief is here used to approach the anisotropic diurnal surface heating (e.g., Bhöner and Antonic, 2009), that could have a role on the ice preservation in glaciers. The resulting maps (Figure 4.12) shows, as expected, a clear difference in between the northern- and southern-facing slopes, as well as the flatter slopes.

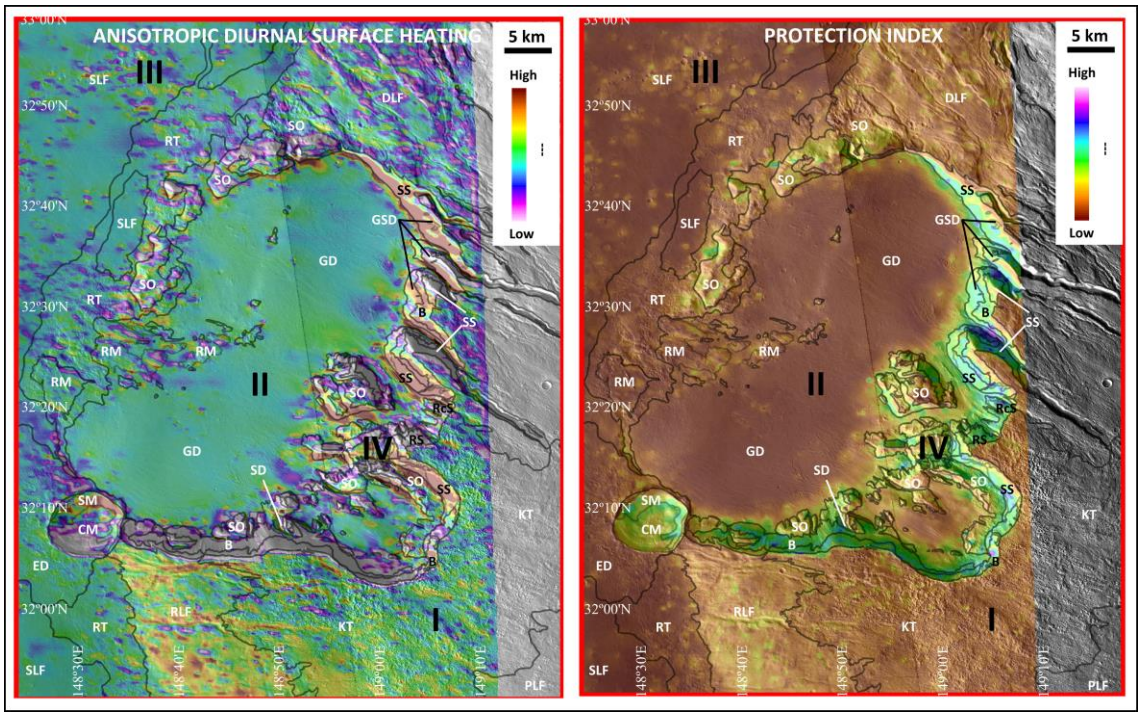

Fig. 4.12: Maps of anisotropic diurnal surface heating and protection Index of the lower NW flank of the Hecates Tholus volcano, Mars.

Sector I shows more variety than the previously described morphometric parameters due to the gradual change on the flank aspect. Consequently, the westernmost part of the flank shows higher heating values than the northwestern part. Sector II has the most continuous and homogeneous distribution of the heating values, although with slightly lower values at the northernmost sector of the depression bottom. On the other hand, Sector III shows the most variable heating values, probably due to the reported behavior and spatial distribution of the ruggedness in the area. Finally, Sector IV shows the most extreme variability on heating values due to the aspect of the walls marking the edges of the depression on the

flank of the volcano. In spite of these spatial patterns, the mean values do not allow to relate any unit to a selected solar heating, although we would like to point that gullies unit (GsD unit) shows the higher mean solar heating of the mapped units (Figure 4.12).

The protection index (Yokoyama et al., 2002) adds an interesting variable to the investigation of ice preservation. Although the surface heating directly depends on slope aspect, the relief variations plays an important role too because the surrounding reliefs could help to protect the surface and any ice mass from the direct sun's heating, in spite the aspect could be not favorable. The protection index shows how the depression walls and their nearest areas have high protection index values, meanwhile the flat areas of the floor of the depression and the surrounding volcanic plains are completely exposed and not protected by any surrounding relief.

4.4.5. Topographic profiles

The transverse and longitudinal topographic profiles of the study area (Figure 4.13), shows the convex topography of the lower flank of the Hecates Tholus volcano (profiles A1, A2, B3, and B6), as well as the flat surface of surrounding volcanic plains (profile A5). However, the detailed analysis of the profiles allows characterize the GD unit and the possible glacial related features.

Transverse to flow profiles are very different when close to the depression limits or cut across the center of the depression. Close to the limits these profiles show an irregular topography and capture the shape of the valleys reaching the main depression (profile A2), that, considering the low resolution of the topographic data, seems to have a U-shaped section. On the other hand, profiles across the depression center (profile A3) show a soft convex profile. However, near the northwestern edge of the depression (profile A4), the topographic profile shows a more variable behavior, remaining flat and smooth the northeastern half, and flat but slightly rougher at the southwestern half of the depression.

Longitudinal to flow profiles also show similar smooth and convex surface at the bottom at the floor of the depression, mainly near the eastern walls (profiles B2, B4 and B5), meanwhile the outer terrain shows rougher surface. Other profiles also show a topographic step on the floor of the main depression (profile B3) with rough terrain between the step and the western edge of the depression. This step is not visible on other sectors of the depression, where the smooth and convex surface reaches the edge of the depression (profiles B4 and B5).

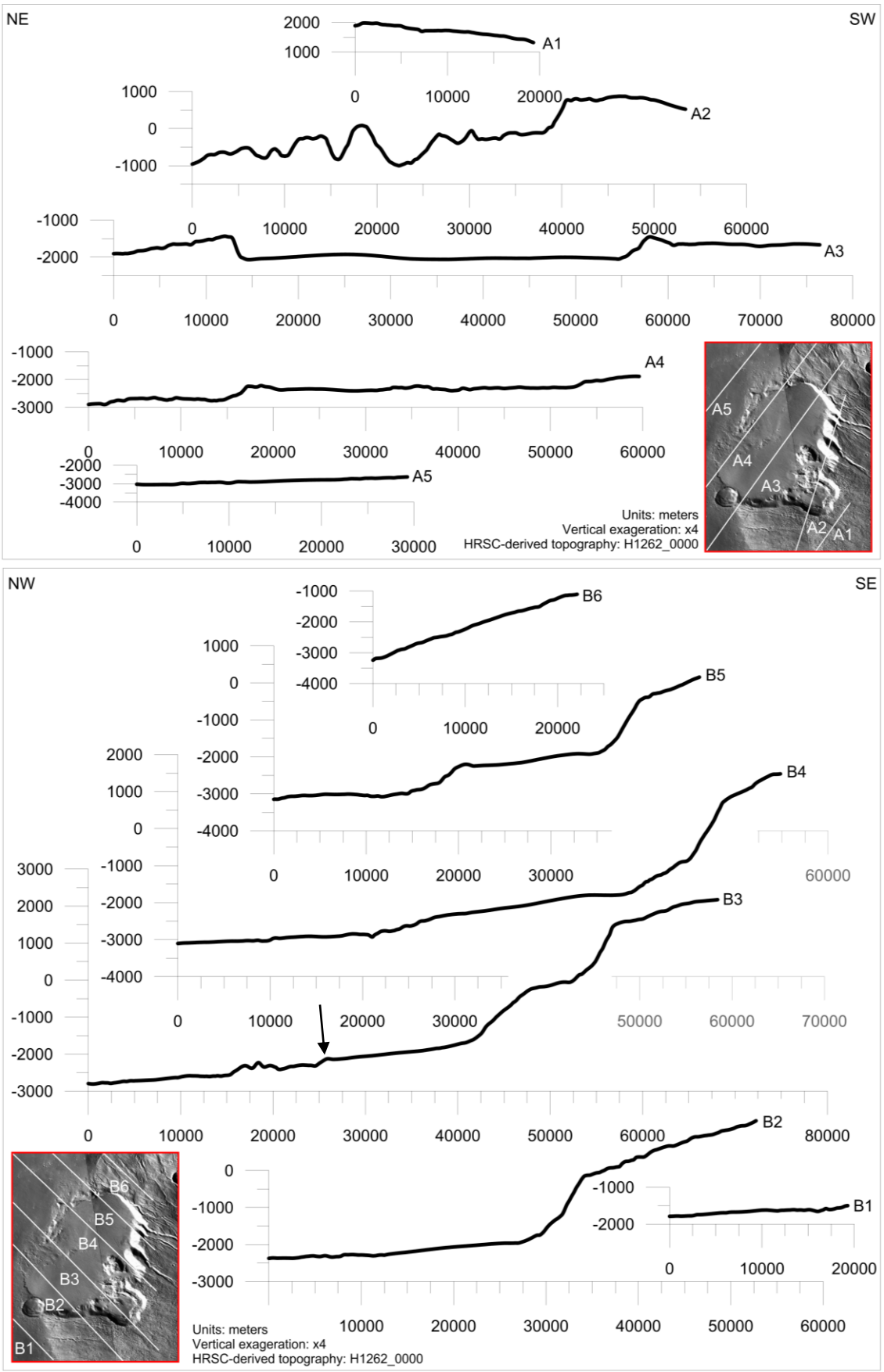

Fig. 4.13: Topographic sections crossing the main depressions at the lower NW flank of the Hecate Tholus volcano (top), and along the flanks slopes (bottom), based on a HRSC-derived DTM. Arrow marks the position of a topographic step at the bottom of depression B.

4.4.6. Valleys cross sections

The northeastern wall of the depression is dissected by three valleys. In the topographic profiles they show smooth slopes and U-shape with a narrow flat floor (Figure 4.14).

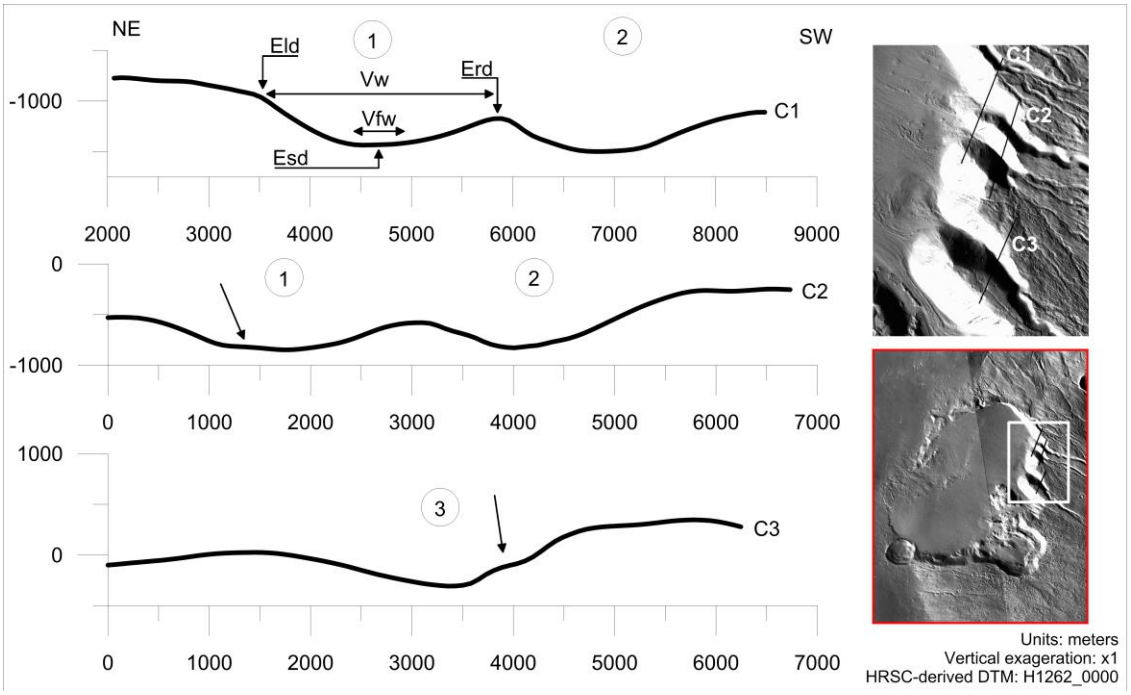

Fig. 4.14: Topographic sections crossing the main depressions at the lower NW flank of the Hecate Tholus volcano (top), and along the flanks slopes (bottom), based on a HRSC-derived DTM.

To support the visual morphological analysis, a power-law fitting analysis of the HRSC-data was done (Harbor and Wheeler, 1992; Pattyn and Huele, 1998; Schaefer, 2011). First, we isolated the valley data by a fourth-order polynomial fit (Table 4.2), and the high correlation coefficient agrees with the adequate extraction of the valleys shoulders (e.g., Schaefer, 2011). Secondly, we used those topographic data on the power-law fit (Pattyn and Huele, 1998), returning b-values near 2 (Table 4.3), typical of the glacial valleys (Svensson, 1959; Graf, 1970; Hirano and Aniya, 1988; Jiao, 1981; Liu, 1989, which *b* value ranges between 1.5 and 2.5 (Graf, 1970; Doornkamp and King, 1971; Aniya and Welch, 1981; Jiao, 1981; Liu, 1989; Li et al., 1999). Those values increase downslope when calculated at different cross sections for the same valleys. Those results support the glacial interpretation of these valleys. Only one b value is out of the glacila valley range, but it can be realted to a former fluvial origin of the valley, such as others described on the flanks of the volcano (e.g., Gulick et al., 1997). Based on this evidence, we suggest that most valleys had a fluvial origin but they were later modified by glacial processes.

Table 4.2: Coefficients of the second- and fourth-order polynomial fit to the HRSC topographic data for each valley, and the correlation coefficient.

Section	Valley	x4	x3	x2	x	a	R2
C1	1	-5E-11	8E-7	-5E-3	-5E-2	11.716	0.9962
	2	-4E-11	1E-6	-1E-2	-1E-2	40.934	0.9965
C2	1	-1E-11	7E-8	7E-5	7E-5	-0.5952	0.9914
	2	-1E-10	2E-6	-1E-2	-1E-2	29.026	0.9943
C3	3	-9E-11	1E-6	-6E-2	-6E-2	12.49	0.9905

Table 4.3: Results from power law fitting to the HRSC-derived topographic data of different cross sections of the three studies valleys.

Section	Valley	a	b	x()	y()	R2	RMSE
C1	1	4.58E-05	2.26	1.25E+03	5.70E+02	0.981662	17.678114
	2	1.25E-03	1.80	9.52E+02	4.94E+02	0.985968	11.930579
C2	1	2.61E-04	1.96	1.17E+03	1.15E+03	0.989024	9.190439
	2	5.82E-03	1.58	8.86E+02	1.17E+03	0.994326	7.565323
C3	3	9.33E-04	1.83	9.70E+02	1.71E+03	0.978771	20.772657

In spite of the indisputable results of the polynomial and power law fittings, other calculated parameters used to distinguish fluvial from glacial valleys, based on the measurement of valley dimensions (Figure 4.13), do not as clearly point toward a glacial origin. Low values (typically near 0) of the Valley height-width ratio (Vf) are interpreted to be related to “V”-shaped valleys on active uplift and deep linear stream incision (Bull an McFadden, 1977; Pedrera et al., 2009). Our calculations returned low values but still nearest to 1 (Table 4.4).

The lower result we obtained (0.51) corresponds to the section in which we already obtained the lower b-value on the power law fitting, what is coherent with a less effective glacial sculpt of the valley. The calculated Form shape (FR) values are lower than 0.22, inside the typical range of values of 0.1 – 0.3 proposed by different authors (e.g., Jiao, 1981; Hyrano and Aniya, 1988, 1989, 1990; Li et al., 2001). Those FR values are also different from each slope of the valley (Table 4.4). This asymmetry on FR values is also observable in the topographic profiles (Figure 4.14), where north-facing slopes are, in general, gentler. However, the HiRISE images show that in many valleys of the entire study area shows higher slope and rock outcrops on the north-facing slopes, and slope deposits and gentler slopes on the south-facing slopes.

Table 4.4: Results from power law fitting to the HRSC-derived topographic data of different cross sections of the three studies valleys.

Section	C1		C2		C3
Valley	**1**	**2**	**1**	**2**	**3**
Eld (m)	-964	-1192	-579	-586	-76
Erd (m)	-1175	-1204	-594	-476	207
Esc (m)	-1436	-1498	-848	-828	-306
Vfw (m)	306	229	302	151	228
Vw (m)	2293	1987	2345	1966	2361
Vf	0.83	0.76	1.15	0.51	0.61
FR_l	0.21	0.15	0.11	0.12	0.10
FR_r	0.11	0.15	0.11	0.18	0.22
b	2.26	1.80	1.96	1.58	1.83

4.5. Discussion: past and present glaciers

4.5.1. Glacial geomorphology

Among a wide variety of mapped geomorphological units (de Pablo and Centeno, 2012) GD and RM units are directly related to glacial processes as we described. In addition we cannot discard that glacial processes may ahave play an important role on the detected resurfacing events of several units –specially those related to Hecates Tholus volcanic activity (as DLF unit).

The study area elevation ranges between 3000 to -3500 m. GD and RM units are only distributed between 1000 and -3000 m in elevation. This range on elevation includes the glacial deposits located inside the channels dissecting the lava flows on the flank of the volcano, although they represent a small percentage of the complete GD unit. In fact, the mean elevation of GD unit is located at -2000 m (Figure 4.9), since the extensive area mapped like GD unit is located inside the two nested depressions on the flank of the volcano, between about 200 and -2500 m in elevation.

Originally, this unit was mapped including the smooth terrain dissected by multiple elongated scarps and lineated valley fill (LDA and LVF; Head et al., 2010 and references therein), and the rough and hummocky surface, interpreted to be accumulation of debris material (including erratic blocks) on the front of the putative glaciers infilling the nested depressions (Figure 4.5). Considering the hummocky texture and their location on the front of

the smoother area dissected by LDA and LVF features, three interpretations about the origin of GD unit are possible:

1) In the first case, debris material forming the rough and hummocky terrain could be the result of debris accumulation due to rockfall activity on the surrounding valleys walls (Whalley et al., 1996), latter accumulated at the front of the glacier after a long time of travel on top of the glacier tongue. In this case, the putative glaciers on the study area should exist on present day below these deposits.

2) On the second hand, although the origin could be the same, they could remain accumulated on the front of the glaciers once it completely disappeared by ablation, forming an extensive field of till, although ice lenses could exist in the core of these deposits.

3) On the third case, the debris material formed below the glacier due to basal erosion caused by meltwater flowing below the ice. If we are able to observe it is because the glacier already disappeared in this area.

Presence of some here described glacial features on the area allow us to favour the second and third cases, and reject the first one in which the ice still remain below these materials at the western sector of the depressions. Rochee moutonèe and pingos are the main evidence of the complete ablation of the glacier at that sector. Rochee moutonèes are erosive landforms formed below the glacier, and Pingos are periglacial landforms formed on cold areas with permafrost, but without glacial ice.

In addition, to further elements help us to discard the presence of ice in the western sector of depression B. The SW-NE topographic step across the main depression (Figure 4.8, Figure 4.10 and Figure 4.13) could be the result of glacial ice ablation. The disappearance of the ice could cause the sedimentation on the floor of the depression of the debris materials what travelled on top of the glacier, or the discovery of the basal debris materials originally covered by the glacier. Then, the topographic step could indicate that the eastern sector still contains an important amount of ice buried by debris material.

The second one is the distribution of the moraines (Figure 4.5), only at the eastern two thirds of the depression just until the topographic steep at about -2150 m in elevation (Figure 4.8, Figure 4.10, and Figure 4.13). Since those materials are moraines, and they extend from more than 15 km from the base of the depression's walls, there are not reason for their

disappearance just at that distance, except, from our point of view, if the glacier was already ablationated. Therefore, when the glacier extended further (see de Pablo et al., 2013 for a reconstruction of the glacier evolution), the eastern part of the depression should also be covered by the glacier. After its ablation, the debris material and moraine materials should be deposited on the floor of the depression, together with the subglacial debris materials losing their original morphology and distribution patterns to result in the present hummocky terrain (till deposits), as well as the discovery of the rochee moutonées (as pointed by de Pablo et al., 2013).

4.5.2. Relict glaciers

The rough and hummocky surface at the western sector on the floor of the depression at the flank of the volcano has been interpreted as till deposits, meanwhile the other sectors of the GD unit could represent debris covered glaciers (de Pablo et al., 2013). We already mentioned the topographic step what separate both sectors, as seen on the topographic profiles of the area (Figure 4.13), what could mark the terminus of the glaciers.

The analysis of topographic data (Figure 4.10) show clear differences between the volcano flanks (Sector I), volcanic plains surrounding the edifice (Sector III), the walls of the depression (Sector IV) and the floor of that depression (Sector II). At this scale, we are not able to see clear differences between the till deposits and the debris-covered glaciers, that could be related with the relative lower resolution of the DTM respect the HRSC, CTX and HiRISE images we used. However, aspect and slope maps shows differences at the easter sector of GD unit, directly at the base of the depression's walls and the mouth of the valleys, revealing a fan-like morphology, also marked by abundant moraine landforms (Figure 4.5). Topogaphic profiles (mainly sections B4 and B5 in Figure 4.13) also show a convex area immediately at the base of the walls.

This morphology is compatible with different processes, including slope mass wasting, alluvial fan and piedmont glaciers. However, considering the geological setting, we favor the glacial origin. Taking into account all those observations, the presence of relict glaciers in the area is feasible. This observations, contribute to the main evidence, what is the presence of possible crevasses and bergschrunds: fracture like landforms that should disappear in case all ice were already completely ablated. Then, if crevasses and bergschrunds are observable in HiRISE images, it means that at least relict glacial ice still remain below the debris, till, dust and/or pyroclastic material what seem to cover the surface on present day. In fact, those areas

show low anisotropic diurnal surface heating and medium protection index, as derived from the HRSC-derived DTM (Figure 4.12). However, the other parts of GD unit show similar surface texture and contains crevasses. Then, relict glaciers can extent to the easternmost 2/3 of the GD unit, west to the already mentioned topographic step. In fact, buried ice has been proposed to exist few meters below the surface (Helbert et al., 2005) based on the protection effect of the mantle covering the surface.

4.5.3. Glacier flows

As we said above, the presence of crevasses is a fair evidence of present existence of ice (their conservation after ice melting being very difficult). But the existence of the main type of crevasses (Figure 4.15) related to compression and extension of the ice is response of ice flow (e.g., Holdsworth, 1956; Van der Veen, 1990, Bennet and Glasser, 2009) suggest that ice is still flowing, even if we can´t measure it.

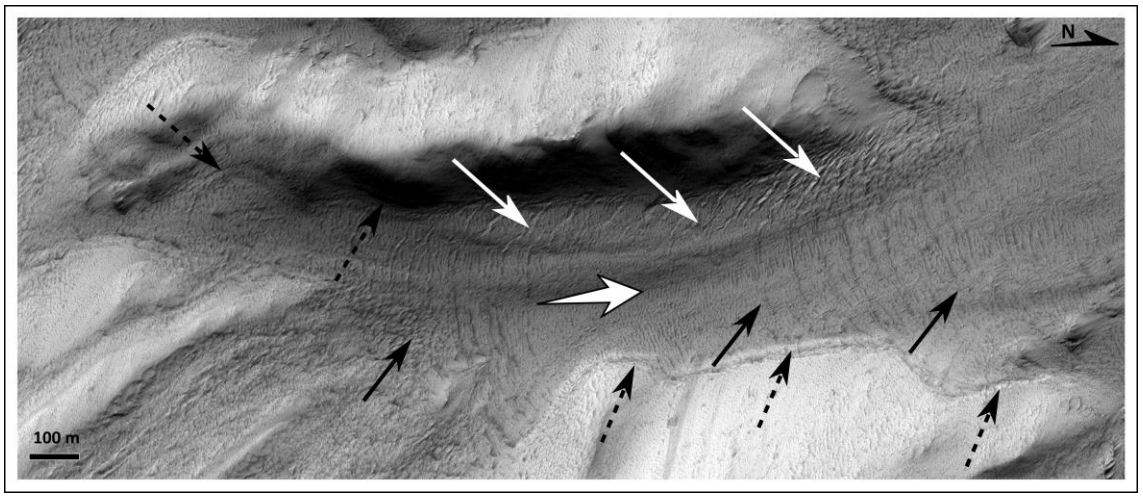

Fig. 4.15: Transverse crevasses (black arrows), chevron crevasses (white arrows) and bergschrund (black dashed arrows) on a glacier at the southern wall on the main depression at the flank of Hecates Tholus volcano, as seen on esp_027029_2125_red HiRISE image. Interpreted glacier flow toward the north (central white arrow). Image centered at 32.146ºN, 148.775ºE.

On the volcano flank, the higher catchment area reach maximum values on the floor of the valleys dissecting the flank (Figure 4.11), as expected. However, on the smoother surface of GD unit on the floor of the depressions, values increase following a radial pattern at the mouth of the valleys dissecting the walls of the depression, but also extend downslope to the northwest of the depression. Areas in which this increase on values remains parallel are observable (Figure 4.11), and we interpret this pattern as the areas corresponding to different glacial tongues. Most of them finish at the SW-NE topographic step crossing the depression. However, in few cases they extent until the NW edge of the depression. This pattern is also observed on the spatial distribution of moraines (Figure 4.5).

This catchment area map agrees with the idea of multiple pulses of advance ad retreat on the glaciers, as well as a complex glacial dynamics (de Pablo et al., 2013) due to the presence of different possible glacial tongues in the area, what require a detailed analysis to refine the glacial evolution on this region.

4.5.4. Glacier thermal regime

Present conservation of crevasses and bergschrunds on the eastern sector of the depression seems to support our model in which the ice still remains on that sector, but melted on the western sector, as it was already discussed by de Pablo and Centeno, 2013.

However, these glacial features, and the already discussed till deposits, open the discussion about the thermal regime of the glaciers in this area. Hambrey and Glasser (2012) summarized the main characteristic of temperate (warm or wet) glaciers, cold (dry) glaciers, and polythermal glaciers, although exceptions to the general behavior of each type of glaciers had been also described. The type of thermal regime of the glaciers on the lower NW flank of the Hecates Tholus volcano is not easy, but, based on our observations, they were temperate glaciers.

Mapped eskers on the study area point to the presence of relative abundant melting water, that it is typical of temperate glaciers. This type of glaciers is very effective on erosion on the valley walls, accumulating important quantities of debris on their surface, but not below the surface, with thin subglacial till deposits. Presence of hanging valleys, rochees moutonèes and flutes and smooth outcrops (SO unit) at different sites could be evidences of an effective erosive glacier, like temperate glaciers. As we discussed above, the hummocky terrain (till deposits of eastern part of GD unit) on the eastern edge could be related to accumulation of basal, surficial or both debris materials, what explain their abundance. Then, based on those observations, we consider that the evidences point toward temperate glacier, in spite supraglacial meltwater evidences has not been observed on HiRISE or MOC images.

This thermal regime could be initially opposite to the environment in which the glaciers in the lower NW flank of the Hecates Tholus volcano could be formed. However, we should remember that 1) not all the glaciers formed during a glaciation are cold glaciers, 2) the glaciers could evolve from cold to temperate thermal regimes, and 3) some of the observed glacial features we observe are remants of the different episodes of the glacier, and mostly of the last events. In fact, ages of the main glacial events in these glaciers (Neukum et al., 2004; Hauber et al., 2005; de Pablo et al., 2013) seems to be related to the last ice ages on Mars. It

means cold conditions at the mean latitudes in which Hecates Tholu is located. In fact, de Pablo and Centeno (2013) proposed important events of increase on ice accumulation, and consequently increase on glaciers extension and thickness. In those conditions, like occurred on Antarctica, glaciers with cold thermal regime seem to be the most feasible. However, although under extremely low surface temperatures, the geothermal heat-flux could not be overcome to produce cold glacier if they are thick enough (Hambrey and Glasser, 2012).

We do not have evidences of the present thickness of the hypothetical glaciers filling the depressions A and B. However, the walls of the depression where hanging valleys are located, are as high as 500 meters. Therefore, considering the steep observed on the topography (profile B3 on Figure 4.13), the total thickness of the glaciers could reach more than 600 meters, what is much more than the thickness of Antarctic glaciers on the edge of the continent, where cold glaciers could exist due to the cold conditions and thin thickness (Hambrey and Glasser, 2012).

On the other hand, we do not discard a high geothermal flux like other factor affecting the existence of temperate glaciers on the study area. The volcanic origin of the study area is enough to consider this possibility, as well as the existence of multiple volcanic events, some of them as young as 350 Ma (Neukum et al., 2004; Hauber et al., 2005; Werner, 2009; de Pablo et al., 2013), as well as episodes of activity that melted the ice cap on the summit of the volcano (e.g., Gulick et al., 1998; Fasset and Head 2006, 2007).

4.5.5. Glacier dynamics

In order to have a first approach to the glacier dynamics, we analyzed the b and FR parameters, as proposed by Hirano and Aniya (1988), for the several valleys of the study area (Figure 4.14). The b-FR correlation (Figure 4.16) agrees with the “Patagonia-Antarctic” evolutionary model where ice sheets excavated wide valleys, characterized by large b values and low FR (Hirano and Aniya, 1988), what agrees with the extensive valleys and glaciated surface we observed in the study area (e.g., Neukum et al., 2004, Hauber et al., 2005; Werner, 2009; de Pablo and Centeno, 2012). However, the results do not return a discernible trend. For that reason, to derive an evolutionary conclusion is not appropriate (Harbor, 1990; Augustinus, 1992, 1995; Li et al., 2001; Brook et al., 2005), especially taking into account the limited data we used, the relative low resolution of the DTM and the models were been developed based only on terrestrial data.

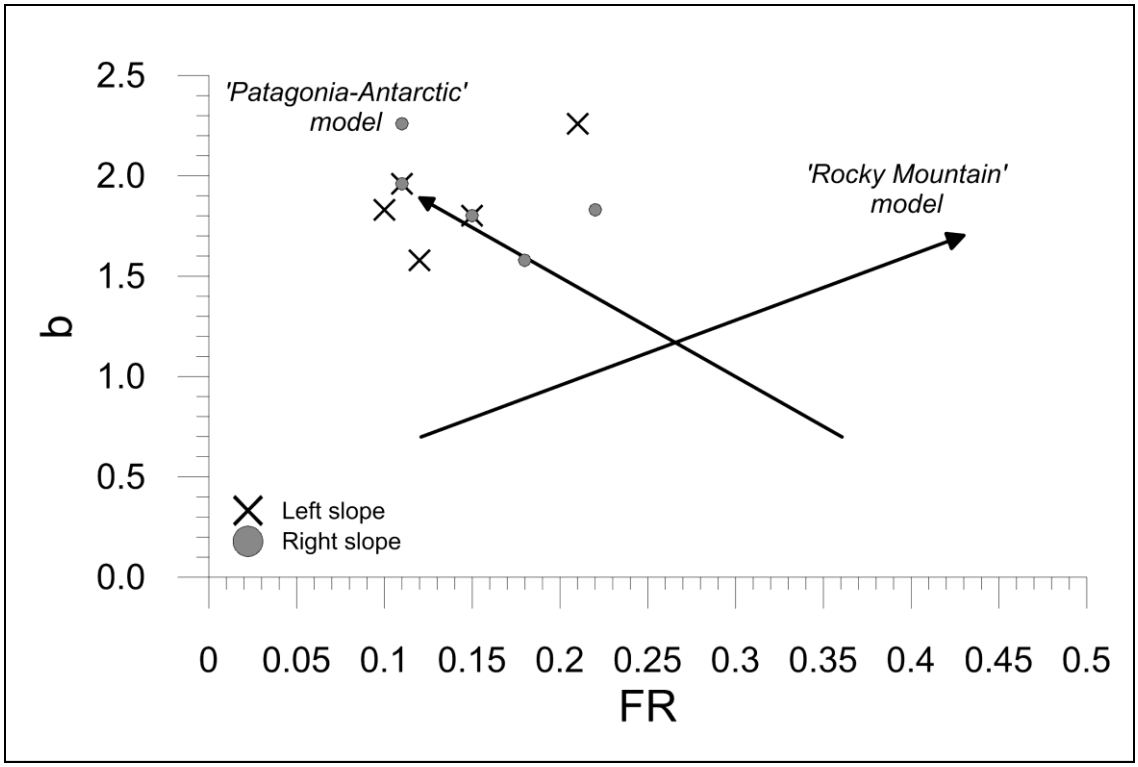

Fig. 4.16: Plot showing b-FR parameters calculated of left and right slopes of 3 different valleys dissecting the eastern wall of the main depression at the flank of Hecates Tholus volcano (see Figure 4.4.14). Arrows show the expected correlations between those values on the Patagonia-Antarctic and Rocky mountain type of glacial valleys, as proposed by Hirano and Aniya (1988).

This limited morphometric analysis of the three glacial valleys reaching the depression points toward a complex origin with glaciers resurfacing older fluvial valleys. In fact, cross sections across of the valleys shows a scarp on the slope (see arrow on sections C2 and C3 in Figure 4.14) that we are not able to interpret: an eroded fluvial terrace or a spur on the glacial valley are the most likely interpretations. Both interpretations are feasible and agree with the context and the possible fluvial and glacial origin and modification of the valley. The observations on HiRISE images also reveals the existence of flat areas near the floor of the valleys, but due to the heavily erosion and dust/fine-grained materials accumulation in the area, it is not possible for us to discern between the fluvial and the glacial origins.

4.5.6. Interstitial ice

Apart from glacial ice, important quantities of buried ice could exist in the area filling the pores or instersticial pace of sediments and slope materials, especially in the area with higher thermal protection index. The obvious asymmetrical difference in walls heating (Figure 4.12) could be the responsible of the asymmetrical distribution of slope features observed in the HiRISE images (Figure 4.17): Lobated sloped deposits, corresponding to the mapped Creep Deposit unit (CD unit), slope creeping marks and smooth homogeneous mantle slope deposits,

partially corresponding to the Smooth Slopes unit (SS unit). All of them are widely distributed by the depression walls as well as valleys slopes.

Creep Deposits slope unit is characterized by rough deposits generally located at the lower part of the slopes, with undulated to wavy surface. Bottom limit is smooth and sometimes indistinguishable from valley's floor deposits, but the upper limit is irregular, contrasting with the smooth slope deposits (Figure 4.17). In all cases, Creep Deposits are located on west- and south-facing slopes. In most of the cases, they are related to slope creeping marks: narrow (less than 2 m wide) and short (typically short than 100 m) lineal marks widely distributed at middle to lower of valleys's slopes and depression walls, forming parallel trains with variable separation, but in the range of 2 to 15 m, normal to the slope (Figure 4.17).

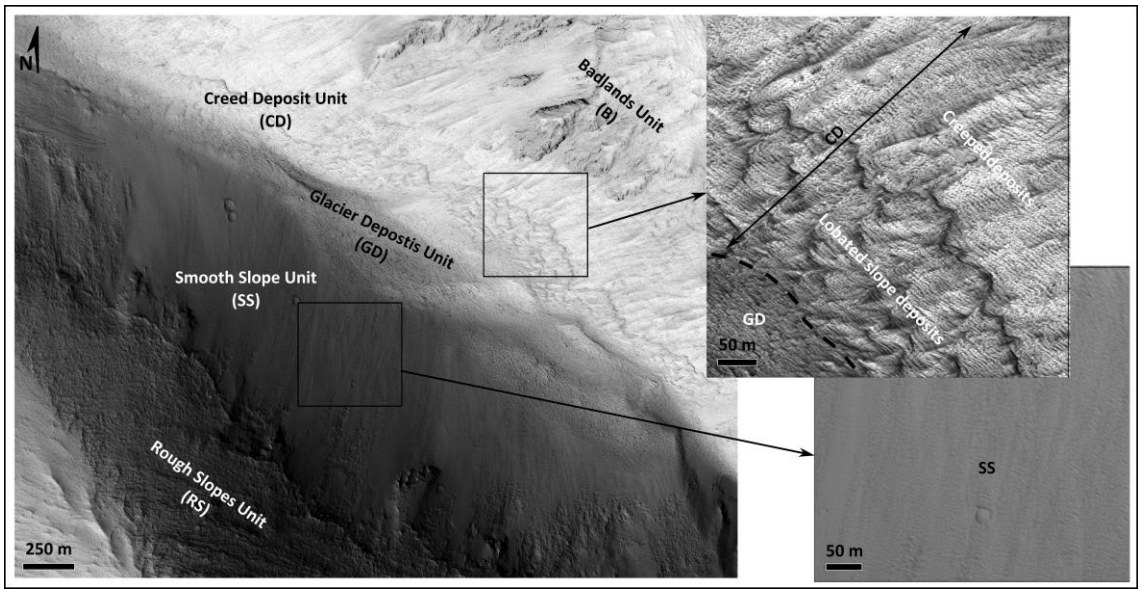

Fig. 4.17: HiRISE image (esp_024418_2125_red) showing the asymmetrical distribution of smooth slope deposits (north-facing flank), and creep deposits (south-facing flank) and details to show how creep deposit unit (CD) could be divided into lobatated slope deposits, and creeped deposits theyself, both marked by the presence of sloep creeping marks (SCM), what does not appear in smooth slope unit (SS).

They are not only related to CD unit but to any kind of materials on the west- and south-facing slopes and walls. Both CD unit and slope creeping marks are related to relatively low protection index and high solar heating areas in the above described maps. We could not discard other origin for those marks, such as aeolian deposits due to the extensive distribution of dunes and other aeolian deposits everywhere in the study area, but we favor the creeping origin due to high their aspect constrains in slopes and walls.

On the other hand, Smooth Slope unit (SS unit) mapped by de Pablo and Centeno (2012) by the use of CTX imagery (Figure 4.4) looks very different in HiRISE images. In some cases, they do not look like slope deposits, but like cemented sheet deposits. Its higher apparent cementation stage is observable by the presence of fractures, showing scarps with subvertical wall of few meters in height. Although the distribution of this material is not as frequent as the SS and CD units, when it exists it is related to north-facing slopes on narrow valleys, and, in some cases, only restricted to the lower part of the slopes. Those sites correspond with high protection index and low solar heating values on the above described maps. Shallower and/or wider valleys in the study area also show the asymmetric distribution on the materials, with CD unit and slope creeping marks on the south-facing slopes, but without cemented materials on the north-facing slopes, probably due to the lower topographic protection and the consequent higher solar heating. In fact, in some cases, although less evident than in the other slopes, deposits from possible creeping on (not completely similar to CD unit materials) the north-facing slopes is also observable only in few selected cases.

Gully deposits (GsD unit) have also important aspect dependence, like occurs in many other sites of the planet (Malin and Edget, 2000, 2001; Edget et al., 2003) since they are only observable on west and south-facing slopes, in relation with relatively high solar heating index values. In the study area, there are a dozen of gullies observed on CTX and the few available HiRISE images. They are characterized by a dark-toned surface, but not thick deposits such as in other Martian gullies, without apron deposits. Their apex are located few cents of meters below the valleys and depression walls and scarps, and could extend for more than 1 km downslope until reach the floor of the valleys. The direct relation between GsD unit and solar heating is revealed the relative higher mean values respect all the other mapped units in the study area (Figure 4.9), what is other observation what could help to explain their locations.

Considering the geological setting, we interpret those slope cemented deposits, and Slope creeping marks such as the result of the differential solar heating on the walls and slopes of the area due to their slope angle, aspect and relative low protection by the surrounding reliefs. In the same way than gullies has been classically related to slopes with higher isolation rates (e.g., Malin and Edget, 2000, 2001; Edget et al., 2003; Christensen, 2003; Heldmann and Mellon, 2004; Dickson et al., 2007; Dundas et al., 2012; Harrison et al., 2015), CD unit could be the results of the creep movement of the slope materials. However, their dependence to the aspect, in our opinion, indicates the existence of water on the porous of those slope materials. Its melting due to the solar heating could facilitate the downslope creep movement. The

presence of slope creeping marks on the same walls (not only related to CD unit) could be other indicative of this process, as well as the absence of both CD unit and SCM on the north-facing slopes but, when it appears, the cemented deposits.

To explain the existence and distribution of all these features, we propose a model (like a working hypothesis to be tested when new data will be available) in which the surface is covered by mantle deposits with an aeolian, pyroclastic, slope or mass-wasting origin, which could contain some quantities of water in the porous, freeze and cementing the fine-grained materials. The differential solar heating in the area could allow to those deposits, when not eroded, to remain in the north-facing, topographically protected and low heated slopes, forming the above describe slope cemented deposits. However, on the west- and south-facing slopes, with lower topographic protection and the consequently higher solar heating, the ice melts allowing the downslope movement of the fine-grained materials (creeping). This movement produces extensive creeping marks on the slopes. Due to a long duration of this process, the higher slopes and/or the thicker deposits, the materials moved downslope more quickly to form lobated and wavy deposits, mainly at the middle and lower parts of the slopes (CD unit). Since the slope creeping marks are also observable dissecting the CD unit materials, it means that this process repeated also after the lobated deposits formed.

This model, is compatible with the classical conditions required for gullies formation on the sun-facing slopes, and agrees with the different observations and models about the presence and distribution of ice-cement materials, ice-rich deposits, layering mid-latitudes deposit during the recent ice-ages on Mars (e.g., Carr, 1982; Mellon and Jakosky, 1995; Mustard et al., 2001; Milliken et al., 2003; Kostama et al., 2006; Schon et al., 2009).

4.6. Conclusions

A detailed analysis of HiRISE, MOC, CTX and HRSC images allowed to provide a detailed description and interpretation of the 18 different geomorphological units what were mapped by de Pablo and Centeno (2012) on CTX images of the lower NW flank of the Hecates Tholus volcano, as well as to briefly describe the wide variety of geomorphological landforms they mapped, but also others visible only on HiRISE images. To complete our research about the geomorphology of the area, different morphometrical analyses have been conducted, deriving slope, aspect, curvature, rudgeness, catchment slope and area, solar anisotropical diurnal heating ad protection index, based on the use of a HRSC-derived DTM. Finally, other detailed morphometrical analyses of different topographic valleys cross-sections has been conducted

used to discuss their possible glacial origin. This research complete and extend the previous works by de Pablo and Centeno (2012) and de Pablo et al. (2013). For that reason, our discussion is only focused on glacial- or ice-related features, trying to understand on the evolution of the glacial events, as well as on the characteristics of the glaciers of this area.

Based on those analyses, we conclude that the glacial origin of the materials at the floor of main valleys and the nested depressions at the flank of the volcano is the most feasible. In fact, we distinguish between till deposits and debris-covered glaciers, due to the morphology presence of different features like hummocky terrains or moraines, respectively. A topographic step on the floor of the depression helps to divide both terrains, as well as to point toward the possible existence of relict glaciers, covered by dust and debris deposits, in agreement with topographic sections, and slope and aspect maps.

The different glacial-related geomorphological units and element like rochees mountonèes, flutes, till deposits and moraines, among others, allowed us to discuss the thermal regime of the glaciers that sculpted this region. Although indisputable conclusion could not be provided, temperate glaciers are the most feasible. The great ice thickness of about 600 meters we suggest for the possible glaciers that existed in the area is not a problem for the existence of temperate glaciers, as occurs on many Antarctic glaciers on Earth due to the effect of the pressure and geothermal heat-flow.

Morphometrical analysis allowed us to make a first approach to the glacial origin of the glacier based on the b-FR relation of three of the main valleys dissecting the eastern wall of the nested depression at the flank of the volcano. However, we point a primary fluvial origin, in agreement with many other authors what studied the channels on the flanks of Hecates Tholus volcano.

Finally, nowadays, relict glaciers could still remain in the area due to the topographic and geomorphological evidences. However, different creep slope marks on south-facing slope, as well as an asymmetrical distribution of smooth slope deposits allow us to propose the presence of ice cementing surficial materials like slope deposits.

PhD thesis

Glacial geomorphology of the NW flank of the Hecates Tholus volcano, Mars

5

Thermal characterization

Miguel Ángel de Pablo Hernández

2015

Abstract:

Many glacial features has been described in the lower NW flank of Hecates Tholus , but there is no absolute evidence of the present existence of ice. However, debris materials in the area could be mantling an ice body, a relict of the ancient extensive glaciers that most authors recognize in the area. Previously, some authors have proposed the existence of ice lenses as shallow as 2 meters in depth. Here, we look for new evidences of buried ice using the thermal characterization of the surficial materials of the study area. We used data from the Mars Climate Database to have a first regional approach, but this research derives from the analyses of surface brightness temperature derived from THEMIS-IR both daytime and nighttime. We characterize the different sectors of the area, and try to define a pattern for each geomorphological unit previously mapped. The study of the relations between surface temperature and topography, elevation, slope, aspect, ruggedness, insulation, apparent thermal inertia, thermal inertia and general mineral composition define some thermal anomalies in the area. We discuss possible origins for those anomalies, and we finally conclude that they can reflect buried ice bodies locate on the botton of the depression on the flank of the volcano.

Resumen:

En la base del flanco Noroeste del volcán Hecates Tholus de Marte se han descrito numerosas morfologías glaciares, pero no se han encontrado evidencias indiscutibles de la existencia de hielo en la zona en la actualidad, aunque trabajos previos propusieron la existencia de lentes de hielo a tan solo 2 m de profundidad. En este trabajo se buscan nuevas evidencias de la presencia de dicho hielo enterrado bajo la superficie en esta zona. Se emplea la base de datos climáticos de Marte como primera aproximación, pero este trabajo se fundamenta en el análisis de temperatura del brillo de la superficie derivada de los datos THEMIS-IR, tanto diurnos como nocturnos. Con ellos, se ha caracterizado térmicamente cada sector del territorio de estudio, y se ha intentado establecer patrones térmicos para cada una de las unidades geomorfológicas previamente cartografiadas. Tras discutir la posible relación entre el comportamiento térmico con factores como el relieve, la altitud, la pendiente, orientación, rugosidad, insolación, inercia térmica aparente, inercia térmica, o composición mineralógica general, se ha encontrado posibles anomalías térmicas. Se discute el posible origen de dichas anomalías, que podrían estar causadas por la presencia de posibles cuerpos de hielo enterrado bajo del depósitos que rellenan las depresiones en la ladera de éste volcán.

Related publications:

de Pablo, M.A. Orosei, R., and Centeno, J.D. 2014. Looking for buried ice relict of glacial activity at the lower NW flank of the Hecates Tholus volcano, Mars. Lunar and Planetary Science Conference, 45. Abstract #1151.

de Pablo, M.A. and Centeno, J.D. 2013. Qualitative analysis of THEMIS-derived brightness temperature of the lower NW flank of the Hecates Tholus volcano, Mars. Lunar and Planetary Science Conference, 44. Abstract #1589.

Centeno, J.D. and de Pablo, M.A. 2012. Preliminary analysis of surface temperature in the depression at the lower NW flank of the Hecates Tholus volcano, Mars. Lunar and Planetary Science Conference, 43. Abstract #1097.

5.1. Introduction

The Hecates Tholus volcano (32.12ºN, 150.24ºE) is one of the three edifices forming the Elysium volcanic province of Mars (Figure 5.1), and the unique of them showing glacial-related landforms in the northwestern flank (e.g., Neukum et al., 2004; Hauber et al., 2005; de Pablo and Centeno, 2012). These features also occur in other volcanoes of Mars at similar tropical latitudes like Olympus Mons, Arsia Mons, Ascraeus Mons or Pavonis Mons (Head et al., 2005). Occurrence of relevant amounts of ice capable to form ice patches, ice caps, and glacial flows only on the NW-facing slopes has been explained by ice precipitation during high obliquity periods (e.g., Jakosky and Carr, 1985; Laskar et al., 2004; Forget et al., 2006), although ice-deposits formation at tropical latitudes during low obliquity periods has been also proposed (Levrard, 2004). These glacial events could occur both on recent times related to the last ice ages on Mars (e.g., Laskar et al., 2004; Head et al., 2003, 2005, 2006; Neukum et al., 2004; Hauber et al., 2005; Forget et al., 2006), but also in more ancient times (e.g., de Pablo et al., 2013).

Hauber et al. (2005), de Pablo and Centeno (2012) and de Pablo et al. (2013) described, mapped and dated the glacial-related landforms existing in the NW flank of the Hecates Tholus volcano by the use of Mar Orbiter Camera (MOC), High Resolution Stereo Camera (HRSC), and Context (CTX) images, but not evidences of ice at the surface has been reported. However, de Pablo and Centeno (2012) mapped some pingos in the main depression that could be indicative of existence of ice-lenses close to the surface (see Burr et al., 2009 for a detailed overview of pingos formation). In addition, there are previous works in many other sites of Mars, where pingos have been described (e.g., de Sakimoto, 2005a, 2005b; Bacastow and Sakimoto, 2006; de Pablo and Komatsu, 2008). In fact, on Earth, the ice lenses forming pingos does not require to be buried deeper than 1 meter (Mackay, 1987).

On Mars, based on crater counting technique, Hauber et al. (2005) propose that the glacial activity could have stopped about 5 Ma ago, meanwhile de Pablo et al. (2013) proposed that this glacial activity could remain also during the last ice ages on Mars, between 2 Ma and 400 Ka ago (Head et al., 2003; Laskar et al., 2004). In both cases, due to sublimation, the presence of remnant ice in the surface from the last glacial event in this area is not feasible, but Helbert et al. (2005) model that ice could exist only a few meter below the surface, protected by a mantle of sediments (till, pyroclasts or aeolian dust). Then, if ice could exist in the lower NW flank of the Hecates Tholus volcano, it could be relevant from different points of

view, including geological or volcanical among others. However, to corroborate this result is not possible by the use of visible images because the study area does not show evidences of ice on the surface, but glacial-related landforms (Neukum et al., 2004; Hauber et al., 2005; de Pablo and Centeno, 2012; de Pablo et al., 2013), what has been interpreted to mark the location of debris-covered glaciers. Then, if ice still exist in the area below the surface, other research techniques different than satellite images on visible range need to be used. Then, it is possible that surface temperature could reflect thermal anomalies on the area, and may be the few ground penetration radar sections could corroborate it.

Assuming this hypothesis, the aim of this chapter is to characterize the thermal behavior of the study area, in relation to season, elevation, aspect, materials, and geomorphological units, and to locate possible thermal anomalies what could contribute to support the numerical models what predict the existence of remnant ice lenses, or ice-rich or ice-cemented materials near the surface in the NW flank of the Hecates Tholus volcano, such as it was proposed by other authors (Helbert et al., 2005; Aharonson and Schorghofer, 2006). Complementarily, radargrams of the study area are been analyzed looking for possible evidences of buried ice in the main depression of the NW flank of the Hecates Tholus volcano, restricting our research area to 31.8ºN-33.08ºN and 148.37ºE-149.38ºE (Figure 5.1).

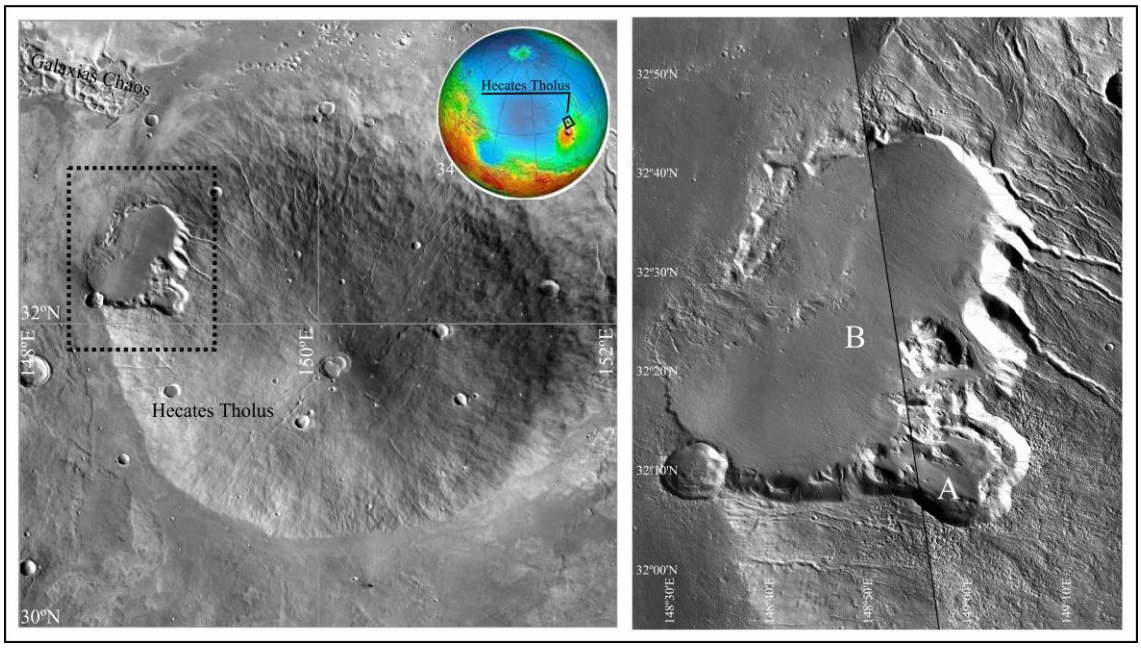

Figure 5.1: Location map of the Hecates Tholus volcano (left) on Mars, and the study area (black dash lined box) at the lower NW flank of the edifice. CTX images mosaic of the study area what includes a nested depression system (depression A and B).

5.2. Data and methods

Thermal characterization of the lower NW flank of the Hecates Tholus volcano was possible thanks to the analysis of different data. First, we analyzed the regional surface temperature by the use of the Mars Climate Database (MCD) based on climatical models supported by data from different robotic missions to Mars (Lewis et al., 1999; Forget et al., 1999). These data provided the context thermal behavior depending of the scenario: cold, warm, and the conditions existing during Martian year 24 (year during the Mars Global Surveyor mission was active around Mars), depending of the dust content in the atmosphere. We extracted 12 values for each mean monthly day provided by the database (corresponding to a 2 hours local time period at meridian 0, what are 12 pm at the study area local time zone) surface and air (about 2 meters above the surface) temperature of a 3.75º x 5.625º region in which the study area is located. We used these data to calculate maximum, mean and minimum temperature for mean day what represent each month in the database, as well as the increment on temperature (AT) and the difference between surface and air temperatures per each month.

Second, we derived surface brightness temperature (BT) from band 9 (centered at 12.57 μm) of both daytime and nighttime infrared images acquired by THermal Emission Imaging System (THEMIS) instrument on board of Mars Odyssey (MO) spacecraft mission (Christensen et al., 2004, Saunders et al., 2004). BTR products were processed under request by the use of THMPROC on-line tool developed and maintained by the Arizona State University (http://thmproc.mars.asu.edu). Processing included signal drift corrections (UnDrift/DeWobble-UDDW), image rectification (Unslant), correlated noise removal (Deplaid), automated radiance correction (Auto-radcorr), and image unrectification (Return to projected (Slanted) image). Resulting product were obtained in 32-Bits ISIS cube format, from which we extracted the projection information by the use of ISIS2World script by USGS Astrogeology, available at http://webgis.wr.usgs.gov/pigwad/tutorials/scripts/perl.htm. We developed our own batch script to conduct this operation in an automatic way (Appendix A.1.).

From the 54 THEMIS IR images available until January 2015 release, only 24 images were included into the final analyses (Table 5.1). The other images were discarded due to the low coverage of the study area (less than 15%); the errors in the image or during the processing with THMPROC, or due to they were acquired at very different solar longitudes to allow to produce homogeneous temperature maps. The resulting cover both daytime and

nighttime and they were acquired at different solar longitudes (Ls) covering all the seasons files (Table 5.1). They were integrated into a Geographic Information System (GIS) based on the use of ArcGIS software (by ESRI). The USGS Images toolbox for ArcGIS (http://webgis.wr.usgs.gov/pigwad/tutorials/scripts/)has been used to assign the projection information, obtained by ISIS2World PERL script, to each image, as well as to remove the null values from the brightness temperature images.

Table 5.1: THEMIS-IR images used on the thermal characterization of the Lower NW flank of the Hecates Tholus volcano, Mars, showing their acquirement date, Solar longitude of that date, and minimum and maximum brightness temperature of the image.

Type	Image	Date	Solar long.	Min. Temp.	Max. Temp.
Night	I05394011	3-Mar-2003	146.216	158.518	188.373
	I05731008	31-Mar-2003	160.583	89.846	160.924
	I06480019	1-Jun-2003	195.067	140.907	178.731
	I06842009	30-Jun-2003	212.963	149.714	180.225
	I06867006	2-Jul-2003	214.223	157.835	191.032
	I07204010	30-Jul-2003	231.475	150.825	178.18
	I07591013	31-Aug-2003	251.64	154.644	174.627
	I07616010	2-Sep-2003	252.943	166.736	191.578
	I09925004	10-Mar-2004	2.446	152.25	184.18
	I14817023	17-Apr-2005	194.705	95.532	170.439
	I14842018	19-Apr-2005	195.916	90.171	167.64
	I16689007	18-Sep-2005	290.491	160.764	178.109
	I23740011	22-Apr-2007	223.646	159.739	195.823
	I31813030	14-Feb-2009	209.965	151.803	184.235
Day	I02404005	30-Jun-2002	34.53	220.07	251.703
	I02429005	2-Jul-2002	35.464	215.753	252.217
	I04289002	2-Dec-2002	103.059	210.281	252.162
	I08034021	6-Oct-2003	274.696	184.129	229.299
	I09644004	16-Feb-2004	350.787	209.676	238.581
	I16695015	19-Sep-2005	290.808	163.485	195.118
	I17319013	9-Nov-2005	321.059	185.27	222.349
	I17344019	11-Nov-2005	322.221	182.559	227.577
	I17631022	5-Dec-2005	335.272	196.194	230.84
	I17943008	30-Dec-2005	348.868	201.332	232.009
	I18567014	20-Feb-2006	14.393	201.071	233.366
	I18879012	17-Mar-2006	26.467	208.706	239.91
	I19503018	8-May-2006	49.662	221.209	236.232
	I20726008	16-Aug-2006	93.827	196.559	237.726
	I28538002	21-May-2008	74.612	188.945	231.571

Differences on surface brightness temperature could have different origins, including different thermal inertia of the materials at the surface (due to grain size, mineralogy, etc.) thickness of the dust cover, topography, elevation or aspect. For that reason, only a proxy or qualitative analyses could be used (e.g., Tisch, 2008). A 1000 m regular grid was created covering the full study area, and surface temperature, elevation and aspect at each node has been measured in order to analyze these possible relationships, by the use of zonal statistics

tools of a GIS (ArcGIS 9.3 by ESRI), using the limits of the geomorphological units by de Pablo and Centeno (2012). Those samples were used to plot diagrams of temperature versus elevation and aspect for each season (spring, summer, fall and winter), and time (daytime and nighttime), for each geomorphological unit.

On the other hand, in order to try to reduce the influence of topographic variables into our interpretations, we also produced an Apparent Thermal Inertia (ATI) (Prize, 1977) map of the study area with a resolution of 100 m/pixel, calculated as:

$$ATI = (1 – A) / (Tday – Tnight) \quad \text{(Eq. 5.1)}$$

where A represent albedo, and Tday and Tnight the surface brightness temperatures on daytime and nighttime, respectively.

Because the available Viking-based and TES-derived albedo map has low resolution (60 km/pixel and 7.5 km/pixel, respectively) for the relatively small study area, we made an approach to albedo by the recalculation to 0-1 range of the digital numbers of the mosaic of two images (B06_011957_2127_XI_32N211 and B04_011324_2128_XI_32N211W) acquired by the CTX instrument on board MRO mission to Mars, with a spatial resolution of about 6 m/pixel.

On the other hand, we obtained daytime and nighttime temperatures from a mosaic of the THEMIS-IR images acquired in similar Solar Longitude in order to reduce the spatial variability on surface temperature, taking into account the partial coverage of each image, and that those images where acquired in different Martian years (Table 5.1). Considering these limitations, the resulting ATI is only used as a qualitative approach. However, quantitative analysis of the thermal inertia (TI) was possible thanks to the use of a tile (30N120E) of the THEMIS-derived Thermal Inertia global mosaic (Christensen et al., 2014), available at USGS Astrogeology division (http://astrogeology.usgs.gov/maps/mars-themis-derived-global-thermal-inertia-mosaic), which error inside each image in about 10%, but about 20% between different images (Fergason et al., 2006). The spatial resolution of the TI map is 100 m/pixel.

THEMIS IR images were also used to derive Decorrelation Stretch images (DCS) of 3 bands (Gillespie et al., 1986) assigned to Red-Blue-Green (RGB) colors: 8-7-5, 9-7-5, 9-6-4, 6-4-2, 8-6-4, 3-5-8, or 2-6-9, among others. DCS images were also produced from radiance daytime THEMIS IR images by the mean of THMPROC on-line tool. From all the possible bands combinations, we focused on 8-7-5, 9-6-4, 9-7-5, and 6-4-2, what are those combinations

usually analyzed by other authors (e.g., Bandfield et al., 2004a, 2004b; Rogers et al., 2005, 2009; Bandfield, 2008; Osterloo et al., 2010). Here we used the approach made by other authors, what relate different colors on each bands combination to the presence of different minerals. The results are not detailed and accurate, but provide an initial approach when no other accurate spectrometric data are available, such data from Compact Reconnaissance Imaging Spectrometer (CRISM) instrument (Murchie et al., 2002) on board of MRO spacecraft.

Because we hypothesize that surface brightness temperature could reflect the effect of putative subsurficial ice lenses, we completed this research with the use of ground penetration radar data acquired by Mars Shallow Radar Sounder (SHARAD) instrument on board of MRO mission (Seu et al., 2004; 2007a). We used SHARAD data they were already used to study the characteristics and properties of the Martian polar caps (e.g. Seu et al., 2007b; Phillips et al., 2008). SHARAD works by transmitting radar pulses with a 10 MHz bandwidth at a central frequency of 20 MHz, which penetrate below the surface and are reflected by any dielectric discontinuity in the subsurface. Such discontinuities are caused by changes in composition (ice vs. rock) or in structure (lava flow vs. loose regolith), or both.

SHARAD Instrument team processed echoes to obtain a vertical resolution of 15 m in free space (resolution in other media improves as the inverse of the square root of the relative dielectric permittivity), and a horizontal resolution of 0.3-1 km along the ground track of the spacecraft (depending on processing), and of 3-6 km across-track (depending on surface roughness) (Seu et al., 2007a). Data are usually represented in the form of radargrams, showing radar echoes acquired continuously during the movement of the spacecraft as grey-scale images, in which the horizontal dimension is distance along the ground track, the vertical dimension is the round trip time of the echo, and the brightness of the pixel is a function of the strength of the echo. The resulting image is a radar cross-section of the ground track of the spacecraft.

At present time, only 7 radargrams derived from SHARAD data exist of the NW flank of the Hecates Tholus volcano, but only a couple of them (Table 5.2) cross the study area: the main depression on this flank of the volcano, where the glacial landforms has been described and mapped (e.g., Neukum et al., 2004; Hauber et al., 2005; de Pablo and Centeno, 2012). We analyzed those radargrams in order to determine the possible subsurficial structure what could help us to interpret the surface brightness temperature, apparent thermal inertia, or thermal inertia.

Table 5.2: SHARAD radargrams of the region dissecting the study area at the lower NW flank of the Hecates Tholus volcano, Mars.

Data	Date	Max. Lat.	Min. Lat.	Max. Long.	Min. Long.
S_00191602	2006-12-23	34.7438	15.0102	149.3778	146.7634
S_00212701	2014-12-27	34.7747	15.0418	148.7742	146.1588
S_01328201	2009-05-27	75.2198	29.8731	160.7205	148.9281
S_01349301	2009-06-12	75.2731	29.8725	160.1278	148.2952
S_02574302	2012-01-23	75.1666	29.8083	160.883	149.0415
S_02595402	2012-02-08	75.1636	28.9736	160.5457	148.5909
S_02616501	2012-02-25	72.7198	27.2986	158.2356	147.7149

5.3. Results

5.3.1. Regional surface and near surface air temperatures

Surface temperature data extracted from the MCD (Lewis et al., 1999; Forget et al., 1999) provide a general thermal characterization of the study area (Figure 5.2; Table 5.3). Surface temperatures ranges between 274.7 K to 159.6 K under the Cold scenario, between 274.5 K to 161.0 K under the MY24 scenario, and between 272.5 K to 166.7 K under the Warm scenario. Mean annual values of surface temperatures ranges are 206.7 K, 205.9 K and 294.8 K for the Cold, MY24 and Warm scenarios, respectively. On the other hand, near surface air temperatures ranges between 236.4 K to 162.4 K under the Cold scenario, between 236.6 K to 163.6 K under the MY24 scenario, and between 242.5 K to 168.8 K under the Warm scenario. In all these scenarios, the maximum surface and near surface air temperature are reached in month 5 (Ls 120-150) and the minimum in month 10 (Ls 270-300). Only in Cold and MY24 scenarios the maximum surface temperature is higher than the water freezing point (273.15 K). Mean surface and near surface air temperatures varies in less than 10 K for all scenarios, and thermal amplitudes range between 44 to 98 K on the surface and 23 to 58 on the air.

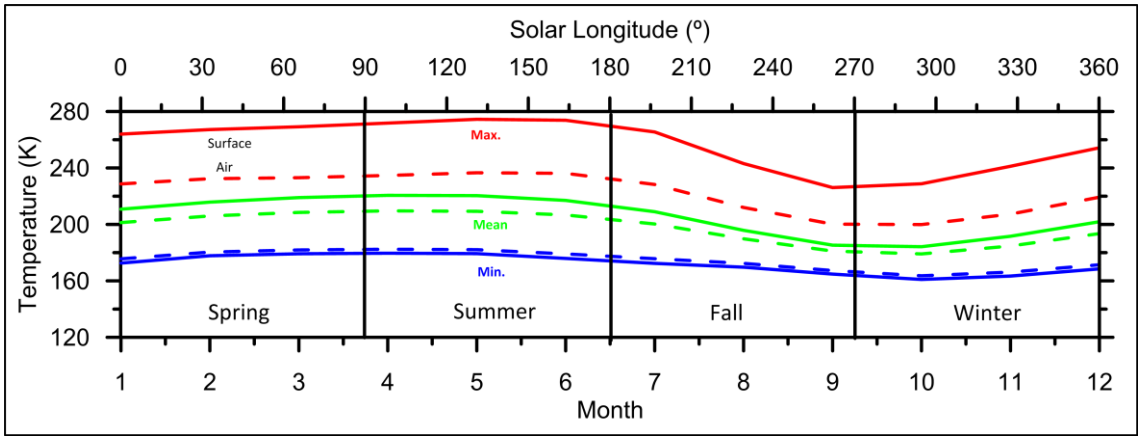

Figure 5.2: Maximum, mean and minimum surface and air temperatures for a mean day per month derived from Mean year (MY24) model of the Mars Climate Database (Lewis et al., 1999; Forget et al., 1999).

Table 5.3: Maximum, mean and minimum surface and air temperatures for the mean day of each month derived by three different scenarios (cold, mean and warm) at the Mars Climate Database (Lewis et al., 1999; Forget et al., 1999), and calculated thermal range (AT) and surface-air mean temperatures differences.

Model	COLD									
	Surface Temperature (K)				Surf-Air difference		Air temperature (K)			
Month	Max	Mean	Min	AT		Month	Max	Mean	Min	AT
1	263.9	210.6	172.1	91.8	10.1	1	227.0	200.5	175.1	51.9
2	267.6	216.1	177.4	90.2	9.9	2	232.0	206.1	180.1	51.9
3	269.4	219.1	179.0	90.4	10.6	3	232.7	208.5	181.8	50.9
4	272.1	220.7	179.7	92.4	11.0	4	234.3	209.7	182.5	51.8
5	274.7	220.5	179.4	95.3	11.0	5	236.4	209.6	182.1	54.3
6	274.1	217.1	175.6	98.5	10.5	6	236.1	206.6	178.3	57.8
7	266.4	209.3	171.7	94.7	9.1	7	228.1	200.2	174.8	53.3
8	251.5	197.6	166.0	85.5	8.6	8	212.0	188.9	168.9	43.1
9	238.1	188.4	161.4	76.7	6.6	9	203.4	181.7	164.4	39.0
10	235.3	186.2	159.6	75.7	6.8	10	199.9	179.3	162.4	37.5
11	244.6	192.7	162.0	82.6	8.1	11	206.4	184.6	165.4	41.0
12	256.3	202.5	167.3	89.0	9.4	12	218.2	193.1	170.4	47.8

Model	MY24									
	Surface Temperature (K)				Surf-Air difference		Air temperatura (K)			
Month	Max	Mean	Min	AT		Month	Max	Mean	Min	AT
1	264.0	210.8	172.6	91.4	9.5	1	228.7	201.3	175.6	53.1
2	267.2	215.8	177.8	89.4	9.8	2	232.4	206.0	180.4	52.0
3	269.2	219.0	179.2	90.0	10.5	3	233.1	208.5	181.9	51.2
4	271.8	220.6	179.6	92.2	11.0	4	234.7	209.6	182.4	52.3
5	274.5	220.4	179.3	95.2	11.1	5	236.6	209.3	182.1	54.5
6	273.8	217.0	175.9	97.9	10.3	6	236.2	206.7	179.1	57.1
7	265.5	209.0	172.4	93.1	8.7	7	228.3	200.3	175.7	52.6
8	243.1	195.8	169.7	73.4	5.9	8	212.0	189.8	172.4	39.6
9	226.1	185.3	164.8	61.3	4.3	9	200.2	181.1	167.3	32.9
10	228.8	184.2	161.0	67.8	5.0	10	199.9	179.1	163.6	36.3
11	241.2	191.6	163.4	77.8	6.9	11	207.3	184.7	166.2	41.1
12	254.3	201.9	168.5	85.8	8.3	12	219.3	193.5	171.4	47.9

Model	WARM									
	Surface Temperature (K)				Surf-Air difference		Air temperatura (K)			
Month	Max	Mean	Min	AT		Month	Max	Mean	Min	AT
1	257.7	210.0	178.8	78.9	5.5	1	232.2	204.5	182.1	50.1
2	264.3	215.7	182.3	82.0	6.8	2	237.3	209.0	184.8	52.5
3	267.3	218.7	182.7	84.6	7.9	3	237.9	210.8	185.3	52.6
4	270.3	220.3	182.9	87.4	8.3	4	239.7	212.0	185.7	54.0
5	272.5	220.2	183.3	89.2	7.9	5	242.5	212.3	186.0	56.5
6	269.6	216.7	181.3	88.3	6.5	6	241.4	210.1	185.0	56.4
7	256.1	207.3	178.2	77.9	5.3	7	228.8	202.0	181.5	47.3
8	234.1	194.5	173.7	60.4	3.9	8	210.7	190.6	176.3	34.4
9	214.6	183.6	168.6	46.0	3.3	9	194.9	180.4	170.8	24.1
10	211.6	181.4	166.7	44.9	3.3	10	192.3	178.2	168.8	23.5
11	225.1	188.6	169.5	55.6	3.6	11	203.5	185.1	171.9	31.6
12	243.9	200.0	174.3	69.6	4.6	12	218.8	195.4	177.2	41.6

5.3.2. Regional surface brightness temperature

Daytime surface brightness temperature derived from THEMIS-IR images shows temperatures ranging between 200 and 275 K, mean while for the nighttime, surface temperatures ranges between 100 and 200 K. On both, daytime and nighttime, the surface brightness temperatures distribution made possible to define four sectors (Figure 5.3), what correspond to the four sectors already defined based on the topographical analysis of the study area (Chapter 4).

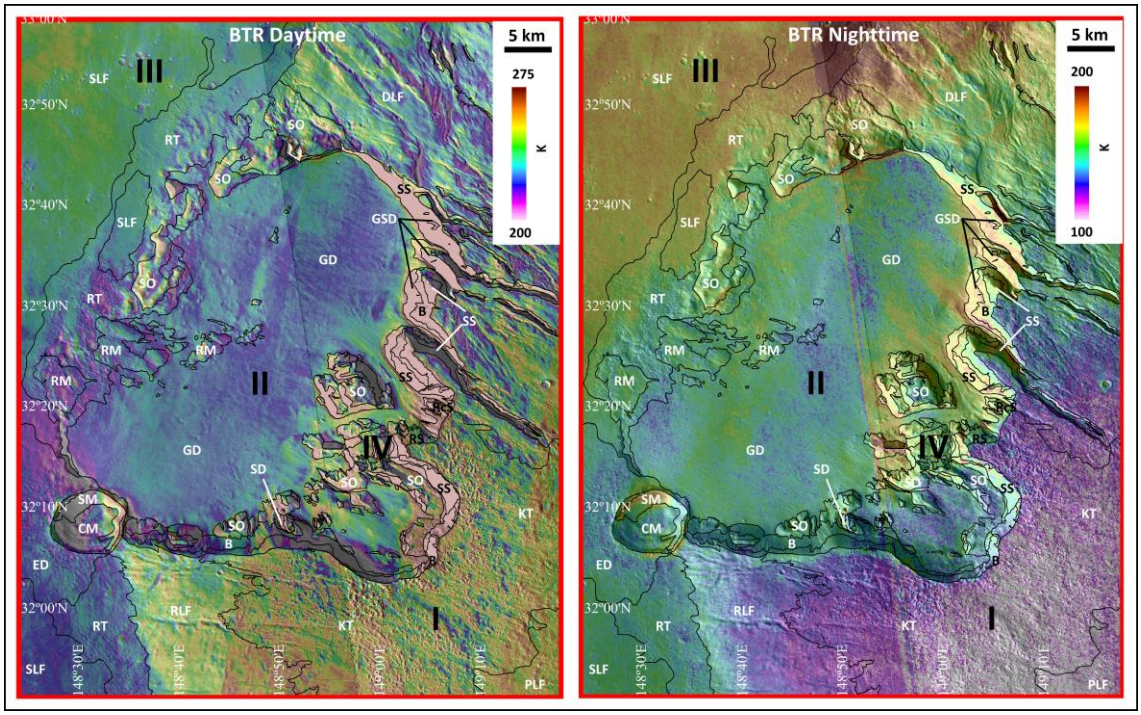

Fig. 5.3: Mosaics of THEMIS-IR images derived daytime (left) and nighttime (right) surface brightness temperatures of the lower NW flank of the Hecates Tholus volcano, Mars, and sectors (I, II, III and IV) with similar thermal behavior.

On daytime, higher temperatures are observed at both sectors, the lava flows from the Elysium Mons volcano, surrounding the base of the Hecates Tholus volcano (sector III), but mainly in the NW sector of the studied area, and the materials forming the western flank of the volcano (sector I), although with slightly lower temperature values. Low temperatures are located on the floor of the main depression of the flank (sector II). However, the most extreme temperatures are located on the walls of the depressions on the flank (sector IV). In fact, the wall of the depressions, valleys and channels on the flank of the volcano show also a pristine pattern, with lower temperatures at north-facing walls and higher values at the south-facing walls.

Surface temperature behavior during the nighttime follows a slightly different pattern (Figure 5.3). The higher temperatures are also related to the lava flows from the Elysium Mons volcano bordering the Hecates Tholus edifice (sector III), however, this temperature clearly decrease with the increase on elevation along the flank of the volcano. Then, the higher part of the NW flank (Sector I) shows lower surface temperatures, following a clear gradient with elevation. Channels in the lower part of the northern sector of the study area also show low temperatures, but not as lower as during the daytime and with small differences respect the surrounding slopes. The walls of depressions and main valleys (sector IV) remain the north-south facing variability, although their temperatures are not now the most extreme measured. Finally, the surface temperatures of the floor of the depressions are also low temperatures, lower than expected form the altitudinal gradient we described above. In fact, areas of low temperatures are located in the middle of the floor of the depression.

5.3.3. Surface brightness temperature *versus elevation and aspect*

The regional distribution on surface brightness shows some kind of relationship with elevation, aspect, or both. In order to clarify these relationships, we describe here the correlation, for each geomorphological unit mapped in the study area (de Pablo and Centeno, 2012), based on samples from a regular grid 1 km in distance between each correlative nodes. The number of samples per geomorphological unit depends of each area. Moreover, we produced separate plots per daytime/nighttime periods as well as for spring/summer/fall/winter seasons, and the availability of THEMIS images covering each area is neither the same for each unit. Consequently, the resulting plots (Figure 5.4) contain a different number of samples per geomorphological unit, time period and season.

In general, all the geomorphological units of the area show a similar pattern, with decrease on the surface temperature with the increase on elevation (Figure 5.4), although their aspect is, in general, more restricted. For those units with a wider elevation distribution, both daytime and nighttime temperatures reduce with elevation, or remain slightly constant. Some units, when more than one image is available, show parallel distribution on temperatures versus elevation and also versus aspect, what correspond to the evolution on the temperature along the time (increase on solar longitude). Daytime-Nighttime variability is also observable (Figure 5.4), with differences what could be higher than 100 K.

In spite the elevation/aspect influence on the surface brightness temperature is evident, no special patterns could be deduced from the data for each geomorphologic unit.

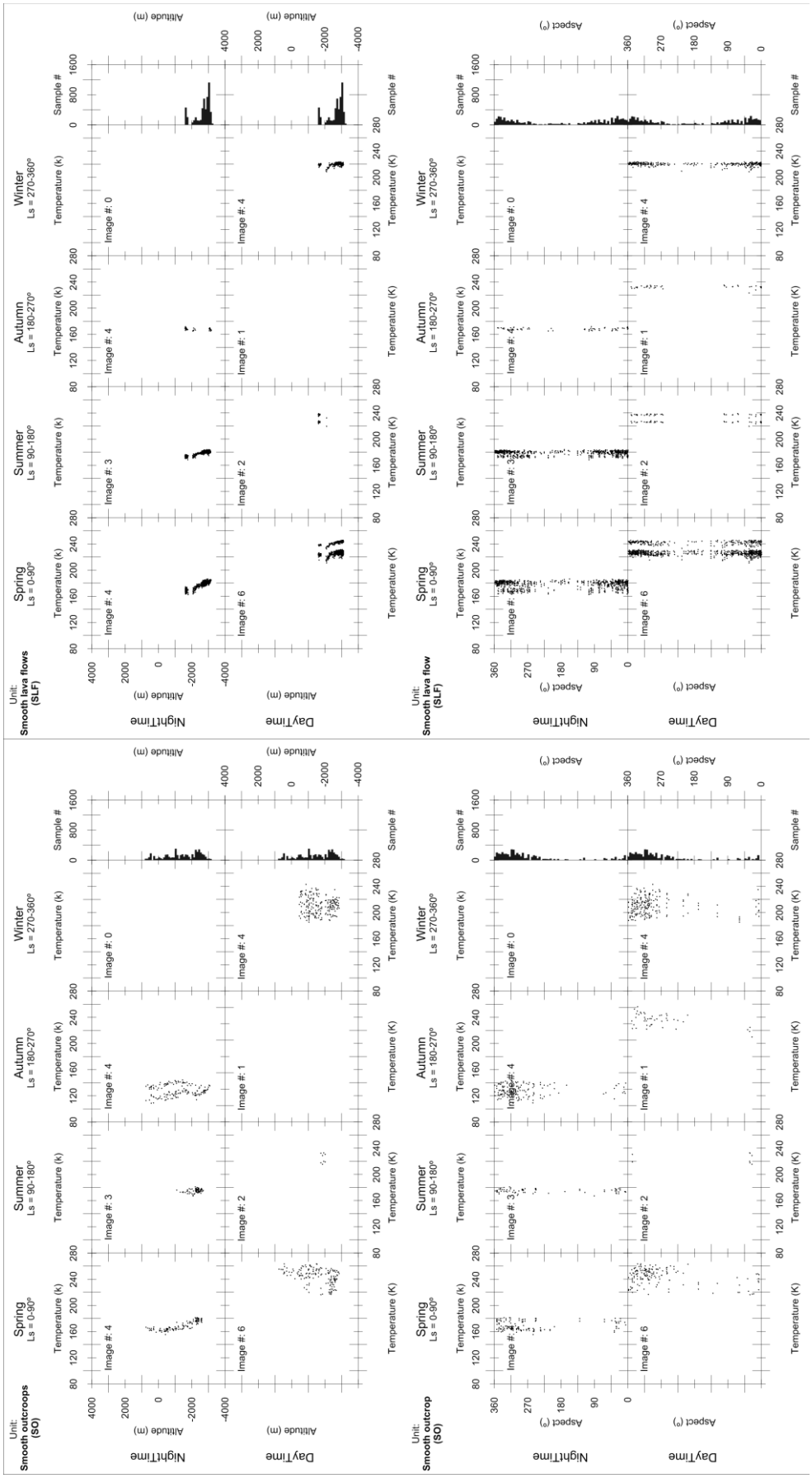

Fig. 5.4: Plots showing THEMIS-IR-derived daytime and nighttime surface brightness temperature versus elevation and aspect per each season. Sheet 1: geomorphological units SLF (Smooth Lava Flows) and SO (Smooth Outcrops) (de Pablo and Centeno, 2012).

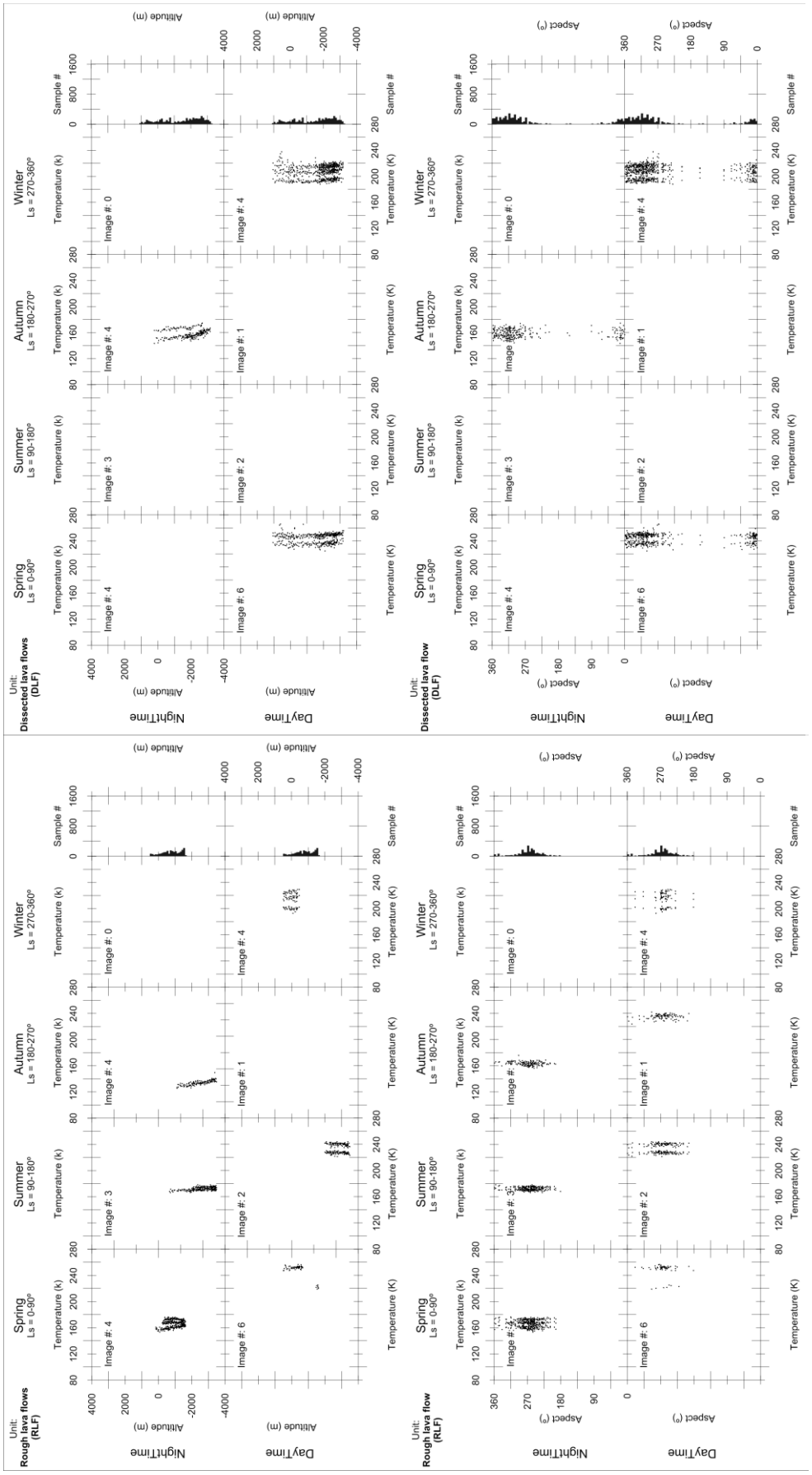

Fig. 5.4: Plots showing THEMIS-IR-derived daytime and nighttime surface brightness temperature versus elevation and aspect per each season. Sheet 2: geomorphological units DLF (Dissected Lava flows) and RLF (Rough Lava Flows) (de Pablo and Centeno, 2012).

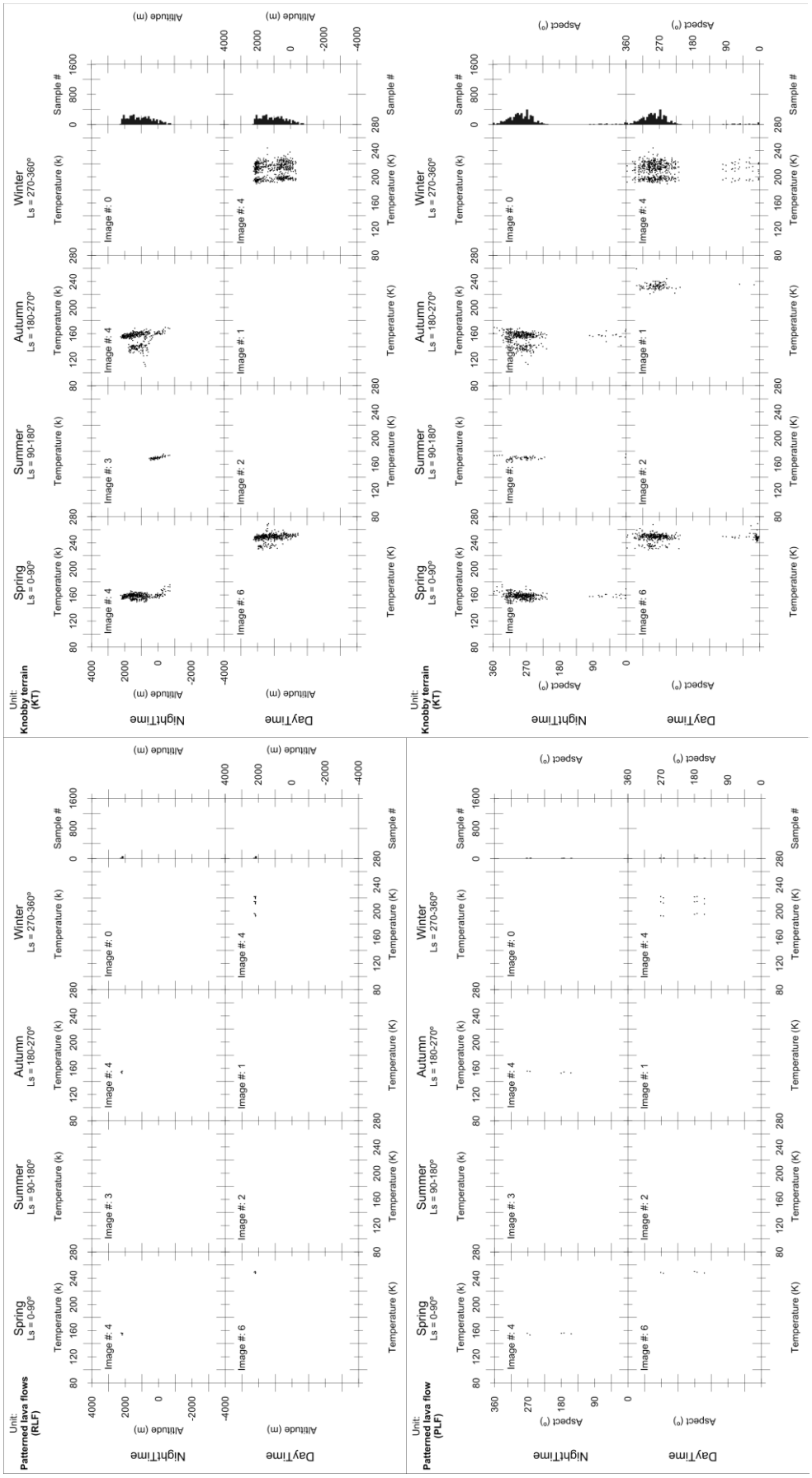

Fig. 5.4: Plots showing THEMIS-IR-derived daytime and nighttime surface brightness temperature versus elevation and aspect per each season. Sheet 3: geomorphological units KT (Knobby Terrain) and PLF (Patterned Lava Flows) (de Pablo and Centeno, 2012).

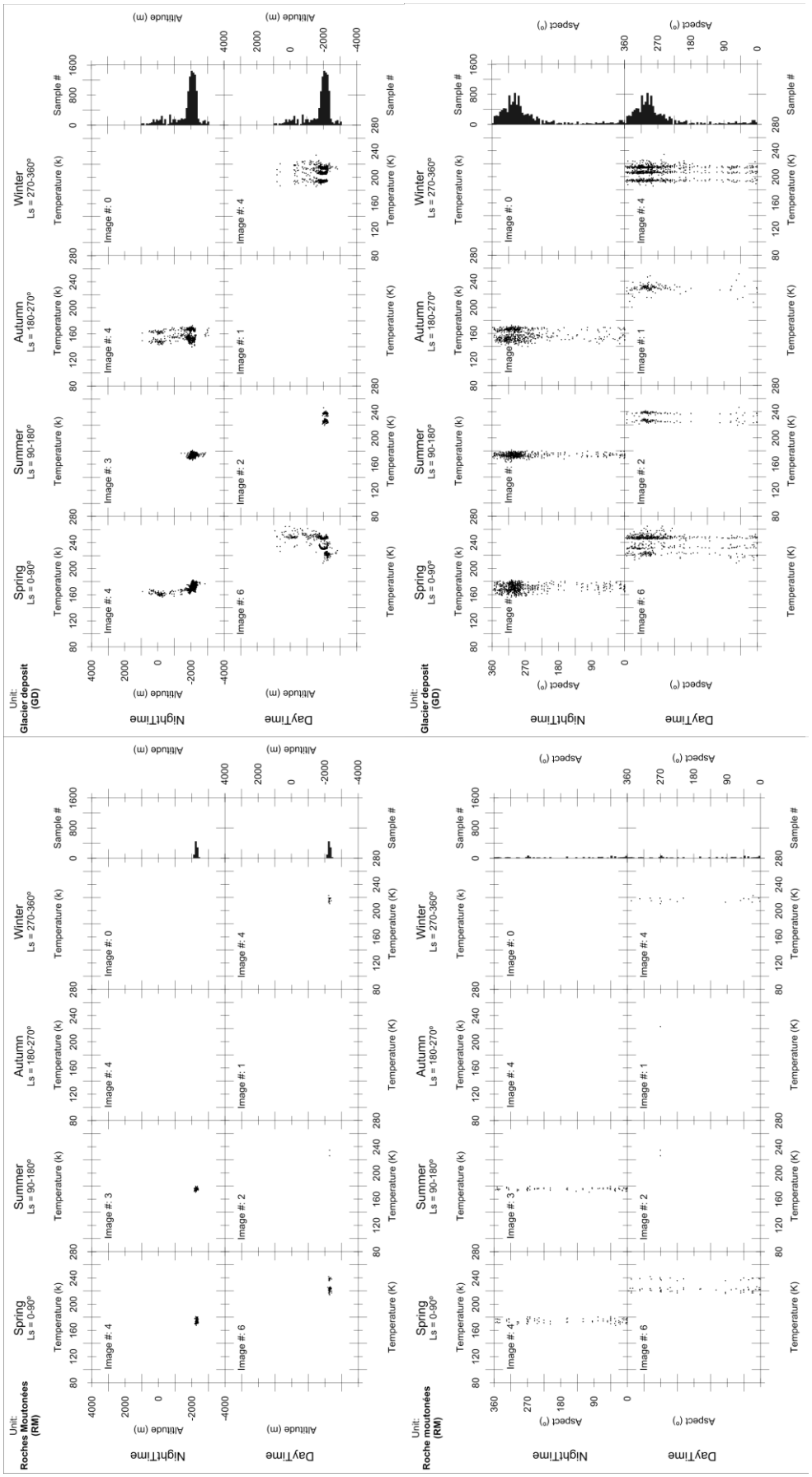

Fig. 5.4: Plots showing THEMIS-IR-derived daytime and nighttime surface brightness temperature versus elevation and aspect per each season. Sheet 4: geomorphological units GD (Glacial Deposits) and RM ((Roche Moutonèe) de Pablo and Centeno, 2012).

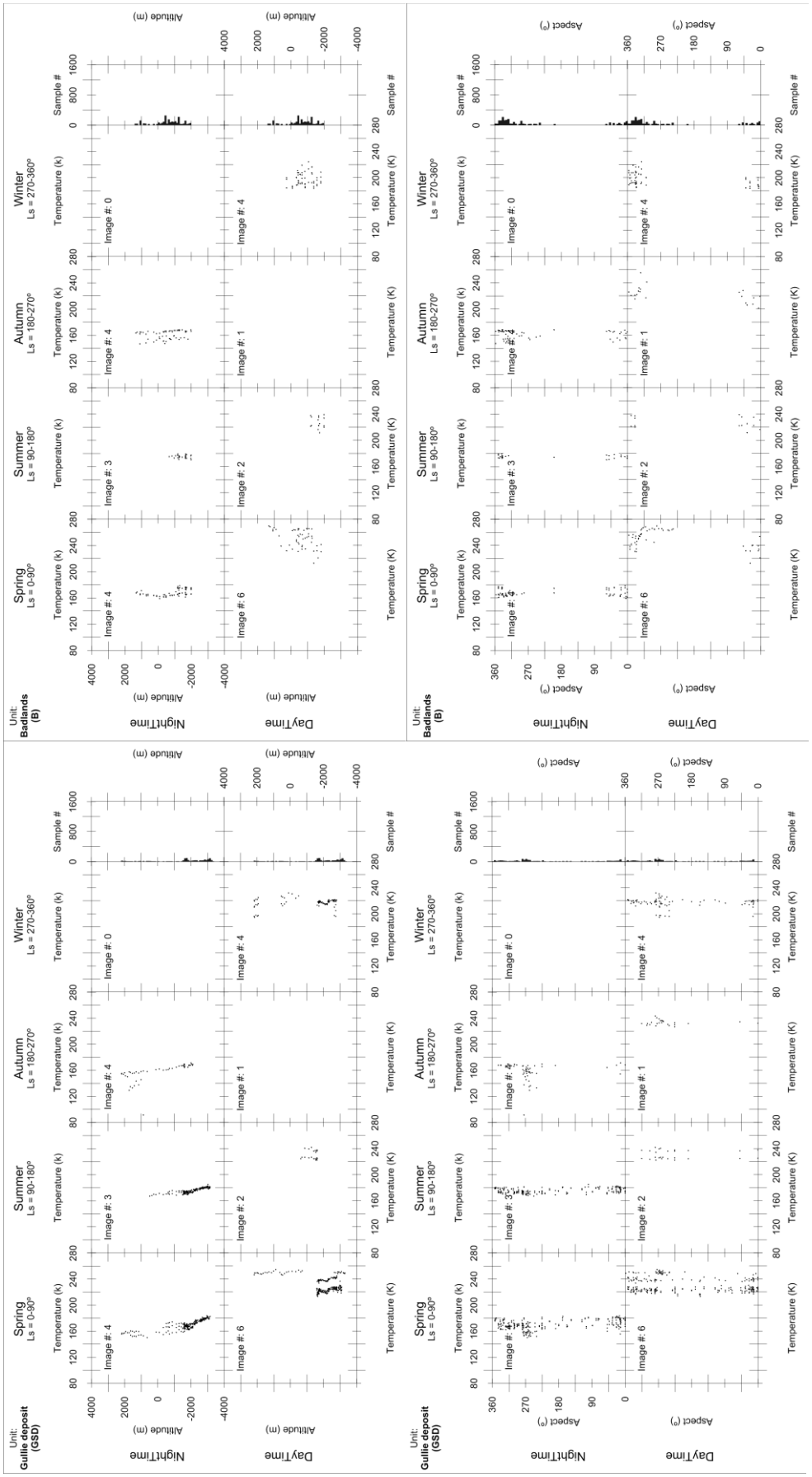

Fig. 5.4: Plots showing THEMIS-IR-derived daytime and nighttime surface brightness temperature versus elevation and aspect per each season. Sheet 5: geomorphological units B (Badlands) and GsD (Gullies Deposits) (de Pablo and Centeno, 2012).

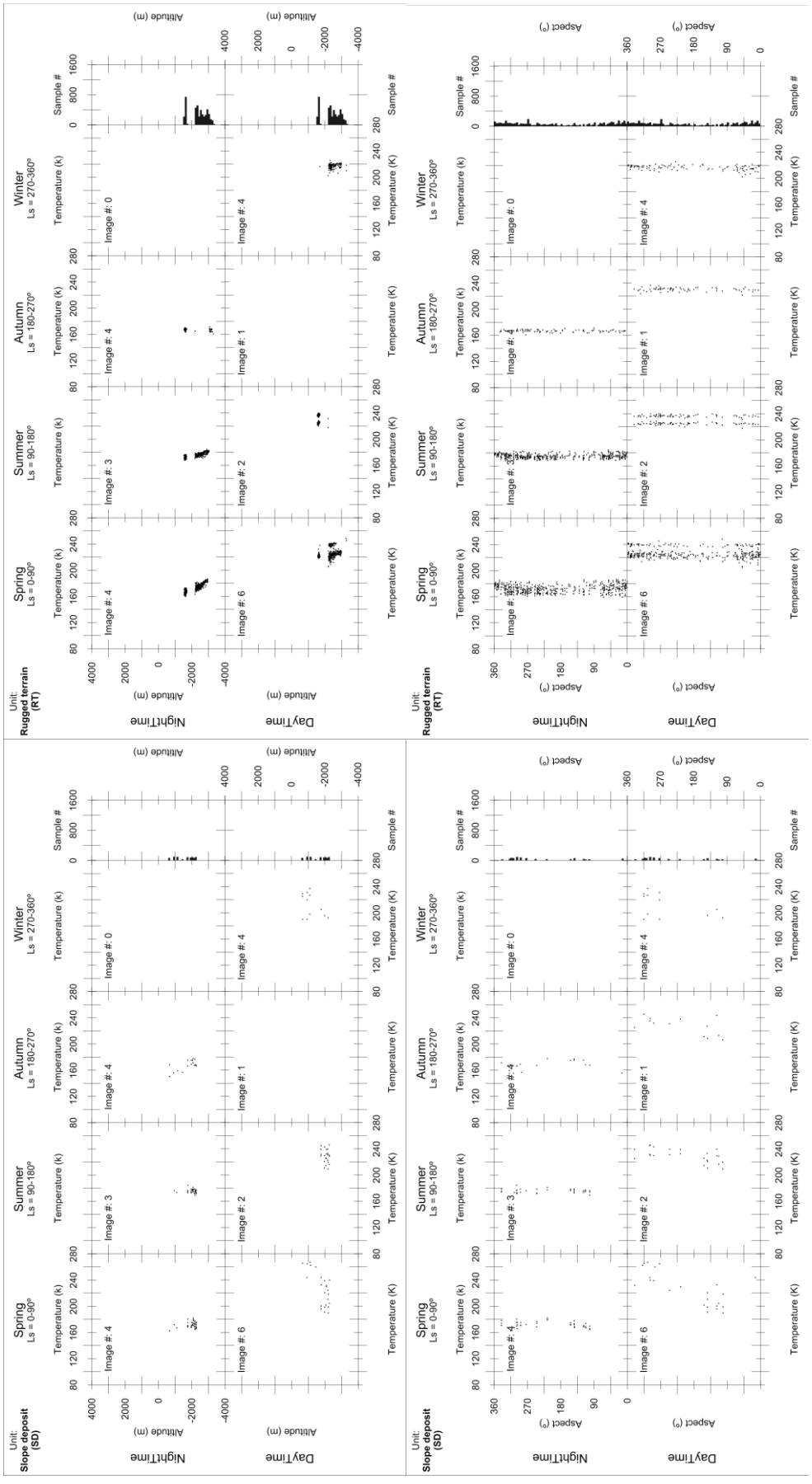

Fig. 5.4: Plots showing THEMIS-IR-derived daytime and nighttime surface brightness temperature versus elevation and aspect per each season. Sheet 6: geomorphological units RT (Rugged Terrain) and SD (Slope Deposits) (de Pablo and Centeno, 2012).

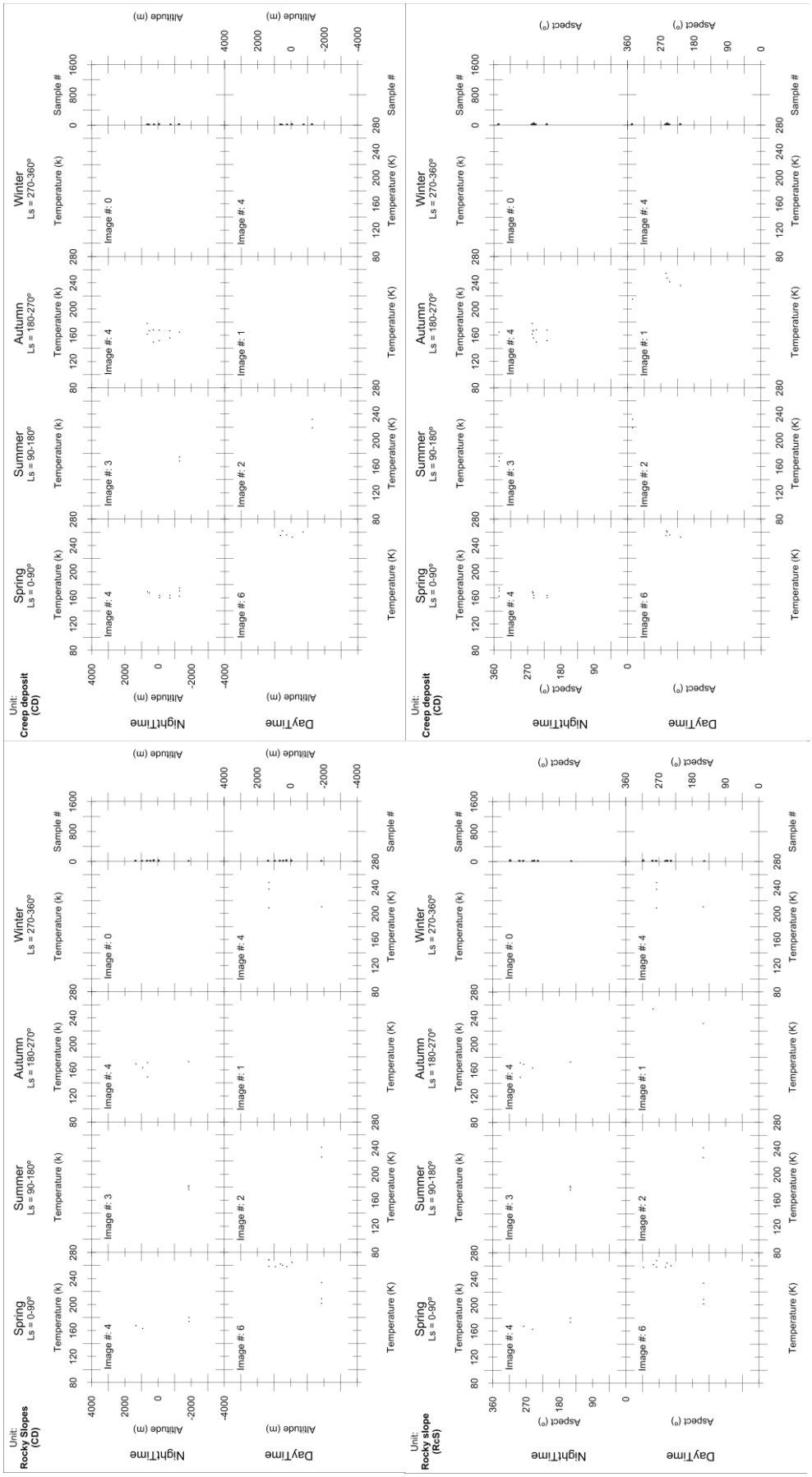

Fig. 5.4: Plots showing THEMIS-IR-derived daytime and nighttime surface brightness temperature versus elevation and aspect per each season. Sheet 7: geomorphological units CD (Creep Deposits) and RcS (Rocky Slopes) (de Pablo and Centeno, 2012).

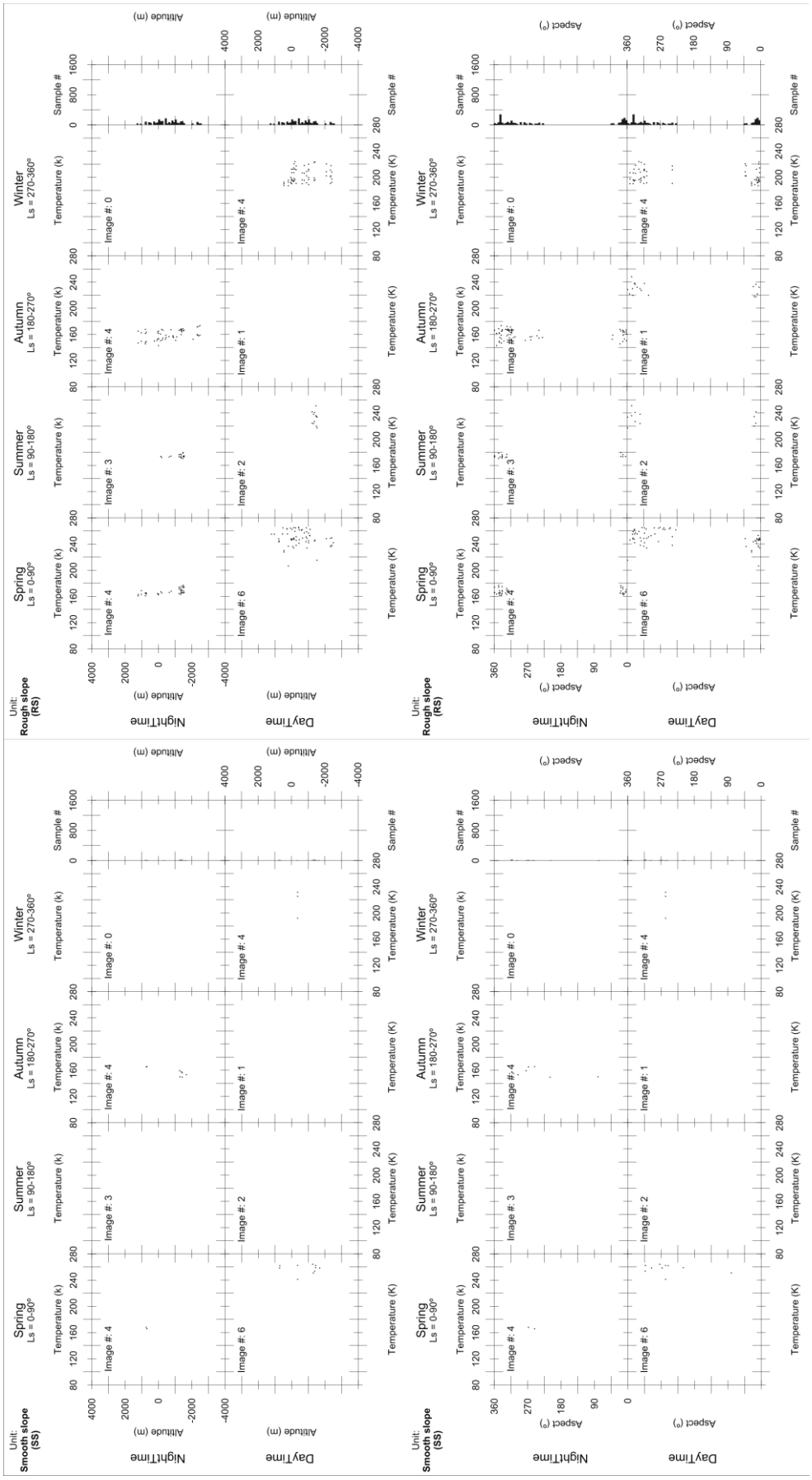

Fig. 5.4: Plots showing THEMIS-IR-derived daytime and nighttime surface brightness temperature versus elevation and aspect per each season. Sheet 8: geomorphological units RS (Rough Slope) and SS (Smooth Slopes) (de Pablo and Centeno, 2012).

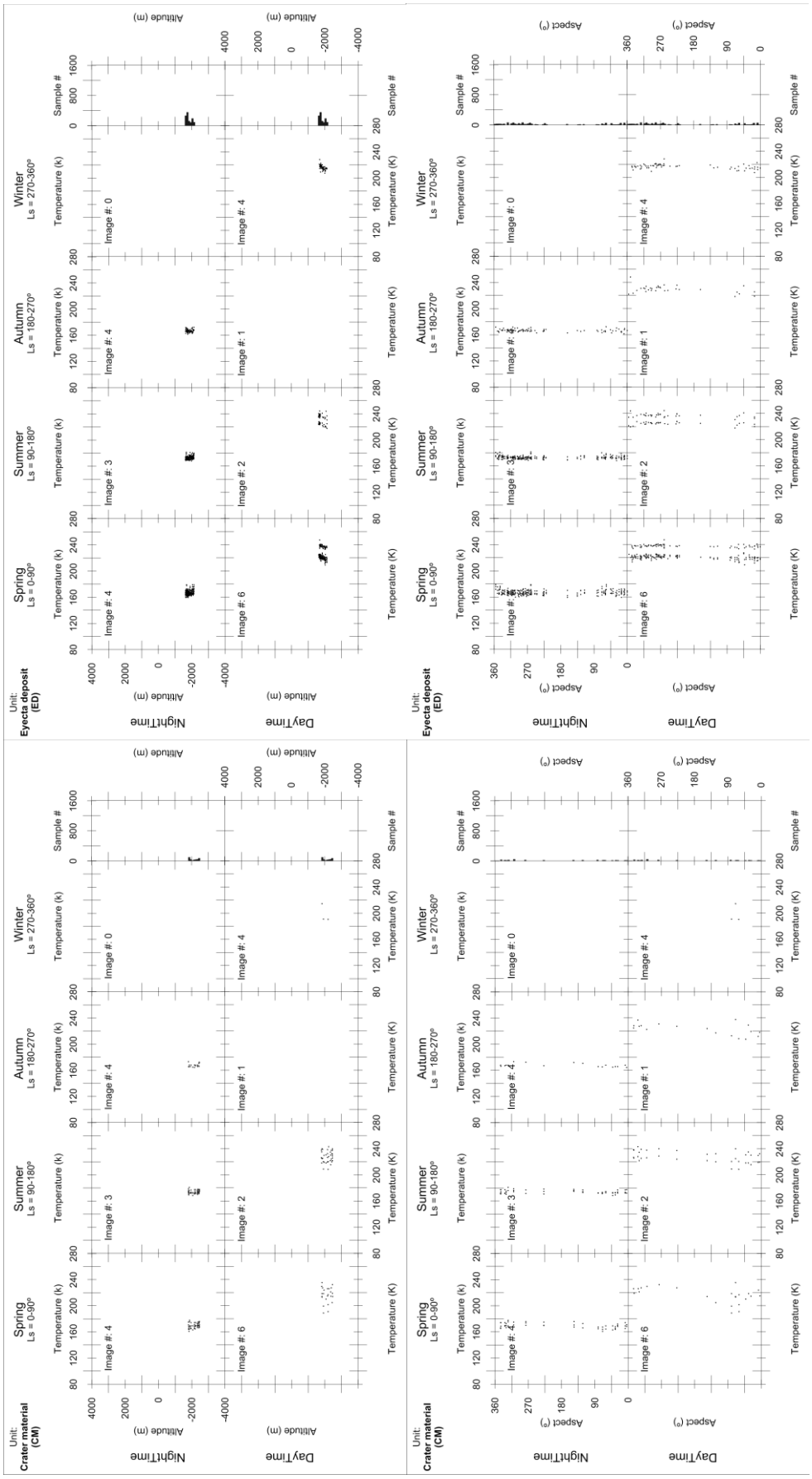

Fig. 5.4: Plots showing THEMIS-IR-derived daytime and nighttime surface brightness temperature versus elevation and aspect per each season. Sheet 9: geomorphological units ED (Ejecta Deposit) and CM ((Crater Material) de Pablo and Centeno, 2012).

5.3.4. Apparent Thermal Inertia (ATI)

The ATI map of the study area (Figure 5.5) was derived by the use of equation 5.1, using digital numbers of CTX images as an approach to the albedo. This is the main reason why the resulting map should be considered only a semi-quantitative approach to thermal inertia. In any case, ATI map reveals the materials have 4 different sectors corresponding to the previously defined sectors depending of both the topographical properties and surface temperature patterns. Limits are clear and, for some units, they follow precisely the limits of the geomorphological units mapped in the area (de Pablo et al., 2012).

Sector I, corresponding to the materials forming the flank of the Hecates Tholus volcano, shows very low values. Higher variability exists in the proximity of depression A (KT unit). Meanwhile, the most uniform area correspond to the lower west-facing flank of the volcano (RLF unit), with higher ATI values in the area of narrow channels (DLF unit).

Sector II, corresponding to the materials forming the floor of the depressions on the NW flank of the volcano (GD unit), is characterized by medium to high values, except the edges, where low values are most frequent, as well as in small areas inside the main plains at the floor of the depressions.

Sector III, corresponding to the planes surrounding the Hecates Tholus volcano (SLF unit), and it is characterized by high ATI values. The limits of this unit are gradual and they could include other geomorphological units located surrounding the volcanic edifice (e.g., RT, ED, RM, SO units).

Finally, sector IV, corresponding to the walls of the depressions on the flank of the volcano, is characterized by the highest and lowest ATI values, with and evident pattern on the distribution of lower ATI values at the south-facing walls, and contrarily on the north-facing slopes, where the higher values are located. We could not discard this is an artifact caused by the effect of scenes illumination on the CTX images used for the ATI calculation.

Even if the map should be limited to qualitative analysis, it shows an evident difference between the materials forming the Hecates Tholus volcano, those materials at the plains surrounding it, and the materials at the floor of the nested depressions. Pristine limits between those three sectors, that are not evident on the CTX images, contribute to the reliability of the approach on ATI calculation.

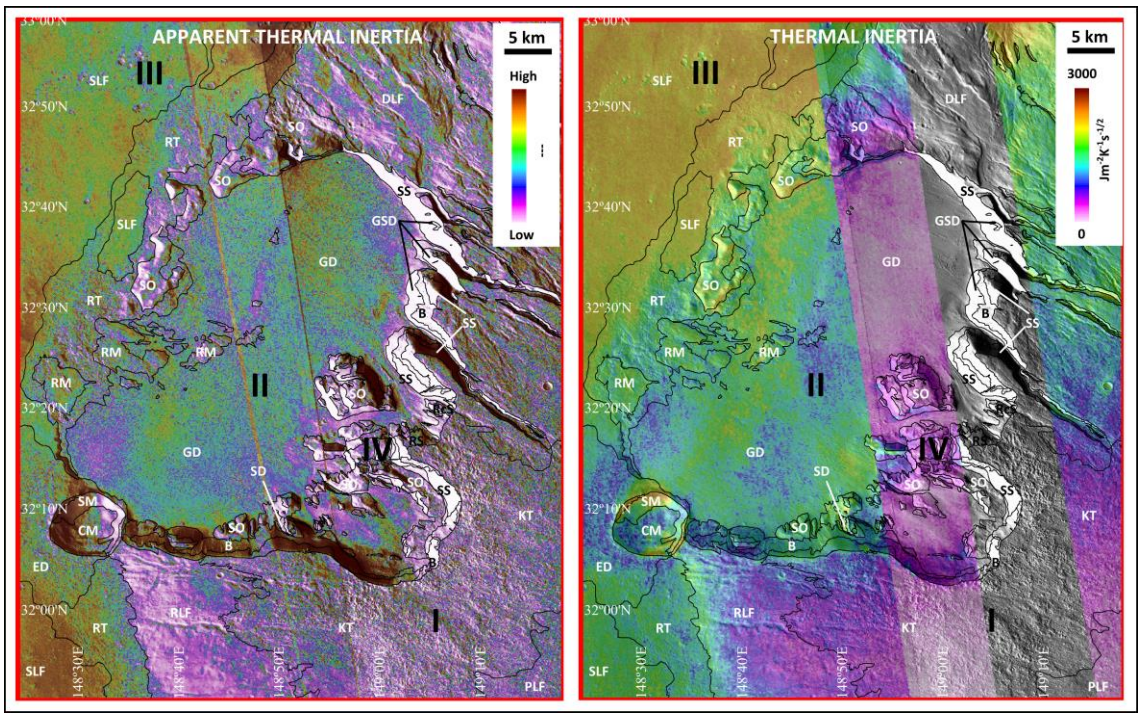

Fig. 5.5: Maps of Apparent Thermal Inertia (left) calculated from surface brightness temperature, and Thermal Inertia (right) (Christensen et al., 2014) of the lower NW flank of the Hecates Tholus volcano, Mars. Note that Apparent Thermal Inertia is a qualitative approach; meanwhile Thermal Inertial is in $Jm^{-2}K^{-1}s^{-1/2}$. Sectors with different thermal behavior is marked (sectors I, II, III and IV).

5.3.5. Thermal inertia

Scene of the Thermal inertia (TI) maps of Mars (Christensen et al., 2014), shows a general and gradual increase on TI values from the highest part of the study area, at the middle part of the Hecates Tholus volcano flank, to the plains surrounding the edifice (Figure 5.5), very similar to the qualitative values of the API map. Lower values, 80 to 130 $Jm^{-2}K^{-1}s^{-1/2}$, correspond to Sector I, meanwhile sector III shows the higher values, 160 to 325 $Jm^{-2}K^{-1}s^{-1/2}$. Moreover those values, sectors I and III are characterized by their uniform TI distribution, meanwhile Sector II is characterized by both, variable TI values from 150 to 250 $Jm^{-2}K^{-1}s^{-1/2}$, and their spatial variability, with sectors of low values surrounded by high values at the central part of the main depression of the volcano's flank. Sector IV is not completely covered by available data, and could not be characterized, although higher variability, compared to ATI values, is visible (Figure 5.5).

Thermal inertia values are related to surface properties such as particle size, abundance of rocks, surface moisture, exposure of bedrocks, but could be influenced by many factors such as presence of dust, pressure, topography, among many others (e.g., Jakosky, 1986; Edgett and Christensen, 1991, 1994; Presley and Christensen, 1997; Christensen et al.,

1998; Jakosky et al., 2000; Mellon et al., 2000; Pelkey et al., 2001; Christensen et al., 2001; Presley, 2002; Fergason and Christensen, 2003; Fenton et al., 2003; Fenton and Mellon, 2006; Fergason et al., 2006; Putzig and Mellon, 2007; Mellon et al., 2008). Considering the bibliography, the surface should be characterized by silt to coarse sand in grain-size (Edgett and Christensen, 1994). Then, the surface of Sector I, with lower values should be made of silt, meanwhile Sector III, with higher values, should be made of very find to medium sand in grain size.

5.3.6. Regional compositional analysis

Because surface temperature, and therefore, thermal inertial, could be influenced by the composition of materials at the surface, we analyzed the regional composition by mean of the use of decorrelation stretch (DCS) (Gillespie et al., 1986) of 3-bands of THEMIS-IR images, in order to provide a general knowledge about the presence of different type of materials in the area. We used the most frequent combinations used on the regional study of Mars: 8-7-5, 6-4-2, 9-6-4, and 9-7-5 (Figure 5.6).

Rogers et al. (2005) summarize the expected results for the DCS 8-7-5 based on their own studies but also in previous works (e.g., Bandfield et al., 2004a, 2004b): pink, purple and magenta colors marks the presence of olivine-rich and low pyroxene materials, orange color indicate presence of basaltic materials, and yellow color are evidences of rich-silica materials. Green color in this type DCS combination was interpreted to be dust deposits with an undefined mineralogy what mask the mineralogy of the underneath materials (Pelkey et al., 2004; Hamilton et al., 2007), meanwhile cyan colors has been also related to water ice clouds (Hamilton et al., 2007) and also to olivine presence (Lane and Goodrich, 2010). Other DCS combinations result in different colors for the same compositions. On DCS 6-4-2, green color marks the presence of olivine-rich and low plagioclase materials, blue color is characteristic of basaltic material, and pink color indicative of silicic materials. On DCS 9-6-4, olivine-rich and low plagioclase materials is marked by purple color, basaltic materials by pink color, and silicic material by yellow color, including sulphate and phyllosilicates in agreement with Baldridge et al. (2011). Finally, on DCS 9-7-5, olivine-rich materials are also visible as purple color (Hamilton and Christensen, 2005). Based on those criterions, DCS 8-7-5 images of the study area shows that pink, purple and green colors are the characteristics color of the area, marking the presence of olivine-rich materials (basaltic/mafic materials), locally covered by dust deposits. There are not areas with yellow color and, consequently, we cannot report the presence of silicic materials.

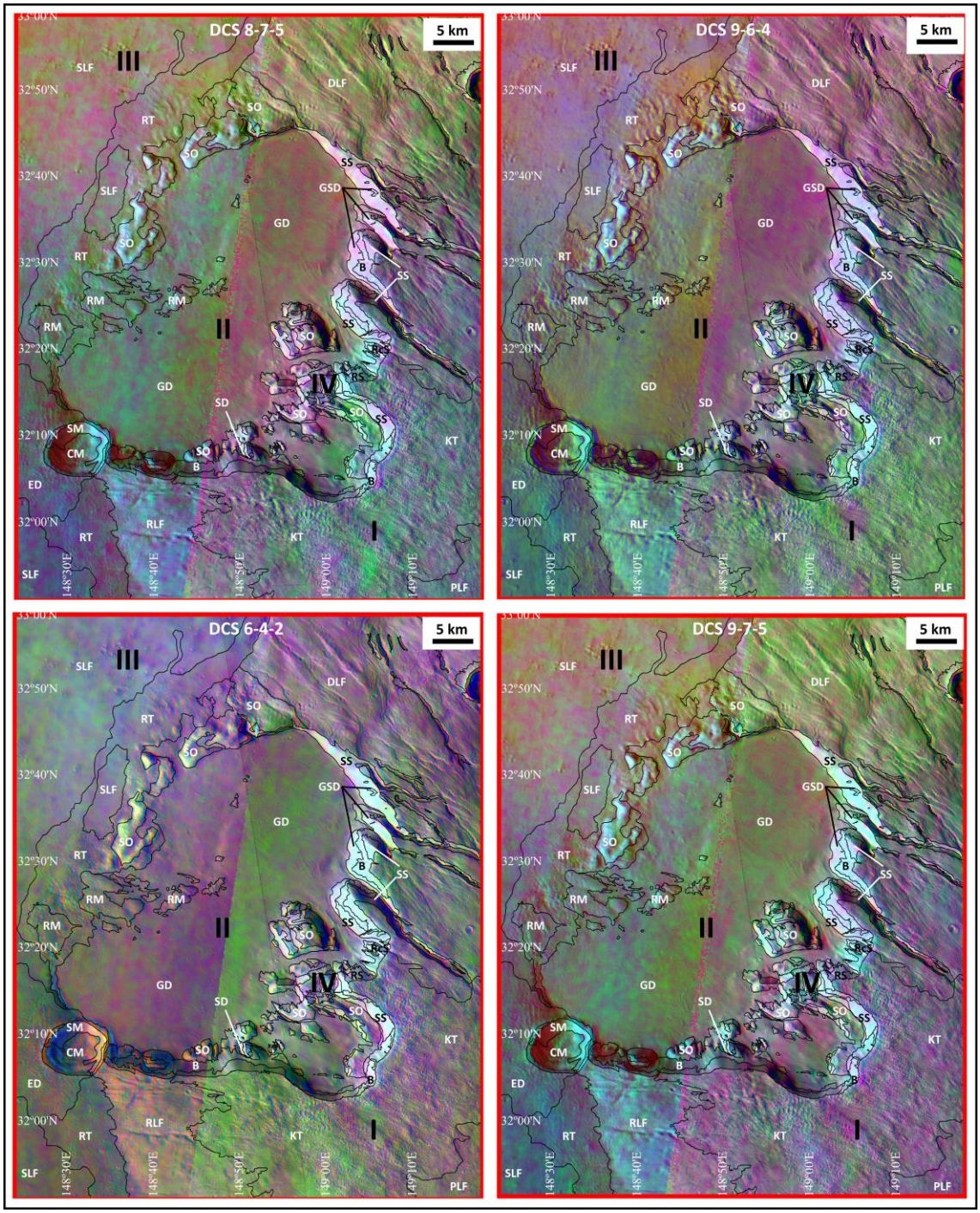

Fig. 5.6: Maps showing DCS images of 8-7-5 (upper left), 9-6-4 (Upper right), 6-4-2 (lower left) and 9-7-5 (lower right) bands combinations of I36935017 and I38994009 THEMIS-IR daytime images.

Although colors intensity change from one image to other, all the images shows a similar color pattern with frequent pink, purple, magenta and cyan colors in the southern part of the study area, meanwhile the green color is dominant on the central and northern part (Figure 5.6). In detail, the NW flank of the Hecates Tholus volcano shows variable composition,

marked by pink and purple colors in the southern part that changes to green with pink spots and small areas in the northern part. The two nested depressions show different color, mainly purple-pink in depression B, and a mixture between pink-purple and green in depression A. Pink, purple, magenta and cyan colors are dominant in the walls of both depressions. The smooth reliefs forming the western edge of depression B also shows cyan color, marking the presence of olivine-rich materials. The surrounding area of the Hecates Tholus volcano in the study area is characterized by purple colors in the southern part, and pink and purple in the northern part although green areas are also observed in this sector. In selected sites, cyan colors are also observable, mainly in the higher part of the volcano flank, but also inside the depressions, without masking the underneath green and purple colors. On the other hand, silicic materials (yellow color) has not been observed on DCS 9-6-4 images, and neither chlorine deposits has been observed by the combination of 8-7-5, 9-6-4, and 6-4-2 DCS images (Osterloo et al., 2010).

Based on this visual analysis of DCS images, we cannot clearly define a compositional difference between the 18 geomorphological units mapped in the area (de Pablo and Centeno, 2012) and neither on each one of the 4 sectors of the area (Figure 5.6), since all of them, shows similar color patterns, and compositional limits could be not be mapped based on these data.

5.3.7. Subsurface characteristics

In order to correlate the surface temperature patterns with the subsurface characteristics, we used SHARAD data to analyze the subsurface structure. Firstly we should consider that SHARAD transmits through a dipole, which has negligible directivity, with the consequence that the radar pulse illuminates the entire surface beneath the spacecraft and not only the near-nadir portion from which subsurface echoes are expected. The electromagnetic wave is thus scattered by any roughness of the surface. This means that areas of the surface that are not directly beneath the radar can scatter part of the incident radiation back towards it, and thus produce surface echoes that will reach the radar after the echo coming from nadir, which can mask, or be mistaken for, subsurface echoes. Because of its small size, so far only a limited number of observations had been collected over the study area (Table 5.2). In most of the cases, it is clear that a second echo past the surface appears when SHARAD flies over the NW flank of Hecates Tholus, caused by the rim of the depression on which the study area is centered. Further observations on the available data have provided similar results, and no subsurface interface has been detected so far (Figure 5.7).

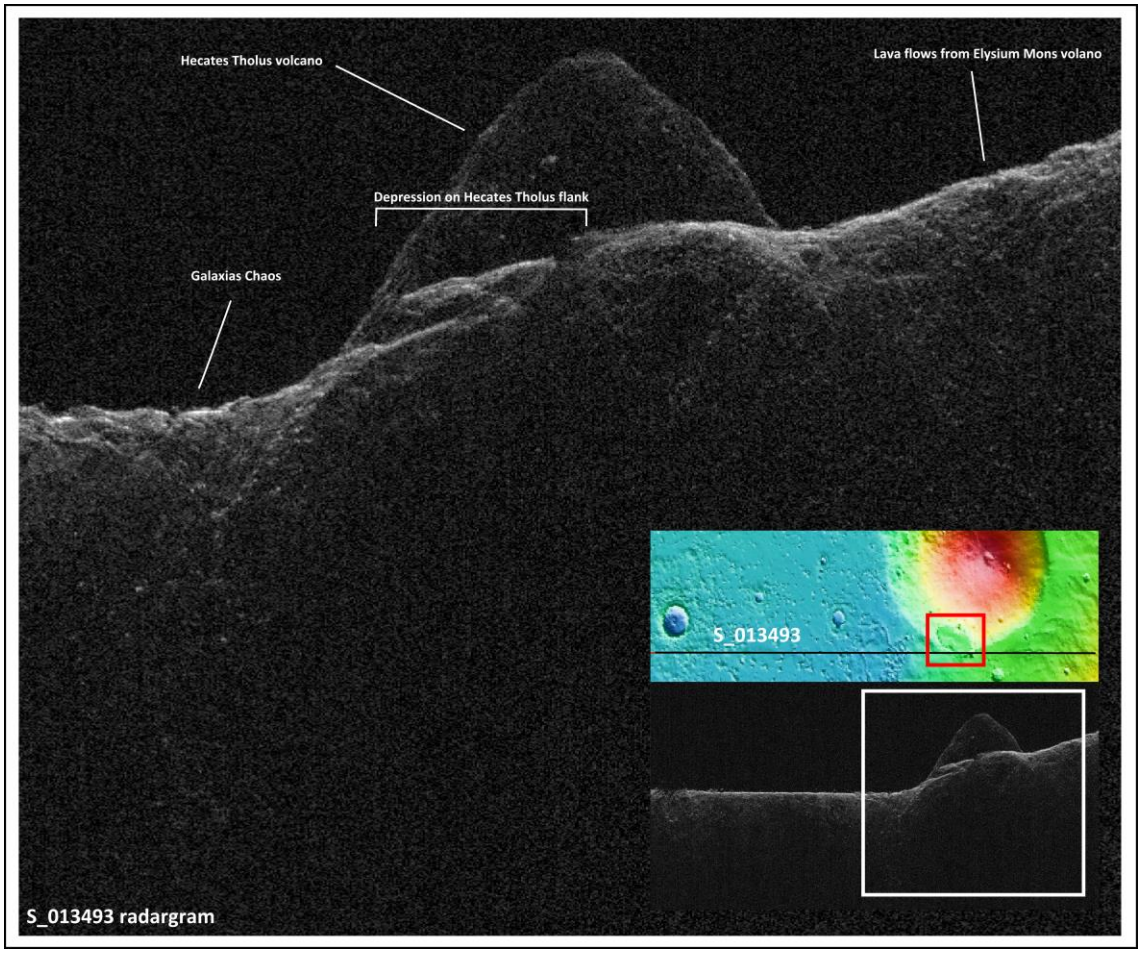

Fig. 5.7: Example of echoes (principal and secondary) observed on a section of S_013493 SHARAD radargram crossing the westernmost part of the main depression on the flank of Hecates Tholus volcano, Mars. Inset shows the track of the radargram on a MOLA topographic map with the location of the study area (red box).

5.4. Discussion: relict ice.

5.4.1. Thermal characterization

Mars Climate Database provides only an overview of the surface temperature data of Hecates Tholus volcano due to its low spatial resolution. In general for the different scenarios, the area is almost ever under freeze conditions due the surface temperature are below 273.15 K (0ºC) (Figure 5.2). Exceptions occur during the summer season (mainly months 5 and 6) when the temperatures slightly goes above this temperature, under Cold and MY24 models. On the other hand, the lower temperatures are as low as 161 K (-112ºC). This range of temperatures is not different than the normal mean conditions in any other mid-latitude region of Mars, in where the sub-surficial water, if it exists, should remain freeze. Without the consideration of other parameters such as soil salinity, elevation, pressure, atmospheric water content, dust opacity, or solar radiation, we could say that only during the summer, the surface temperature

could reach temperatures high enough to cross the temperature boundary for the liquid water stability. Such as we said, this does not mean liquid water existence during the summer due to the many other factors what affect its existence.

However, this temperature range is derived from a low resolution climate model. Analyzing the THEMIS-IR-derived surface brightness temperature, a more detailed analysis of the results could be done, not only spatially, but temporal (day/night and seasonal). Summer daytime surface brightness temperature map (Figure 5.3) reveals that the temperatures are not so high in the study area, although the south-facing walls of depressions and deep valleys (Sector IV) could reach 275 K, what it is approximately the highest temperature we obtained. Similar high temperatures are also observable at high elevation on the flank of the volcano, on Sector I, but with a less spatially continuous distribution. On day time, there is not a clear variation of the temperatures with elevation, meanwhile on nighttime, the gradient is evident (Figure 5.3), with lower temperatures at higher elevation (Sector I), and low temperatures at lower elevation (Sector III).

In detail, the analysis of temperature distribution of the geomorphologic units (Figure 5.4) shows very different patterns: on daytime, some units slightly increase the temperatures with elevation, meanwhile others reduce, and few others remain constant or do not show a clear trend. Meanwhile, on nighttime, the surface temperatures have a more common pattern for all the geomorphological units (at least for those with enough available data), in which temperature decreases with elevation (Figure 5.4). This behavior occurs for all the seasons, with small differences in gradient.

On the other hand, the effect of aspect is not evident. The main aspect of the study area toward the Northwest made most of the units, except those related to walls and flanks of valleys and depressions, to have a similar aspect. For the case of the slope units (sector IV), they are small enough to do not have many samples in our study, what result in a low density cloud of data on the plots (Figure 5.4). In spite of that, the daytime surface temperature map (Figure 4.3) shows the clear difference on surface temperature for north-facing versus south-facing walls on Sector IV. This observation supports the presence of selected geomorphological units mainly in north-facing slopes (e.g., B unit) meanwhile others are mainly related to south-facing slopes (GsD or SS units). The already discussed presence of creeping marks on south-facing slopes (Chapter 4) is also well supported by the differential thermal behavior on the different walls f the study area. This also agrees with the distribution of gullies (GsD unit) on the study area, in a similar way than many other gullies on Mars, related to the walls with

higher isolation, i.e. south-facing slopes (e.g., Malin and Edget, 2000, 2001; Edget et al., 2003; Christensen, 2003; Heldman, 2004; Dickson et al., 2007; Dundas et al., 2012; Harrison et al., 2015). In general, what we observed on the aspect versus temperature plots is that temperature is rather independent of aspect in all geomorphologic units, both daytime and nighttime.

Based on our data and methods, any of the geomorphological units could be characterized by a unique thermal behavior, although regional patterns could be observed, that relate the different units to different approximate temperature ranges. On daytime, Sector I is characterized by temperatures of 240-260 K; Sector II by temperatures of 220-240 K; Sector III by temperatures of about 230 K; and Sector IV by temperatures of 250-270 K for the south-facing walls, and 200-200 K for the north-facing walls. On nighttime, Sector I is characterized by temperatures of 100-130 K; Sector II by temperatures of 130-150 K; Sector III by temperatures of 170-200 K; and Sector IV by temperatures of 160-175 K for the south-facing walls, and 140-160 K for the north-facing walls (Figure 5.3).

5.4.2. Thermal anomalies

The difference on temperature between daytime and nighttime (described above) is evident (Figure 5.8), showing a range between 30 and 130 K. This range is bigger at the upper part of the Hecates Tholus flank in the study area, and decrease with the descent on elevation. The pattern observed in this map is, evidently, similar (but opposite in quantitative value) to the Apparent Thermal Inertia and Thermal Inertia maps (Figure 5.5).

However, the floor of the depressions on the flank of the volcano (depressions A and B in Figure 5.1), corresponding to GD geomorphological unit (de Pablo and Centeno, 2012), shows a difference of about 70 to 80 K, but, about 5 K in difference respect the surrounding terrains (Figure 5.8). This difference is more evident on Depression B, where all the floor of the depression should have a similar origin, but these thermal differences are not the same for all the floor of the depression.

Although it is an small difference compared to others observed in the area, it was not expected to exist due to the floor of the depressions are quite similar from geomorphological and topographical points of view, such as it was already described (Chapter 4). Elevation changes gradually from SE to NW in the floor of the depressions (Figure 4.8), and similar slope, aspect, curvature, and ruggedness index has been described for inner part of the depressions'

floor, i.e. Sector II (Figure 4.10). Only the areas near the walls of the depressions, and surrounding areas have different behavior and consequently differences on those topographic parameters. Moreover, other areas with similar elevation do not show this kind of difference on daytime-nighttime surface brightness temperature, neither for the case of depression A. In fact, the effect of the topography is negligible to explain this anomaly, because the anisotropic diurnal surface heating is similar and about uniform for both depressions, and the protection index is null for both areas (Figure 4.12). Then, we could discard a topographic effect like the cause of the described anomaly.

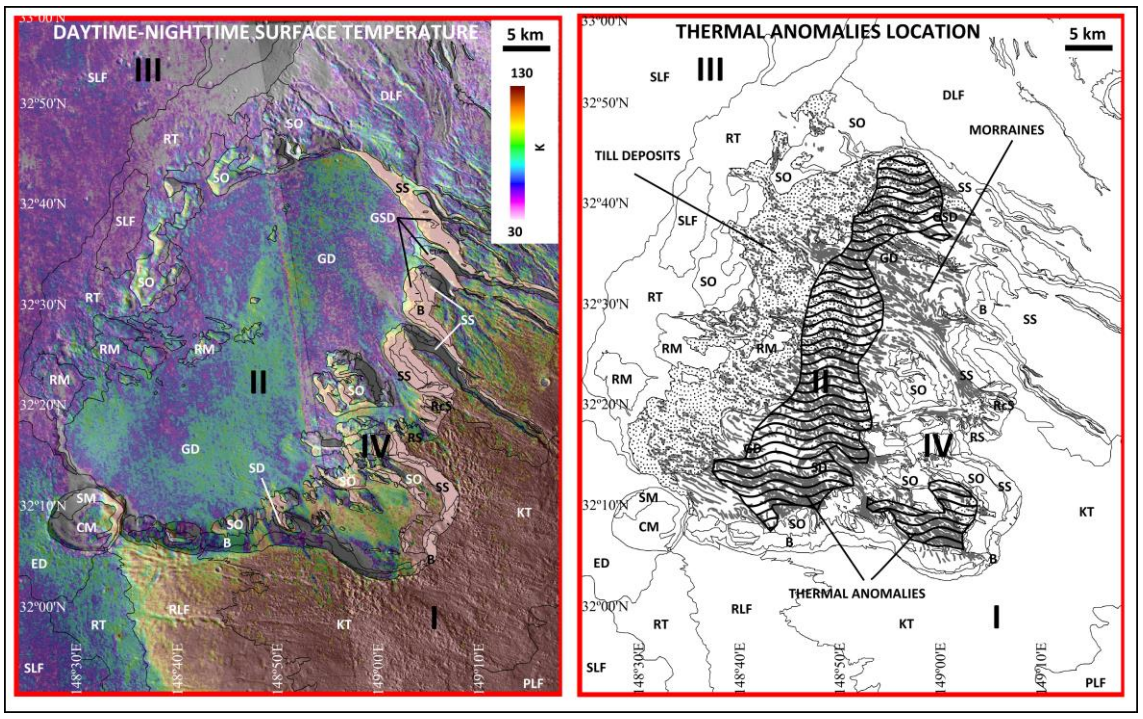

Fig. 5.8: Daytime-nighttime surface brightness temperature difference map of the lower NW flank of the Hecates Tholus volcano, Mars (left), and map showing the location of possible thermal anomalies (sectors with wavy patterns) on the floor of the depressions, where moraines-like landforms are located (right). Boxes a, b, and c mark the location of surface examples as seen on CTX images (Figure 5.9).

This different on the thermal behavior on the floor of the depression is also visible on nighttime surface brightness temperature map (Figure 5.3) and, consequently, on Thermal Inertia map (Figure 5.5). A difference on thermal inertia means differences on grain size, soil moisture, chemical composition, etc. About the grain size, the values on thermal inertia of the whole map are lower than 325 $Jm^{-2}K^{-1}s^{-1/2}$ (Figure 5.5). These low values correspond to silt to medium sand in grain size (Edgett and Christensen, 1994). By observing the few available HiRISE and CTX images of the floor of the depressions (Figure 5.9), the materials seems to be fine grained, except the westernmost sector of depression B, where more coarse and rugged

surface is observed, mapped like glacial erratic fields (de Pablo and Centeno, 2012) and interpreted to be till deposits (Chapter 4).

In fact, daytime-nighttime surface temperature difference (Figure 5.8), and the thermal inertia map (Figure 5.5) shows clearly the limit of the westernmost till deposits (Figure 5.8). However, all the other sectors of the floor of the depressions seem to have the same kind of surface, similarly covered by dust, aeolian deposits, and moraine deposits (Figure 5.9). Then, the grain size distribution on the easternmost sector of depression B, and the whole depression A, seems to have similar surficial texture, i.e., similar grain size. For that reason, we could also discard differences on grain size such as the main cause of the thermal anomaly we observe on the floor of depressions A and B.

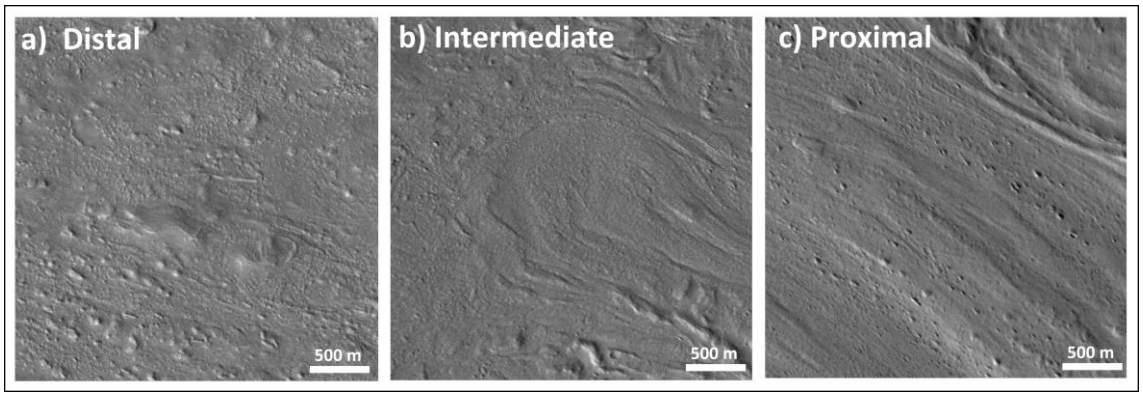

Fig. 5.9: Tiles of CTX images showing distal (a), intermediate (b) and proximal (c) areas of the glacial related deposits filling the depressions at the lower NW flank of the Hecates Tholus volcano of Mars, marking the difference on surface between distal (rugger) and intermedium and proximal areas (smoother) (Location map in Figure 5.8).

Changes on composition on surface materials on the floor of both depressions could neither explain the anomalies. DCS maps (Figure 5.6) show a random-like distribution of purple and green colors, related to mafic/basaltic composition of the surface materials. This composition is reasonable considering the volcanic origin of the edifice. The abundance of fine-grained materials on the surface was deduced from thermal inertia data and the texture observed in the imaginary. It is compatible with the presence of pyroclastic materials, some of them related to the putative lateral volcanic eruption that was proposed for the origin of depression A, and its surrounding materials (those mapped like KT unit by de Pablo and Centeno, 2012) (Neukum et al., 2004; Hauber et al, 2005). Moreover, other processes could explain the presence of fine-grained materials in the area, such as aeolian or glacial processes, (Chapter 4).

In both cases, fine-grained materials could be involved, but their composition should be mainly the composition of the materials affected by them, i.e., the volcanic materials. Then, the absence of relevant chemical variations on the surficial materials is expected for the whole study area in general, and for the floor of the depressions A and B in particular. In this way, the anomalies observed on the daytime-nighttime surface temperature map cannot reflect differences in composition and, therefore, differences in thermal inertia.

5.4.3. Buried ice?

These are all the data we have to analyze and discuss in order to solve the origin of the thermal anomalies. If the anomalies are not related to the topography, elevation, grain size, or composition, an abnormal thermal behavior of materials below the surface could be the only explanation for these thermal anomalies.

Long time ago, at the beginning of thermal infrared remote sensing as a tool for buried ice detection on glacial and periglacial environments, it was confirmed that ice-cored surfaces could have contrast on surface temperature due to differential energy budget, as well as the thickness of the mantle materials causing different thermal flux rates. That means that, a surface with similar characteristics, where buried ice exist could cause different infrared emission (e.g., Lougeay, 1972, 1974, 1982; Santeford and Smith, 1974; Hall and Martinec, 1985), still applied today on Earth (e.g., Shukla et al., 2010; Kääb et al., 2014).

Then, if the anomalies we detected reveal the presence of ice lenses below the surface, two effects could be expected: a lower surface temperature, and a surface topographic anomaly. In the first case, the lower surface brightness temperature on nighttime already exist (Figure 5.3). In the second case, we said that the terrain does not show an evident topographic change where the thermal anomalies are located. However, topographic profiles across the depressions (Figure 4.13, sections A3, B4 and B5) show the terrain is slightly convex in that places in spite the curvature map does not show that effect (Figure 4.10).

Other topographic cross sections (Figure 5.10) show similar effects on different sites of the study area. At these sites, the night temperature is lower than expected from the surrounding terrain, and it happens at different slope aspects and elevations. The convex areas, what are not visible on curvature map (Figure 4.10), is detected on a normalized heights map (Böhner and Selige, 2006) based on HRSC-derived DTM (Figure 5.10), and it shows the areas of the floor of the depressions which elevation is slightly higher than surroundings.

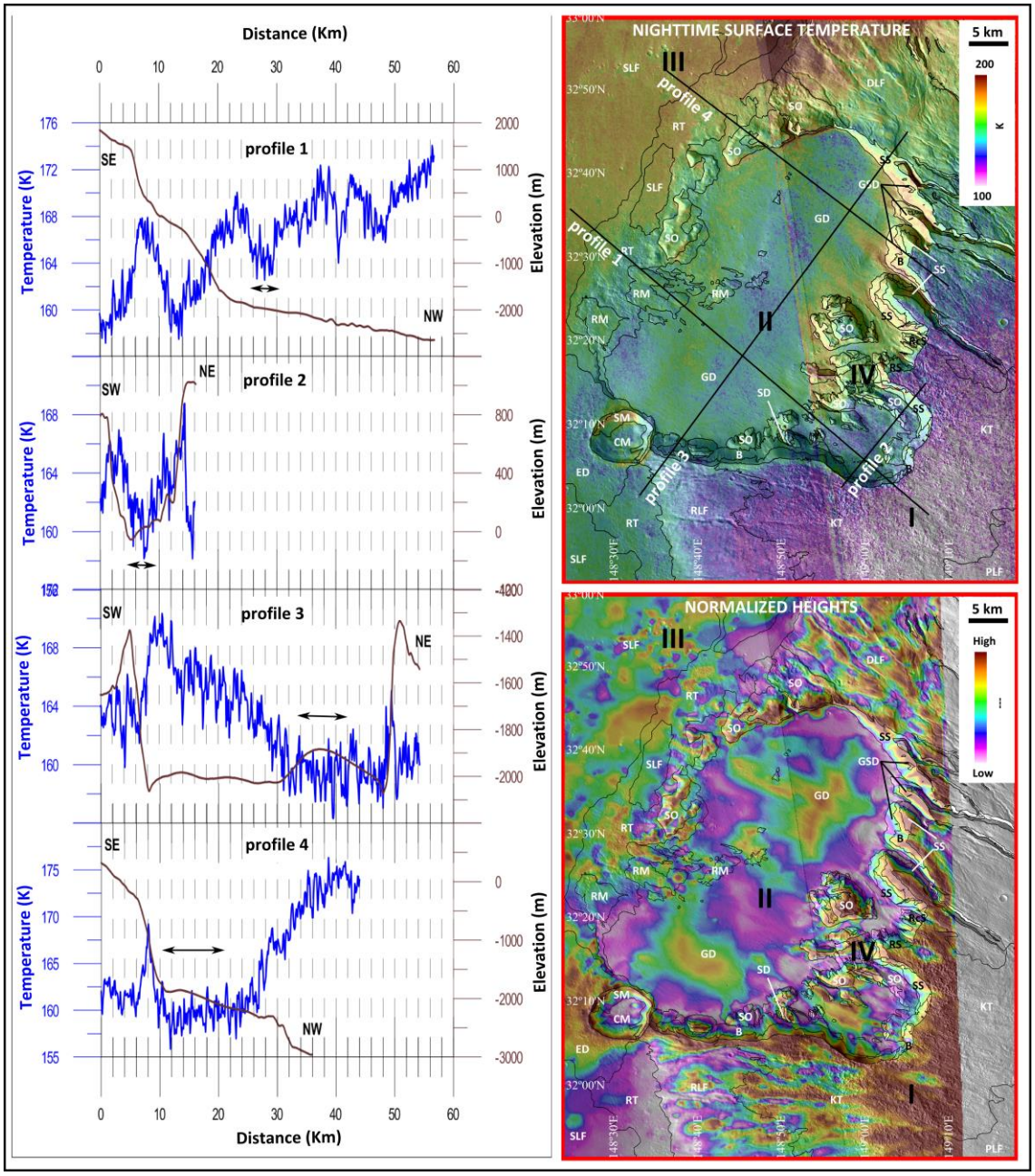

Fig. 5.10: Topographic (black lines) and nighttime surface brightness temperature (blue lines) profiles (left) across the nested depression at the lower NW flank of the Hecates Tholus volcano, Mars (upper right), and normalized heights maps (lower right) of the study area. Note the presence of convex profiles in selected sites (mainly in profile 3), what is not visible on topography, but clearly marked on normalized heights map. On these areas (arrows), lower surface temperatures than expected by the surroundings temperature behavior has been measured.

We interpret this convex structure such as a possible evidence of the existence of a buried ice body below the areas where the anomalies are located on the floor of both depressions. If the complete area was covered by extensive glaciers (Neukum et al., 2004; Hauber et al., 2005; de Pablo and Centeno, 2012; de Pablo et al., 2013), the ice thickness should reduce toward their front due to ablation processes during the last retreat episode of these glaciers (de Pablo et al., 2013). If the background surface is homogeneous without

changes on slope, then, the convex topographic section and the higher normalized heights (Figure 5.10) can reveal covered relict ice. In the western part of the depression B, glacier retreat left a field of till (de Pablo et al., 2013), while to the east, the glacier could followed a partial sublimation, reducing slightly the elevation of the terrain, but left some remnant ice until today.

However, ice did not completely disappear at the eastern sector, because the geomorphologic evidences points to its existence, such as crevasses or bergschrunds (Chapter 4). In fact, if the thermal anomaly is not located at the easternmost sector of the main depression could be due to a thicker debris mantle due to the accumulation at the mouth of the valleys dissecting the walls of the depression. In the case of depression A, there are no valleys dissecting this depression (Figure 5.1), and only a thinner mantle of debris material could cover the floor, allowing a higher thermal effect of the ice lenses on the surface temperature.

In any of those cases, some ices lenses could remain at the central area of the floor of both nested depressions, buried under the debris materials what originally covered the glacier (Figure 5.11), such as it was already proposed to exist, also based on the analysis and modelization of spectrometric data (Helbert et al., 2005; Aharonson and Schorghofer, 2006).

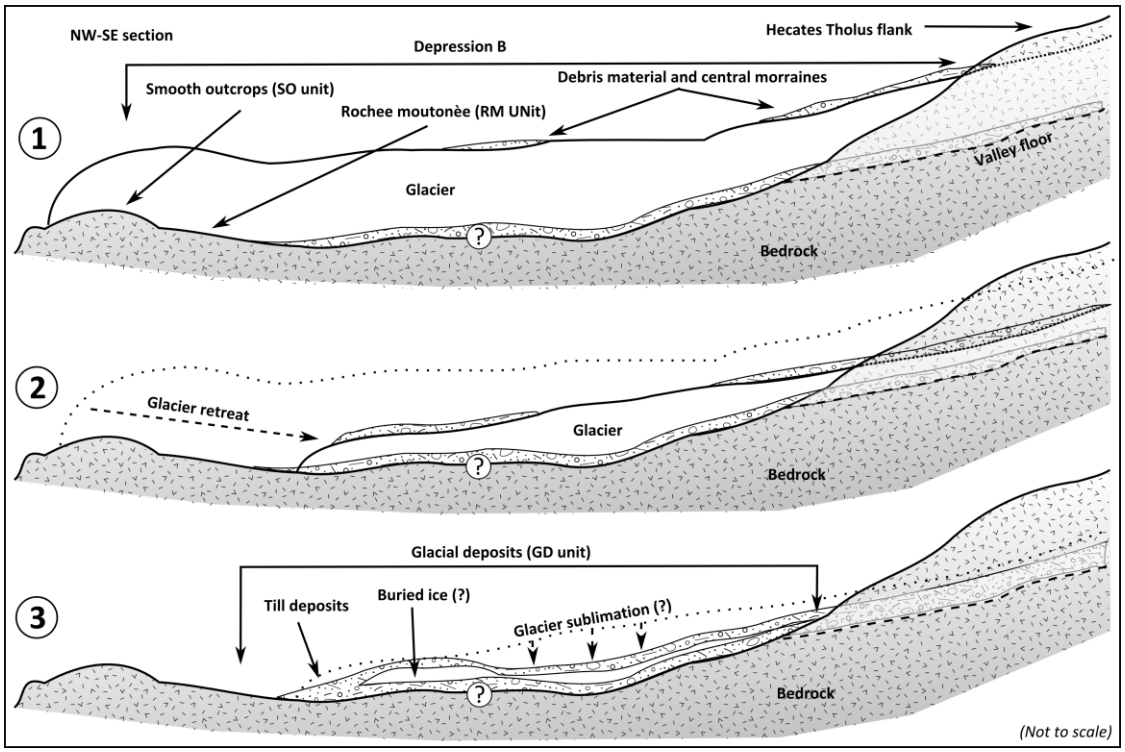

Fig. 5.11: Model showing the possible evolution of the glaciers at the lower NW flank of Hecates Tholus volcano what could explain the presence of buried ice at the floor of depressions on the flank (based on de Pablo et al., 2013 glaciers evolution.

We are not able at this stage to propose a model to explain why this happened, or how it occurred, but this could be the working hypothesis for further future research. Assuming the buried ice exist, based on our observations on daytime-nighttime surface brightness temperature and normalized heights maps, we propose areas of preferential research for future investigations on the floor of both nested depressions on the flank of the volcano(Figure 5.12).

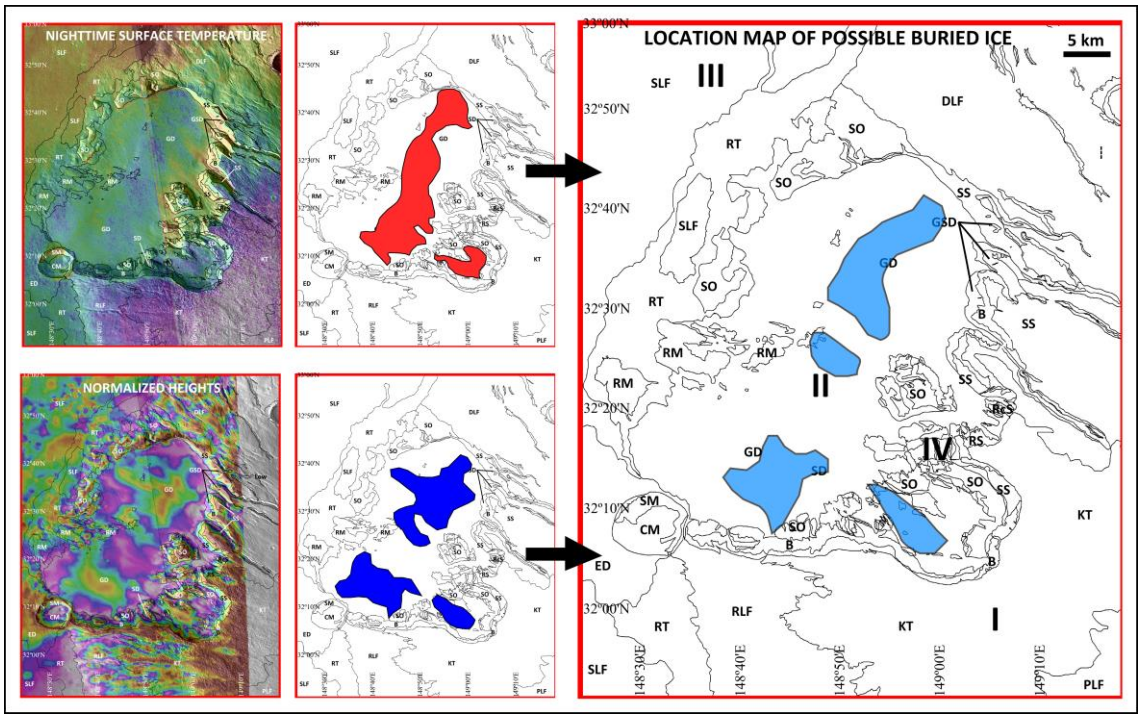

Fig. 5.12: Map of the lower NW flank of the Hecates Tholus volcano, Mars, showing the areas of preferential location of buried ice lenses (right) based on the spatial distribution of anomalies on daytime-nighttime surface brightness temperatures (top left), and normalized heights (bottom left).

If these ice bodies really exist, they should be visible on ground penetration radar data from SHARAD instrument. In fact, SHARAD data were already used to study the subsurficial structure and ice and water subsurface distribution studies (e.g., Holt et al., 2008; Carter et al., 2009; Plaut et al., 2009; Spagnuolo, 2011). However, our analysis of SHARAD radargrams (Figure 5.7) does not allow to confirm the presence of buried ice at the floor of both depressions. If ice was the main component of the materials filling the depression where the thermal anomalies where described, then these sectors itself should have been mostly transparent to radar pulses, and a clear detection of its bottom should have been possible. We didn´t observed this effect on the studied radargrams (Figure 5.7), but the lack of a subsurface radar echo does not automatically rule out the presence of ice. For example, a very rough subsurface interface, such as caused by chaotic or collapsed terrain, would result in the

diffuse scattering of radar signal that could weaken the backscattered echo below the threshold for detection. Another factor potentially affecting detection is data processing: radar echoes are processed in such a way to enhance the signal coming from nadir, filtering out echoes arriving from different directions. The flanks of Hecates Tholus are tilted, however, and to get the strongest echo from any subsurface interface, echoes should be focused in a direction perpendicular to the flanks themselves, that is away from nadir. Until a more specialized processing can take place, a final result on the lack of detection of subsurface interfaces cannot then be ruled out.

In summary, the data we analyzed does not allow to indisputably confirm the presence of buried ice below the surface, like relic ice from the glaciers existed in the area in the past for a long period at the lower NW flank of the Hecates Tholus volcano (Neukum et al., 2004; Hauber et al., 2005; Werner, 2009; de Pablo et al., 2013). However, its presence is feasible, not only because it was predicted to exist (Helbert et al., 2005; Aharonson and Schorghofer, 2006), but because of the presence of thermal anomalies on the floor of the depressions what are not able to explain by the regional distribution of topography, elevation, grain-size, or compositional factors.

5.5. Conclusions

The analysis of surface brightness temperature, derived from THEMIS-IR data, made possible to characterize thermally the lower NW flank of the Hecates Tholus volcano, although it was not possible to individually characterize each geomorphological unit already mapped in the area (de Pablo and Centeno, 2012).

Four sectors have been differentiated, depending of their thermal behavior: Sector I, related to the flank of Hecates Tholus volcano, where the daytime surface temperature is higher than nighttime temperature. Sector II, related to the floor of depressions on the NW flank of the volcano. Sector III, related to the lava flows from Elysium Mons surrounding Hecates Tholus volcano, characterized y high temperatures on both daytime and nighttime. Sector IV, related to the walls of the nested depressions and narrow and deep valleys, where there is a heavy contrast on daytime-nighttime temperatures, but also evident differences on south- and north-facing slopes due to differential insulation.

In general, the different geomorphological units do not show significant temperature changes depending of the aspect, meanwhile, in general, the surface temperature reduce with

elevation. This behavior remains during the night, and also along the different seasons, although with changes on the temperature ranges.

We detected thermal anomalies on nighttime surface temperature map also on daytime-nighttime surface temperature difference map. They are located on the central area of the floor of the main depression on the flank of the Hecates Tholus volcano, and also in most of the area of the floor of the smaller and nested depression in the same flank. This anomaly consists on a variation of about 5 K in the daytime-nighttime surface temperature difference in areas where this thermal changes in not expected due to the uniform surface characteristics. We discussed the relationships of these anomalies with elevation, topography (slope, aspect, curvature, ruggedness index, diurnal anisotropic heating, or protection index), thermal inertia and mineral composition, and any of them seems to explain the anomaly.

A slightly convex relief on the topographic cross sections of the area is observable at sites where the anomaly is located allowed us to hypothesize about the existence of ice lenses at these sites. Those lenses could be relict from the extensive glaciers active in the area for millions of years (Neukum et al., 2004; Hauber et al., 2005; de Pablo et al., 2013). However, ground penetration radar data from SHARAD instrument did not made possible to clearly distinguish any inner subsurface structure, neither to locate the base of the hypothesized buried ice body in the floor of the nested depressions. In spite of that, those data neither allow to discard this hypothesis.

Although we are not able to confirm the presence of buried ice, remnant from the past glacial events in the area, the anomalies are a solid evidence of present ice, provided that they are not directly related to topographic or elevation effects, differences on grain size, or the main mineral composition of surface materials.

Although the bibliography about Mars do not pay so much attention to the analysis of brightness temperature, except as a qualitative approach to thermal inertia, our work revealed that this data could have more applications on Mars -for example, thermal anomalies could help on the study of several geological processes, including the glacial process. On the other hand, the calculation of Apparent Thermal Inertia using daytime and nighttime mosaics of THEMIS-IR-derived surface brightness temperature images, and the use the CTX images as a substitute of surface albedo, resulted a good approach for qualitative analysis, due to its similarities to the quantitative Thermal Inertia maps.

PhD thesis

Glacial geomorphology of theNW flank of the Hecates Tholus volcano, Mars

6

Mars-Earth analogues

Miguel Ángel de Pablo Hernández

2015

Abstract:

Deception Island is an active volcano at the South Shetland Archipelago, Antarctica (62º58'37''S, 60º39'00''W) about 12 km wide, and with a maximum altitude of 540 m. Glaciers cover the 57% of the island, flowing from the ice caps that cover the higher elevations. The volcanic activity during the 1960's and 1970's produced a layer of pyroclastic material that covers almost half of the glaciers surface. However, glacial features could be still recognized in those covered glaciers, converting them into a perfect analogue to compare the features that could be observed on the NW flank of the Hecates Tholus volcano of Mars (and other Martian volcanoes), where ice is not visible on satellite images provided by the multiple missions sent to Mars. Here, we show and compare the glacial geomorphological forms of Deception Island (Antarctica) and Hecates Tholus (Mars), including crevasses, bergschrunds, moraines, erratic blocks, depressions, terminus, or ridges, among others. Those geomorphological similarities and the distribution of them at the Hecates Tholus area allow us to discuss the possible existence of glaciers covered by debris materials, pyroclastic deposits and dust layers on Mars, in agreement with other similar proposal existing on the bibliography for this volcano. Finally, we briefly discuss the interest of this island to conduct different researches to increase our knowledge about the covered glaciers on Mars and their dynamics.

Resumen:

La isla Decepción es un volcán activo del archipiélago de las Shetland del Sur, Antártida (62º58'37''S, 60º39'00''W), de unos 12 km de diámetro y una altitud máxima de 540 m. Los glaciares cubren el 57% de la isla. La actividad volcánica durante los años 60 y 70 del pasado siglo XX generaron materiales piroclásticos, muchos de los cuales cubren en la actualidad parte de dichos glaciares. A pesar de estar cubiertos, aún son reconocibles muchos rasgos glaciares, convirtiendo así a estos glaciares antárticos en un análogo perfecto con el que comparar los rasgos que se pueden observar, entre otros, en la base del flanco Noroeste del volcán Hecates Tholus de Marte, donde no se observa hielo en las imágenes de las diferentes misiones. Aquí se muestran y comparan los rasgos geomorfológicos glaciares de la isla Decepción (Antártida) y Hecates Tholus (Marte), incluyendo crevasses, rimayas, morrenas, boques erráticos, depresiones, frentes glaciares, o crestas. Estas similitudes geomorfológicas y su distribución en Hecates Tholus permiten discutir la posible existencia de glaciares relictos cubiertos por derrubios, piroclastos o polvo en Marte, de acuerdo con otros trabajos previos de la zona. Finalmente, se discute brevemente el interés de la isla Decepción como análogo terrestre para comprender mejor los posibles glaciares cubiertos de Marte y su dinámica.

Related publications:

Centeno, J. D., de Pablo, M. A., Molina, A., and Ramos, M.2013. Glaciers on Deception Island, Antartica: Analogue of the Debris-Covered Glaciers on the Hecates Tholus Volcano of Mars. Lunar and Planetary Science Conference, 44. Abstract #1495.

de Pablo, M.A., Ramos, M., Vieira, G., Gilichinsky, D., Gómez, F., Molina, A. and Segovia, R. 2009. Deception island, Antarctica: a terrestrial analogue for the study and understanding of the Martian permafrost and subsurface glaciers. Geophysical Research Abstracts, 11, EGU2009-1292.

6.1. Introduction

The study of terrestrial analogues has been a fundamental methodology to identify and recognize the existence of different geological landforms and processes on the surface of Mars (e.g., Chapman, 2007; Hipkin et al., 2013; Breed, 1977; Berkley and Drake, 1981; Lucchitta, 1981; Rotshchild, 1990; Hartmann et al., 2003; Ormö et al., 2004; Arfstrom and Hartmann, 2005; Komatsu et al., 2007; Kochel and Trop, 2008; Pacifici, 2009; Chan et al., 2010; Fernández-Remolar et al., 2011; Ulrich et al., 2012; Bishop et al., 2013; Hipkin et al., 2013, and references there in). In this sense, the description of glaciers and glacial features on Mars has been essentially based on their image analogy with the landforms previously studied on the surface of our own planet.

Ice and glaciers have never been found on the surface of Mars outside the polar caps, or small ice patches at selected sites of the planet (e.g., Carr, 2006). However, previous works on Mars have described many geomorphological elements similar to those caused by glacial activity on Earth (e.g., Milkovich et al., 2006; Fastook et al., 2008, 2011; Morgan et al., 2009; Baker et al., 2010; Dickson et al., 2010, 2012; Fasset et al., 2010; Levy et al., 2010; Hubbard et al., 2011; Souness et al., 2012). Their existence, as well as other forms related to the existence of ice under the surface (pingos, and corroded, scalloped or polygonal terrains, etc.) and above the surface (like subglacial volcanoes), evidence the presence and the role of ice agent in the past of the planet (e.g., Rossbacher and Judson, 1981; Carr, 1986, 2006; Anderson, 1992; Chapman, 1994; Fairén et al., 2003; Head et al., 2004, 2004; Madeleine et al., 2009; Page et al., 2009; Carr and Head, 2010; Fairén, 2010; Martínez-Alonso et al., 2011; Koutnik et al., 2013).

Glacial landforms have been described in the Martian polar caps, and in other areas such as Deuteronilus Mensae, Neredium Montes, Hellas Planitia or the Middle and Northern Plains (e.g., Fishbaugh and Head, 2005; Banks et al., 2008; Tanaka et al., 2008; Hubbard et al., 2011; Fastook et al., 2011, 2012; Dickson et al., 2012). In addition, several volcanoes of Mars show glacial landforms in their flanks. In fact, some volcanoes located at tropical latitudes show glacial features on their northwestern flanks, such as Olympus Mons, Arsia Mons, Ascraeus Mons, Pavonis Mons on the Tharsis volcanic province (e.g., Head and Marchant, 2003; Head et al., 2004, 2005; Milkovich et al., 2006; Shean et al., 2005, 2007; Fassett and Head, 2007; Kadish et al., 2008; Fastook et al., 2008; Robbins et al., 2011). Different mechanisms has been proposed to explain the occurrence of relevant amounts of ice capable to form ice patches, ice caps, and glacial flows only on the NW-facing slopes, including snow

precipitation during high obliquity periods (e.g., Jakosky and Carr, 1985; Laskar et al., 2004; Forget et al., 2006) or ice-deposits formation at tropical latitudes during low obliquity periods (e.g., Levrard et al., 2004). These glacial events could have occur on ancient times, but also in more recent times related to the last ice ages on Mars (e.g., Laskar et al., 2004; Head et al., 2003, 2004, 2005, 2006; Neukum et al., 2004; Hauber et al., 2005; Forget et al., 2006).

In the Elysium volcanic province of Mars, Hecates Tholus (32.12ºN, 150.24ºE) is the unique volcano showing possible glacial features (e.g., Neukum et al., 2004; Hauber et al., 2005; de Pablo and Centeno, 2012), and they concentrate in its lower NW flank (Figure 6.1a), such as revealed by the presence of different geomorphological features, that has been described and mapped on this area thanks to the use of the high-resolution images from different orbiters. However, no ice has been observed on the surface at this flank of the volcano, neither on the high-resolution images provided by the most recent missions to Mars (Mars Reconnaissance Orbiter). Then, although geomorphological features (such as crevasses or moraine deposits; de Pablo and Centeno, 2012) point toward the existence of very shallow ice under the surface, its presence has not been still confirmed because ice has not been directly observed.

Different researchers have focused on the detection of ice in the first meters below the surface at this site. They report thermo-physical evidences and models based on remote sensing data, such as brightness temperature or thermal inertia (Helbert et al., 2005; Aharonson and Schorghofer, 2006; Centeno and de Pablo, 2012; de Pablo and Centeno, 2013). They conclude that it is still possible to have some quantities of ice forming lenses at relatively shallow depths of only 1-2 meters, but limited to very selected sites (Helbert et al., 2005) of the area where the glacial-related deposits has been described (Neukum et al., 2004; Hauber et al., 2005; de Pablo and Centeno, 2012).

However, we still lack clear evidence of the presence of important quantities of glacial ice –and this work is an attempt to contribute. We focused on the analysis of the geomorphological features observed in High Resolution Imaging Science Experiment (HiRISE) and Context (CTX) images of the lower NW flank of the Hecates Tholus volcano (Figure 6.1a; Table 6.1). To give a solid foundation to our interpretations, we based our research on the study of a terrestrial analogue, the pyroclast-covered glaciers on Deception Island, Antarctic Peninsula, Antarctica (62°58’37”S; 60°39’00”W, Figure 6.1b). Deception Island is an active volcano at the South Shetland Archipelago, in the Antarctic Peninsula region with glaciers, some of them partially covered by air-fall materials (mainly lapilli) from the last eruptions

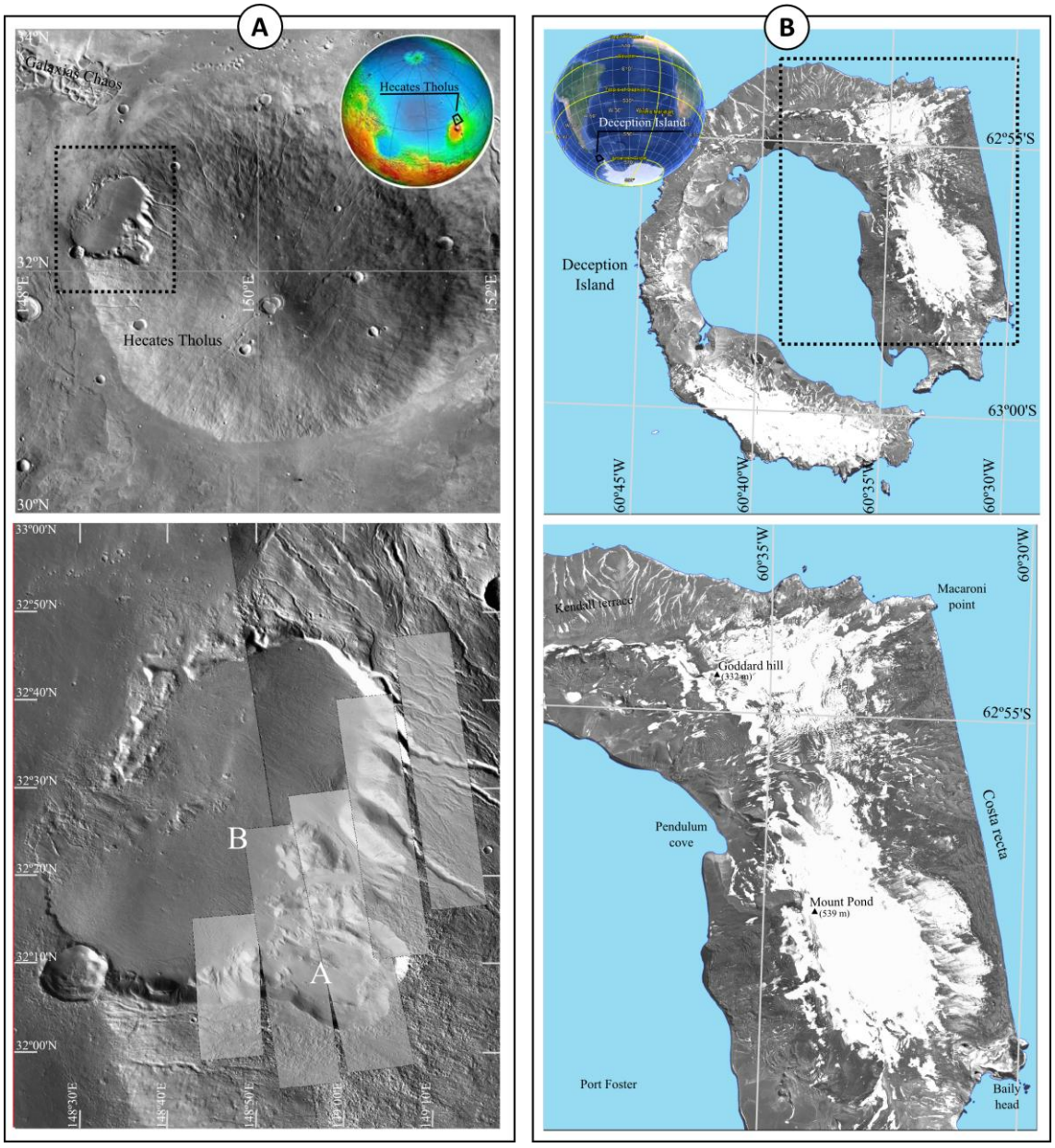

Fig. 6.1: Location map of the study areas, at the lower NW flank of the Hecates Tholus volcano of Mars (A), and at the east side of Deception Island (B), South Shetland Archipelago, Antarctica.

occurred in late 1960's and early 1970's (e.g., Baker et al., 1975; Martini and Giannini, 1988, Vila et al., 1992; Almendros et al., 1997; Aristarain and Delmas, 1998; Cooper et al., 1998; Alguacil et al., 1999; Pallàs et al., 2001; Smellie, 2002a,b; Ibañez et al., 2000). Those materials hide the ice (mainly at the lower half of the glacier tongues) which it is not visible in the satellite images (Figure 1b), such as most likely occurs on the floor of depressions A and B of Hecates Tholus volcano (Figure 1a). However, the thin pyroclastic cover allows to recognize the most representative glacial morphologies related to the glacier that flows under this pyroclastic layer (such as moraines, roches moutonnees, horns, crevasses, ridges, etc.). In this research we carried out a detailed analysis of glacial landforms in satellite images of Deception

Island and compared them with the features we observed on the high resolution images from Hecates Tholus volcano. Based on the analogues, we finally discuss if it is possible the existence of ice at present day under the materials covering the surface of the putative glaciers on Mars.

6.2. Data and methods

This research is based on the analyses of remote sensing data (images) from both, Hecates Tholus volcano on Mars and Deception Island volcano on Earth. However, we also developed some fieldwork on Deception Island in order to confirm our observations on the satellite images.

Panchromatic satellite images from Deception Island were acquired by Quickbird-2 satellite on January 21st, 2003 (Antarctic summer), with a spatial resolution of 0.5 m/ pixel (Figure 6.1b). Those images, in GeoTiff format, did not require a special treatment and they were directly added to a Geographic Information System (GIS) based on the use of ArcGIS software (by ESRI), where they were analyzed. On the other hand, we used high-resolution images of the Martian surface acquired by the HiRISE instrument on board of the Mars Reconnaissance Orbiter (MRO) of NASA, with spatial resolutions ranging between 0.50 and 0.25 cm/pixel. Those images, in JPG2000 format, were obtained through the NASA's Planetary Data System (PDS) Geosciences Node's Orbital Data Explorer (ODE) by the University of Washington in Saint Louis (http://ode.rsl.wustl.edu/; Benneth et al., 2008; Wang et al., 2009, 2010, 2011). We later processed them with PDS2WORLD script, from the Astrogeology branch of the United States Geological Survey (http://webgis.wr.usgs.gov/pigwad/tutorials/scripts/perl.htm), in order to obtain the adequate projection header files. This simple processing of the images were enough to add those images into a GIS for Mars, completing the geodatabase used to develop the geomorphological mapping and age-derivation by the crater-size measurement (de Pablo and Centeno, 2012; de Pablo et al., 2013). Although at present day, there are available 13 HiRISE images covering the study area of the flank of the Hecates Tholus volcano, due to the image overlapping and their different spatial resolutions, we finally analyzed only 6 of those HiRISE images (Figure 6.1a; Table 6.I) to locate and describe possible glacial landforms.

The fieldwork on Deception Island consisted on short fieldtrips along the boundaries of the Black, Red and Green glaciers, located at the inner flank of the eastern side of the island. Their name derive from the main color of the pyroclasts that cover the glacier as seen in its

terminus in Port Foster, the inner bay of Deception Island (Figure 6.1b). Those fieldtrips occurred during five consecutive Antarctic summers in January 2009 to January 2013. Due to security reasons, it was not possible to carry out long fieldtrips to the central part of those debris-covered glaciers, since in general there are many crevasses and thin layers of pyroclastic deposits hiding most of them. For that reason, we also made supplementary fieldtrips to different sites of the island that made possible to recognize the covered glaciers from the distance. In addition, we sailed all around the island in order to have a wider and more complete overview of the island and its glaciers in December 2012. Observations and the pictures taken during all those fieldtrips and sailings, have allowed us to interpret the features we observe in the satellite image of Deception Island.

Table 6.1: CTX and HiRISE images used on the study of analogues between covered glaciers on Hecates Tholus (Elysium region, Mars) and Deception Island (Antarctica, Earth). Coverage of those images is showed in Figure 1.

Instrument	Image	Res. (m/pixel)	Date	Ls
HiRISE	esp_024207_2130_red	0.50	2011-09-25	6.0
HiRISE	esp_024418_2125_red	0.50	2011-10-12	15.0
HiRISE	esp_025275_2125_red	0.50	2011-12-17	44.1
HiRISE	esp_025275_2125_red	0.50	2011-12-17	44.1
HiRISE	psp_001527_2125_red	0.25	2006-11-23	139.7
HiRISE	esp_027029_2125_red	0.25	2012-05-02	104.9
CTX	B04_011324_2128_XI_32N211W	6.00	2008-12-25	180.1
CTX	B06_011957_2128_XI_32N211W	6.00	2009-07-20	209.0

6.3. Hecates Tholus and Deception Island

6.3.1. Geological settings

The Hecates Tholus volcano is one of the three volcanoes of the Elysium Volcanic rise of Mars, in the northern lowlands, formed about 3.8 Ga ago (e.g., Neukum et al., 2004; Hauber et al., 2005; Werner, 2009; Platz and Michael, 2011; de Pablo et al., 2013). This volcano is about 8,000 m high and 180 km in diameter, with a nested complex caldera on the summit, 10 km wide and 600 m deep, caused by five overlapping collapse episodes occurred between 1 Ga and 100 Ma (Neukum et al., 2004; Hauber et al., 2005). The flanks of the volcano have a smooth surface, a radial channels network, and stepped slopes (Mouginis-Mark et al., 1982; Gulick and Baker, 1989, 1990; Fasset and Head, 2006, 2007). The origin of those channels has been discussed, although the fluvial origin seems to be the most feasible, and the proposed sources of water includes: redistribution of water equatorward, such as reveals the presence

of glacial feature in the equator (e.g., Jakosvky and Carr, 1985; Jakosky and Haberle, 1992; James et al., 1992; Carr, 1996; Richardson and Wilson, 2002; Head et al., 2003; Head and Marchant, 2003; Mischna et al., 2003; Shean et al., 2005); geothermal melting of a snow cap on the volcano (Gulick et al., 1997; Zent, 1999; Gulick, 2001; Carr and Head, 2003); remobilization of volatiles on a degassing stage of this volcano (Scott and Wilson, 1999); and basal melting of snowpacks located on the higher parts of the flanks of the volcano (Carr and Head, 2003; Fasset and Head, 2006).

However, the most relevant feature of the edifice (any other volcano on Mars shows something similar) is the presence of two nested depression at the lower NW flank. The higher and smaller depression was interpreted to be caused by a lateral volcanic eruption (e.g., Neukum et al., 2004; Hauber et al., 2005), probably related to magma-water interactions (Mouginis-Mark et al., 1982; Mouginis-Mark and Christensen, 2005) which is in agreement with the presence, near the base of this volcano, of the shoreline of the ancient ocean of Mars (e.g., Baker et al., 1991; Clifford and Parker, 2001; Fairén et al., 2003), and the abundant magma-water interactions described in this region of Mars, including magma-ice interactions (e.g., Mouginis-Mark, 1985; Mouginis-Mark et al., 1982, 1984; Chapman et al., 2000; Mouginis-Mark and Christensen, 2005). The subglacial volcanoes described in the surrounding region of Utopia Planitia support this glacial environment (Chapman, 1997, 2003) and agree with the proposals by different authors on the role of glaciers in the evolution of this volcano (Gulick et al., 1997; Zent, 1999; Gulick, 2001; Carr and Head, 2003; Neukum et al., 2004; Hauber et al., 2005; Fasset and Head, 2006; de Pablo et al., 2012). In detail, bergschrunds, seracs, crevasses, moraines, flow structures, rochee moutonnées, flutes, arêtes and glacial erratics has been described and mapped inside the nested depressions on the base of the volcano (de Pablo and Centeno, 2012), at the area 31.8º to 33.0ºN and 148.37º to 149.3ºE (Figure 1a). However, despite of the presence of those features, ice has been not directly observed, and the whole area is debris-covered. Remnant ice lenses could exist, such as points the existence of mapped pingos (de Pablo and Centeno, 2012), but also such as reveals the analysis of thermophysic properties of the surface based on remote sensing data (Helbert et al., 2005).

Deception Island is part of the South Shetland Archipelago, Antarctica (Figure 6.1b), and one of the main volcanoes of the Antarctic continent along with Penguin Island (at the South Shetland archipelago too) and Mount Erebus (in Ross Island). It is a collapsed caldera, about 12 km in diameter (Baker et al., 1975; Rey et al., 1995; Martí et al., 1996; Smellie et al., 2006) with an inner bay (Port Foster) open to the SE through a gap (Neptune Bellows). Ring-

shaped in plan view, the island is a chain of summits (maximum elevation: Mount Pond with 539 m a.s.l.) mostly covered by glaciers that flow to reach the sea level (Figure 6.1b).

The volcanic activity seems to be related to both subduction of the Drake Plate under the Antarctica Plate (e.g., Hawkes, 1962; Baker et al., 1975; Grad et al., 1992; de Rosa et al., 1995) and of extensional tectonics (e.g., Rey et al., 1995; Martí et al., 1996) since the island is located in the confluence of the southwestern end of the Brandsfield Trough and the Hero Fracture Zone. Besides the main caldera, different volcanic craters related to post-caldera eruptions characterize the inner part of the island, some of them relatively recent. In fact, the last volcanic eruptions occurred in 1967, 1969, and 1970, but fumaroles, geothermal anomalies, thermokarsts and seismic activity remain active. Those eruptions caused the presence of air-fall deposits (volcanic cinders and pyroclasts) mantling some of the glaciers that cover more than half of the island surface. The result is that, during the austral summer (when the winter snow precipitation melts), the ice of the glaciers is covered with pyroclastic materials up to 3 m thick, hiding the ice layer when observed from their surface (e.g., Klay and Orheim, 1969) or from satellite. It is possible to observe the ice mass forming those glaciers, but only at selected sites, mainly in the terminus and some crevasses, but necer from satellite images. Those pyroclasts-covered glaciers show several geomorphological features characteristic of glacial flow (crevasses, seracs, moraines, and other flow structures). These landforms allow to recognize and to map the glacier extension from the satellite imagery in spite the pyroclastic cover.

There are additional effects on their pyroclastic cover: the insulation of the glaciers from the environmental conditions, due to the low thermal conductivity of those materials (Klay and Orheim, 1969) that could help to preserve the ice of the glacier. The volcanic activity and the presence of glaciers in the island caused magma-ice and magma-water interaction that had an important role on the recent volcanic events, such as on the 1969 eruption (Smellie, 2002b) as well as on more recent activity (Somoza et al., 2004).

6.3.2. Climatic conditions

The Mars Climate Database (MCD), supported by data from different robotic missions to Mars (Lewis et al., 1999; Forget et al., 1999), shows that the climate in the lower NW flank of the Hecates Tholus volcano should be cold, with mean air temperature near the surface ranging between -108.0ºC to 1.3ºC. In all scenarios contained in the MCD (cold, warm, and mean conditions), the maximum temperature is reached in month 5 (Ls 150º) and the

minimum in month 10 (Ls 270º). Minimum temperatures in coldest scenario reach -112ºC, what it is clearly colder than the lower air temperature we registered at Deception Island during the last decade, about -23ºC.

On the other hand, the climate in Deception Island (and the other islands of the South Shetland Archipelago) shows extreme seasonal variability in temperature and snow cover (Smith et al., 2003). Harsh weather conditions prevail all the year around. In spite of the maritime influence, winters are long with mean daily temperatures below 0ºC, and summers are short and characterized by freezing and thawing cycles. The mean annual air temperature at sea level ranges between -3.9ºC and -1.6ºC, with an increase of 0.25ºC/decade since 1951 (Turner et al., 2005). Precipitations (mainly snow, also during the Antarctic summers) range between 470 and 700 mm of water equivalent with an extremely variable inter annual snow regimen (Styszynska, 2004).

6.4. Morphological analogues

6.4.1. Analogues

Deception Island shows many reliefs, features and landscapes that could be considered analogues of some Martian landforms (e.g., Smellie, 2002a; Martínez-Frías et al., 2003; de Pablo et al., 2009; Prieto-Ballesteros et al., 2012; Molina et al., 2013). In fact, the morphological similarities and harsh weather conditions on this island allowed to test the ground temperature sensors of the Rover Environmental Monitoring Station (REMS) instrument on board of Mars Science Laboratory Mission (Ramos et al., 2012; Gómez-Elvira et al., 2012). The analogues include a wide variety of reliefs, from different origins including volcanic, fluvial, aeolian or periglacial, among others (de Pablo et al., 2009; Molina et al., 2013). However, our main target is to establish the morphological analogues between Deception Island and the possible glacial features and reliefs and landscapes described or observed on the lower NW flank of the Hecates Tholus volcano, especially those that could be caused only by very recent glacial activity.

6.4.2. Covered glaciers

Most glaciers of East Deception Island are covered with pyroclastic material, and the ice is exposed and free from pyroclastic cover only in the higher areas were ice flow has revove an important part of the pyroclastic cover (Figure 6.2). The middle and lower sectors of the glaciers remain partially to completely covered by a layer of unconsolidated pyroclastic

material (mainly lapilli) from the last eruptions in 1960's. At the visited sites, the thickness of this mantle-like layer could reach 3 meters, hiding completely the glacial ice (Figure 6.2). The ice is only visible in the front (terminus) of the glaciers (in the shore of Port Foster or the Antarctic Ocean in Costa Recta -as shown in Figure 6.3), in narrow and elongated depressions on the glaciers, or at located sites on their edges. In spite of the presence of the pyroclastic deposit covering the surface of the glaciers, the morphology of the glacier tongues are mostly recognizable, as well as some of their inner structures (such as we will see below). Only at selected sites, the pyroclastic surface remains completely smooth, hiding any possible morphology or structure of the glaciers (Figure 6.2). In those cases, the reconnaissance of the glacier existence below the surface is difficult and requires field contextual observations, because the surface does not show characteristic features (Figure 6.2). Then, without the presence of additional evidences (as textures or structures) is it not possible to establish the presence of a glacier under the surface. On Mars, many different sites show features that different authors proposed to be debris-covered glaciers (e.g., Squyres, 1978; 1979; Lucchitta, 1984; Milliken et al., 2003; Pierce and Crown, 2003; Head and Marchant, 2003, 2009; Shean et al., 2005; Head et al., 2006a,b, 2010; Levy et al., 2007, 2009, 2010; Kadish et al., 2008; Chuang and Crown, 2009; Byrne et al., 2009; Baker et al., 2010; Souness et al., 2012), including those on the lower NW flank of the Hecates Tholus volcano (e.g., Hauber et al., 2004; Neukum et al., 2005; de Pablo and Centeno, 2012). Obviously, being impossible the direct observation of ice, only contextual analysis of images, morphology and structures suggested the glacier existence. With such difficulties to confirm the presence of glacial ice, only a characteristic set of glacial features can be hold as clear evidence, such as lobate debris aprons, lineated valleys, or others

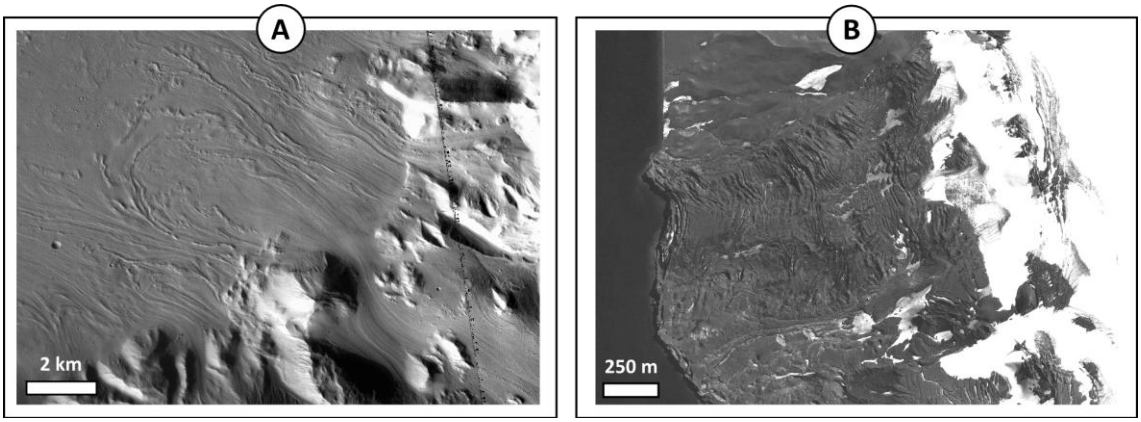

Fig. 6.2: (1) Example of covered glaciers on both Hecates Tholus (A) and Deception Island (B). The general morphology and the presence of selected features on both areas could be explained by glacial activity, only confirmed on Deception Island thanks to the presence of ice (B), which is not visible in the HiRISE image of Mars (A). (2) In some cases, the surface remains smooth and ice is not visible, because the glacier remains hided under a layer of material on Deception Island (B) and possibly also on Hecates Tholus (A).

summarized by Dickson et al. (2012) (Figure 6.2). Some of these elements are clear results of glacial activity although only fe of them are proxy data of present glacial ice and glacial activity. We observed some of them on both Hecates Tholus and Deception Island volcanoes, such as we described in the next paragraphs.

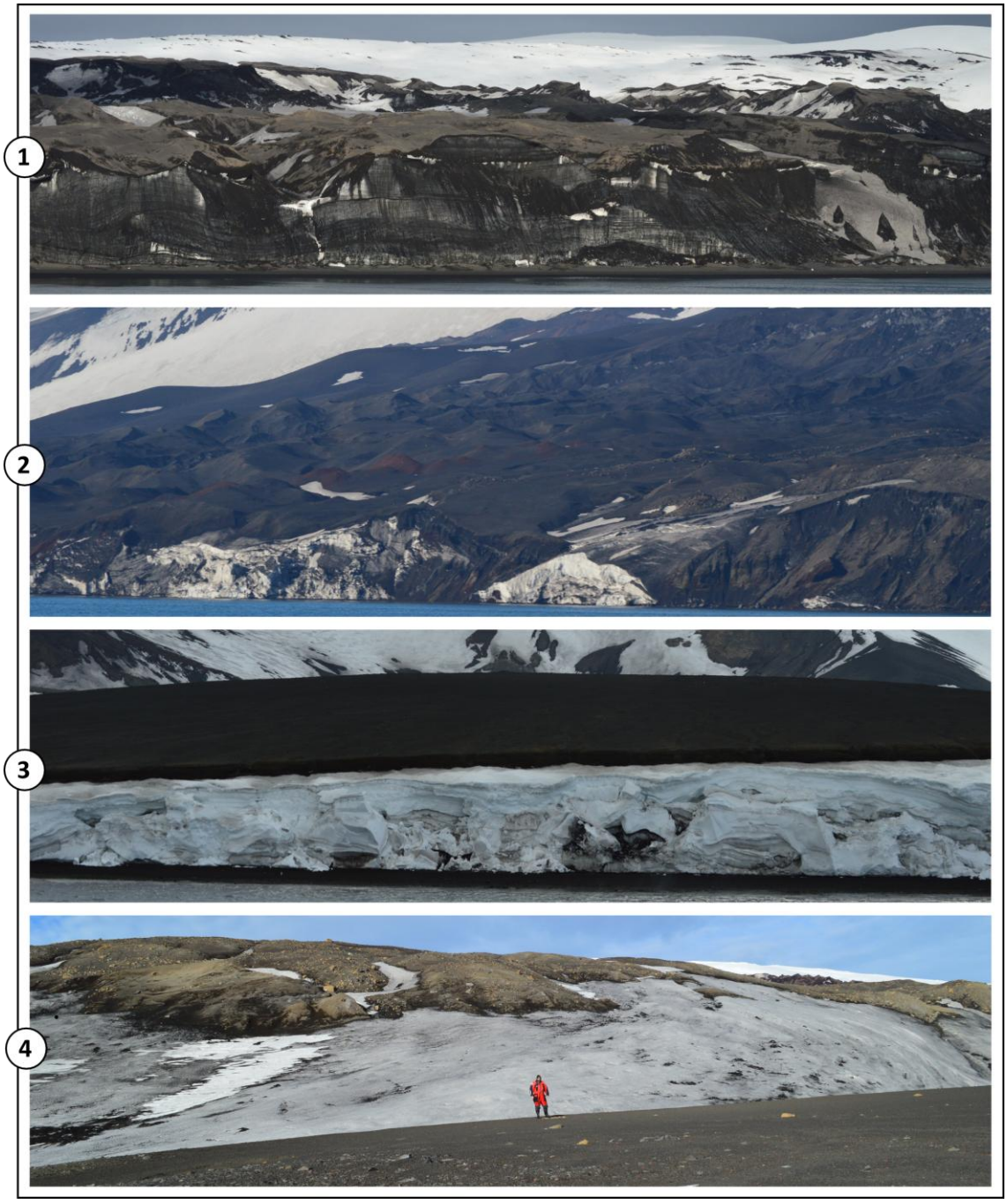

Fig. 6.3: Pictures of debris- and pyroclastic-covered glaciers on Deception Island. Cover thickness varies from 0.3 to 3 m. (1) View from Costa Recta of the covered glaciers at the eastern external flank (front height: 45 m.); (2) View from Port Foster of the covered glaciers flowing to the west from the ice cap at Mount Pond (front height: 25 m.). Note the hummocky surface; (3) View from Port Foster of a remnant ice mass from an old glacier covered by pyroclastic layers (front height: 10 m.); (4) View of a gradual inland terminus of a covered glacier. Note the variable roughness of the materials covering the glacier as well as the existence of erratic blocks and volcanic bombs on top (Pictures: M.A. de Pablo).

6.4.3. Cirques

The laterally open bowl-shaped depressions are the head of a number of glaciers on the Earth. On Deception Island, since the main ice mass flowing downslope comes from an ice cap located at the rim of the collapse caldera, there are not many cirques. However, small cirques are located at the head of other small covered glaciers located on the northern part of the island (Figure 6.4). Due to the intense tectonic control, those cirques do not have a clear bowl-shaped morphology and they show resurfacing by recent fluvial and slope processes. On Hecates Tholus, we don't find so many cirques (Figure 6.4), because the ice seems to came from ice patches on the top of the volcano (Gulick and Baker, 1989, 1990; Gulick et al., 1997; Zent, 1999; Gulick, 2001; Carr and Head, 2003; Fasset and Head, 2006), flowing downslope on the NW flank, and spreading at the inner depression, after a short travel through some valleys originally excavated by streams (e.g., Mouginis-Mark et al., 1981; Gulick et al., 1997; Fasset and Head, 2006). Actual glacial cirques on Hecates Tholus are anecdotic and small, but their morphology is similar to those observed on Deception Island, and latter modified by more recent processes as well (mainly slope processes, as it will be discussed below).

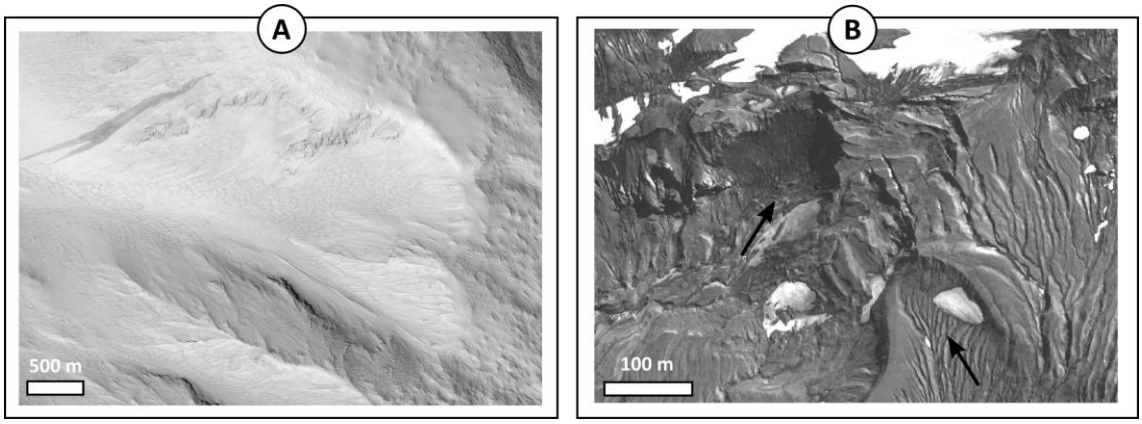

Fig. 6.4: Example of glacial cirques on Hecates Tholus (A) and Deception Island (B). On the terrestrial examples (arrows), they are isolated and were clearly latter modified by streams, meanwhile on the Martian ones, they are nested at the head of a valley, and filled by solifluction deposits.

6.4.4. Glacial Valleys

Later erosive or sedimentary processes in Earth very often destroy the typical U-shaped transversal topographic profiles of glacial valleys. Some valleys seem to be excavated by glaciers in Deception Island, although on present times they only show fluvial, periglacial and slope processes (Figure 6.5). Field observations and topographic data analysis allow to observe that those valleys have regular straight flanks with steep slopes, generally covered by

slope deposits, and a flat floor formed by consecutive erosion and sedimentation processes caused by seasonal streams. This morphology is not U-shaped, but trough-shaped, that is also a typical morphology for glacial valleys.

On the Hecates Tholus area, U-shaped hanging valleys have been described (de Pablo et al., 2013), which supports the existence of glacial events in the area in the past. However, the main valleys reaching the depression B, where the possible glacial deposits are abundant, do not show this U-shaped transversal topographic profile, but a V-shaped (Figure 6.5). This could be caused because most of those valleys where originally carved by streams coming from the summit of the volcano (e.g., Gulick and Baker, 1989, 1990; Gulick et al., 1997; Zent, 1999; Gulick, 2001; Carr and Head, 2003; Hauber et al., 2004; Neukum et al., 2005; Fasset and Head, 2006), and later used by the glacial ice masses to flow downslope. However, at the bottom of some of those valleys, surrounding the materials filling the valleys, steeped slopes are observable on HiRISE images, that could be interpreted to be shoulders caused by glacial net ablation, such as occurs on Earth. Others valleys show a trough profile, with flat floors and regular and straight slopes, similar to those of Deception Island.

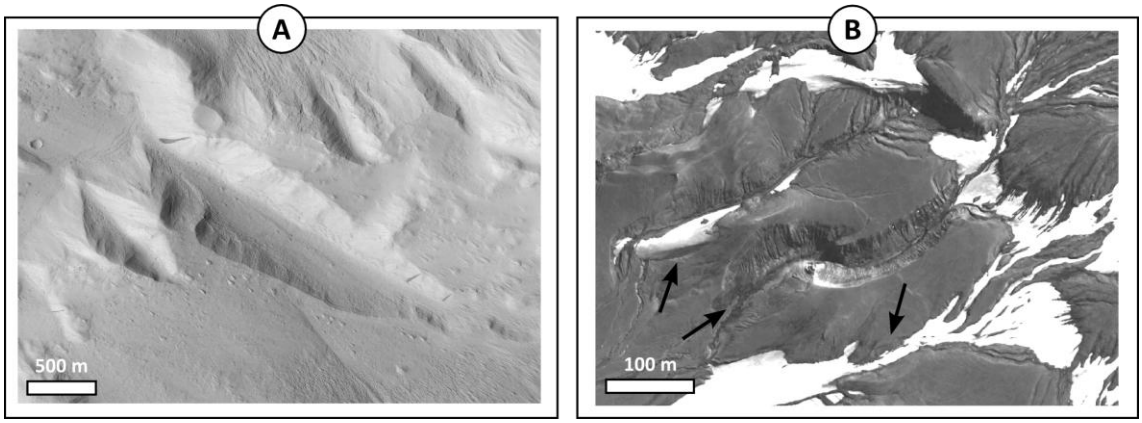

Fig. 6.5: Example of valleys modified by glacial activity on Hecates Tholus (A) and Deception Island (B). They are "V"-shaped valleys but with an evident flat floor. On the Terrestrial case, there is more recent fluvial activity, such as reveals the streams and fluvial deposits, although some of them still retain small ice patches and snow accumulated during the winter (arrows).

6.4.5. Crevasses

Differences in ice-flow speed (due essentially to geometry of the valley bottom) produce compression and extension fractures (crevasses) whose geometry in plan is easily identifiable. These crevasses can be transverse to the flow direction, caused by subglacial irregularities; longitudinal, caused by lateral ice spreading (when the glacier enters a whiter valley or a plain); or marginal crevasses, oblique to the margins of ice caused by compressive

and/or extensive stress due to differences on the ice flow velocity (see Hooke, 2005; Bennett and Glasser, 2009 for a review). On Deception Island, there are many of those fractures, irregularly distributed on glacial tongues, but mainly near their head, where the steepest slopes can be found. They are normally straight although curved crevasses are also visible (Figure 6.6). At selected sites, crevasses form blocks of ice (seracs), also covered by pyroclastic materials, in some cases with a chaotic distribution. On Hecates Tholus we do not observe those seracs, but the crevasses are visible on HiRISE images (Figure 6.6). They are located on the deposits mapped such as covered glaciers (de Pablo and Centeno, 2012), mainly near the mouth of the valleys reaching the floor of the main depression, with a slightly curved path in plant view, as seen on the satellite images. Moreover, we also observed similar features inside the valleys that reach the depression. They are visible on both CTX and HiRISE images, showing similar characteristics but in a more dense accumulation at the bottom parts of the valleys only. Other crevasses has been observed near the edges of the possible glacial tongues on Hecates Tholus, oblique to the valleys but with straight patterns, and pointing both downslope and upslope, that could be related to compressive and extensive efforts on the ice mass due to the differential movement caused by the differential velocity.

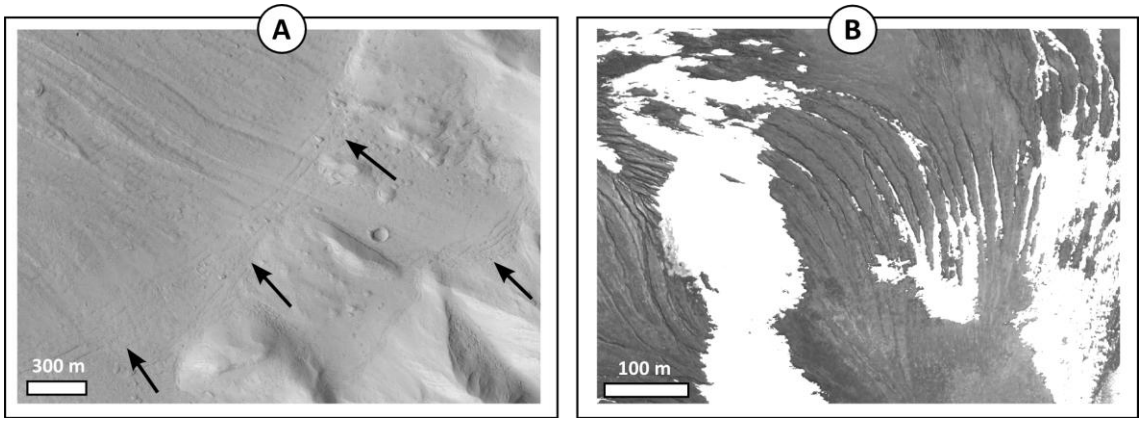

Fig. 6.6: Example of crevasses on Hecates Tholus (A) and Deception Island (B), one of the features that evidence the presence of ice under the surface. They are typically curved in plant (arrows on A) caused by the flow of the glacier downslope. In the case of Hecates Tholus (A), they longest ones are located at the mouth of the valleys dissecting the depression B (arrows on B), but shorter ones are widely distributed in the material filling the floor of the depression.

6.4.6. Bergschrunds

A bergschrund is a deep crevasse between the moving ice and the stationary nevé, firn or ice, at the head limit of the glacier. It is often visible only during summer, because in winter it is concealed by snow. On Deception Island, many bergschrunds are visible at the edge of the

ice cap on top of the volcano rim, where the different glacial tongues start and flow downslope (Figure 6.7). The high slope at these sites could be the main reason to explain the presence of those fractures.

On Hecates Tholus volcano, HiRISE images allow to observe several bergschrunds. Some of them were already mapped (de Pablo and Centeno, 2013) using CTX images. They are generally located on the mouth of the valleys reaching the floor of the depression on the flank of the volcano, although they are also visible on the base of small closed depressions in the area (Figure 6.7).

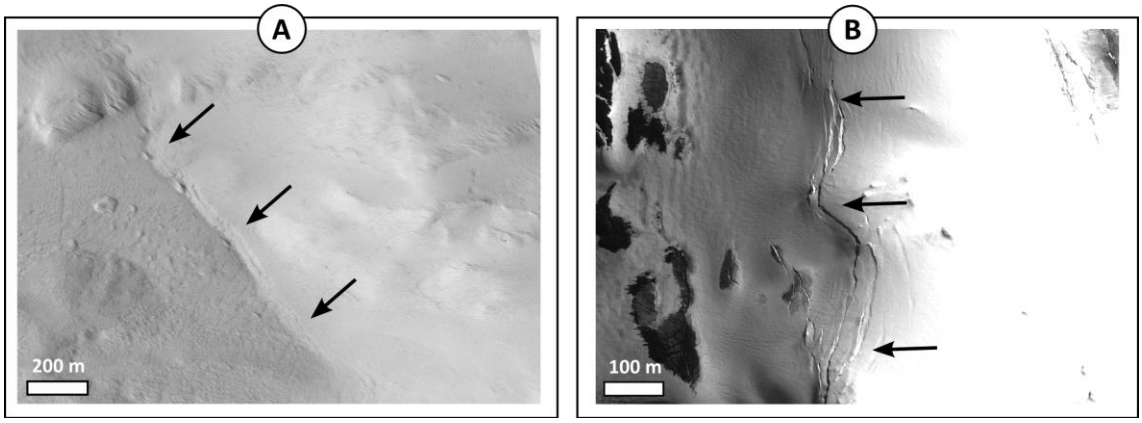

Fig. 6.7: Example of bergschrunds (long, deep and narrow crevasse at the head of the glacial flow) on Hecates Tholus (A) and Deception Island (B), marking where the glacier ice separate from the firn above starting to flow downslope. They are recognized in the ice of the glaciers at the summit of Deception Island (black arrows on B), but also on the covered glacier of Hecates Tholus (arrows on A), that is other of the features supporting the hypothesis of subsurface ice masses existence.

6.4.7. Ridges

The advance of the glaciers usually produces the formation of ridges on the front due to overlapping of ice wedges. The result is a wavy surface on the terminal section of the glacier flow. In these areas, some subglacial debris move to higher levels, and could form surficial accumulations of debris, highlighting the wavy surface. On Deception Island, those ridges are recognizable only in the shorter glaciers, which terminus is located inland. The longer ice flows reaching the shore of the island (both on Port Foster and Costa Recta) do not show this type of morphologies (Figure 6.8). They provide a wavy surface to the front of the glaciers, bordering the edge of the own front (lobate plant morphology). On Hecates Tholus, this wavy surface is not visible on satellite images, and topographic data does not have enough spatial resolution to allow their recognition. However, CTX and HiRISE images reveal the presence of abundant ridges, lobated in shape (Figure 6.8), similar to those previously named like Lobate Debris Aprons (Pierce and Crown, 2003; Mangold, 2003; Li et al., 2005; Chuang and Crown, 2005,

2009) and Lineated Valley Fill (Head et al., 2006a,b; Baker et al., 2010). Their morphology was one of the keys to propose the existence of glaciers in this site of Mars (e.g., Neukum et al., 2004; Hauber et al., 2005; de Pablo and Centeno, 2012).

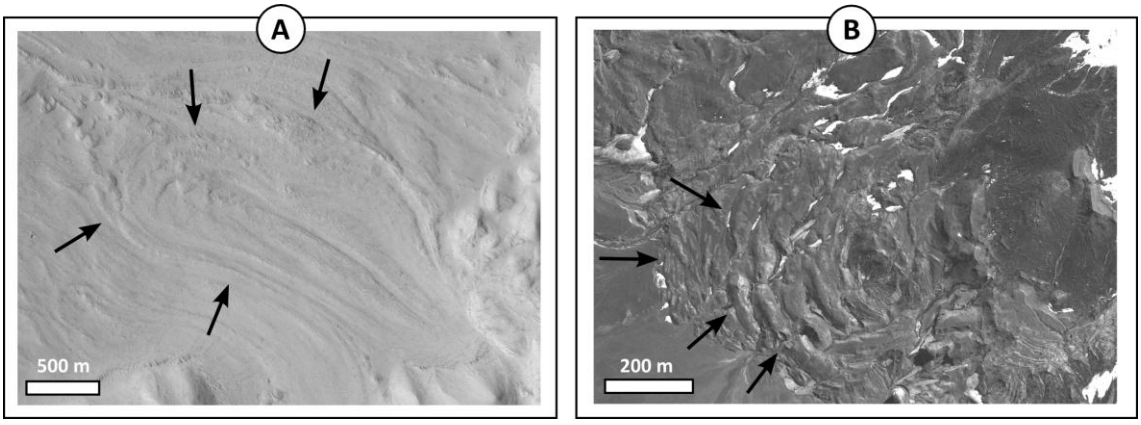

Fig. 6.8: Example of the ridges observed on Hecates Tholus (A) and Deception Island (B) (arrows) formed by accumulation of ice and the consequent compressive efforts on the front of the glacial flows.

6.4.8. Moraines

Glaciers erode the valleys out of several processes (plucking, entrainment, abrasion, etc.) and receive materials from the valley slopes (mainly as a result of gravity, runoff and wind erosion). The sediments are incorporated into the flow of the glacier, organized in marginal moraines (lateral, central and frontal moraines) or bottom moraines (under ice and exposed only when the glacier is destroyed). The ablation on the glacier front could produce very rough surfaces caused by the exhumation of basal moraine, but also by the accumulation of a till deposit by progressive down-wasting of buried ice (see Bennett and Glasser, 2009 for a review of those processes). On Deception Island, central, lateral and terminal moraines are recognizable although in general they are not extensive, probably due to the small size of the island and the consequently reduced length of the glaciers. However, some terminal moraines are clearly recognizable showing a hummocky surface rough in texture due to the coarse and heterogeneous materials accumulated (Figure 6.9). On Hecates Tholus, rough surfaces formed by irregular, lobated and multiple-size mounds, and has been mapped on the western sector of the floor of depression B (de Pablo and Centeno, 2012), and could be interpreted such as relict materials from possible ancient basal moraines and/or supraglacial meltout till (Figure 6.9). This type of materials are also recognizable slightly outside the depression B, just on the area that could marks the maximum extension of the glaciers on the NW flank of this Martian volcano (de Pablo and Centeno, 2012; de Pablo et al., 2013).

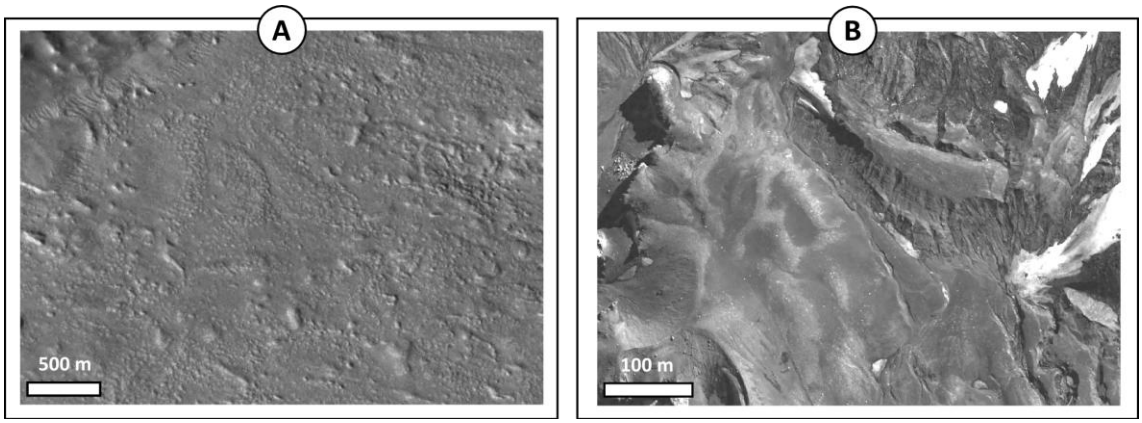

Fig. 6.9: Example of moraine deposits on Hecates Tholus (A) and Deception Island (B) showing hummocky and chaotic distribution of coarse and poorly classified materials.

6.4.9. Erratic blocks

Blocks of rocks could be transported by the glaciers for hundreds of kilometers and could appear isolated or forming clusters far away from their original position. Erratic blocks are visible at selected sites of Deception Island, in some cases, not far from the place where they seems to came from, still on top of glaciers; and in other cases, they are related to moraine deposits outside the glaciers. The origins of some of those blocks on Deception Island (Figure 6.10) are rockfall processes from outcrops at high slopes, and pyroclastic deposition of volcanic bombs what later traveled on the glacier after the volcanic eruption that produced them. Furthermore, entrainment and plucking add very often block to the ice flow, and many erratics of Deception Island may be the result of such processes. On the Hecates Tholus glacial region, CTX images show a rough surface apparently formed by blocks with an increase of the density of blocks toward the west. These fields of blocks had been mapped and interpreted as

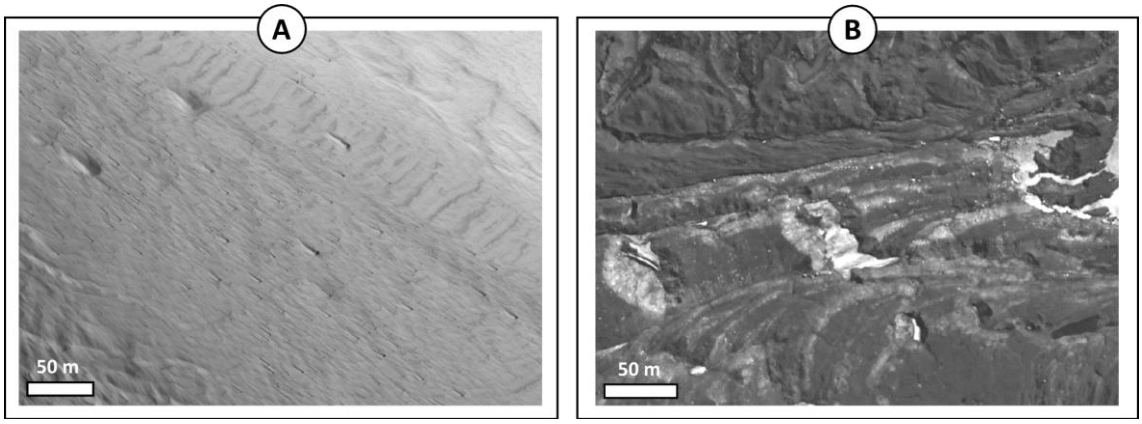

Fig. 6.10: Example of erratic blocks, metric in diameter, on Hecates Tholus (A) and Deception Island (B). In the case of Hecates Tholus, they are visible on the HiRISE image such as more or less dark blocks on the floor of a glacial valley. Moreover, most of them support the existence of wind streaks downwind of them (arrows on A). On the case of Deception Island, they are distributed at the surface, along the glacial flows showing very different diameters too (arrows on B).

blocks all along the valleys as well as in the depression floor. Most of those blocks are related to wind streaks and wind shallow deposits (Figure 6.10).

6.4.10. Pits and depressions

Depressions are common on the ice surface, on sediment-covered glaciers and on glacial deposits. On ice, the flow of thawing water turns out into a network of conducts connected to surficial depressions. On sediment-covered ice, termokarst or adaptation to crevasses can produce depressions. Finally, in terminal moraines and when sediment-covered glaciers are receding, the fusion of ice can produce the collapse of the sediment cover. Besides, termokarst can contribute to any of these processes. On Deception Island, depressions up to 5 to 15 meters in diameter are common and appear forming groups (Figure 6.11). Their origin has not been previously investigated (a safe access to most of them has been not found at present day during our short field campaigns) althought could include kettles, thermokarst, glacial moulines, or collapse of surficial pyroclastic deposits due to presence of crevasses under the surface. However, outside the glaciers, has also been observed some of those depressions, and interpreted to be thermokarst due to local melting of permafrost (e.g., Smellie, 2002a,b; Vieira et al., 2008; Melo et al., 2009).

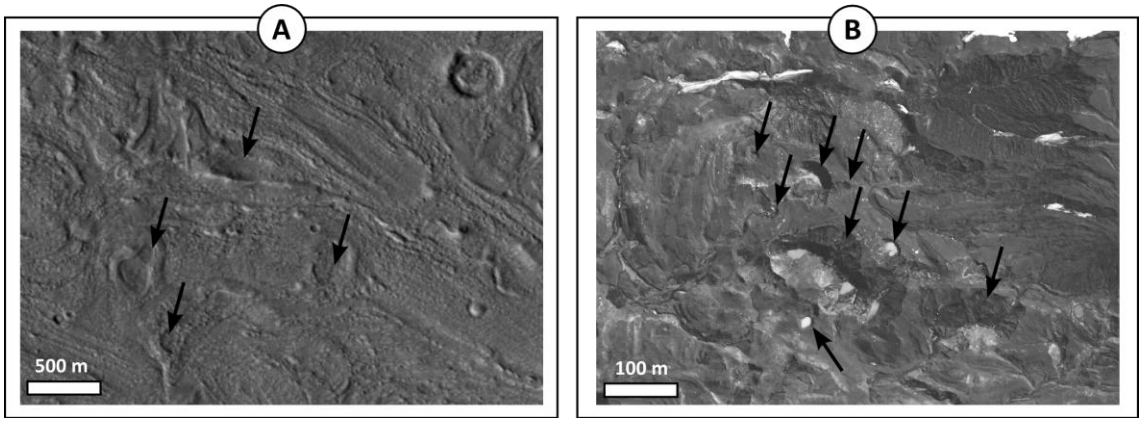

Fig. 6.11: Example of depressions on Hecates Tholus (A) and Deception Island (B). In the case of the depressions on Hecates Tholus, the CTX image shows few depression, hundreds of meters in diameter and lobated in morphology (black arrows on A), but they are clearly different than the impact craters, such as this located near the upper right corner of the image. In the case of the Deception Island depressions, their diameter range between few meters to more than one hundred meter (arrows on B).

On Hecates Tholus volcano, depressions other than the impact craters has also been observed at CTX and HiRISE images (Figure 6.11), although their presence is not frequent. All of them are located at the surface of the materials filling the depression B. The main difference with those observed on Deception Island (moreover of the diameter) is the morphology: in

Deception Island, they are approximately conical or bowl depressions -on Hecates Tholus a flat bottom is the most common geometry. The origin has been never discussed, and could be as wider as those on Deception Island, including thermokarst, because Hecates Tholus volcano and the surrounding area are characterized by features caused by magma-ice interactions (e.g., Mouginis-Mark, 1985; Mouginis-Mark et al., 1982, 1984; Chapman et al., 2000; Mouginis-Mark and Christensen, 2005).

6.4.11. Terminus or snouts

The end of a glacial, named terminus or snout, can show different morphologies and structures, from vertical walls marked by a scarp to gently and long slopes. Frequently, accumulations of materials (till, debris deposits, terminal moraines, pinnacles, etc.) near the snout can be observed. On Deception Island, there are examples of all types of terminus (Figure 6.12). On Port Foster and Costa Recta the glacier front is a series of walls showing the bended and fractured ice interstratified with pyroclastic materials (Figure 6.3). In other sites of the island, the glaciers end with very gently slopes where the ablation made possible to see the interstratifications of ice and pyroclasts, as well as rough terrains formed by pinnacles, and terminal moraines (Figure 6.3).

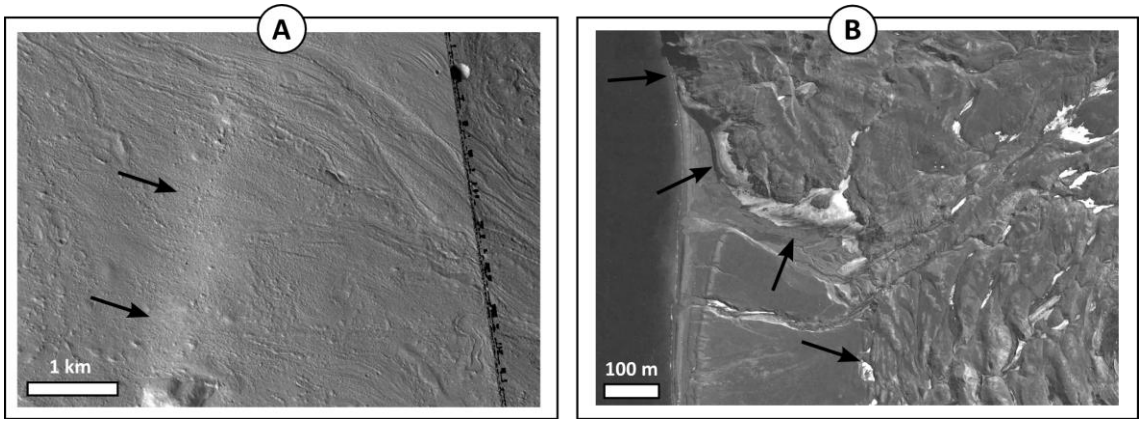

Fig. 6.12: Example of glacier terminus on Hecates Tholus (A) and Deception Island (B): In the case of Hecates Tholus, the terminus is marked by a topographic step, although it is not so evident (arrows on A), except by the effect of the light (HiRISE image illuminated from the west). Note that other glacial flow seems to flow more to the NW such as visible on northern of the upper arrow. In the case of the terminus on Deception Island, they could be both smooth and progressive (lower black arrows on B), and scarped and abrupt (higher black arrows on B), sometimes raising the sea on Port Foster.

On Hecates Tholus, there are not abrupt terminuses such as on Port Foster, but relatively gently slopes of the deposits filling the main depression with a rough surface (Figure 6.12) that could be caused by the presence of erratic blocks or ice thawing (such as described before), but also by pinnacles and remnants of the debris materials and medial moraines.

However, the images illumination allows to observe a topographic step (Figure 6.12), that is not such as evident on the topographic data. Toward the NW of this possible terminus, the terrain of the floor of depression B is more rough, irregular and hummocky, such as we presented above.

6.4.12. Outwash

Outwash is a fluvial processes caused by ice fusion in the periphery of temperate and warm glaciers –and the term outwash deposits refers to the sediments produced by outwash rivers. Outwash is active during the whole existence of glaciers (as thawing dominates once a year) and during glacier retreat periods (when ablation is dominant). Braided rivers characterize the outwash drainage and, consequently, braided bars and channels are the main landform in these environments. On Deception Island, outwash deposits and structures are also visible but there are not changes on the surface color respect the covered glaciers or the surrounding areas (Figure 6.13). The mantle-like deposits of pyroclasts cover all the surfaces in the region. Moreover, the sediments transported by the streams are mainly pyroclasts (moreover of fragments of other different types of volcanic rocks). However, the streams are clearly visible, as well as, in some cases, the fluvial terraces, alluvial fans and deltas.,In the case of Hecates Tholus, de Pablo and Centeno (2012) mapped some eskers, channels and sedimentary materials just outside the northwestern edge of the depressions on the flank of the volcano, thanks to the use of CTX images (Figure 6.13). On the other hand, de Pablo et al. (2013) proposed a sequence of the glacial events to explain the presence of those features advances and retreats of the glacier fronts along the geological history of the volcano.

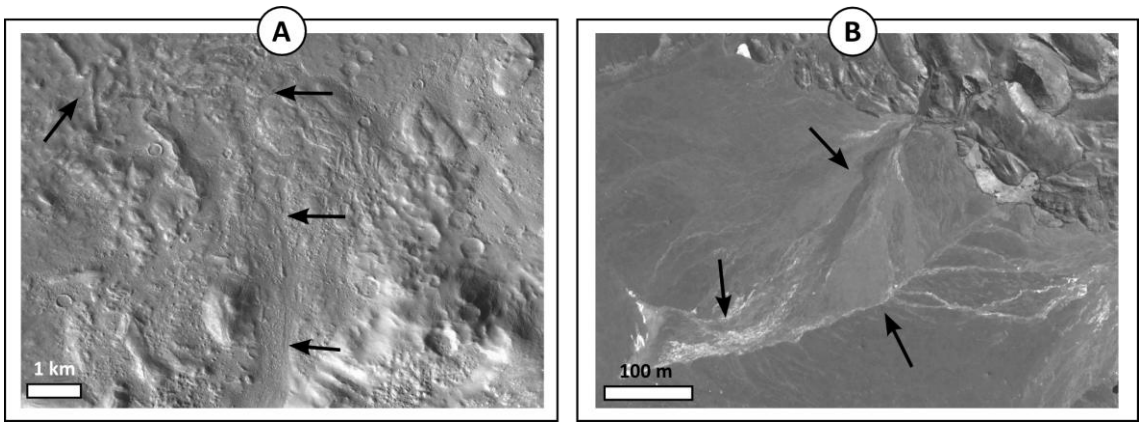

Fig. 6.13: Example of outwash plain at the glaciers fronts on Hecates Tholus (A) and Deception Island (B), showing channels and streams. The channels disappear far away from their head. In the case of Hecates Tholus, they show possible eskers related to extensive period of the glaciers (upper left arrow on A).

6.4.13. Other features

Apart from the glacial landforms presented before, Deception Island shows other features that are similar to those mapped and observed at the lower NW flank of the Hecates Tholus volcano (de Pablo and Centeno, 2012), as well as many other features what could also serve such as analogues of Mars, as the volcanic (lava flows, calderas) fluvial (streams, terraces, deltas), aeolian (dunes, dust-mantles), and coastal morphologies (shorelines), moreover of mineral and geochemical similarities (such as summarized in Molina et al., 2013). Here we briefly present some of them (Figure 6.14) because of their similarities and interest to understand the geological and glaciological history of the glacial processes on the Hecates Tholus volcano.

Gullies: on Deception Island, they are frequent and one of the most characteristics forms to be observed in the island. They result from seasonal snow, permafrost and active layer melting. On Mars, Gullies has been widely described all around the planet, mainly related to the inner walls of impact craters (e.g., Malin and Edgett, 2000), and caused by groundwater, or surficial ice deposition, among others (e.g., Malin and Edgett, 2000, Hetch, 2002; Arfstrom and Hartmann, 2005; Márquez et al., 2005; Williams et al., 2009; Raak et al., 2012). In the case of the Hecates Tholus volcano (Figure 6.14-1), very few of those gullies have been observed using both CTX and HiRISE images (e.g. de Pablo and Centeno, 2012). They are isolated and mainly located at south-facing walls of valleys and the walls of the nested depressions of this volcano. In some cases, they are characterized by smooth dark-toned deposits, what contrast with the surrounding smooth light-toned materials of the walls and slopes.

Talus slope or screep deposits: on Deception Island, the high slope walls are not frequent, but when exist, it is frequent to observe these slope deposits, but they are also usually resurfaced by other processes (rockfall and solifluction, among others). On Mars, most of the slopes forming the walls of depressions A and B on Hecates Tholus are characterized by a smooth surface, mainly due to the accumulation of materials at their lower part (Figure 6.14-2). Those deposits are usually smooth, regular and featureless, except by the presence of gullies; meanwhile the upper part of the slopes, not covered by those deposits, is usually rough.

Solifluction deposits: on Deception Island, those deposits are not often, and when exist, they are small, only visible from the surface (not clearly distinguishable on satellite images). Those characteristics could be related to the small slopes and low walls height in which they appear. They neither show the clear differential pattern depending of the slope aspect. However, the

slope deposits on the walls of depressions A and B on Hecates Tholus shows a differential behavior depending of their aspect. Mainly on south-facing slopes, the deposits show a pristine and extensive wavy pattern here interpreted to be caused by solifluction processes (Figure 6.14-3).

Rock outcrops and rockfall deposits: an important number of the higher part of the scarps and walls on Deception Island are characterized by it rough texture caused by volcanic rocks outcrops, including pyroclastic tuff, and basaltic lava flows (Figure 6.14-4). On Hecates Tholus, they are visible such as rough materials at the head of scarps, in a similar way to what could be observed in the CTX and HiRISE images of the wall of the valleys dissecting the depression on the base of Hecates Tholus volcano. In some cases, on both Deception Island and the study area in Hecates Tholus volcanoes, on the base of the walls could be observed rock fall deposits.

Craters: the volcanic activity on Deception Island is the origin of the rounded depressions manly located on the inner northern sector. Successive volcanic eruptions caused the formation of those depressions, which morphology is similar to the morphology of the eroded impact craters on Mars -with the exception of the ejecta deposits, that do not exist on Deception Island. However, the craters in Deception show a rim-shaped relief forming the crater flank deposit due to the accumulation of the pyroclastic materials instead. However, on Deception Island, there also many rounded depressions and pits that could be caused, not only by volcanic eruptions, but collapses, subsidences, or thermokarst. On Hecates Tholus those depressions are not as pristine and frequent, and they also show more lobated and irregular morphologies than those on Deception Island (Figure 6.14-5).

Fig. 6.14 (next page): Examples of other non-glacial features that appear on Hecates Tholus (A) and Deception Island (B) related to the covered glaciers, including gullies (1), smooth slopes (2), and solifluction deposits (3), rocky slopes and rockfall deposits (4), and craters (5).

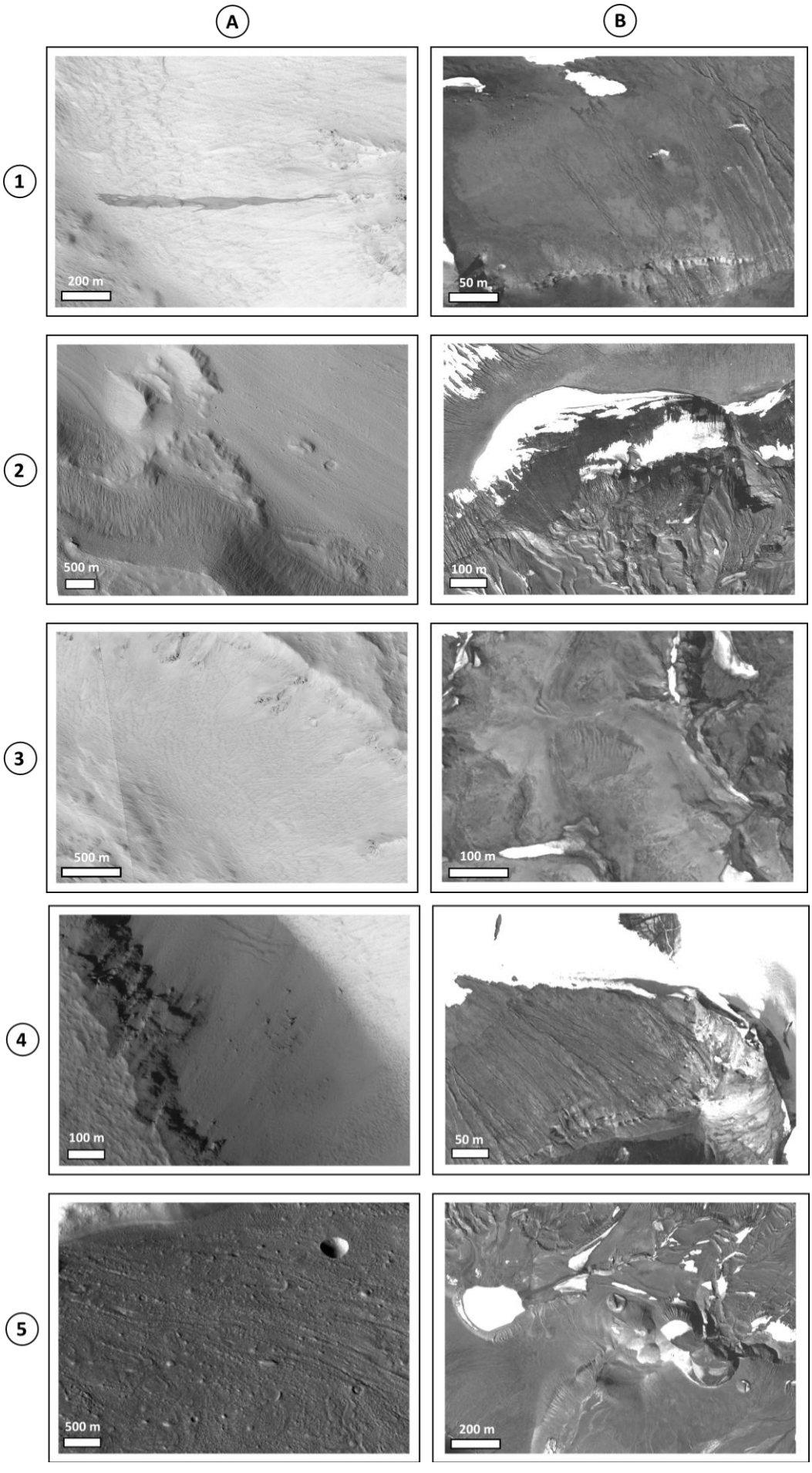
A
B
1
200 m
50 m
2
500 m
100 m
3
500 m
100 m
4
100 m
50 m
5
500 m
200 m

6.5. Discussion: Covered glaciers

6.5.1. Covered glaciers, rock glaciers or remnant deposits on Hecates Tholus?

The observed analogues between the covered glaciers on Deception Island and Hecates Tholus volcano let us attempt to understand the environmental and geological conditions of the Martian site.

The first issue to consider is the nature of the materials padding the bottom of depressions A and B on the NW flank of the Hecates Tholus volcano. From our point of view, the materials covering the area could be any combination of the following cases (Figure 6.15-1): (1) debris deposits from slope processes (including solifluction and rockfalls, among others) at the base of the high walls forming the depressions A and B, as well as the valleys dissecting them; (2) pyroclastic deposits (from cinder to bomb-size particles) from eruptive events, such as occurs on Deception Island, taking into account the volcanic origin of this region –in fact, some authors proposed a possible eruption on the flank of the volcano about 350 Ma ago (e.g,, Neukum et al., 2004; Hauber et al., 2005); and (3) dust deposits caused by the periodic Martian storms responsible of cover the surface of the planet with a very fine-grained material (e.g., Christensen, 1986; Ruff and Christensen, 2002). Whatever is the origin of these materials, glacial reworking is a possibility. Other type of materials are not discarded, such as impact ejecta deposits, but due to the low density of extensive impacts craters in the area, we think the floor covering effect on the depressions is not relevant. In any case, they could explain what type of materials could we have there, but not the morphologies mapped and described in the area (e.g., Neukum et al., 2004; Hauber et al., 2005; de Pablo and Centeno, 2012), especially those we compared with the features observed in the eastern sector of Deception Island described above.

Three possible scenario are possible assuming that the features described on the lower NW flank of the Hecates Tholus volcano of Mars are related to glacial processes, based on their similarities with the Deception Island features, and given that the ice is not visible on the available CTX or HiRISE images of Hecates Tholus three possible scenarios are possible: they could be covered glaciers, rock glaciers or remnant deposits of an ancient glacial activity in the area (Figure 6.15-2).

The here described Hecates Tholus-Deception Island analogues support the glacial interpretation of the features observed on Hecates Tholus, and the possibility of ice existence

under the surface at present day (Helbert et al., 2005). These interpretations are in agreement with the other many glacial features mapped in the area (e.g., Neukum et al., 2004; Hauber et al., 2005; de Pablo and Centeno, 2012).

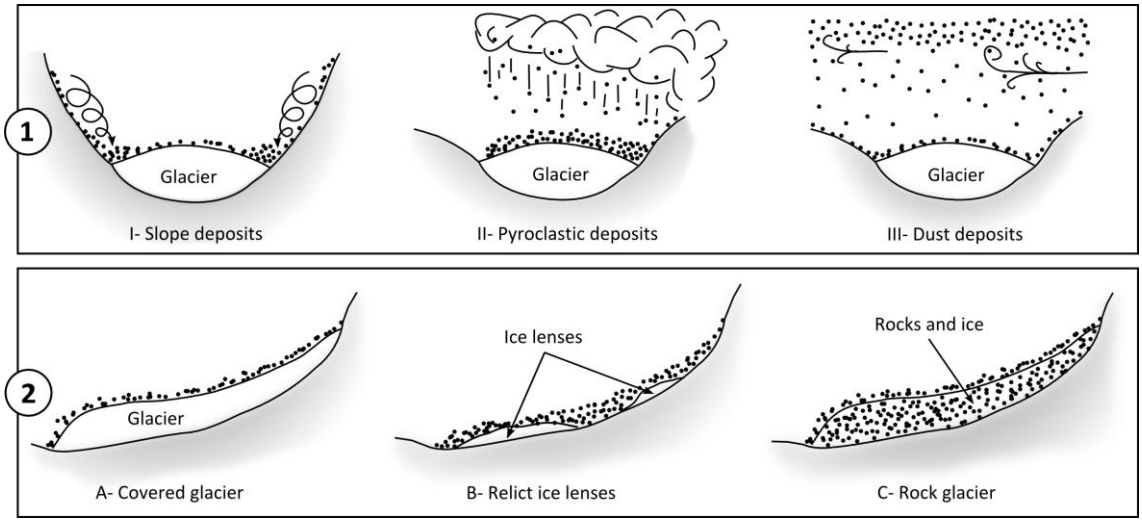

Fig. 6.15: (1) Three of the most feasible processes that could cause the Hecates Tholus's glaciers coverage by different type of materials: (I) slope processes (from falls to creeping) causing the accumulation, mainly in the laterals of the glacier; (II) volcanic eruptions causing fall of ash, cinder, pyroclasts and bombs, irregularly distributed on space and thickness, and (III) dust storms that cause the widespread sedimentation of fine-grained materials. (2) Three possible scenarios to explain the presence of the features observed on the floor of depressions on the flanks of the Hecates Tholus volcano: A) a glacier covered by different type of materials (1); B) a relict glacier where only few ice lenses remains under the surface covered by different type of materials, not necessarily transported by the own glacier in the past; and C) a rock glacier, in which the ice is only an small portion of the mass of the flow.

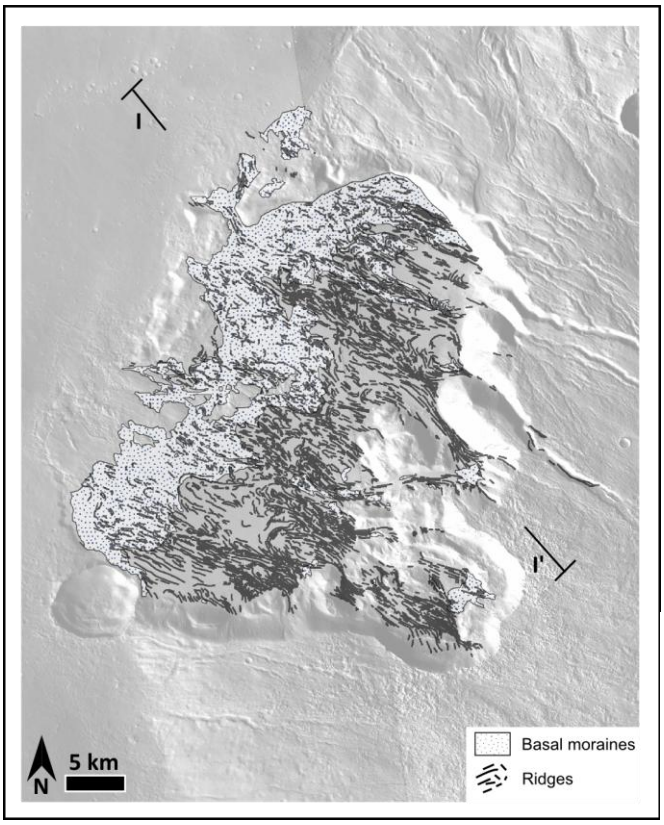

On the other hand, the distribution of ridges and possible moraines mapped in the area (de Pablo and Centeno, 2012), reveals a maximum glacial phase followed by a retreat of the glaciers from NW to SE (Figure 6.16) (de Pablo et al., 2013). At the maximum glacial extension in the area, the glaciers covered all the surface of the depressions A and B, and also overflowed their NW edge.

Fig 6.16: Maps of possible rough terrain (possible moraines) and ridges at the floor of the nested depression on the flank of Hecates Tholus volcano (modified from de Pablo and Centeno, 2013). I-I' items mark the location of the topographic profile on Figure 6.18.

When the glaciers started their retreat, could leave a rough deposit on the floor of the western sector of the depression B. These materials could be exposed on basal moraines or sublimation-fusion till deposits, such as we described above. The remnant glaciers should be then located at the eastern part of depression B and filling most of the depression A, which are the areas where the ridges are distributed (Figure 6.16).

At this stage, there are some important questions: (1) Is there today any glacial ice in Hecates Tholus? (2) If there is any ice, is it located in ice lenses, in covered-glaciers (with clean ice below a blanket of sediments) or in rock glaciers (with interstitial ice)? Both are common in the final stage of the glacial evolution and, in fact, both can coexist in the area (Figure 6.15-2).

The key elements to answer are the crevasses (Figures 6.6) and bergschrunds (Figure 6.7) on the bottom of depression A and the western sector of depression B. If our interpretation of the features like fractures is correct, they could not be tectonic in origin because 1) their curved shape, 2) their pattern following the scarp general morphology, 3) they do not have other morphological expression outside the area where they appear, and 4) they do not follow regional fractures patterns. Then, those fractures should be produced by adjustment on the terrain materials, probably ice due to all the other glacial features described in the area. From our point of view, they are so long and wide to be contraction cracks due to desiccation. Moreover, in most of the cases, they have a common pattern, normal to the general slope direction, with their extremes downslope curved. This also occurs on the floor of the main valleys dissecting the depression B, where those fractures have been also observed, but not in the area of possible moraine deposits, such as observed on the available CTX and HiRISE images. There is other observation that corroborates the glacial origin of those fractures, the presence of downslope and upslope curved fractures in the bottom of a valley due to compressive and extensive stress due to the downslope movement of the glaciers (Figure 6.17).

We put forward the present-day existence of glacial ice, below the pyroclastic cover, on Hecates Tholus, at least in the areas where crevasses and bergschrunds can be identified. As explained above, crevasses and bergschrunds are certainly linked to active glaciers –in Deception Island they are only visible on the area where glaciers exist, including covered-glaciers. In addition, crevasses and bergschrunds are very frail forms, easy to destroy, and subjects to be buried and concealed by any pyroclastic event (we should remind that terrestrial bersgchrunds are covered every winter by snow). Those glaciers are located on the

eastern sector of depression B, filling the main valleys dissecting this depression, as well as on the floor of depression A, but not at the western part of the depression B, were moraines remnants of a more extensive glacial episode (de Pablo et al., 2013) are located. We could do not discard that other glaciers could exist outside the depression filling, for example, the valleys that dissect the NW flank of the volcano.

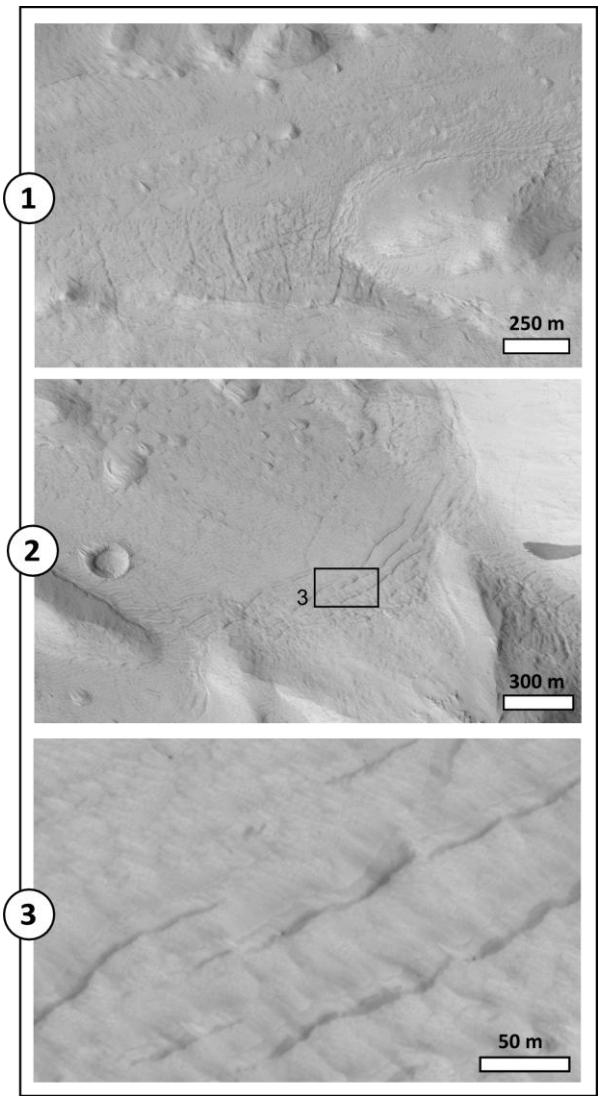

Fig 6.17: Examples of possible crevasses as seen on HiRISE images at different scales.

Then rock glaciers and ice lenses are very likely to exist in Hecates Tholus. In most terrestrial deglaciated areas, these two elements coexist with glacier in the late stages of glacial recession, which seems to be the present state of those glaciers (de Pablo et al., 2013). Although to distinguish between glacier and rock glaciers existence in the area is far from the objectives of this work, we found that the glaciers are the most feasible hypothesis, such as we discuss in the next paragraphs.

Furthermore, if crevasses are visible in the images, it means that the materials covering them are not very thick to allow to recognize the glacial crevasses below it. Otherwise, the crevasse should be also completely filled and hided, and indistinguishable respect to the surrounding terrains. In fact, on Deception Island (as well as in any other glacier of the Earth), the snow precipitation each winter is enough to hide the fractures and crevasses. Then, the thickness of these mantle deposits should not be so thick and this could point to aeolian and dust deposits. The abundant wind streak deposits related to the erratic blocks observed on the floor of a valley at the lower NW flank of the Hecates Tholus volcano (Figure 6.10) could support this interpretation. This thin layer, that could partially fill the crevasses (or some of them) but allow

to recognize most of them, it is compatible with the existence of ice 1 − 2 meters below the surface (Helbert et al., 2005), and explain why we could not observe ice in this region, but the morphology derived from its glacial flow. On Deception Island, the thickness of the pyroclastic layer covering some parts of the glaciers reach 3 meters at located sites, but in general they are about 2 meters, and they also allow to recognize the morphology of the crevasses, but not the ice that forms the glacier (Figure 6.6).

Then, taking into account our observations on CTX and HiRISE images and their analogues in Deception Island, the geomorphological map of the area (de Pablo and Centeno, 2012), and the evolutionary model of the glaciers in the area (de Pablo et al., 2013), and assuming these interpretations are correct, we propose a geological model of the present state of the floor of the nested depressions on the lower NW flank of the Hecates Tholus volcano (Figure 6.18). This model propose that the floor of the valleys dissecting the depression B, as well as the floor of depression A and the eastern sector of depression B are filled by glaciers. The ice of them is not visible on satellite images because they are covered by debris, pyroclastic and aeolian/dust deposits. Those glaciers are the remnants of extensive glaciers that filled completely those depression in the past (de Pablo et al., 2013) and probably other areas of the Hecates Tholus volcano. Here, the glaciers show central and lateral moraines (ridges), as well as erratic blocks and crevasses and bergschrunds related to the recent flow. The western sector of depression B is characterized by moraine deposits (basal moraines or

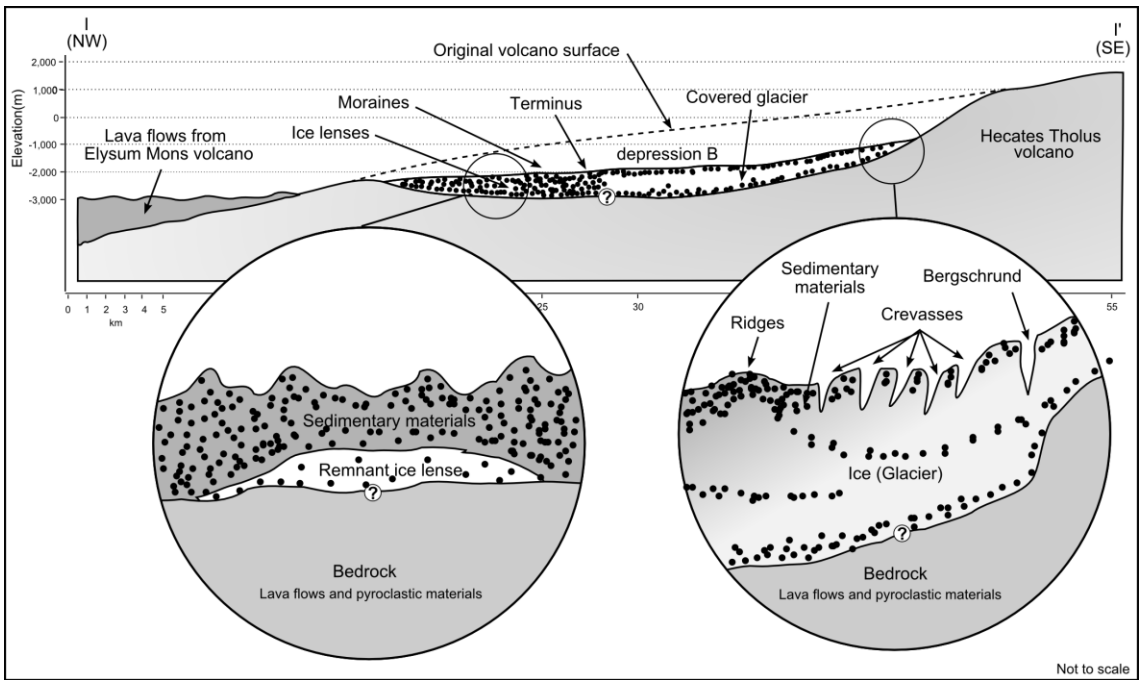

Fig 6.18: HRSC-derived topographic profile showing a schematic model of the possible glaciers distribution in the main depression at the NW flank of the Hecates Tholus volcano. Circles show details of the location of possible remnant ice lenses as well as covered glaciers with their crevasses. Not to scale. Profile location is showed in Figure 6.16.

meltout till deposits) during the retreatment of the glaciers. We could not discard the presence of small ice lenses in this sector of the depression, as would indicate the pingos in the area (such as suggested and mapped by de Pablo and Centeno, 2012). However, the presence of lobated and lineated landforms at the eastern sector of depression B, the presence of knobby terrain at the western sector if that depression, and the topographic step at the limit between those sectors (Figure 6.12) could be indicative of the presence of a covered glacier in the eastern sector nowadays, which terminus is marked by the topographic step respect the western sector probably formed by ancient basal moraine deposits.

To study HiRISE-derived digital elevation models, THEMIS-derived surface temperature data and MARSIS/SHARAD ground penetration radar data could provide the necessary information to corroborate (1) if there is still ice (extensive masses or just only ice lenses) under the surface; (2) the presence of crevasses and their characteristics; and (3) the real thickness of the materials filling the depressions at the lower NW base of the Hecates Tholus volcano. Both things would provide the necessary information to understand both the geological origin of the depressions, and the glacial (and geological) history of this region of Mars.

6.5.2. About analogues

Our detailed examination on Deception Island (using both satellite images and field observations) resulted in the first description of many features and reliefs that are similar to those described at the lower NW flank of the Hecates Tholus volcano (de Pablo and Centeno, 2012). Many other Deception Island landforms are also analogues to other features observed on other sites of Mars (e.g. Molina et al., 2013), but here we focused on the glacial landforms of Hecates Tholus to confirm if the features observed on Mars are enough evidence of the existence of a covered glacier.

Although in some cases, other origins are feasible for those reliefs on Mars, if we consider them individually, we think that the presence of such a wide set of forms make evident their glacial origin. In fact, in this work we only report reliefs that are present on Deception Island and Mars. De Pablo and Centeno (2012) observed on Hecates Tholus more glacial features such as flutes, roches moutonèes, arêtes, among others, that are not visible on Deception Island because (1) the presence of a thick deposit of pyroclastic material covering the surface due to the eruptions occurring on this volcano in very recent times (during the 1960's; e.g., Baker et al., 1975; Pallàs et al., 2001) could cover them (such as flutes); (2) the

unconsolidated materials (tuff and pyroclasts) versus the lava flows that seems to form the Hecates Tholus volcanic edifice could avoid their formation (such as arêtes or roche moutonneès); and 3) the relative low glacial dynamics during the last centuries on Deception Island compared to the long glacial activity reported to occurs on Hecates Tholus along the last 3.8 Ga (e.g., Hauber et al., 2004; Neukum et al., 2005; de Pablo et al., 2013) could avoid their formation.

The reliefs we observed on Deception Island are not different from the reliefs that could be observed on other glacial regions of the Earth, including other debris-covered glaciers (e.g., Douglas et al., 1994; Levy et al., 2006; D'Agata and Zanutta, 2007; or Mihalcea et al., 2008, among many others). However, from our point of view, the reasons that convert this terrestrial volcano, and its glaciers, into a realistic analogue for the glaciers proposed to exist on the lower NW flank of the Hecates Tholus volcano are:

a) The volcanic origin of the bedrock and mantling materials. Both on Hecates Tholus and Deception Island are volcanic edifices formed by lava flows and pyroclastic materials. Then, all type of deposits (debris, moraines, or slope among others) observed on Hecates Tholus, should be more similar to their analogues in Deception Island than their analogues in other glacial sites of the Earth outside a volcanic region.

b) The presence of covered glaciers. Although other glaciers are also located at volcanic regions, such as occurs on Iceland or the Andes mountain ranges, they are not covered glaciers. So, they do not work such as analogues for those proposed to exist on Hecates Tholus (and other sites of Mars) where the ice, if it exists or existed, should be located some meters below the surface of a debris or mantle deposit.

c) The cold and harsh climate conditions. Although other volcanic areas of the Earth show glacial features (e.g., Iceland or Andes), the weather conditions are not as cold and harsh as they could be on Deception Island. On the other hand, the weather conditions on Deception Island are not as cold as they could be on Erebus volcano (in Antarctic continent too), but this last volcano is completely covered by glaciers, then, it does not work such as an analogue of the covered glaciers on Hecates Tholus. Finally, although the weather conditions on Deception Island are not as cold and harsh as they could be on Mars, the range of temperatures and the strong winds are nearby.

Considering the similarities presented in this work between the covered glaciers on the eastern side of Deception Island, and the possible covered glaciers on Hecates Tholus (and probably other many possible glaciers described on Mars), we considered to summarized the most important information (scientific and logistical) concerning this site to fit to the recently proposed templates to create an analogues database for further researches and planetary (Mars) missions design (Hipkin et al., 2013), including an abstract (Table 6.2), a list of important features and processes observed at the site (Table 6.3), and the logistic rubric (Table 6.4). Those tables have been developed due to the increasing interest of the scientific and engineering communities (see Hipkin et al., 2013 for a short overview) involved on the planetary exploration, and show a brief summary of our observation on both satellite images and field observations. The information provided is mainly focused on the study area and the topic here discussed: the possible debris-covered glaciers on Hecates Tholus. Other topics could be studied in this Antarctic volcano (e.g., Martínez-Frías et al., 2003; de Pablo et al., 2009; Prieto-Ballesteros, 2012; Molina et al., 2013) and the tables could be then completed with additional information affecting those topics.

The main concern about the area such as a terrestrial analogue to develop in-situ studies is the special regime of the island because, it is included into the Antarctic Treaty (http://www.ats.aq/), that have some limitations to develop studies there such as null environmental impact. Moreover, Deception Island is an Antarctic Special Management Area (ASMA), and includes Antarctic Specially Protected Areas (ASPAs), that require special authorizations for accessing and take samples or develop activities inside. However, although the extensive study area here presented (about 46 km^2) include some of those areas, it is not required to go inside them to develop a complete study of the local geology and geomorphology, or other types of study, such as confirm the testing of the ground temperature sensor of REMS/MSL instrument (Ramos et al., 2012; Gómez-Elvira et al., 2012). A minor concern is the access to the area, because it is an island and the access could be only done by ship (and also helicopter from the nearest airfield in King George Island, in the same archipelago, or from ships equipped with helicopter dock). In spite of those concerns, there are established Research Antarctic Stations in Deception Island: “Gabriel de Castilla” Spanish Antarctic Station and “Decepción” Argentinian Antarctic Station, what provide the necessary logistics support to work all around the island to the researches during the Antarctic summer periods (normally from December to March).

Table 6.2: Deception island analogue site summary, according to Hikpin et al. (2013) analogues database template.

Abstract title		Covered glaciers on Deception Island: analogues of possible glaciers on the Martian volcanoes
Authors		M.A. de Pablo, J.D. Centeno, M. Ramos, A. Molina
Most important question		Is there a covered glacier on present day with an important ice mass?
Logistic and environmental constraints		Accessible by ship/helicopter Possibility to have logistic support by the Antarctic Stations existing in the island. Protected by the Antarctic Treaty Less harsh weather conditions from November to March
Summary table	Site name	Eastern sector of Deception Island
	Centre coordinates	62º55'36''S; 60º34'15''W
	Elevation	Max: 539 m. (Mount Pond); Min: 0 m. (sea level);
	Areal extent	~ 46 km^2
	Prime science questions	Glacial/periglacial geomorphology and evolution Climate evolution Surface temperature
	Distance from airstrip	~ 140 km by ship to/from the "Teniente R. Marsh" airfield located at Fildes Peninsula, King George Island, South Shetland Archipelago, Antarctica.
	Environmental characteristics	Harsh weather conditions, main from April to October Temperatures: Max: +10ºC; Mean: 1ºC; Min: −28ºC Humidity: ~ 95% Important snow coverage during the winter; and strong wind and storm all the year around No vegetation coverage
	Previous studies at analogue site	Geological and geomorphological cartographies Tectonics and seismic activity
	Primary landing site	Main depression at the lower NW flank of the Hecates Tholus volcano of Mars (32º28'34''N, 148º55'13''E, −1830 m)
	References	*Smellie et al., 2002* (Geological and geomorphological maps of Deception Island) *de Pablo and Centeno, 2012 and de Pablo et al., 2013* (Geomorphological cartography and glacial evolution of the lower NW flank of Hecates Tholus volcano).

Table 6.3: Most important features and processes of eastern side of Deception Island such as Terrestrial analogue for possible debris-covered glaciers on Hecates Tholus, Mars, according to Hikpin et al. (2013) analogues database template.

Rank	Category of features	Applicability
2	Mineralogy/petrology	Define the petrology and mineralogy of the materials covering the glaciers to define their origin
4	Chemistry	Study water/ice chemistry
6	Sedimentology	Define the characteristics of the materials observed in the area: tills, pyroclastic deposits
6	Stratigraphy	Establish the stratigraphic sequence of the different materials to approach the geological evolution
1	Geomorphology	Recognize the glacial landforms, specially crevasses and moraines.
4	Hydrology	Study runoff (supraglacial and/or subglacial)
7	Biology	Search for forms of life associated to the ice
-	Ecology	-
5	Geological setting	To know the origin of the materials covering the glaciers
3	Environmental setting	Measure the environmental conditions in order to
-	Gradients	-
8	Fluxes and transport	Heat flux and energy interchange related to the glacier and the volcano
-	Metabolism	-

6.5.3. Analogues exploitation

The interest of this terrestrial analogue, beyond helping us to interpret the glacial origin of Martian landforms, is the possibility to develop different field experiment which could allow to characterize these debris-covered glaciers in order to help us to understand the covered glaciers on the Martian volcanoes. Here we provide an example of this experiment that could be carried out thanks to the logistics provided by the Deception Island local logistic facilities (Table 5). We propose to establish here an experimental field station to measure the surface and ground temperature, similar to those stations the Ground Temperature Network – Permafrost (GTN-P) already have all around the world to analyze the thermal behavior of permafrost and active layer (http://www.gtnp.org). The measurement of the surface temperature at the pyroclastic materials covering the glaciers on different locations (also outside the glaciers) could provide the necessary data to derive detailed surface temperature

maps. Under the same boundary conditions (the same cold climate and weather, and similar materials covering the surface) changes on the surface temperature could reveal the effect of the ice presence below the surface. The experimental station in the surface would provide us the ground true data to test thermal satellite images of the island from where to derive more detailed and extensive surface temperature maps to study the thermal effect of the covered glacier on the surface. This procedure would help to test the previous models proposed by several authors suggesting present ice lenses a few meters below the surface in NW Hecates Tholus, based on the analyses of Thermal Emission System (TES) data (from Mars Global Surveyor mission to Mars), (Helbert et al., 2005). Nowadays, the THermal EMmision Imaging System instrument (THEMIS) on board of Mars Odyssey mission allows us to determinate the surface temperature and thermal inertia by the use of the band 9 (e.g., Fergason et al., 2006). By deriving surface temperature maps, we could be able to locate thermally anomalous areas, and by deriving thermal inertia maps we are able to establish the presence of thermally different materials covering the surface. Those boundary conditions should be able to determine the location of possible remnants of ice lenses under the surface, that should be later studied by ground penetration radar data from MARSIS or SHARAD instruments. A similar approach has been also carried out in other debris-covered glaciers on the Earth by deriving surface temperature maps from ASTER data (e.g., Suzuki et al., 2007).

This experiment is focused on the study of the own glacial features, but this is just one of the possible research activities that could be conducted on this terrestrial analogue from different points of view, including astrobiology (e.g., the search for forms of live living under the surface or into the glacier) or volcanology (e.g., magma-ice interactions, such as those proposed to widely occurs on the Elysium volcanic province - Mouginis-Mark, 1985; Mouginis-Mark et al., 1982, 1984; Chapman, 1994; Chapman et al., 2000; Mouginis-Mark and Christensen, 2005, among others).

6.6. Conclusions

Our analysis of satellite images from Mars and Earth allowed us to recognize morphological analogues between the features observed on the lower NW flank of the Hecates Tholus volcano and the Deception Island volcano. The analogue features include: crevasses, bergschrunds, erratic blocks, terminus, moraines, ridges, depressions, and other not glacial features (gullies, rockfall deposits, solifluction, etc.).

Table 6.4: Logistics rubric for Deception Island, according to Hikpin et al. (2013) analogues database template.

Feature of concern	No concerns	Minor concerns	Significant concerns but mitigable	Some concerns may be not mitigable	Concerns make research impractical	Comments
Permitted access to the site	Access restrictions ensure that there is not human influence in the area.		Access and sampling require authorization by the National Antarctic Committee			Protected by Antarctic Treaty and included into the ASMA. Some sites are ASPA (see text)
Feasible of site access for researches		Accessible by ship and helicopter Harsh weather conditions from April to October Vehicles are not permitted				Accessible also in winter if required. Working in the glacier does not require a vehicle
Suitability for in situ equipment/instrumentation deployment	Harsh weather conditions made necessary to ensure the instrumentation Pyroclastic materials are dusty during the summer when dry					Actually, a wide variety of instruments are working under harsh weather condition all year around
Human influences on the Site	No human activities in the area					Antarctic tourist visit some places outside the here proposed study area, and they are so respectful with scientific instrument when exist, following the Antarctic Treaty.
Environmental impact of research	None, since the instrumentation is not invasive and is installed for short periods of time, and the fieldtrips follow the ASMA guidelines.					Antarctic Treaty requires an Environmental Impact Report for each activity to develop in the area to ensure the null or transitory environmental impact
Cost for site access			Requires dedicated transport, because it is outside the commercial routes.			Different National Polar programs develop summer research campaigns that share logistics if required
Logistical support and local infraestructures	2 Antarctic stations in the island (Spain and Angentina), with full equipped installations and communications (telephone, radio, internet), as well as scientific laboratories and logistical support (boats) and mountain expertise crew. 24 hours of power supply 220V					Spanish Antarctic Station provide all the necessary requirement to develop fieldworks in the island, as well as logistical support to stay for some months in the island with a more than acceptable comfort under the Antarctic environment restrictions.
Safety issues	Connected by helicopter with airfield in King George island in case of emergency. Different Polar Research vessels normally located in the area in case of emergency (or logistical support) Spanish station is connected to the military hospital in Spain in real time (telemedicine) Spanish station have a crew expert on mountain activities	The island is an active volcano, and volcanic activity is visible (fumaroles and small earthquakes). Seismic activity is monitorized 24h at different locations in the island from the Spanish Antarctic Station, and it provides the alarm system to evacuate the island if necessary.				The Spanish Antarctic Station is ready for an evacuation in case of a volcanic eruption, and material to survey in the island, under the volcanic activity and the harsh Antarctic weather is provided to each person at the station if necessary. Evacuation routes exist and coordinated with the different Spanish Polar Vessels.

The main relevance of those analogues is that they are related to covered/buried and active glaciers, however. On Deception Island, the glaciers are partially covered by pyroclastic deposits from the last eruption in the 1960's. Those analogies point toward the existence of present day remnant glaciers on the depression at the lower NW flank of the Hecates Tholus volcano of Mars. This interpretation is supported by the existence of crevasses and berschrunds on Mars, a set of landforms that only can be preserved if glacial ice exists and the mantle deposited above the glacier is not thick enough to hide it.

Based on those analogues, we propose a scenario in which the eastern part of the depression B on the lower base of the Hecates Tholus volcano could currently be filled by glaciers covered by debris materials, pyroclastic deposits and/or dust mantles, meanwhile the western sector of the main depression shows features remnant of ancient glaciers after the disappearance of the ice. The presence of crevasses is for us a clear marker of the ice existence at low depths.

The extensive analogues observed on the covered glaciers of Deception Island allow us to propose this sector of the island such as an interesting terrestrial analogue of the debris-covered glaciers of the Martian volcanoes, where to carry out further researches thank to the logistics facilities –not common remotes sites of the Earth where covered-glaciers on the flanks of volcanoes exist. On the other hand, to study the thermal behavior of the pyroclastic blanket of the terrestrial volcano could help to define a method to detect ice under the Martian pyroclastic surfaces, using the THEMIS-derived surface temperature data.

PhD thesis

Glacial geomorphology of the NW flank of the Hecates Tholus volcano, Mars

7

Discussion

Miguel Ángel de Pablo Hernández

2015

Abstract:

The geomorphological analysis and mapping of the study area, the morphometrical and thermal characterization, and the study of terrestrial analogues, provide a wide variety of evidences to discuss the presence of relict ice on recent and present times on the bottom of the depressions at the NW flank of Hecates THolus. This section includes a discussion about the possible existence of ice, the inner structure of the glacial till deposits (GD geomorphological unit) and the most likely distribution of ice. An important subject is the discussion on the dynamics of recent and present glaciers of Hecates Tholus based on the distribution of crevasses and bergschrunds in the area. Considering the volcanic setting of the study area, we discuss a possible scenario that could explain that recent dynamics. Finally, we make some suggestions on the research necessary to check our hypothesis and to probe the existence of ice in the flank of Hecates Tholus volcano.

Resumen:

El análisis y cartografía de los distintos rasgos geomorfológicos de la zona de estudio, junto con la caracterización morfométrica y térmica de la misma, y mediante el apoyo de los análogos terrestres, han permitido establecer una amplia serie de evidencias de la posible existencia de hielo relicto en tiempo recientes (e incluso en la actualidad) en el fondo de las depresiones que caracterizan el flanco noroeste del volcán Hecates Tholus de Marte. Aquí desarrollamos una discusión sobre la posible existencia de hielo, así como de cómo podría ser la estructura interna de los depósitos interpretados en este trabajo como till glaciar (unidad GD), y dónde se localizaría dicho hielo en el interior de estos materiales. También se discute la posible dinámica más reciente de estas masas glaciares teniendo en cuenta la existencia de crevasses y rimayas en la zona. Finalmente, y teniendo en cuenta el contexto volcánico de la zona de estudio, se discute cuáles podrían haber sido los procesos que explicarían dicha dinámica más reciente, y proponemos qué otras investigaciones podrían llevarse a cabo en el futuro para completar este trabajo y comprobar si estos procesos ocurrieron y si realmente existe hielo enterrado en este flanco del volcán Hecates Tholus.

7.1. Introduction

Glacial-related landforms have been widely described in all Mars latitudes (such as summarized in Dickson et al., 2012), pointing toward a complex glacial history with multiple ice ages (Head et al., 2003). According to Lascar et al (2004) several glaciations happened during the last 20 Ma, probably related to variations in the planet obliquity. The main volcanoes of Tharsis region, as well as other tropical volcanoes of Mars, show many glacial "marsforms" from the last Martian ice ages (e.g., Head et al., 2003, 2005). This is the case, of the Hecates Tholus volcano on the Elysium volcanic region (Figure 7.1), where a wide variety of glacial features have been mapped and described at the lower sector of its NW flank, revealing a long and complex glacial evolution (e.g., Neukum et al., 2004; Hauber et al., 2005).

The most recent geological cartography of this volcano (Neukum et al., 2004; Hauber et al., 2005) was based on the use of the new (in that days) HRSC images which resolution is about 12 m/pixel. However, those maps, although cover an important extension of the NW flank, are not detailed enough to distinguish geomorphological features except lobate debris aprons (LDA) and lobate valley fills (LVF), similar to other features described in different

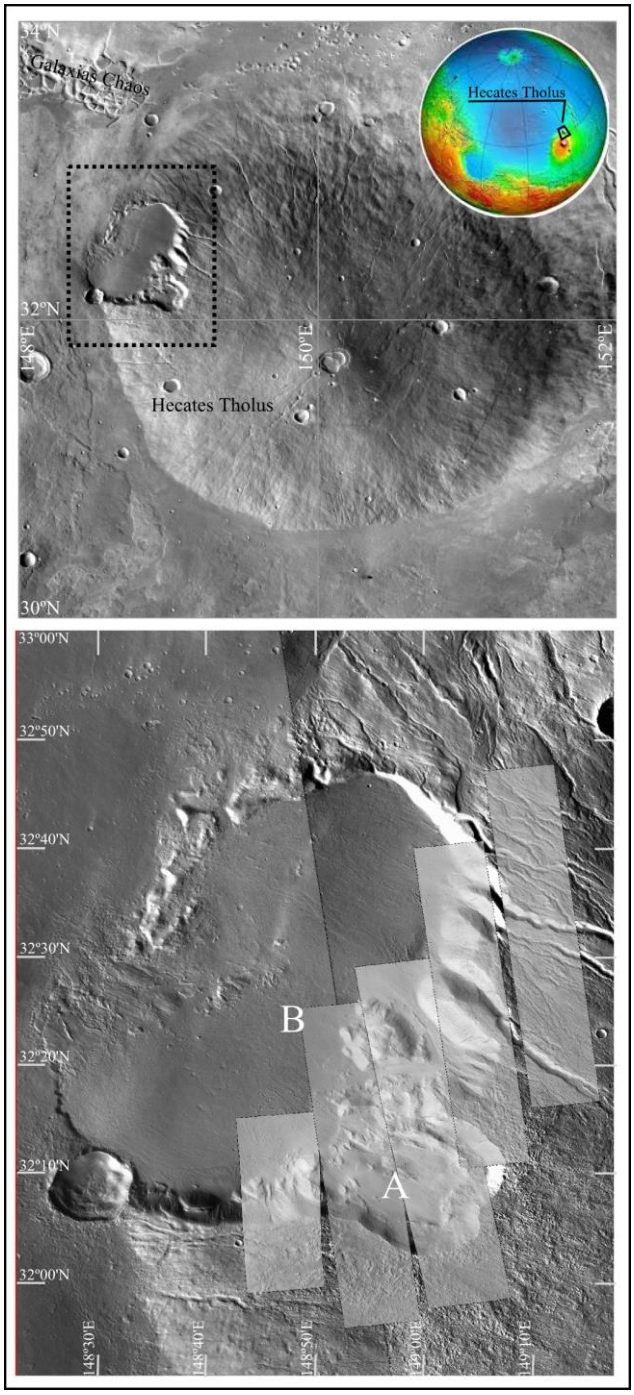

Fig. 7.1: Location map of the Hecates Tholus volcano of the Elysium volcanic province, Mars (top), and the study area (bottom, showing the location of the available HiRISE images partially covering the floor of depressions A and B on the NW flank of the volcano.

regions of Mars (e.g., Head et al., 2006, 2010). The detailed description of those features was done by the use of MOC images which resolution is about 2 m/pixel. Our map in a previous work (de Pablo and Centeno, 2012), is based on the use of CTX images (which resolution is about 6 m/pixel), and the detailed description of each mapped feature and units is based on the use of MOC and HiRISE images (which resolution is about 0.35 m/pixel). The result is a more detailed map (scale 1:100.000), of the lower NW flank of the volcano, which shows a wide variety of "marsforms". A respect previous map, this detailed map is an important advance on the knowledge of this volcano and its geological and glacial histories.

In a similar way, previous works to date the different units of the area (e.g., Neukum et al., 2004; Hauber et al., 2005; Werner, 2009), were based on regional mapped units. Our crater size-frequency distribution study (de Pablo et al., 2013) allowed date different geomorphological units better than the regional units dated by previous authors. Our results agree with previous, extend back the history of the volcano to 3.8 Ga, and introduce new ages for many other glacial events, which agree with the last ice ages of Mars (Head et al., 2003). The result is a very detailed age narrowing for the different units and, therefore, a detailed history of the glacial events on the study area. We can say that, at the moment of writing these lines, it is the most detailed reconstruction of glacial processes in any of the glaciated areas of Mars.

We also conducted detailed description of the geomorphological units and elements mapped, and the first morphometrical study ever done for this area. This description and morphometry allow the geomorphological characterization of the area, the thermal modelization of the glaciers, the proposal of a glacial origin of the valleys dissecting the depression walls, and the discussion on the possible existence of ice on present time in the area.

Our first suspect of present buried ice derived from the observation of crevasses and thermal anomalies, both impossible to preserve long after ice thawing. A good important part of this work is devoted to find sound evidence of this buried ice.

Present existence of ice (or very recent existence) in the study area related to glacial geomorphological units, was also discussed thanks to the thermal characterization of the area, mainly based on THEMIS-derived brightness temperature of the surface. Although our results should be considered as a starting point for further and detailed researches, we were able to produce serious evidence supporting the presence of buried ice in some places of the study

area. These interpretations were based on the location of possible surficial thermal anomalies what were not able to relate to differences on composition, elevation, or relief, as well as to the existence of landforms that could be easily destroyed during glacier ablation. Moreover, the location of that thermal anomalies, partially coincide with the area that other authors proposed the existence of buried ice (e.g., Helbert et al., 2005). We tried to confirm it by the use of ground penetration radar data from SHARAD instrument but, unfortunately, we were not able to distinguish any reflector that could be interpreted as ice layers or lenses under the surface. Moreover, data were excessively noisy due to the local relief, the depressions in the flank, and the proper volcano edifice.

The idea of buries glacial-ice is also supported by the terrestrial analogues we studied in Deception Island, Antarctica. The pyroclastic deposits covering the glaciers on that Antarctic island hide the ice surface of the glaciers, but many glacial-related features could be still recognizable on satellite images. Then, absence of ice on the surface at the study area on Mars (as well as in any other glaciated areas of the planet except the polar caps), as seen on images from any instrument, is not a handicap for the ice existence below the surface. Dust deposits and debris accumulations could cover the remnant ice from the last ice age on Hecates Tholus, protecting the ice from the sublimation under present cold climate conditions. But the presence of crevasses indicates that ice flow happened not very long ago -or the crevasses should have been erased or covered by aeolian processes.

Then, along this work we provided an answer to each one of all those initial questions what inspired this research: what are the glacial-related features existing in the area? How is their distribution? When they formed? How many events were required to form them? In which climatic conditions they formed? How was their evolution? Is there still any ice there?

7.2. Inner structure

Thank to recent advances in the study of the area, further questions arise: Are those glaciers active on present time? If they are actic, are they growing or retreating? How could the glaciers flow without ice accumulation at the head? Or without a clear mass-balance gradient? Are there evidences of glacial dynamics? How is the inner structure? The observations we provided along this work could help us to provide an answer to that questions, or, at least, to speculate about it.

Along this work we showed, described and characterized geomorphological evidences of glacial activity in the area (de Pablo and Centeno, 2012), that made possible, together with crater size-frequency distribution analyses , to propose how was the evolution of glaciers in this flank of Hecates Tholus (de Pablo et al., 2013).

We also discussed briefly the existence of ice lenses and their possible location in the floor of the depressions at the flank of the volcano, as well as discussed the inner structure of the glacial deposits (GD unit) (Figure 6.15): Debris-covered glaciers, relict ice lenses, or rock glaciers were here discussed. We already said that SHARAD ground penetration radar data didn´t allow to study the inner structure of the deposits and, therefore, to establish which model of those three is the correct. However, there is an observation what still captures our attention: if frontal lobate moraine deposits result from the glacier retreatment, why we still are able to observe crevasses and bergschrunds in the floor of the depression and valleys related to GD unit? Why we still have thermal anomalies (of lower temperatures than expected) on the central part of the main depression? Why there is a topographic steep in that floor?

We could speculate about one unique scenario: a glacier that was covered and buried under some meters of materials (debris, pyroclastic and/or dust). This glacier, that extended until the middle part of the depression, where the topographic step is located, was later covered by new piedmont glaciers during a more recent glacial event. That new glaciers later disappeared by retreat, leaving numerous moraine deposits, all around the depression on the flank of the volcano. Since that moment, the remnant ice located in depth, and protected by mantle deposits, including moraines, could have some kind of flow, since new crevasses and bergschrunds formed on more recent times in the floor of the depression and also in the floor of the valleys, related to GD unit (Figure 7.2).

Considering the volcanic setting of the area, the existence of numerous pulses and events on the glacial activity, with advance and retreat of glacial tongues in the depression (de Pablo et al., 2013), we consider that this scenario is feasible, and explain all the above observations, including moraine deposits, crevasses, bergschrunds and thermal anomalies.

Then, the inner structure of GD unit depends of the sector (Figure 7.2). On the western sector of the depression, GD unit could be formed by basal moraine deposits from the different glacial episodes (de Pablo et al., 2013), later overlapped by frontal moraine deposits abandoned by the glaciers retreat pulses. However, on the central and eastern sector of the

depression (as well as in the floor of the main valleys dissecting in the flank of the volcano), we could have extensive ice covered by mantle deposits, and overlapped by the same frontal moraine deposits. The limit between each sector is marked by the topographic step previously described.

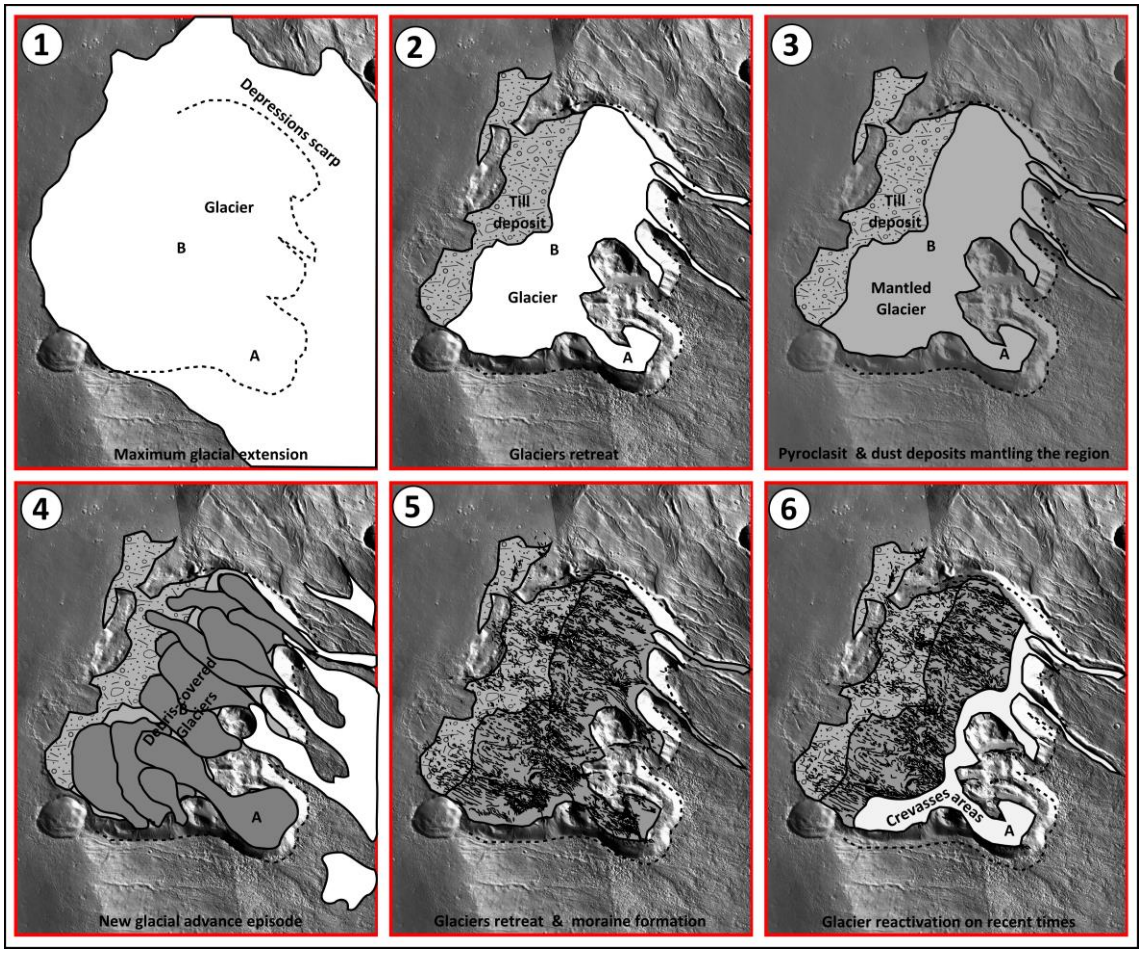

Fig. 7.2: Sketch sowing the proposed evolution model of glaciers on depressions A and B at the flank of the Hecates Tholus volcano, an how an important ice layer could exist in the area, later overlapped by retreat moraines and the crevasses sector could be indicative of a recent reactivation of the glaciers flow.

The mantle deposits could have very variable thickness: where it is thick enough, crevasses do not exist or, if exist, they are filled and then indistinguishable; where the thickness is low enough we were able to identify crevasses on HiRISE images (Figure 4.6; Figure 4.7; Figure 4.15). However, we could not establish the thickness of the ice layer, or the ice content. Considering the three scenarios we proposed in this work: debris-covered glaciers, relict glaciers, or rock glaciers (Figure 6.15), two observations allow us to preliminarily discard the rock glaciers scenario, because it could not explain the existence of crevasses and bergschrunds. We consider so complex to conserve crevasses during 440 Ka, which is the

youngest age we obtained for the glacial activity in GD unit (de Pablo et al., 2013). Aeolian and pyroclastic materials should erase those features along this period.

It is more difficult to decide between the other two cases, because if ice forms a continuous layer like it is expected on the case of buried ice, why there are not thermal anomalies everywhere in the area? We do not discard that a further and a more detailed and accurate research could reveal it, but it is not evident as we saw before in this work. On the other hand, if ice lenses existed, a more irregular topography should be expected due to the irregular distribution of ice in the floor of the depression. However, topographic data shows a smooth and regular slope (Figure 4.10), such as expected if a regular and continuous buried ice layer exists in the eastern sector of depression B.

7.3. Glacier dynamics

Although we are not able to establish if a continuous buried ice layer exist in the depression, crevasses and bergschrunds give good information on glacier dynamics. Crevasses form due to ice flowing. Depending of the local efforts, transverse, radial, and chevron crevasses form (Figure 4.7; e.g., Paterson, 1981; Nye, 1952), and bergschrunds form on the head of a glacier because the initial downslope movement of the ice. Then, we could ask three questions: When they formed? Why they formed?, and How they formed?

To answer the question about when they formed we could consider again that it could be difficult to preserve the ice fractures during 440 Ka that is the age of the last glacial event we obtained in this work (de Pablo et al., 2013). Although the recent climate conditions on Mars and on the study area (Figure 5.2; Figure 5.3) are enough cold to preserve the ice, the sublimation should made them to disappear because of sublimation of the seracs. On the other hand, if this process was not effective enough, aeolian deposits should fill and cover the crevasses along this long period.

Therefore, from our point of view, the crevasses and bergschrunds should be pretty young. We also described the wide distribution in the area of solifluction deposits related to south-facing slopes (Figure 4.17). We consider that if the solar radiation flux was high enough to produce the surficial ice-cemented slope deposits melting, the same process should make disappear the ice where the crevasses are located along the last 440 Ka. Then, if spite the solar radiation flux, and the low protection index, the crevasses and bergschrunds are still recognizable what, from our point of view, means that they are really young.

To answer to why question, we could consider that crevasses and bergschrunds form because tensional efforts in the ice mass. On Earth, they form because the irregular inner efforts caused by ice flow (e.g., Liboutry et al., 1976). In a static mass of ice, there are not that efforts, and therefore, crevasses do not form. Then, from our point of view, the downslope movement of the ice mass is the unique cause of the crevasses of the area.

Finally, to answer the how question, we could consider the distribution of bergschrunds in the study area (Figure 7.3). They are located at the eastern part of each depression in the flank of the volcano, related to the base of the walls. They are more frequent on north- and northwest-facing slopes, but it could be due to the south- and southeast facing slopes are characterized by slope and solifluction deposits (Figure 4.17) what could be covering the bergschrunds. Together with widely distributed crevasses, they point to a regional movement of the glaciers better than the flow of selected glaciers tongues. Then, if all the glaciers move, the cause should be also a regional force, for instance a regional mass balance gradient.

No evidences of ice accumulation on recent times have been reported on Mars in general, and on Hecates Tholus in particular. Then, three possibilities are feasible: (1) an increase on the ablation change the balance of a glacier in equilibrium; (2) the presence of a subglacial lubricant favor the flow of an unbalances glacier; and (3) a combination of them. In all cases, the flow could produce the reported features: crevasses and bergschrunds.

Surficial sublimation is feasible (e.g., Mangold, 2011 and references there in), but this could explain only a small volume of ablation. Moreover, landforms related to surficial ice sublimation should exist in the area like those described in other sites of Mars: basketball terrains, sublimation polygons, thermokarsts, scalloped terrains, etc. (e.g., Kreslavsky and Head, 2000; Malin and Edgett, 2001; Marchant et al., 2002; Head et al., 2003; Mangold et al., 2004; Kotama et al., 2006; Levy et al., 2008; Costard and Kargel, 1995; Morgenstern et al., 2007; Soare et al., 2008; Lefort et al., 2009, 2010; Zanetti et al., 2010), and they were not observed on MOC or HiRISE images off the study area. Then, glacier basal fusion could be more efficient because it changes the mass balance and also helps glacial flow with its lubricant effect. This is in agreement with the temperate glacial thermal regime we deduced on the basis of the presence of many geomorphological landforms in the area.

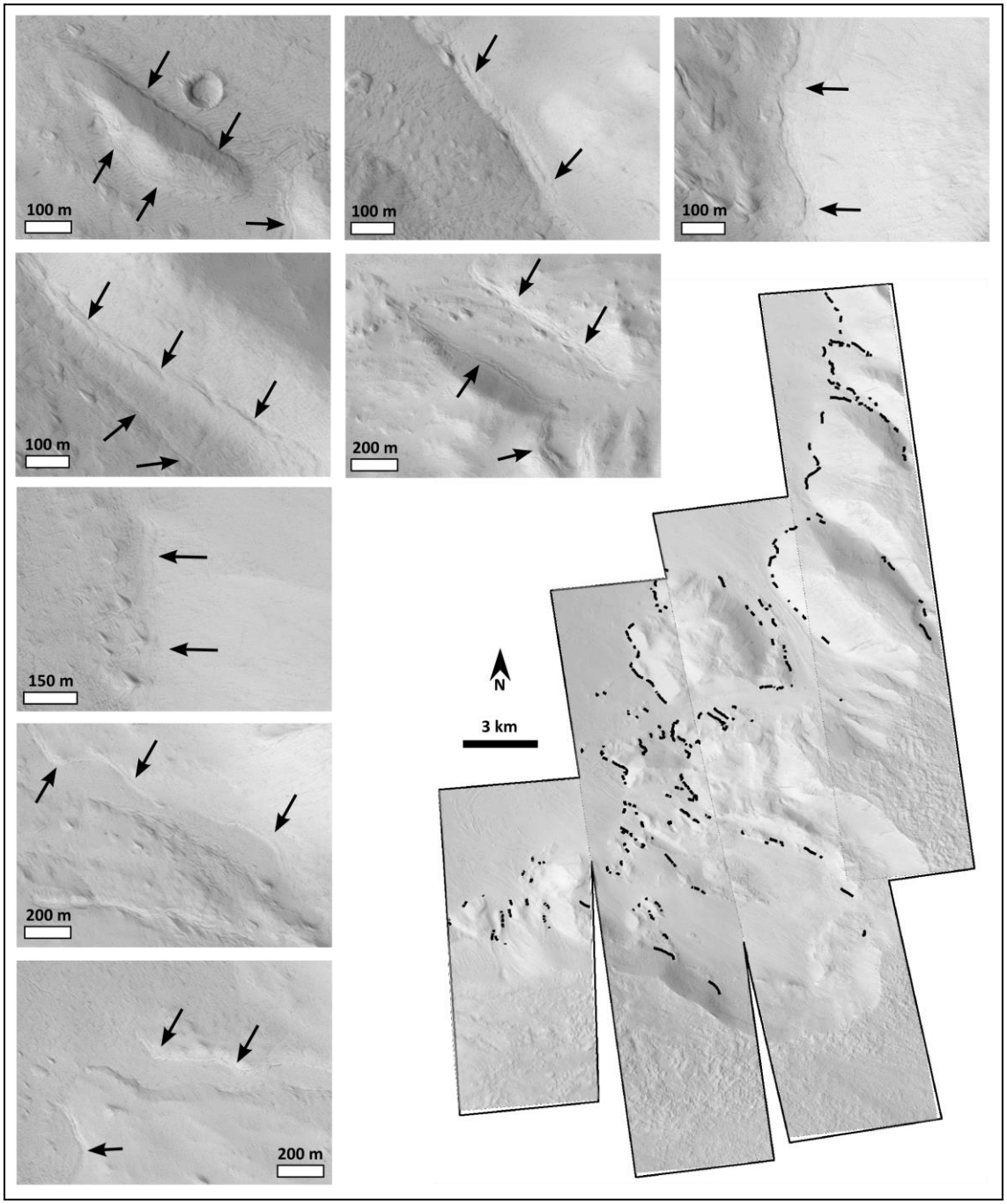

Fig. 7.3: HiRISE images mosaic (bottom right) showing the distribution of bergschrunds in the boundaries of the floor of depression A and the eastern sector of depression B (see location in Figure 7.1), and different examples from this area showing the distribution of that bergschrunds (black arrows) at the head or the flanks of the remnant ice masses.

7.4. Geological and environmental implications

Assuming that basal glacier melting could be the cause of the glacier flow, the next question to answer is which process caused the basal melting. On Earth, different processes could cause the basal melting: basal pressure caused by pressure, due to thick ice masses or to irregularities in the bedrock, like on rochee moutonèes , surficial melting water that reach the

base through moulines, runoff water on the base of the glacier coming from the surrounding non-glaciated terrains, or basal ice melting because of a local increase on heat flux, until the extreme of volcanic eruptions and jökulhlaups formation (e.g., Hooke, 1989; Fountain and Walder, 1998; Singh and Singh, 2001; Schoof, 2010; Irvine-Fynn et al., 2011). Basal pressure and geothermal flux could cause the direct basal ice melting, meanwhile surficial melting and runoff water accumulation on the base, could indirect help to melt the basal ice due to its relative higher temperature.

We already said that we are not able to calculate or to derive the thickness of the ice mass under the surface at the depressions and neither to calculate the pressure on the base. However, the key is that crevasses and bergschrunds are relatively recent (as discussed above), then, if there was not new accumulation of ice, the mantle deposits seems to be regularly distributed, debris deposits, and increase on the basal pressure could be discarded as the cause of the recent movement of the ice.

On the other hand, the flank of the volcano that surrounds the depressions (Figure 7.1) do not show recent reactivation of streams or the formation of new ones. This discards the runoff water accumulation. In the same way, HiRISE images do not show any evidence of surficial melting and water accumulation or flow, what discard the surficial water infiltration as a cause of basal melting or flow. Moreover, sublimation should be the most feasible mechanism of ablation under the present environmental conditions, such as occurred in many other sites on Mars that explain the existence of basketball terrains or scalloped terrains, among other landforms (e.g., Kreslavsky and Head, 2000; Malin and Edgett, 2001; Marchant et al., 2002; Head et al., 2003; Mangold et al., 2004; Kotama et al., 2006; Levy et al., 2008; Costard and Kargel, 1995; Morgenstern et al., 2007; Soare et al., 2008; Lefort et al., 2009, 2010; Zanetti et al., 2010). A gradient on sublimation, for example related to a different in surficial temperature such as this one we observed exist in the different geomorphological units (Figure 5.4), could cause an unbalance on the glacier mass and, therefore, the ice flow.

However, we did not observe any feature (topographic, geomorphological, or textural) to point toward a surficial sublimation of the ice.Then, although we could not definitively discard the effect of differential ablation by sublimation caused by differential surface temperature, an abnormal geothermal flux in the base of the depressions A and B should be the possible mechanism to produce the basal melting, after discard the other three possible causes.

Then, if an increase on the normal geothermal flux could produce the melting of the basal ice of the glacier, it could flows downslope, to form bergschrunds on the head of the glacier, and create crevasses in the glacier mass. Moreover, any melt water in the glacier bottom can flow and, under pressure conditions, have a lubricant effect. This melting water could reach the terminus area of the glacier (in the topographic step described above) and, when unprotected by the glacial ice should freeze or sublimate. This would also explain the lack of recent fluvial "marsforms" or activity at westernmost part of depression (although there are not available HiRISE images of this sector on present date). The water could infiltrate into the till deposits what characterize this sector of the depression (de Pablo and Centeno, 2012). However, a possible evidence of this process is the existence of possible pingos in the area, such as those we mapped in the western sector of the main depression (de Pablo and Centeno, 2012), although we could not ensure that pingos form in that moment of the history of the region.

Considering the volcanic origin of the area, an increase on the geothermal flux is a feasible process. Moreover, ground heating by magmatic activity has been already used by different authors to explain the radial network of channels on the flanks of Hecates Tholus volcano (e.g., Mouginis-Mark et al., 1982, 1984; Gulick, 1990; Head et al., 2004; Carr and Head, 2003; Fassett and Head, 2006) as well as many other features of this volcano (see de Pablo, 2009 for a review) along its geological history. Magma-water interactions have been widely studied in the area and it could also cause the formation of Galaxias Chaos, located immediately at the Northwest of the study area (e.g., Mouginis-Mark et al., 1984; Mouginis-Mark, 1985; Greeley and Guess, 1987; Tanaka et al., 1992), although sublimation and many other processes has been proposed like its origin (see a review in Pedersen, 2011).

Other fact could merge to help to understand the geothermal activity in this area: the proper depressions. The glaciers we studied here are mainly located inside two huge depressions on the flank of the volcano (Figure 7.1). Although the higher one, depression A, could be formed during a lateral volcanic explosion (Neukum et al., 2004; Hauber et al., 2005; Werner, 2009), an origin for the lower and extensive depression, depression B, has been still not confirmed, although different mechanism has been discussed (see de Pablo, 2009 for a detailed review).

Independently of their origin, fractures should exist, since these depressions seems do not formed by glacial erosion. Then, if fractures or any other conduct exist related to the depressions, a possible increase on the geothermal activity in the area, related to the volcanic

origin of Hecates Tholus, could help on the heat transportation to the surface, producing the basal melting what could cause the recent flow of the glaciers and, therefore, the crevasses and bergschrunds we observed in the HiRISE images of the area (Figure 7.4).

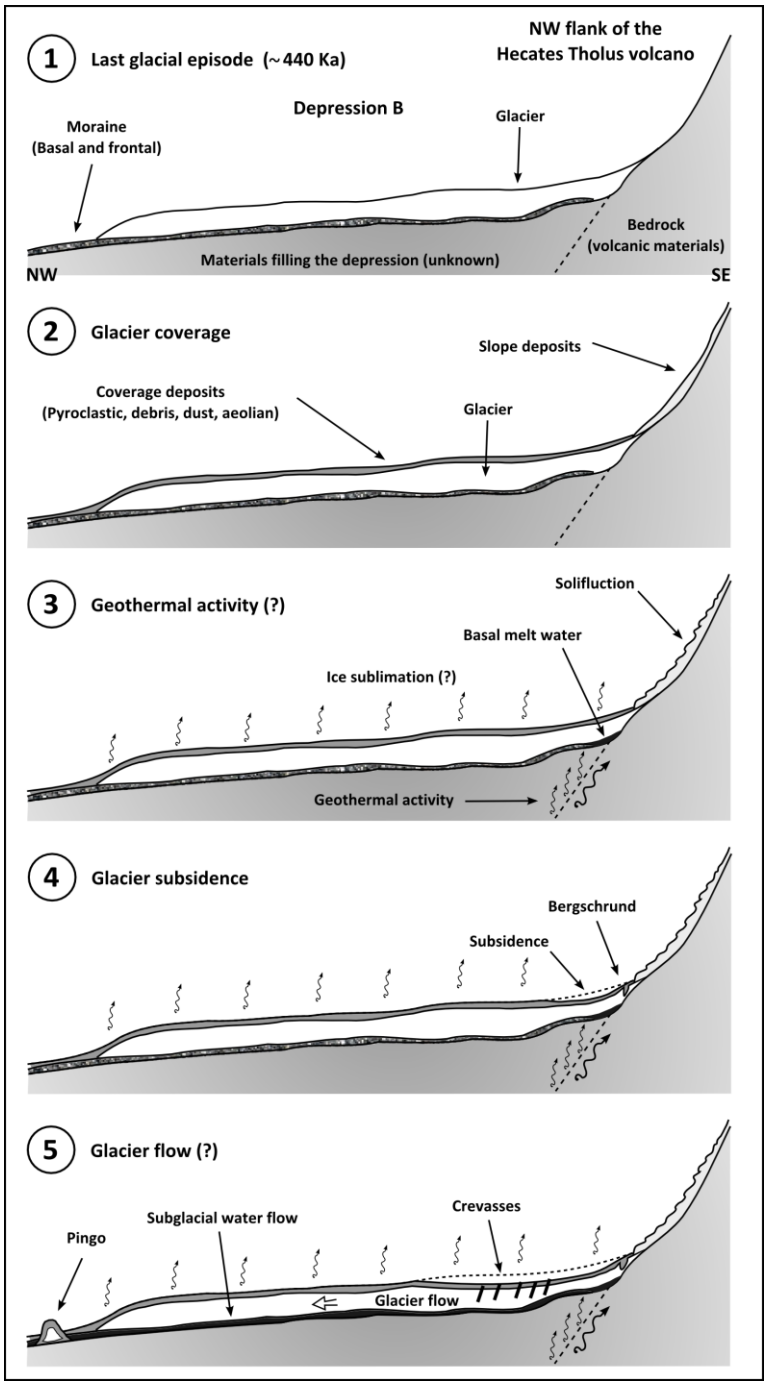

Fig. 7.4: Sketch showing the possible recent evolution of the glaciers . This possible evolution can explain the origin of bergschrunds, as well as other features such as crevasses and pingos in the area. Basal melting caused by geothermal flux, possible related to the geological structures caused by the proper depressions formation and the volcanic nature of the area, could help to the recent formation of those landforms and the flow of the glacier on recent times.

In fact, recent geological activity on the planet has been already proposed (e.g., Márquez et al., 2005), and an extensive corridor related to Tharsis and Elyisum volcanic provinces concentrate many evidences of recent geological activity, including magma-water interactions (e.g., Dohm et al., 2008). On the other hand, the glaciers of Hecates Tholus could be active although there is not a current Martian ice age, as it happens in present Earth mountain glaciers. Is it true? Does it occur in the same way in other glaciers of Mars? Are other regions showing the same evolution? Is it possible to establish a global history of glacial activity on the last 100 Ka based on geomorphological observations?

7.5. Further research

In this chapter we speculated, based on the evidences we presented along the different part of this work, about the possible recent glacial activity in the depressions at the lower NW flank of Hecates Tholus volcano, as well as about a possible mechanism to trigger that activity. Evidently, further research is required to check this hypothesis, and to accumulate other evidences that could confirm the exposed scenario here. Further investigations should focus on four subjects or approaches to complete the research we present here: geomorphological, spectrometrical, radar, and thermal analyses.

A detailed geomorphological analysis, based on HiRISE images is required in order to allow a more detailed geomorphological cartography to allow crevasses and bersgchrunds mapping, as well as moraine deposits. On present date, the available HiRISE images only cover depression A and the western sector of depression B. When in the future the spatial coverage of those types of images will extend to the eastern sector, till deposits pingos, roches moutonèes, flutes, or hanging valleys could be studied in detail. Extensive image coverage will also allow a more detailed crater counting and, therefore, a more detailed age determination for the different geomorphological units.

Spectrometrical analysis has been carried out here in this work based on THEMIS images, but it only provided a big picture of the geochemical composition of the study area. The use of CRISM spectrometrical data will made possible to identify the chemical composition of the different materials at the surface, including the bedrocks, dust, morraines and, may be, the ice. Nowadays, only few images of the westernmost sector of depression B are available. When a more extensive coverage will exist, this type of studies will help on the understanding of the geological evolution of the area. In fact, the hypothesis of geothermal activity in the area could be checked, may be by the search of mineral related to geothermal alterations on young materials.

Ground penetration radar data from SHARAD and MARSIS instruments should be analyzed in detail. Here we could only made a general overview of the few available SHARAD data, but a research focused on the use of them, including a more precise and accurate processing, will may be help on locate reflectors in the materials forming the GD unit on the floor of the depressions of the study area. This can confirm or reject the presence of ice layers or lenses. This data, may be could also help to locate the bottom of the depression and, perhaps, geological structures related to their origin.

Although we conducted an investigation to thermally characterize the study area, due to the presence of possible thermal anomalies we revealed, a more detailed and accurate analysis should be done, considering the develop of thermal models to confirm and precisely locate thermal anomalies, not only related to ice presence, but the possible presence of small spots of higher temperature, may be related to the geothermal flux what could produce the basal melting we propose is the possible cause of glaciers flow. At present time, this research depends on the use of THEMIS data, but the Mars Odyssey mission is still active and sending new data, that will allow detailed and also regional thermal studies, as well as analysis of the thermal evolution along the last decade.

In any case, the better way to confirm the existence of buried ice near the surface of the depressions is to carry out a borehole there. Depression B would be a perfect landing site for a mission with drilling capacity, such as the future In-Sight mission. The smooth surface between the moraine deposits we mapped, formed by fine grained material, and with low slope, would grant a safe landing place, and the presence of the here described crevasses point towards the ice presence at shallow depth within reach of the relative small drilling elements could be on board an spacecraft.

In this sense, Deception Island, Antarctica, is a perfect place to test the drilling instruments, providing the required experience to the scientific and enginery teams to test the instruments and the operations procedures under really cold climatic conditions. The pyroclastic covered glaciers on this Antarctic volcano are an indisputable adequate analogue for the study of glaciers on the flank of Hecates Tholus, as well as on the NW flanks of many other volcanoes on Mars. In this sense, Deception Island glaciated and active volcano is a perfect scenario to learn about the geomorphological, spectrometrical, radar and thermal properties of buried glaciers on volcanoes flanks, in order to test the results of the same type of studies on Mars.

7.5. Conclusions

The different evidences we obtained along this work made possible to consider in this chapter the most recent dynamics of the glaciers in the depressions A and B on the lower NW flank of Hecates Tholus volcano. The presence of crevasses and bergschrunds could be only explained if they are really young. In fact, they should be younger than 440 Ka which is the age of the last glacial event we date in this work. Coexistence of crevasses and bergschrunds, and moraine deposits is difficult to explain, except if the moraines are related to the retreatment of glaciers what covered, in a more recent age, ancient debris or pyroclastic deposits that mantled the extensive glaciers partially filled the floor of both depressions on the flank of the volcano. We explained here how this is possible considering the multiple glacial episodes of advance and retreatment of the glaciers in this region, as well as the volcanic nature of Hecates Tholus.

Moreover, those features imply ice mass movement, and we relate it to some kind of mass balance gradient. After discarding accumulation and surficial ablation, the basal melting seems to be the most feasible process. Considering the volcanic environment, we propose that an increase on the geothermal flux on the floor of the depressions could be the cause of basal melting of the glaciers. In addition, it helps to explain the unbalance of the remnant and buried ice layers, how the melting water could favor the ice flow, and the formation of crevasses and bergschrunds in recent times.

Finally, we propose different research techniques that could help to obtain more evidences to support or reject our hypothesis.

PhD thesis

Glacial geomorphology of the NW flank of the Hecates Tholus volcano, Mars

8

Conclusions

Miguel Ángel de Pablo Hernández

2015

8.1. Partial conclusions

The lower NW flank of the Hecate Tholus volcano of Mars is the unique volcano of the Elysium volcanic province showing glacial-related landforms, as reported by different authors. In order to study in detail those glaciers and their characteristics, we conducted different researches. Here we show the main partial conclusions resulting from each partial research.

The geomorphological analyses and mapping of the CTX images of the area resulted into a 1:100.000 scale geomorphological map, what allow concluding:

- The studied area is rich in possible glacial features (landforms, deposits, etc.), including moraines, covered glacial tongues (or possibly, rocky glaciers), lineated deposits, eskers, roches moutonèes, etc. It also reveals the existence of other interesting relief related to several processes, including: tectonics (ridges, faults and graben, or morphological alignments), fluvial and water-related (gullies, channels, or terraces), periglacial (pingos), gravitational (mass wasting deposits or creeping slopes) and impact-related (impact craters or ejecta deposits) forms.

The crater Size Frequency distribution (SFD) analyses in the main geomorphological units are the most detailed and extensive ever done in the NW flank of Hecates Tholus volcano. These analyses allow concluding:

- The general ages provided agree with the ideas of previous authors, and suggest a complex hydrological, climatic and geological history for this volcano in very recent times, perhaps as recent as 0.4 Ma.

- Volcanic activity was more important during the Late Noachian–Hesperian forming the volcanic edifice between 3.8 and 3.4 Ga, although later events could be as recent as 350 Ma in this sector of the edifice.

- Glacial activity had an important role in the resurfacing of the volcano flanks at relatively early times, as far back as 1.4 Ga, and the younger events could have occurred 60 Ma, 30 Ma, 16 Ma and 6 Ma ago, although other intermediate events could not be excluded at about 980 Ma, 800 Ma, 500 Ma, 415 Ma, 340 Ma, or 110 Ma ago. We also obtained ages of resurfacing events of 1.3 Ma, 1 Ma, and 0.44 Ma which could be related to glacial activity during the last ice age of Mars.

- A long-lasting glacial activity could have formed an extensive and very dynamic glacier that produced erosion and polishing of the outcrops forming smooth outcrops, roches moutonnées and hanging valleys. We deduced the probable glacier thickness at the edge of the depression B, to be about 600 meters.

A detailed geomorphological and morphometrical studies of CTX, HiRISE images, as well as some MOC and THEMIS images allow to conclude:

- Glacial origin of the materials at the floor of main valleys and the nested depressions at the flank of the volcano is the most feasible. In fact, we distinguish between till deposits and debris-covered glaciers, due to the presence of different marsforms like hummocky terrains or moraines, respectively. A topographic step on the floor of the depression helps to divide both terrains, as well as to point toward the possible existence of relict glaciers, covered by dust and debris deposits, in agreement with topographic sections, and slope and aspect maps.

- The different glacial-related geomorphological units and elements like roches moutonèes, flutes, till deposits and moraines, among others, allowed us to discuss the thermal regime concluding that temperate glaciers that are the most feasible.

- Morphometrical analysis allowed a first approach to the glacial origin of the marscape, based on the b-FR relation of three of the main valleys dissecting the eastern wall of the nested depression. However, we accept a primary fluvial origin, in agreement with many other authors that studied the channels on the flanks of Hecates Tholus volcano.

- Nowadays, relict glaciers could remain in the area due to the topographic and geomorphological evidences, not completely explained by the protection index. However, different creep slope marks on south-facing slope, as well as an asymmetrical distribution of smooth slope deposits allow us to propose the presence of ice cementing surficial materials like slope deposits.

Brightness temperature data, apparent thermal inertia, thermal inertia, or decorrelation stretch images analyses provide a different point of view and new conclusions has been made about the glaciers of the lower NW flank of Hecates Tholus:

- The analysis of surface brightness temperature products made possible to thermally characterize the study area and define four sectors in the depressions. Sector I, related to the flank of Hecates Tholus volcano, where the daytime surface temperature is higher

than nighttime temperature. Sector II, related to the floor of depressions on the NW flank of the volcano. Sector III, related to the lava flows from Elysium Mons surrounding Hecates Tholus volcano, characterized y high temperatures on both daytime and nighttime. Sector IV, related to the walls of the nested depressions and narrow and deep valleys, where there is a heavy contrast on daytime-nighttime temperatures, but also evident differences on south- and north-facing slopes due to differential insolation.

- Possible thermal anomalies reveal on daytime-nighttime surface temperature maps. They are located on the central area of the floor of depression B, and in most of the area of the floor of the depression A. These anomalies consists on a variation of about 5 K in areas where this thermal changes in not expected due to the uniform surface characteristics, after to discuss the relationships of these anomalies with elevation, topography (slope, aspect, curvature, ruggedness index, diurnal anisotropical heating, or protection index), thermal inertia and mineral composition. Any of them seems to explain the anomalies.

- A slightly convex relief on the topographic cross sections of the area is observable at sites where the anomaly is located allowed us to hypothesize about the existence of ice masses at these sites. Those lenses could be relict from the extensive glaciers active in the area for millions of years.

Our analysis of satellite images from Mars and Earth allowed us to recognize morphological analogues between the features observed on the lower NW flank of the Hecates Tholus volcano and the Deception Island volcano. Based on our comparative analysis, we conclude:

- The analogue features include crevasses, bergschrunds, erratic blocks, terminus, moraines, ridges, depressions, and other non glacial features (gullies, rockfall deposits, solifluction, etc.).

- The main relevance of those analogues is that they are related to covered/buried and active glaciers. Those analogies point toward the existence of present day remnant glaciers on the depression at the lower NW flank of the Hecates Tholus volcano of Mars. This interpretation is supported by the existence of crevasses and bergschrunds on Mars, a set of landforms that only can be preserved if glacial ice exists and the mantle deposited above the glacier is not thick enough to hide them.

- Based on those analogues, we propose a scenario in which the eastern part of the depression B could currently be filled by glaciers covered by debris materials, pyroclastic deposits and/or dust mantles, meanwhile the western sector of this depression shows till deposits. The presence of crevasses is for us a clear marker of the ice existence at low depths.

- The extensive analogues observed on the covered glaciers of Deception Island allow us to propose this sector of the island such as an interesting terrestrial analogue of the debris-covered glaciers of the Martian volcanoes, where to carry out further researches thank to the logistics facilities. On the other hand, to study the thermal behavior of the pyroclastic blanket of the terrestrial volcano could help to define a method to detect ice under the Martian pyroclastic surfaces by the use of THEMIS-derived brightness temperature.

The evidences we obtained along this work made possible to consider the most recent dynamics of the glaciers in the depressions A and B.

- The presence of crevasses and bergschrunds could be only explained if they are really young (younger than 440 Ka). Coexistence of crevasses and bergschrunds, and moraine deposits is difficult to explain, except if we consider an scenario where ancient glaciers were buried by pyroclastic (or debris o dust deposits). New glaciers flew on top of that deposits but during their retreat the leaved moraine deposits. Then, nowadays, moraine could cover ancient buried glaciers what today could be fractured by crevases and bergschrunds because it is movement again. This speculative scenario is possible considering the multiple glacial episodes of advance and retreatment of the glaciers in this region, as well as the volcanic nature of Hecates Tholus what could cover ancient glaciers with pyroclastic deposits.

- The presence of those crevasses and bergschrunds implies recent ice mass movement, and we relate it to some kind of mass balance gradient. After to discarding ice accumulation and surficial ablation, basal melting seems to be the most feasible process. Considering the volcanic environment, an increase on the geothermal flux on the floor of the depressions could be the cause of the recent basal melting of the glaciers, the unbalance of the remnant and buried ice layers, and how the melting water could favor the ice flow, and the formation of crevasses and bergschrunds in recent times.

8.2. Final conclusions

After to complete all the partial researches, the final conclusions of this research about the glacial geomorphology of the NW flank of the Hecates Tholus volcano are:

- The lower NW flank of the Hecates Tholus volcano shows a wide variety of landforms caused by glacial activity in the area, supporting the previous and less detailed studies about this region.

- Glacial-related landforms include erosive (hanging valleys, flutes, roches moutonèes) and depositional features (till deposits, glacial erratic, moraines, eskers), that points toward a long and complex geological, climatic and glacial histories – as shown also by many other fluvial, tectonic, or periglacial features.

- The glacial activity in the region occurred along the last 1.4 Ga, with multiple pulses on the advance and retreat, at about 980 Ma, 800 Ma, 500 Ma, 415 Ma, 340 Ma, 110 Ma, 1.3 Ma, 1 Ma, and 0.44 Ma.

- Although the last important glacial events in the area could occur during the last ice ages of Mars, possible surface thermal anomalies and existence of crevasses and bergschrunds point toward the presence of buried ice and its flow on recent times.

- Deception Island, Antarctica, is a perfect terrestrial analogue to study the geomorphology and thermal behavior of buried glaciers on Hecates Tholus in particular, and on Mars in general, where no surficial ice has been ever observed (except on the polar caps).

- Although we provided a detailed approach to the geomorphological characterization of the study area, and the established a detailed history of the glacial events, new more questions appeared that require further investigations to compliment and to complete it.

PhD thesis

Glacial geomorphology of the NW flank of the Hecates Tholus volcano, Mars

References

Miguel Ángel de Pablo Hernández

2015

Aharonson, O., and Schorghofer, N. 2006. Subsurface ice on Mars with rough topography. Journal of Geophysical Research, 111. E11007.

Alguacil, G., Almendros, J., del Pezzo, E., García, A., Ibáñez, J.M., la Rocca, M., Morales, J., and Ortiz, R. 1999. Observations of volcanic earthquakes and tremor at Deception Island, Antarctica. Ann. de Geofisica, 42. 417–436.

Almendros, J., Ibáñez, J.M., Alguacil, G., del Pezzo, E. Ortiz, R., 1997. Array tracking of the volcanic tremor source at Deception Island, Antarctica. Geophysical Research Letters, 24. 3069–3072.

Anderson, D.M. 1992. Glaciation in Elysium. In MSATT Workshop Polar Regions of Mars. Lunar and Planetary Institute Technical Report 92-08. p.1. (Abstract).

Anderson, R.C., Dohm, J.M., Golombek, M.P., Hadelmann, A.F.C., Franklin, B.J., Tanaka, K.L., Lias, J., and Peer, B. 2001. Significant centers of tectonic activity through time for the western hemisphere of Mars. Journal of Geophysical Research, 106. 20563-20585.

Aniya, M. and Welch, R. 1981. Morphological analyses of glacial valleys and estimates of sediment thickness on the valley floor: Victoria Valley system, Antarctica. Antarctic Record, 71. 76–95.

Arfstrom, J. and Hartmann, W.K. 2005. Martian flow features, moraine-like ridges, and gullies: Terrestrial analogs and interrelationships. Icarus, 174(2). 321-335.

Aristarain, A.J., and Delmas, R.J. 1998. Ice record of a large eruption of Deception Island volcano (Antarctica) in the XVIIth century. J. Volcanol. Geotherm. Res., 80, 17–25.

Augustinus, P.C. 1992. The influence of rock mass strength on glacial valley cross-profile morphometry: a case study from the Southern Alps, New Zealand. Earth Surf. Processes Landforms, 17. 39–51.

Augustinus, P.C. 1995. Glacial valley cross-profile development: the influence of in situ rock stress and rock mass strength, with examples from the Southern Alps, New Zealand. Geomorphology, 14. 87–97.

Bacastow, A.L., Sakimoto, S.E.H., 2006. Martian north polar crater morphology: implications for an aquifer. Lunar and Planetary Science Conference, XXXVII (abstract 2239).

Baker, D.H.M., Head, J.W., and Marchant, D.R. 2010. Flow patterns of lobate debris aprons and lineated valley fill north of Ismeniae Fossae, Mars: Evidence for extensive mid-latitude glaciation in the Late Amazonian. Icarus, 207(1). 186-209.

Baker, P.E., McReath, I., Harvey, M.R., Roobol, M.J. and Davies, T.G. 1975. The geology of the South Shetland Islands: V. Volcanic evolution of Deception Island. British Antarctic Survey Scientific Reports, 78. 1-81.

Baker, V.R., Strom, R.G., Dohm, J.M., Gulick, V.C., Kargel, J.S., Komatsu, G., Ori, G.G. and Rice, J. 2000. Mars' Oceanus Borealis, Ancient Glaciers, and the MEGAOUTFLO Hypothesis. Lunar and Planetary Science Conference, XXXI. Abstract #1863.

Baker, V.R., Strom, R.G., Gulick, V.C., Kargel, J.C., Komatsu, G. and Kale, V.S. 1991. Ancient oceans, ice sheets and the hydrological cycle on Mars. Nature, 352. 589–594.

Baker, V.R., Strom, R.G., Kargel, J.S., Dohm, J.M., and Ferris, J.C. 2001. Very recent, water-related landforms on Mars. Lunar and Planetary Science Conference, 32. Abstract #1619.

Baldridge, A.M., Lane, M.D., Wray, J.J. 2011. The earlier Mars Odyssey orbit time reveals aqueous mineralogy in mid-IR data. Lunar and Planetary Science Conference, 42. Abstract #1608.

Bandfield, J.L. 2008. High-silica deposits of an aqueous origin in western Hellas Basin, Mars. Geophysical Research Letters, 35. 1220510.1029/2008GL033807.

Bandfield, J.L., Hamilton, V.E., Christensen, P.R., and McSween, H.Y. 2004a. Identification of quartzofeldspathic materials on Mars. Journal of Geophysical Research, 109. 1000910.1029/2004JE002290.

Bandfield, J.L., Rogers, D., Smith, M.D., and Christensen, P.R. 2004b. Atmospheric correction and surface spectral unit mapping using Thermal Emission Imaging System data. Journal of Geophysical Research, 109. 1000810.1029/2004JE002289.

Banks, M.E., McEwen, A.S., Kargel, J.S., Baker, V.R., Strom, R.G., Mellon, M.T., Gulick, V.C., and the HiRISE team. 2008. High Resolution Imaging Science Experiment (HiRISE) Observations of Glacial and Periglacial Morphologies in the circum-Argyre Planitia Highlands, Mars. J. Geophys. Res. Planets, 113. E12.

Bennett, K. J.; Scholes, D.; Arvidson, R. E.; Slavney, S.; Guinness, E. A.; Stein, T. C. 20008. Accessing Mars Data Using PDS Geosciences Node's Orbital Data Explorer. Lunar and Planetary Science Conference, 39th. Abstract #1391.

Bennett, M. and Glasser, N. 2009. Glacial geology. Willey-Blackwell, Oxford. 385 pp.

Berkley, J.L. and Drake, M.J. 1981. Weathering of Mars: Antarctic analog studies. Icarus, 45(1). 231-249.

Bishop, J.L., Franz, H.B., Goetz, W., Blake, D.F., Freissinet, C., Steininger, H., Goesmann, F., Brinckerhoff, W.B., Getty, S., Pinnick, V.T., Mahaffy, P.R., and Dyar, M.D. 2013. Coordinated analyses of Antarctic sediments as Mars analog materials using reflectance spectroscopy and current flight-like instruments for CheMin, SAM and MOMA. Icarus, 224(2). 1019-1035.

Blaszczynski, J.S. 1997. Landform characterization with Geographic Information Systems. Photogrammetric Enginnering and Remote Sensing, 63(2). 183-191.

Böhner J. and Selige T. 2006. Spatial prediction of soil attributes using terrain analysis and climate regionalisation. In: Böhner J., McCloy K., Strobl J., editors. SAGA—Analysis and Modelling Applications. Vol. 115. Verlag Erich Goltze GmbH & Co; KG, Göttingen. Pp. 13–28.

Böhrner, J. and Antonic, O. 2009. Land surface parameters specific to topo.climatology. In: Heng, T. and Reuter, H.I. (eds). 2009. Geomorphometry: concepts, software, applications. Elsevier, Oxford, UK. 195-226.

Breed, C.S. 1977. Terrestrial analogs of the hellespontus dunes, Mars. Icarus, 30(2). 326-340.

Brook M.S., Purdie H.L., and Crow T.V.H. 2005. Valley cross-profile morphology and glaciation in Park Valley, Tararua Range, New Zealand. Journal of the Royal Society of New Zealand, 35. 399-407.

Bull, W.B., and McFadden, L.D. 1977. Tectonic geomorphology north and south of the Garlock Fault, California. In Geomorphology in Arid Regions: Annual Binghamton Conference, D.O. Doehring, ed., State University of New York at Binghamton, pp. 115–136.

Burr, D.M., Soare, R.J., Wan Bun Tseung, J.M., and Emery, J.P. 2005. Young (late Amazonian), near-surface, ground ice features near the equator, Athabasca Valles, Mars. Icarus, 178. 56–73.

Byrne, P.K., van Wyk de Vries, B., Murray, J.B., and Troll, V.R. 2009. The geometry of volcano flank terraces on Mars. Earth and Planetary Science Letters, 281. 1-13.

Byrne, S., Dundas, C.M., Kennedy, M.R., Mellon, M.T., McEwen, A.S., Cull, S.C., Daubar, I.J., Shean, D.E., Seelos, K.D., Murchie, S.L., Cantor, B.A., Arvidson, R.E., Edgett, K.S., Reufer, A., Thomas, N., Harrison, T.N., Posiolova, L.V., Seelos, F.P. 2009. Distribution of Mid-Latitude Ground Ice on Mars from New Impact Craters. Science, 325. 1674.

Cabrol, N. and Grin, E. 2001. Composition of the drainage network on early Mars. Geomorphology, 37. 269-287.

Carr, M.H. 1982. Periodic climate change on Mars - Review of evidence and effects on distribution of volátiles. Icarus, 50. 129-139.

Carr, M.H. 1986. Mars: A water-rich planet? Icarus, 68(2). 187-216.

Carr, M.H. 1996a. Channels and valleys on Mars: cold climate features formed as a result of a thickening cryosphere. Planetary and Space Science, 44. 1411-1423.

Carr, M.H. 1996b. Water on Mars. Oxford University Press, New York. 248 pp.

Carr, M.H. 2001. Mars Global Surveyor observations of Martian fretted terrain. Journal of Geophysical Research, 106. 23571-23594.

Carr, M.H. 2006. The surface of Mars. Cambridge: Cambridge University Press.

Carr, M.H. and Head, J.W. 2003. Basal melting of snow on early Mars: A possible origin of some valley networks. Geophysical Research Letters, 30. PLA 3-1.

Carr, M.H. and Head, J.W. 2010. Geologic history of Mars. Earth and Planetary Science Letters, 294(3-4). 185-203.

Carr, M.H. and Schaber, G.G. 1977. Martian permafrost features. Journal of Geophysical Research, 82. 4039-4054.

Carter, L.C., Campbell, B.A., Watters, T.R., Phillips, R.J., Putzig, N.E., Safaeinili, A., Plaut, J.J., Okubo, C.H., Egan, A.F., Seu, R., Biccari, D., and Orosei, R. 2009. Shallow radar (SHARAD) sounding observations of the Medusae Fossae Formation, Mars. Icarus, 199(2). 295–302.

Carter, L.M., et al. 2009. Shallow radar (SHARAD) sounding observations of the Medusae Fossae Formation, Mars. Icarus, 199(2). 295–302.

Casertano, L., 1967. Volcanic activity at Deception Island. Antarctic Geology, 33–47, Sci. Comm. on Antarct. Res, London, 1967.

Chamberlin, T.C. 1897. The method of multiple working hypotheses. Journal of Geology, 5. 837-848.

Chan, M.A., Ormö, J., Murchie, S., Okubo, C.H., Komatsu, G., Wray, J.J., McGuire, P., McGovern, J.A., and the HiRISE Team. 2010. Geomorphic knobs of Candor Chasma, Mars: New Mars Reconnaissance Orbiter data and comparisons to terrestrial analogs. Icarus, 205(1). 138-153.

Chapman, M. 2007. The Geology of Mars: evidence from Earth-based analogs. Cambridge University Press, Cambridge. 484 pp.

Chapman, M.G. 1993. Evidence for an ice sheet/frozen lake in Utopia Planitia, Mars. Workshop on the Martian Northern Plains: Sedimentological, Periglacial, and Paleoclimatic Evolution. Abstracts, 4-5.

Chapman, M.G. 1994. Evidence, age and thickness of a frozen paleolake in Utopia Planitia, Mars. Icarus, 109, 393–406

Chapman, M.G. 2003. Sub-ice volcanoes ad ancient oceans/lakes: a Martian challenge. Global and Planetary changes, 35. 185-198.

Chapman, M.G., Allen, C.C., Gudmundsson, M.T., Gulick, V.C., Jakobsson, S.P., Lucchitta, B.K., Skiling, I.P., and Waitt, R.B. 2000. Volcanism and ice interactions on Earth and Mars. In: Gregg, T.K.P. and Zimbelman, J.R. (Eds.) Deep oceans to deep space: environmental effects on volcanic eruptions. Plenum Press, New York. 39-74.

Chapman, M.G., Smellie, J.L. 2007. Mars interior layered deposits and terrestrial sub-ice volcanoes compared: observations and interpretations of similar geomorphic

characteristics. In: Chapman, M.G. (Ed.). The geology of Mars: evidence from Earth-based analogs. Cambridge University Press. 178-210.

Chassefière, E. and Leblanc, F. 2004. Mars atmospheric escape and evolution; interaction with the solar wind. Planetary and Space Science, 52. 1039-1058.

Christensen, P.R. 1986. Regional dust deposits on Mars: Physical properties, age, and history. J. Geophys. Res., 91(B3), 3533–3545.

Christensen, P.R. 2003. Formation of recent martian gullies through melting of extensive water-rich snow deposits. Nature, 422 (6927). 45–48.

Christensen, P.R., Anderson, D.L., Chase, S.C., Clancy, R.T., Clark, R.N., Kieffer, H.H., Kuzmin, R.O., Malin, M.C., Pearl, J.C., Roush, T.L., and Smith, M.D. 1998. Results from the Mars Global Surveyor thermal emission spectrometer. Science, 279. 1692-1698.

Christensen, P.R., Bandfield, J.L., Hamilton, V.E., Ruff, S.W., Kieffer, H.H., Titus, T.N., Malin, M.C., Morris, R.V., Lane, M.D., Clark, R.L., Jakosky, B.M., Mellon, M.T., Pearl, J.C., Conrath, B.J., Smith, M.D., Clancy, R.T., Kuzmin, R.O., Roush, T., Mehall, G.L., Gorelick, N., Bender, K., Murray, K., Dason, S., Greene, E., Silverman, S. and Greenfield, M. 2001. The Mars Global Surveyor Thermal Emission Spectrometer experiment: Investigation description and surface science results. Journal of Geophysical Research, 106. 23,823-23,871.

Christensen, P.R., Jakosky, B.M., Kieffer, H.H., Malin, M.C., McSween, H.Y., Nealson, K., Mehall, G.L., Silverman, S.H., Ferry, S., Caplinger, M. and Ravine, M. 2004. The Thermal Emission Imaging System (THEMIS) for the Mars 2001 Odyssey Mission. Space Science Reviews, 110. 85-130.

Chuang, F.C. and Crown, D.A. 2005. Geomorphic Analyses of Lobate Debris Aprons in Deuteronilus Mensae, Mars. American Geophysical Union Fall Meeting 2005, abstract #P23A-0176.

Chuang, F.C. and Crown, D.A. 2009. Geologic map of MTM 35337, 40337, and 45337 quadrangles, Deuteronilus Mensae region of Mars: U.S. Geological Survey Scientific Investigations Map 3079.

Clark, D.H., Clark, M.M., Gillespie, A.R. 1994. Debris-Covered Glaciers in the Sierra Nevada, California, and Their Implications for Snowline Reconstructions. Quaternary Research, 41(2). 139-153.

Clarke, G.K.C. 2005. Subglacial processes. Annual Review of Earth and Planetary Sciences 33(1): 247–276.

Clifford, S.M. 1993. A model for the hydrologic and climatic behavior of water on Mars. Journal of Geophysical Research, 98 (E6). 10,973–11,016.

Clifford, S.M. and Parker, T.J. 2001. The evolution of the Martian hydrosphere: implications for the fate of a primordial ocean and the current state of the northern plains. Icarus, 154. 40-79.

Coles, R.J. 2014. The cross-sectional characteristics of glacial valleys and their spatial variability. PhD thesis, University of Sheffield.

Cooper, A.P.R., Smellie, J.L. and Maylin, J. 1998. Evidence for shallowing and uplift from bathymetric records of Deception Island, Antarctica. Antarctic Science, 10. 455-461.

Costard, F.M. and Kargel, J. 1995. Outwash plains and thermokarst on Mars. Icarus, 114. 93–112.

D'Agata, C. and Zanutta, A. 2007. Reconstruction of the recent changes of a debris-covered glacier (Brenva Glacier, Mont Blanc Massif, Italy) using indirect sources: Methods, results and validation. Global and Planetary Change, 56(1–2). 57-68.

de Hon, R.A. 1997. The relationship of subdued grooved terrain, mesas and knobs in northeast Elysium Planitia. Lunar and Planetary Science Conference, XXVIII. Abstract #1446.

de Hon, R.A., Mouginis-Mark, P.J. and Brick, E.E. 1999. Geologic map of the Galaxias quadrangle (MTM 35217) of Mars. U.S. Geological Survey. Geologic Serie, Map I-2579.

de Pablo, M. A.; Ramos, M.; Vieira, G.; Gilichinsky, D.; Gómez, F.; Molina, A.; Segovia, R. 2009. Deception Island, Antarctica: a terrestrial analogue for the study and understanding of the Martian permafrost and subsurface glaciers. EGU General Assembly, 2009. Abstract 1292.

de Pablo, M.A. 2009. Geological cartography of the Elysium volcanic region of Mars: Magma-water-climate interactions. PhD Thesis. Universidad Rey Juan Carlos, Madrid. Spain. 500 pp.

de Pablo, M.A. and Centeno, J.D. 2012. Geomorphological map of the lower NW flank of the Hecates Tholus volcano, Mars. Journal of Maps, 2012. 8(3) 208-214.

de Pablo, M.A. and Komatsu, G. 2008. Pingo Fields in the Utopia Basin, Mars: Geological and Climatic Implications. Icarus, 199(1). 49–74.

de Pablo, M.A., Michael, G.G., and Centeno, J.D. 2013. Age and evolution of the lower NW flank of the Hecates Tholus volcano, Mars, based on crater size frequency distribution on CTX images. Icarus, 226(1). 455-469.

de Rosa, R., Mazzuoli, R., Omarini, G., Ventura, J.G., and Viramonte, A. 1995. Volcanological model for the historical eruptions at Deception Island (Bransfield Strait, Antarctica). Terra Antart., 2. 95–101.

Dickson, J., Head, J., and Kreslavsky, M. 2007. Martian gullies in the southern mid-latitudes of Mars: Evidence for climate-controlled formation of young fluvial features based upon local and global topography. Icarus, 188. 315–323.

Dickson, J.L., Head, J.W. and Fassett, C.I. 2012. Patterns of accumulation and flow of ice in the mid-latitudes of Mars during the Amazonian. Icarus, 219(2). 723-732.

Dickson, J.L., Head, J.W., and Marchant, D.R. 2010. Kilometer-thick ice accumulation and glaciation in the northern mid-latitudes of Mars: Evidence for crater-filling events in the Late Amazonian at the Phlegra Montes. Earth and Planetary Science Letters, 294. 332-342.

Dingle, R.V. 1977. The anatomy of a large submarine slump on a sheared continental margin (SE Africa). Journal of Geological Society London, 134. 293-310.

Dobinson, E., Curkendall, D., Plesea, L. and Hare, T.M. 2006. Adaptation and Use of Open Geospatial© Web Technologies for Multi-Disciplinary Access to Planetary Data. Lunar and Planetary Science Conference, XXXVII. Abstract #1463.

Dohm, J.M., Ferris, J.C., Baker, V.R., Anderson, R.C., Hare, T.M., Strom, R.G., Barlow, N.G., Tanaka, K.L., Klemaszewski, J.E., and Scott, D.H. 2001. Ancient drainage basin of the

Tharsis region, Mars: potential source for outflow channel systems and putative oceans or paleolakes. Journal of Geophysical Research, 106. 32943-32958.

Doornkamp, J.C. and King, C.A.M. 1971. Numerical Analysis. In Geomorphology. Arnold, London, 372 pp.

Dundas, C.M., Diniega, S., Hansen, C., Byrne, S., and McEwen, A. 2012. Seasonal activity and morphological changes in Martian gullies. Icarus, 220. 124-143.

Dundas, C.M., Mellon, M.T., McEwen, A.S., Lefort, A., Keszthelyi, L.P., Thomas, N. and the HiRISE Team. 2008. HiRISE observations of fractured mounds: possible Martian pingos Geophys. Res. Lett., 35(4). L04201

Dundas, C.M., Diniega, S., Hansen, C. J., Byrne, S., McEwen, A.S. 2012. Seasonal activity and morphological changes in martian gullies. Icarus, 220(1). 124-143.

Edgett, K., Malin, M.C., Williams, R.M.E., andDavis, S.D. 2003. Polar-and middle-latitude martian gullies: A view from MGS MOC after 2 Mars years in the mapping orbit. Lunar and Planetary Science Conference, 34. Abstract #1038.

Edgett, K.S. and Christensen, P.R. 1991. The particle size of Martian aeolian dunes. Journal of Geophysical Research, 96(E5). 22765–22776.

Edgett, K.S. and Christensen, P.R. 1994. Mars aeolian sand: Regional variations among dark-hued crater floor features. Journal of Geophysical Research, 99(E1). 1997–2018.

Evans, D.J.A., Twigg, D.R., Rea, B.R., and Orton, C. 2009. Surging glacier landsystem of Tungnaarjokull, Iceland. Journal of Maps, v2009, 134–151.

Fairén, A.G. 2010. A cold and wet Mars. Icarus, 208(1). 165-175.

Fairén, A.G., Dohm, J.M., Baker, V.R., de Pablo, M.A., Ruiz, J., Ferris, J.C. and Anderson, R.C. 2003. Episodic flood inundations of the northern plains of Mars. Icarus, 165. 53-67.

Fassett, C.I. and Head, J.W. 2006. Valleys on Hecates Tholus Mars: origin by basal melting of summit snowpack. Planetary and Space Science, 54. 370-378.

Fassett, C.I. and Head, J.W. 2007. Valley formation on Martian volcanoes in the Hesperian: Evidence for melting of summit snowpack, caldera lake formation, drainage and erosion on Ceraunius Tholus. Icarus, 189. 118-135.

Fassett, C.I., Dickson, J.L., Head, J.W., Levy, J.S., and Marchant, D.R. 2010. Supraglacial and proglacial valleys on Amazonian Mars. Icarus, 208. 86-100.

Fastook, J.L., Head, J.W. and Marchant, D.R. 2005. Tropical mountain glaciers on Mars: accumulation conditions, formation times, glacier dynamics, and implications for planetary spin-axis obliquity values. American Geophysical Union, Fall Meeting 2005. Abstract #P34A-03.

Fastook, J.L., Head, J.W., Forget, F., Madeleine, J.-B., and Marchant, D.R. 2011. Evidence for Amazonian northern mid-latitude regional glacial landsystems on Mars: Glacial flow models using GCM-driven climate results and comparisons to geological observations. Icarus, 216(1). 23-39.

Fastook, J.L., Head, J.W., Marchant, D.R., and Forget, F. 2008. Tropical mountain glaciers on Mars: Altitude-dependence of ice accumulation, accumulation conditions, formation times, glacier dynamics, and implications for planetary spin-axis/orbital history. Icarus, 198. 305-317. doi: 10.1016/j.icarus.2008.08.008.

Fastook, J.L., Head, J.W., Marchant, D.R., Forget, F., and Madeleine, J.-B. 2012. Early Mars climate near the Noachian–Hesperian boundary: Independent evidence for cold conditions from basal melting of the south polar ice sheet (Dorsa Argentea Formation) and implications for valley network formation. Icarus, 219(1). 25-40.

Feldman, W.C., Boynton, W.V., Tokar, R.L., Prettyman, T.H., Gasnault, O., Squyres, S.W., Elphic, R.C., Lawrence, D.J., Lawson, S.L., Maurice, S., McKinney, G.W., Moore, K.R. and Reedy, R.C. 2002. Global distribution of neutrons from Mars: results from Mars Odyssey. Science, 297. 75-78.

Fenton, L.K., Bandfield, J.L. and Ward, A.W. 2003. Aeolian processes in Proctor Crater on Mars: Sedimentary history as analyzed from multiple data sets. Journal of Geophysical Research, 108(E12). 5129.

Fenton, L.K. and Mellon, M.T. 2006. Thermal properties of sand from Thermal Emission Spectrometer (TES) and Thermal Emission Imaging System (THEMIS): Spatial variations within the Proctor Crater dune field on Mars. Journal of Geophysical Research, 111(E6). E06014.

Fergason, R.L., Christensen, P.R. and Kieffer, H.H. 2006. High-resolution thermal inertia derived from the Thermal Emission Imaging System (THEMIS): Thermal model and applications. J. Geophys. Res., 111, E12004.

Fergason, R.L. and Christensen, P.R. 2003. Thermal Inertia Using THEMIS Infrared Data. Lunar and Planetary Science Conference, 34. Abstrct # 1785.

Fernández-Remolar, D.C., Prieto-Ballesteros, O., Gómez-Ortíz, D., Fernández-Sampedro, M., Sarrazin, P., Gailhanou, M., and Amils, R. 2011. Río Tinto sedimentary mineral assemblages: A terrestrial perspective that suggests some formation pathways of phyllosilicates on Mars. Icarus, 211(1). 114-138.

Fishbaugh, K.E. and Head, J.W. 2005. Origin and characteristics of the Mars north polar basal unit and implications for polar geologic history. Icarus, 174(2). 444-474.

Forget, F., Haberle, R.M., Montmessin, F., Levrard, B., and Head, J.W. 2006. Formation of glaciers on Mars by atmospheric precipitation at high obliquity. Science, 311. 368-371.

Forget, F., Hourdin, F., Fournier, R., Hourdin, C., Talagrand, O., Collins, M., Lewis, S.R., Read, P.L., and Huot, J.-P. 1999. Improved general circulation models of the Martian atmosphere from the surface to above 80 km. Journal of Geophysical Research, 104. E10. 24,155-24,176.

Fountain, A.G. and Walder, J.S. 1998. Water flow through temperate glaciers. Reviews on Geophysics, 36(3). 299–328.

French, H.M. 1993. Cold-climate processes and landforms. In: French, H.M., Slaymaker, O. (Eds.), Canada's Cold Environments. McGill Queens Univ. Press, Montreal. 271–290.

Gillespie, A. R., Kahle, A.B., and Walker, R.E. 1986. Color enhancement of highly correlated images. I. Decorrelation and HSI contrast stretches, Remote Sensing Environment, 20(3). 209–235.

Gómez-Elvira, J., Armiens, C., Castañer, L., Domínguez, M., Genzer, M., Gómez, F., Haberle, R., Harri, A., Jiménez, V., Kahanpää, H., Kowalski, L., Lepinette, A., Martín, J., Martínez-Frías, J., McEwan, I., Mora, L., Moreno, J., Navarro, S., de Pablo, M.A., Peinado, V., Peña, A., Polkko, J., Ramos, M., Renno, N.O., Ricart, J., Richardson, M., Rodríguez-Manfredi, J., Romeral, J., Sebastián, E., Serrano, J., de la Torre Juárez, M., Torres, J., Torrero, F., Urquí,

R., Vázquez, L., Velasco, T., Verdasca, J., Zorzano, M., and Martín-Torres, J. 2012. REMS: The environmental sensor suite for the Mars science laboratory rover. Space Science Reviews, 2012. 1-58.

Grad, M., Guterch, A., and Sroda, P. 1992. Upper crustal structure of Deception Island area, Bransfield Strait, West Antarctica. Antarctic Science, 4. 469-476.

Graf, W.L. 1970. The geomorphology of the glacial valley cross-section. Arctic and Alpine Research, 2. 303–312.

Greeley, R. 1985. Planetary landscapes. Allen and Unwin, London. 265 pp.

Greeley, R. and Guest, J.E. 1987. Geologic map of the eastern equatorial region of Mars (1:15,000,000). U.S. Geological Survey Geologic Investigations Series, Map I-1802-B.

Greeley, R., Bleacher, J.E., Cave, S.R., Williams, D.A., Werner, S.C., Neukum, G.and the HRSC Co-Investigator Team. 2005. Flank volcanism on Pavonis Mons, Mars revealed by HRSC on Mars Express. Bulletin of the American Astronomical Society, 37. 656.

Gulick, V.C. 1998. Magmatic intrusions and a hydrothermal origin for fluvial valleys on Mars. Journal of Geophysical Research, 103. 19365-19389.

Gulick, V.C. 2001. Origin of the valley networks on Mars: a hydrological perspective. Geomorphology, 37. 241-268.

Gulick, V.C. and Baker, V.R. 1989. Fluvial valleys and martian paleoclimates. Nature, 341. 514–516.

Gulick, V.C. and Baker, V.R. 1990. Origin and evolution of valleys on martian volcanoes. Journal of Geophysical Research, 95. 14325–14344.

Gulick, V.C. and Tyler, D., McKay, C.P. and Haberle, R.M. 1997. Episodic Ocean-induced CO2 greenhouse on Mars: Implications for fluvial valley formation. Icarus, 130. 68-86.

Gurney, S.D. 1998. Aspects of the genesis and geomorphology of pingos: perennial permafrost mounds. Progress on Physical Geography, 22(3). 307–324.

Haberle, R.M., Montmessin, F., Forget, F., Levrad, B., Head, J.W., and Laskar, J. 2004. GCM simulations of tropical ice accumulations: implications for cold-based glaciers. Lunar and Planetary Science Conference, XXXIII. Abstract #1711.

Hall, D.K. and Martinec, J. 1985. Remote Sensing of Ice and Snow. Chapman & Hall, London. 189 pp.

Hamilton, V.E., and Christensen, P.R. 2005. Evidence for extensive, olivine-rich bedrock on Mars. Geology, 33(6). 433–436.

Hamilton, V.E., Osterloo, M.M., and McGrane, B.S. 2007. THEMIS decorrelation stetched infrared mosaic of candidate 2009 Mars Science Laboratory landing sites: evidence for significant diversity. Lunar and Planetary Science Conference, 38. Abstract #1725.

Harbor, J.M. 1990. A discussion of Hirano and Anyia's 1988, 1989 explanation of glacial-valley cross profile development. Earth Surf. Processes Landforms, 15. 369–377.

Harbor, J.M. and Wheeler, D.A., 1992. On the mathematical description of glaciated valley cross-sections. Earth Surf. Processes Landforms, 17. 477–485.

Hare, T.M. and Tanaka, K.L. 2000. Using MOLA and MOC in a GIS. Lunar and Planetary Science Conference, XXXI. Abstract #1907.

Hare, T.M., Kirk, R.L., Archinal, B.A. and Tanaka, K.L. 2005. Working with planetary coordinate reference system. Lunar and Planetary Science Conference, XXXVI. Abstract #2213.

Hare, T.M., Plesea, L., Dobinson, E. and Curkendall, D. 2007. Advanced uses of Open Geospatial Web technologies for planetary data. Lunar and Planetary Science Conference, XXXVIII. Abstract #2364.

Harrison, T., Osinski, G., Tornabene, L., and Jones, E. 2015. Global documentation of gullies with the Mars Reconnaissance Orbiter Context Camera and implications for their formation. Icarus, 252. 236-254.

Harrison, T.N., Osinski, G.R., Tornabene,L.L., and Jones,E. 2015. Global documentation of gullies with the Mars Reconnaissance Orbiter Context Camera and implications for their formation, Icarus, 252.236-254.

Hartmann, W.K. 1973. Martian cratering 4: Mariner 9 initial analysis of cratering chronology. Journal of Geophysical Research, 78. 4096-4116.

Hartmann, W.K. 1984. Does crater "Saturation Equilibrium" exist in the Solar System? Icarus, 60. 56-74.

Hartmann, W.K. 2005. Martian cratering 8: Isochron refinement and the chronology of Mars. Icarus, 174. 294-320.

Hartmann, W.K., Neukum, G., 2001. Cratering chronology and the evolution of Mars. Space Science Review, 96. 65–194.

Hartmann, W.K., Thorsteinsson, T., and Sigurdsson, F. 2003. Martian hillside gullies and icelandic analogs. Icarus, 162(2). 259-277.

Hattestrand, C., and Stroeven, A.P. 2002. A relict landscape in the centre of Fennoscandian glaciation: Geomorphological evidence of minimal Quaternary glacial erosion. Geomorphology, 44, 127–143.

Hauber, E., van Gasselt, S., Ivanov, B., Werner, S., Head, J.W., Neukum, G., Jauman, R., Greeley, R., Mitchell, K.L., Muller, P., and the HRSC Co-Investigator Team. 2005. Discovery of a flank caldera and very young glacial activity at Hecates Tholus, Mars. Nature, 434. 356-361.

Hawkes, D.D. 1962. The structure of the Scotia Arc. Geol. Mag., 99. 85-91.

Head, J.W., and Marchant, D.R. 2003a. Cold-based glaciers in the western Dry Valleys of Antarctica: terrestrial landforms and Martian analogs. Sixth International Conference on Mars. Abstract #3087.

Head, J.W., and Marchant, D.R. 2003b. Cold-based mountain glaciers on Mars: Western Arsia Mons. Geology, 31, 641–644.

Head, J.W. and Marchant, D.R. 2009. Inventory of Ice-related Deposits on Mars: Evidence for Burial and Long-Term Sequestration of Ice in Non-Polar Regions and Implications for the Water Budget and Climate Evolution. Lunar and Planetary Science Conference, 40. Abstract No. 1356.

Head, J.W. and Wilson, L. 2007. Heat transfer in volcano–ice interactions on Mars: synthesis of environments and implications for processes and landforms. Annals of glaciology, 45. 1-13.

Head, J.W., Fassett, C., Hiesinger, H., Neukum, G., Hauber, E. and the HRSC Team. 2004. Snow and ice on martian volcanoes: valley networks and glaciers at Hecates Tholus. Geophysical Research Abstracts, 6. 07937.

Head, J.W., Marchant, D.R., Agnew, M.C., Fassett, C.I., and Kreslavsky, M.A. 2006b. Extensive valley glacier deposits in the northern mid-latitudes of Mars: Evidence for Late Amazonian obliquity-driven climate change. Earth and Planetary Science Letters, 241, 663–671.

Head, J.W., Marchant, D.R., and Ghatan, G.J. 2004. Glacial deposits on the rim of a Hesperian-Amazonian outflow channel source trough: Mangala Valles, Mars. Geophysical Research Letters, 31. L10701.

Head, J.W., Marchant, D.R., Dickson, J.L., Kress, A.M., Baker, D.M. 2010. Northern mid-latitude glaciation in the Late Amazonian period of Mars: Criteria for the recognition of debris-covered glacier and valley glacier landsystem deposits. Earth and Planetary Science Letters, 294. 306-320.

Head, J.W., Mustard, J.F., Kreslavsky, M.A., Milliken, R.E. and Marchant, D.R. 2003. Recent ice ages on Mars. Nature, 426. 797-802.

Head, J.W., Nahm, A.L., Marchant, D.R. and Neukum, G. 2006a. Modification of the dichotomy boundary on Mars by Amazonian mid-latitude regional glaciations. Geophysical Research Letters, 33. L08S03.

Head, J.W., Neukum, G., Jaumann, R., Hiesinger, H., Hauber, E., Carr, M., Masson, P., Foing, B., Hoffmann, H., Kreslavsky, M., Werner, S., Milkovich, S., van Gasset, S, and The HRSC co-investigator team. 2005. Tropical to mid-latitude snow and ice accumulation, flow and glaciation on Mars. Nature, 434. 346-351.

Helbert, J., Reiss, D., Hauber, E., Benkhoff, J. 2005. Limits on the burial depth of glacial ice deposits on the flanks of Hecates Tholus, Mars. Geophys. Res. Lett., 32 (17).

Heldmann, J. 2004. Observations of martian gullies and constraints on potential formation mechanisms. Icarus, 168. 285–304.

Heldmann, J.L. and Mellon, M.T. 2004. Observations of martian gullies and constraints on potential formation mechanisms. Icarus, 168, 285-304.

Hickson, C.J. 2000. Physical controls and resulting morphological forms of Quaternary ice-contact volcanoes in western Canada. Geomorphology, 32. 239-261.

Hipkin, V.J., Voytek, M.A., Meyer, M.A., Léveillé, R., and Domagal-Goldman, S.D. 2013. Analogue sites for Mars missions: NASA's Mars Science Laboratory and beyond – Overview of an international workshop held at The Woodlands, Texas, on March 5–6, 2011. Icarus, 224(2). 261-267.

Hirano, M. and Aniya, M. 1989. A rational explanation of cross-profile morphology for glacial valleys and of glacial valley development: a further note. Earth Surf. Processes Landforms, 14. 173–174.

Hirano, M. and Aniya, M. 1990. A reply to 'A discussion of Hirano and Anyia's 1988, 1989 explanation of glacial valley crossprofile development' by Jonathan M. Harbor. Earth Surf. Processes Landforms, 15. 379–381.

Hirano, M. and Aniya, M. 1988. A rational explanation of cross-profile morphology for glacial valleys and of glacial valley development. Earth Surf. Processes Landforms, 13. 707–716.

Holdsworth, G. 1956. Primary Transverse Crevasses. Journal of Glaciology, 8(52). 107–129.

Holt, J.W., et al. 2008. Radar sounding evidence for buried glaciers in the southern mid-latitudes of Mars. Science, 322. 1235–1238.

Hooke, R.L. 1989. Englacial and Subglacial Hydrology: A Qualitative Review. Arctic and Alpine Research, 21(3). 221-233

Hooke, R.L. 2005. Principles of glacier mechanics. Cambridge University Press, UK, 429 pp.

Howard, A.D. and Moore, J.M. 2004. Scarp-bounded benches in Gorgonum Chaos, Mars: Formed beneath an ice-covered lake? Geophysical Research Letters, 31.

Hubbard, B., Milliken, R.E., Kargel, J.S., Limaye, A., and Souness, C. 2011. Geomorphological characterisation and interpretation of a mid-latitude glacier-like form: Hellas Planitia, Mars. Icarus, 211(1). 330-346.

Ibáñez, J.M., Pezzo, E.D., Almendros, J., La Rocca, M., Alguacil, G., Ortiz, R., and García, A. 2000. Seismovolcanic signals at Deception Island volcano, Antarctica: Wave field analysis and source modeling. J. Geophys. Res., 105(B6), 13905–13931.

Irvine-Fynn, T.D.L., Hodson, A.J., Moorman, B.J., Vatne, G. and Hubbard, A.L. 2011. Polythermal glacier hydrology: a review. Reviews of Geophysics, 49.

Irwin, R.P. and Howard, A.D. 2002. Drainage basin evolution in Noachian Terra Cimmeria, Mars. Journal of Geophysical Research, 107.

Irwin, R.P., Maxwell, T.A., Howard, A.D., Craddock, R.A. and Leverington, D.W. 2002. A large paleolake basin at the head of Ma'adim Vallis, Mars. Science, 297. 2209–2212.

Ivanov, B.A., 2001. Mars/moon cratering rate ratio estimates. Space Science Review, 96. 87–104.

Jakosky, B.M. 1986. On the thermal properties of Martian fines, Icarus, 66(1). 117-124.

Jakosky, B.M. and Carr, M.H. 1985. Possible precipitation of ice at low latitudes of Mars during periods of high obliquity. Nature, 315. 559-561.

Jakosky, B.M. and Haberle, R.M. 1992. The seasonal behaviour of water on Mars. In: Kieffer, H.H., Jakosky, B.M., Snyder, C.W., and Matthews, M.S. (Eds). Mars. The University of Arizona Press, Tucson. 969-1016.

Jakosky, B.M., Mellon, M.T., Kieffer, H.H., Christensen, P.R., Varnes, E.S., and Lee, S.W. 2000. The thermal inertia of Mars from the Mars Global Surveyor Thermal Emission Spectrometer. Journal of Geophysical Research, 105(E4). 9643–9652.

James, P.B., Kieffer, H.H. and Pige, D.A. 1992. The seasonal cycle of the atmosphere of Mars. In: Kieffer, H.H., Jakosky, B.M., Snyder, C.W., and Matthews, M.S. (Eds). Mars. The University of Arizona Press, Tucson. 934-968.

Jaumman, R., and Hauber, E. 2003. Evidence for a surging ice-sheet in Elysium Planitia, Mars. International Conference on Mars, VI, 3018.

Jiao, K.Q. 1981. Cross-section of glacial valley at the head of Urumqi River, Tian Shan. J. Glaciol. Geocryol., 3. 92–96 in Chinese.

Kääb, A., Bolch, T., Casey, K., Heid, T.,Kargel, J., Leonard, G., Paul, F., and Raup, B. 2014. Glacier mapping and monitoring based on spectral data. In: Kargel, Leonard, Bishop, Kääb, Raup (Eds.): Global Land Ice Measurements from Space. Springer Praxis. 75-112.

Kadish, S.J., Head, J.W., Parsons, R.L., and Marchant, D.R. 2008. The Ascraeus Mons fan-shaped deposit: Volcano–ice interactions and the climatic implications of cold-based tropical mountain glaciations. Icarus, 197. 84-109.

Kangi, A. 2007. The role of mud volcanoes in the evolution of Hecates Tholus Volcano on the surface of Mars. Acta Astronomica, 60. 719-722.

Kargel, J.S., Baker, V.R., Beget, J.E., Lockwood, J.F., Pewe, T.L., Shaw, J.S. and Strom, R.G. 1995. Evidence of ancient continental glaciation in the Martian northern plains. Journal of Geophysical Research, 100. 5351-5368.

Kerber, L., Head, J.W. Madeleine, J.B., Forget, F., and Wilson, L. 2011. The dispersal of pyroclasts from Apollinaris Patera, Mars: Implications for the origin of the Medusae Fossae Formation. Icarus, 216. 212-220.

Kerber, L., Head, J.W. Madeleine, J.B., Forget, F., and Wilson, L. 2012. The dispersal of pyroclasts from ancient explosive volcanoes on Mars: Implications for the friable layered deposits. Icarus, 219. 358-381.

Kjaer, H.H., Korsgaard, N.J., and Schomacker, A. 2008. Impact of multiple glacier surges – a geomorphological map from Bruarjokull, East Iceland. Journal of Maps, v2008, 5–20.

Klay, J.K. and Orheim, O. 1969. Glaciology and glacial geology on Deception Island. Antarct. Jour. U.S., July-Aug. 125 - 126.

Kneissl, T., van Gasselt, S., Neukum, G. 2011. Map-projection-independent crater size-frecuency determination in GIS environments – New software tool for ArcGIS. Planetary and Space Science, 59. 1243-1254.

Kochel, R.C. and Trop, J.M. 2008. Earth analog for high-latitude landforms and recent flows on Mars: Icy debris fans in the Wrangell Volcanic Field, Alaska. Icarus, 196(1). 63-77. doi: 10.1016/j.icarus.2008.03.006.

Komatsu, G., Arzhannikov, S.G., Arzhannikova, A.V., Ershov, K. 2007. Geomorphology of sugblacial volcanoes in the Azas Plateau, the Tuva Republic, Russia. Geomorphology, 88. 312-328.

Kossacki, K.J., Markiewicz, W.J., Smith,M.D., Page,D., Murray, J. 2006. Possible remnants of a frozen mud lake in southern Elysium, Mars. Icarus, 181(2). 363-374.

Kostama, V.-P., Kreslavsky,M.A., and Head, J.W. 2006. Recent high-latitude icy mantle in the northern plains of Mars: Characteristics and ages of emplacement. Geophysical Research Letters, 33. L11201.

Koutnik, M.R., Waddington, E.D., Winebrenner, D.P., and Pathare, A.V. 2013. Response timescales for martian ice masses and implications for ice flow on Mars. Icarus, 225(2). 949-959.

Kreslavsky, M.A. and Head, J.W. 2000. Kilometer-scale roughness of Mars: Results from MOLA data analysis. Journal of Geophysical Research, 105. 26695–26712.

Kress, A.M., and Head, J.W. 2008. Ring-mold craters in lineated valley fill and lobate debris aprons on Mars: Evidence for subsurface glacial ice. Geophysical Research Letters, 35. L23206.

Lane, M.D., and Goodrich, C.A. 2010. High-Magnesian Olivine in the Argyre Rim: Derived from a Primitive Magma? Lunar and Planetary Science Conference, 41. Abstract #1533.

Laskar, J., Gastineau, M., Joutel, F., Robutel, P., Levrard, B. and Corrieau, A. 2004. Long term evolution and chaotic diffusion of the isolation quantities of Mars. Icarus, 170. 343-364.

Laskar, J., Levrard, B., and Mustard, J.F. 2002. Orbital forcing of the martian polar layered deposits. Nature, 419, 375–377.

Lefort, A., Russell, P. and Thomas, N. 2006. Scallop-shaped Depressions and Mantle Sublimation in the Mid-Latitudes of Mars. Fourth International Conference on Mars Polar Science and Exploration. Abstract. 8061.

Lefort, A., Russell, P.S., and Thomas, N. 2010. Scalloped terrain in Peneus and Amphitrites Paterae region of Mars as observed by HiRISE. Icarus, 2005(1). 259–268.

Lefort, A., Russell, P.S., Thomas, N., McEwen, A.S., Dundas, C.M., and Kirk, R.L. 2009. Observations of periglacial landforms in Utopia Planitia with the High Resolution Imaging Science Experiment (HiRISE). Journal of Geophysical Research, 114. E04005.

Levrard, B., Forget, F., Montmessin, F., and Laskar, J. 2004. Recent ice-rich deposits formed at high latitudes on Mars by sublimation of unstable equatorial ice during low obliquity. Nature, 431. 1072-1075.

Levy, J.S., Head, J.W., and Marchant, D.R. 2007. Lineated valley fill and lobate debris apron stratigraphy in Nilosyrtis Mensae, Mars: Evidence for phases of glacial modification of the dichotomy boundary. Journal of Geophysical Research, 112. E8. E08004.

Levy, J.S., Head, J.W., and Marchant, D.R. 2009. Concentric crater fill in Utopia Planitia: History and interaction between glacial “brain terrain” and periglacial mantle processes. Icarus, 202. 462–476.

Levy, J.S., Head, J.W., and Marchant, D.R. 2010. Concentric crater fill in the northern mid-latitudes of Mars: Formation processes and relationships to similar landforms of glacial origin. Icarus, 209(2). 390-404.

Levy, J.S., Head, J.W., Marchant, D.R., and Kowalewski, D.E. 2008. Identification of sublimation-type thermal contraction crack polygons at the proposed NASA Phoenix landing site: Implications for substrate properties and climate-driven morphological evolution. Geophysical Research Letters, 35. L04202.

Levy, J.S., Marchant, D.R., and Head, J.W. 2006. Distribution and origin of patterned ground on Mullins Valley debris-covered glacier, Antarctica: the roles of ice flow and sublimation. Antarctic Science, 18 (3). 385–397.

Lewis, S.R., Collins, M., Read, P.L., Forget, F., Hourdin, F., Fournier, R., Hourdin, C., Talagrand, O., and Huot, J.-P. 1999. A climate database for Mars. Journal of Geophyscal Research, 104. E10. 24,177-24,194.

Li, H., Robinson, M.S., and Jurdy, D.M. 2005. Origin of Martian northern hemisphere mid-latitude lobate debris aprons. Icarus, 176(2). 382-394.

Li, Y.K., Liu, G.N., and Cui, Z.J. 1989. The morphological character and paleo-climate indication of the cross-section of glacial valleys. J. Basic Sci. Eng., 7(2). 163–170 in Chinese.

Li, Y.K., Liu, G.N., and Cui, Z.J. 2001. Glacial valley cross-profile morphology, Tian Shan Mountains, China. Geomorphology, 38. 153–166.

Liu, G.N. 1989. Research on glacial erosion landforms: casestudy of Luojishan Mt., Western Sichuan. Journal of Glaciology and Geocryology, 11(3). 249–259. in Chinese.

Lliboutry, L., Briat, M., Creseveur, M., and Pourchet, M. 1976. 15 m deep temperatures in the glaciers of Mont Blanc (French Alps). Journal of Glaciology, 16. 197 – 203.

López, D. and Williams, S. 1993. Catastrophic volcanic collapse: relation to hydrothermal alteration. Science, 260. 1794-1796.

Lougeay R 1972. Patterns of surface temperature in the alpine/periglacial environment as determined by radiometric measurements. In: Bushnell VC, Ragle RH (eds) Icefield Ranges Research Project. Sci Results Montreal 3:163–176

Lougeay, R. 1974. Detection of buried glacial and ground ice with thermal infrared remote sensing. In: Advanced concepts and techniques in the study of snow and ice resources. National Academy of Sciences, 1974. 487–493.

Lougeay, R. 1982. Landsat thermal imaging of alpine regions. Photogrammetric Engineering and Remote Sensing. 48(2). 269-273.

Lucchitta, B.K. 1981. Mars and Earth: Comparison of cold-climate features. Icarus, 45(2). 264-303.

Lucchitta, B.K. 1984. Ice and debris in the fretted terrain, Mars. Journal of Geophysical Research, 89. B409 - B418.

Lundgren, P.P., Berardino, M., Coltelli, G., Fornaro, R., Lanari, G., Puglisi, E., Sansosti, and Tesauro, M. 2003. Coupled magma chamber inflation and sector collapse slip observed with synthetic aperture radar interferometry on Mt. Etna volcano. Journal of Geophysical Research, 108.

Mackay, J.R. 1979. Pingos on the Tuktoyaktuk Peninsula area, Northwest Territories. Geographie Physique et Quaternaire, 33. 3-6.

Mackay, J.R. 1987. The first 7 years (1978–85) of ice wedge growth, Illisarvik experimental drained lake site, Western Arctic Coast. Canadian Journal of Earth Sciences, 23. 1782–1795.

Mackay, J.R. 1998. Pingo Growth and collapse, Tuktoyaktuk Peninsula Area, Western Arctic Coast, Canada: a long-term field study. Géographie physique et Quaternaire, 52(3). 271-323.

Madeleine, J.-B., Forget, F., Head, J.W., Levrard, B., Montmessin, F., and Millour, E. 2009. Amazonian northern mid-latitude glaciation on Mars: A proposed climate scenario. Icarus, 203(2). 390-405.

Malin, M.C. and Edgett, K.S. 2000. Evidence for recent groundwater seepage and surface runoff on Mars. Science, 288. 2330–2335.

Malin, M.C. and Edgett, K.S. 2001. Mars Global Surveyor Mars Orbiter Camera: Interplanetary Cruise through Primary Mission. Journal of Geophysical Research, 106(E10). 23,429–23,570

Malin, M.C., Bell, J.F., Cantor, B.A., Caplinger, M.A., Calvin, W.M., Clancy, R.T., Edgett, K.S., Edwards, L., Haberle, R.M., James, P.B., Lee, S.W., Ravine, M.A., Thomas, P.C. and Wolff, M.J. 2007. Context camera investigation on board the Mars Reconnaissance Orbiter. Journal of Geophysical Research, 112.

Malin, M.C., Danielson, G.E., Ravine, M.A. and Soulanille, T.A. 1991. Design and development of the Mars Observer Camera. International Journal of Imaging Systems and Technology, 3. 76-91.

Mangold, N. 2003. Geomorphic analysis of lobate debris aprons on Mars at Mars Orbiter Camera scale: Evidence for ice sublimation initiated by fractures. Journal of Geophysical Research (Planets), 108 (E4). 8021.

Mangold, N. 2011. Water ice sublimation-related landforms on Mars (in Martian geomorphology). Geological Society Special Publications, 356. 133-149

Marchant, D. R., Lewis, A.R., Phillips, W.M., Moore, E.J., Souchez, R.A., Denton, G.H., Sugden, D.E., Potter, N.J., and Landis, G.P. 2002. Formation of patterned ground and sublimation till over Miocene glacier ice in Beacon Valley, southern Victoria Land, Antarctica. Geological Society of America Bulletin, 114. 718 – 730.

Márquez, A., de Pablo, M.A., Oyarzun, R. and Viedma, C. 2005. Evidence of gully formation by regional groundwater flow in the Gorgonum Newton region (Mars). Icarus, 179. 398-414.

Martí, J., Vila, J. and Rey, J. 1996. Deception Island (Bransfield Strait, Antarctica): an example of a volcanic caldera developed by extensional tectonics. Geological Society, London, Special Publications 110, 253-265.

Martínez-Alonso, S., Mellon, M.T., Banks, M.E., Keszthelyi, L.P., McEwen, A.S., and the HiRISE Team. 2011. Evidence of volcanic and glacial activity in Chryse and Acidalia Planitiae, Mars. Icarus, 212(2). 597-621.

Martínez-Frías, J., Delgado, A., Somoza, L., Maestro, A. and Rey, J. 2003. Carbon, oxygen and hydrogen isotopic signatures of cold and hot waters from Deception Island (Antarctica): Lessons for Mars exploration. 3rd European Workshop on Exo/Astrobiology, Madrid.

Martini, M., and Giannini, L. 1988. Deception Island (South Shetlands): An area of active volcanism in Antarctica. Mere. Soc. Geol. It., 43. 117–122.

McGuire, W.J., Jones, A.P. and Neuberg, J. (Eds.) 1996. Volcano instability on the Earth and other Planets. Geological Society Special Publication, 110. 400 pp.

Mellon M.T., Jakosky B.M., Kieffer H.H. and Christensen P.R. 2000. High-resolution Thermal Inertia mapping from the Mars Global Surveyor Thermal Emission Spectrometer. Icarus, 148. 437-455.

Mellon, M.T., and Jakosky, B.M. 1995. The distribution and behavior of Martian ground ice during past and present epochs. Journal of Geophysical Research, 100. 11781 – 11799.

Mellon, M.T., Boynton, W.V., Feldman, W.C., Arvidson, R.E., Titus, T.N., Bandfield, J.L., Putzig, N.E., and Sizemore, H.G. 2008. A prelanding assessment of the ice table depth and ground ice characteristics in Martian permafrost at the Phoenix landing site. Journal of Geophysical Research, 113. E00A25.

Melo, R., Vieira, G., Rocha, J., Caselli, A., Batista, V., and Ramos, M. 2009. Geomorphological dynamics of Deception Island (Maritime Antarctic): a GIS based analysis of the Cerro de la Cruz - Crater Lake area. EGU General Assembly 2009. 4429.

Melosh, H.J. and Vickery, A.M. 1989. Impact erosion of the primordial atmosphere of Mars. Nature, 338. 487-489.

Michael G.G., Platz T., Kneissl T., and Schmedemann N. 2012. Planetary surface dating from crater size-frequency distribution measurements: spatial randomness and clustering. Icarus, 218. 169-177.

Michael, G.G. and Neukum, G. 2010. Planetary surface from crater size-frequency distribution measurements: partial resurfacing events and statistical age uncertainty. Earth and Planetary Science Letters, 294. 223-229.

Mihalcea, C., Mayer, C., Diolaiuti, G., D'Agata, C., Smiraglia, C., Lambrecht, A., Vuillermoz, E., and Tartari, G. 2008. Spatial distribution of debris thickness and melting from remote-

sensing and meteorological data, at debris-covered Baltoro glacier, Karakoram, Pakistan. Annals of Glaciology, 48(1). 49-57.

Milkovich, S.M., Head, J.W., and Marchant, D.R. 2006. Debris-covered piedmont glaciers along the northwest flank of the Olympus Mons scarp: Evidence for low-latitude ice accumulation during the Late Amazonian of Mars. Icarus, 181(2). 388-407.

Milliken, R.E., Mustard, J.F., and Goldsby, D.L. 2003. Viscous flow features on the surface of Mars: Observations from high-resolution Mars Orbiter Camera (MOC) images. Journal of Geophysical Research Planets, 108. 5057.

Mischna, M.A., Richardson, M.I., Wilson, R.J. and McCleese, D.J. 2003. On the orbital forcing of Martian water and CO2 cycles: A general circulation model study with simplified volatile schemes. Journal of Geophysical Research, 108.

Mitrofanov, I., Anfimov, D., Kozyrev, A., Litvak, M., Sanin, A., Tret'yakov, V., Krylov, A., Shvetsov, V., Boynton, W., Shinohara, C., Hamara, D. and Saunders, R.S. 2002. Maps of subsurface Hydrogen from the High Energy Neutron Detector, Mars Odyssey. Science, 297. 78–81.

Molina, A., de Pablo, M. A., and Ramos, M. 2013. Deception Island, Antarctica, an Earth-Mars Analogue. Lunar and Planetary Science Conference, 44th. Abstract #1719.

Morgan, G.A., Head, J.A., and Marchant, D.R. 2009. Lineated valley fill (LVF) and lobate debris aprons (LDA) in the Deuteronilus Mensae northern dichotomy boundary region, Mars: Constraints on the extent, age and episodicity of Amazonian glacial events. Icarus, 202(1). 22-38.

Morgenstern, A., Hauber, E., Reiss, D., van Gasselt, S., Grosse, G., and Schirrmeister, L. 2007. Deposition and degradation of a volatile-rich layer in Utopia Planitia and implications for climate history on Mars. Journal of Geophysical Research, 112. E06010.

Mouginis-Mark, P.J. 1984. Volcanism in Elysium Planitia, Mars. In: NASA. Reports of Planetary Geology Program. NASA, Washington 1983. 138-140.

Mouginis-Mark, P.J. 1985. Volcano/ground ice interactions in Elysium Planitia, Mars. Icarus, 64. 265–284.

Mouginis-Mark, P.J. and Christensen, P.R. 2005. New observations of volcanic features on Mars from THEMIS instrument. Journal of Geophysical Research, 110.

Mouginis-Mark, P.J., Head, J.W., and Wilson, L. 1982. Explosive volcanism on Hecates Tholus, Mars - Investigation of eruption conditions. Journal of Geophysical Research, 87. 9890-9904.

Mouginis-Mark, P.J., Wilson, L. and Zuber, M.T. 1992. The physical volcanology of Mars. In: Kieffer, H.H., Jakosky, B.M., Snyder, C.W., and Matthews, M.S. (Eds). Mars. The University of Arizona Press, Tucson. 424-452.

Mouginis-Mark, P.J., Wilson, L., and Head, J.W. 1981. Explosive volcanism on Hecates Tholus, I: Surface morphology. International Colloquium on Mars, 3Abstract #441

Mouginis-Mark, P.J., Wilson, L., Head, J.W., Brown, S.H., Hall, J.L. and Sullivan, K.D. 1984. Elysium Planitia, Mars - Regional geology, volcanology, and evidence for volcano-ground ice interactions. Earth, Moon, and Planets, 30. 149-173.

Müller, F. 1962. Observations on pingos. Meddelelser om Grønland, 153 (3). 1–117. [Translated by D.A. Sinclair, National Research Council of Canada]

Murchie, S. et al. (2002) CRISM: Compact Reconnaissance Imaging Spectrometer for Mars on the Mars Reconnaissance Orbiter. Lunar and Planetary Science Conference, 33. Abstract #1697.

Murray, J.B., Muller, J.P., Neukum, G., Hauber, E., Markiewicz, W.J., Head, J.W., Foing, B.H., Page, D.P., Mitchell, K.L. and Portyankina, G. 2005. Evidence from the Mars Express High Resolution Stereo Camera for a frozen sea close to Mars' equator. Nature, 434. 352–355.

Mustard, J.F. 2003. Geomorphic indicators of ground ice on Mars and evidence for climate change. American Geophysical Union, Fall Meeting, C12C-07.

Mustard, J.F., Cooper, C.D. and Rifkin, M.F. 2001. Evidence for recent climate change on Mars from the identification of youthful near-surface ground ice. Nature, 412. 411–414.

Neakrase, L.D.V.; Greeley, R. Williams, D.A., Reiss, D., Michaels, T.I., Rafkin, S.C.R., Neukum, G. and The HRSC Team. 2005. Hecates Tholus, Mars: nighttime aeolian activity suggested by thermal images and mesoscale atmospheric model simulations. Lunar and Planetary Science Conference, XXXVI. Abstract #1898.

Neri M. and Acocella V. 2006. The 2004-05 Etna eruption: implications for flank deformation and structural behaviour of the volcano. Journal of Volcanology and Geothermal Research, 158. 195-206.

Neuffer, D.P. and Schultz, R.A. 2006. Mechanisms of slope failure in Valles Marineris, Mars. Quarterly Journal of Engineering Geology and Hydrogeology, 39. 227–240.

Neukum, G. 1983. Meteoritenbombardement und Datierung planetarer Oberflächen. Habilitation Dissertation for Faculty Membership, Ludwig-Maximilians University. Munich, Germany. 186 pp.

Neukum, G., and Hiller, K. 1981. Martian Ages. Journal of Geophysical Research, 86. 3097-3121.

Neukum, G., and Ivanov, B.A. 1994. Crater Size Distributions and Impact Probabilities on Earth from Lunar, Terrestrial-Planet, and Asteroid Cratering Data. In: T. Gehrels (ed.), Hazards due to Comets and Asteroids. The University of Arizona Press, Tucson. 359-416.

Neukum, G., Jaumann, R., Hoffmann, H., Hauber, E., Head, J.W., Basilevsky, A.T., Ivanov, B.A., Werner, S.C., van Gasselt, S., Murray, J.B., McCord, T., and The HRSC co-investigator team. 2004. Recent and episodic volcanic and glaciar activity on Mars revealed by the High Resolution Stereo Camera. Nature, 432. 971-979.

Nussbaumer, J., Hauber, E., and Jaumann, R. 2004. Evidence of recent glaciation in Elysium Planitia, Mars. Lunar and Planetary Science Conference, XXXV. Abstract #1244.

Nye, J. 1952. The mechanics of glacier flow. Journal of Glaciology, 2. 82–93.

Oehler, J.F., van Wyk de Vries, B., and Labazuy, P. 2005. Landslides and spreading of ocean hot-spot and arcshield volcanoes on low strength layers (LSLs): and analogue modeling approach. Journal of Volcanology and Geothermal Research, 114. 169-189.

Ormö, J., Komatsu, G., Chan, M.A., Beitler, B., and Parry, W.T. 2004. Geological features indicative of processes related to the hematite formation in Meridiani Planum and Aram Chaos, Mars: a comparison with diagenetic hematite deposits in southern Utah, USA. Icarus, 171(2). 295-316.

Osterloo, M.M., Anderson, F.S., Hamilton, V.E., and Hynek, B.E. 2010. Geologic context of proposed chloride-bearing materials on Mars. Journal of Geophysical Research, 115. E10012.

Pacifici, A. 2009. The Argentinean Patagonia and the Martian landscape. Planetary and Space Science, 57. 571-578.

Pacifici, A., Komatsu, G., and Pondrelli, M. 2009. Geological evolution of Ares Vallis on Mars: Formation by multiple events of catastrophic flooding, glacial and periglacial processes. Icarus, 202(1), 60–77.

Page, D.P. 2007. Recent low-latitude freeze–thaw on Mars. Icarus, 189. 83-117.

Page, D.P. and Murray, J.B. 2006. Stratigraphic and morphologic evidence for pingo genesis in the Cerberus plains. Icarus, 183. 46-54.

Page, D.P., Balme, M.R., and Grady, M.M. 2009. Dating martian climate change. Icarus, 203(2). 376-389. doi: 10.1016/j.icarus.2009.05.012.

Pallàs, R., Smellie, J. L., Casas, J. M. and Calvet, J. 2001. Using tephrochronology to date temperate ice: correlation between ice tephras on Livingston Island and eruptive units on Deception Island volcano (South Shetland Islands, Antarctica). Holocene, 11(2). 149-160.

Parker, T.J., Gorsline, D.S., Saunders, R.S., Pieri, D.C., and Schneeberger, D.M. 1993. Coastal geomorphology of the Martian northern plains. Journal of Geophysical Research, 98. 11061-11078.

Pasckert, J.H., Hiesinger, H., and Reiss, D. 2012. Rheologies and ages of lava flows on Elysium Mons, Mars. Icarus, 219. 443-457.

Paterson, W.S.B. 1981. The physics of glaciers . Second edition. Pergamon Press, Oxford.

Pattyn, F. and Huele, W.V. 1998. Power law or power flaw? EarthSurf. Processes Landforms, 23. 761–767.

Pedersen, G.B.M., and Head, J.W. 2010. Evidence of widespread degraded Amazonian-aged ice-rich deposits in the transition between Elysium Rise and Utopia Planitia, Mars:

Guidelines for the recognition of degraded ice-rich materials. Planetary and Space Science, 58. 1953-1970.

Pedersen, G.B.M. and Head, J.W., 2011. Chaos formation by sublimation of volatile-rich substrate: evidence from Galaxias Chaos. Icarus, 211. 316-329.

Pedrera, A., Pérez-Peña, J.V., Galindo-Zaldívar, J., Azañón, J.M., and Azor, A. 2009: Testing the sensitivity of geomorphic indices in areas of low-rate active folding (eastern Betic Cordillera, Spain). Geomorphology, 105. 218-231.

Pelkey, S.M., Jakosky, B.M., and Mellon, M.T. 2001. Thermal inertia of crater-related wind streaks on Mars. Journal of Geophysical Research, 106. 23909–23920.

Phillips, R.J., et al. 2008. Mars north polar deposits: Stratigraphy, age, and geodynamical response. Science, 320(5880). 1182–1185.

Pierce, T.L. and Crown, D.A. 2003. Morphologic and topographic analyses of debris aprons in the eastern Hellas region, Mars. Icarus, 163(1). 46-65.

Platz, T., Michael, G., 2011. Eruption history of the Elysium volcanic province, Mars. Earth and Planetary Science Letters, 312. 140-151.

Platz, T., Michael, G., Jodlowski, and Neukum, G. 2010. Construction of an eruption record for the Elysium Volcanic Centre, Mars: Preliminary results. Geophysical Research Abstracts, 12. EGU2010-11285-1.

Plaut, J.J., Safaeinili, A., Holt, J.W., Phillips, R.J., Head, J.W., Seu, R., Putzig, N.E., and Frigeri, A. 2009. Radar evidence for ice in lobate debris aprons in the mid-northern latitudes of Mars. Geophysical Research Letters, 36. L02203.

Plescia, J.B. 2000. Geology of the Uranius Group Volcanic Constructs: Uranius Patera, Ceraunius Tholus, and Uranius Tholus. Icarus, 143. 376-396.

Plescia, J.B. 2001. Elysium Region Tectonics. Lunar and Planetary Science Conference, XXXII. Abstract #1088.

Presley, M. A., and P. R. Christensen (1997), Thermal conductivity measurements of particulate materials 2. Results, Journal of Geophysical Research, 102(E3). 6551–6566.

Price, J.C. 1977. Thermal inertia mapping: a new view of the Earth. Journal of Geophysical Research, 82. 2582–2590.

Prieto-Ballesteros, O., Gómez, F., Moreno, M., de Diego, G., Fernandez-Sampedro, M., Martín-Redondo, M.P., and Parro, V. 2012. European Planetary Science Congress 2012. EPSC2012-466.

Putzig, N.E. and Mellon, M.T. 2007. Apparent thermal inertia and the surface heterogeneity of Mars. Icarus, 191. 68-94.

Raack, J., Reiss, D., and Hiesinger, H. 2012. Gullies and their relationships to the dust–ice mantle in the northwestern Argyre Basin, Mars. Icarus, 219(1). 129-141.

Ramos, M., de Pablo, M.A., Sebastian, E., Armiens, C., and Gómez-Elvira, J. 2012. Temperature gradient distribution in Permafrost Active layer, using a prototype of the Ground Temperature Sensor (REMS-MSL) on Deception Island (Antarctica). Cold Regions Science and Technology. Cold Regions Science and Technology, 72 23–32.

Reid, M.E., Sisson, T.W. and Brien, D.L. 2001. Volcano collapse promoted by hydrothermal alteration and edifice shape, Mount Rainier, Washington. Geology, 29. 779–782.

Rey, J., Somoza, L., and Martínez-Frías, J. 1995. Tectonic, volcanic and hydrothermal event sequence on Deception Island (Antarctica). Geo-Marine, 15. 1-8.

Richardson, M.I. and Wilson, R.J. 2002. Investigation of the nature and stability of the Martian seasonal water cycle with a general circulation model. Journal of Geophysical Research, 107.

Riley, S.J., DeGloria, S.D., and Elliot, R. 1999. A terrain ruggedness index that quantifies topographic heterogeneity. Intermountain Journal of Sciences, 5. 1-4.

Robbins, S.J., di Achille, G., and Hynek, B.M. 2011. The volcanic history of Mars: High-resolution crater-based studies of the calderas of 20 volcanoes. Icarus, 211(2). 1179-1203.

Rogers, A.D., Christensen, P.R., and Bandfield, J.L. 2005. Compositional heterogeneity of the ancient Martian crust: Analysis of Ares Vallis bedrock with THEMIS and TES data, Journal of Geophysical Research, 110(E5). E05010.

Rossbacher, L.A. and Judson, S. 1981. Ground ice on Mars: Inventory, distribution, and resulting landforms. Icarus, 45(1). 39-59.

Rothschild, L.J. 1990. Earth analogs for Martian life. Microbes in evaporites, a new model system for life on Mars. Icarus, 88(1). 246-260.

Ruff, S.W., and Christensen, P.R. 2002. Bright and dark regions on Mars: Particle size and mineralogical characteristics based on Thermal Emission Spectrometer data. Journal if Geophysical Research, 107.

Russell, P.S. and Head, J.W. 2007. The Martian hydrologic system: Multiple recharge centers at large volcanic provinces and the contribution of snowmelt to outflow channel activity. Planetary and Space Science, 55. 315–332.

Russell, P.S. and Head, J.W. 2003. Elysium-Utopia flows as mega-lahars: a model of dike intrusion, cryosphere cracking, and water-sediment release. Journal of Geophysical Research, 108.

Sakimoto, S.E.H. 2005a. Central mounds in Martian impact craters: assessment as possible perennial permafrost mounds (pingos). Lunar and Planetary Science Conference, XXXVI. Abstract #2099.

Sakimoto, S.E.H. 2005b. Martian polar craters: Possible polar materials apparent effects and post-impact modification by apparent perennial permafrost mound (pingo) formation. Workshop on the Role of Volatiles and Atmospheres on Martian Impact Craters, LPI Contribution No. 1273. 94-95.

Santeford, H.S. and Smith, J.L. (eds.). 1974. Advanced concepts and techniques in the study of snow and ice resources. National Academy of Sciences, Washington D.C., USA. 99 pp.

Saunders, R.S., Arvidson, R.E., Badhwar, G.D., Boynton, W.V., Christensen, P.R., Cucinotta, F.A., Gibbs, R.G., Landano, M.R., Mase, R.A., Meyer, M.A., Pace, G.D., Plaut, J.J., Sidney, W.P., McSmith, G.W., Spencer, D.A., Thompson, T.W. and Zeitlin, C.J. 2004. 2001 Mars Odyssey Mission summary. Space Science Reviews, 110. 1-36.

Schaefer, E.I. 2011. Morphometric Analysis of Valleys for Erosive Glacial Modification in the Northern Midlatitudes of Mars.Lunar and Planetary Sciences Conference, 42.Abstract #2796.

Schon, S.C., Head, J.W., and Milliken, R.E. 2009. A recent ice age on Mars: Evidence for climate oscillations from regional layering in mid-latitude mantling deposits. Geophysical Research Letters, 36. L15202.

Schoof, C. 2010. Ice-sheet acceleration driven by melt supply variability. Nature, 468 (7325): 803–806.

Schorghofer, N. 2007. Dynamics of ice ages on Mars. Nature, 449. 192-194.

Schorghofer, N. 2010. Fast numerical method for growth and retreat of subsurface ice on Mars. Icarus, 208. 598-607.

Schorghofer, N., and Forget, F. 2012. History and anatomy of subsurface ice on Mars. Icarus, 220. 1112-1120.

Scott, E.D., and Wilson, L. 1999. Evidence for a sill emplacement event on the upper flanks of the Ascraeus Mons shield volcano, Mars. Journal of Geophysical Research, 104. 27079.

Seu, R., Biccari, D., Lorenzoni, L.V., Phillips, R.J., Marinangeli, L., Picardi, G., Masdea, A., and Zampolini, E. 2004. SHARAD: The MRO 2005 shallow radar. Planetary and Space Science, 52. 157–166.

Seu, R., et al. 2007a. Accumulation and erosion of Mars' south polar layered deposits. Science, 317. 1715–1718.

Seu, R., et al. 2007b, SHARAD sounding radar on the Mars Reconnaissance Orbiter. Journal of Geophysical Research, 112. E05S05.

Shean, D.E., Head, J.W., and Marchant, D.R. 2005. Origin and evolution of a cold-based tropical mountain glacier on Mars: The Pavonis Mons fan-shaped deposits. Journal of Geophysical Research, 110. E05001.

Shean, D.E., Head, J.W., Fastook, J.L., Marchant, D.R. 2007. Recent glaciation at high elevations on Arsia Mons, Mars: Implications for the formation and evolution of large tropical mountain glaciers. Journal of Geophysical Research, 112(E3). E03004.

Shukla, A., Arora, M.K., Gupta, R.P. 2010. Synergistic approach for mapping debris-covered glaciers using optical–thermal remote sensing data with inputs from geomorphometric parameters. Remote Sensing of Environment, 114(7). 1378-1387.

Singh, P., and Singh, V.P. 2001. Snow and Glacier Hydrology. Kluwer Acad., Dordrecht, Netherlands. 754 pp.

Smellie J.L. 2001. Lithostratigraphy and volcanic evolution of Deception Island, South Shetland Islands. Antarctic Science, 13(2). 188-209.

Smellie J.L., McArthur J.M., McIntosh W.C., and Esser R. 2006. Six million years of glacial history recorded in the James Ross Island Volcanic Group, Antarctic Peninsula. Palaeogeography, Palaeoclimate and Palaeoecology, 242. 169.

Smellie, J.L. 2002a. Geology. In: López-Martínez, J.L., Smellie, J.W., and Thomson, M.R.A. Thomson (Eds.). Geology and Geomorphology of Deception Island. 78 pp, with accompanying maps. BAS GEOMAP Series, Sheets 6-A and 6-B, 1:25 000, British Antarctic Survey, Cambridge.

Smellie, J.L. 2002b. The 1969 subglacial eruption on Deception Island (Antarctica): events and processes during an eruption beneath a thin glacier and implications for volcanic hazards. In: Smellie, J.L.; Chapman, M.G., (eds.) Volcano-ice interaction on Earth and Mars. London, Geological Society of London. Geological Society Special Publication, 202. 59-79.

Smellie, J.L. and Chapman, M.G. (Eds) 2002. Introduction: volcano-ice interaction on Earth and Mars. Geological Society of London, Special Publications, 202. 430 pp.

Smith, K.L., Baldwin, R.J., Glatts, R.C., Chereskin, T.K., Ruhl, H., and Lagun, V. 2003. Weather, ice, and snow conditions at Deception Island, Antarctica: long time-series photographic monitoring. Deep-Sea Research II, 50. 1649-1664.

Smith, M.J., Rose, J., and Booth, S. 2006. Geomorphological mapping of glacial landforms from remotely sensed data: An evaluation of the principal data sources and an assessment of their quality. Geomorphology, 76, 148–165.

Soare, R.J., Burr, D.M., and Wan Bun Tseung, J.M. 2005. Pingos and a possible periglacial landscape in Utopia Planitia. Icarus, 174(2). 373–382.

Soare, R.J., Osinski, G.R., and Costard, F.M. 2008. Recent, Late Amazonian pingos, ice-rich landscapes and periglacial ponding in Utopia and western Elysium Planitia, Mars. Lunar and Planetary Science Conference, XXXIX. Abstract #1315.

Soare, R.J., Osinski, G.R., and Thomson, L. 2009. Perennial mounds in Utopia Planitia: (HiRISE) evidence of a glacial origin. Lunar and Planetary Science Conference, 40, 1278.

Somoza, L., Martinez-Frías, J., Smellie, J.L., Rey, J. and Maestro, A. 2004. Evidence for hydrothermal venting and sediment volcanism discharged after recent short-lived volcanic eruptions at Deception Island, Bransfield Strait, Antarctica. Marine Geology, 203. 119-140.

Souness, C., Hubbard, B., Milliken, R.E., and Quincey, D. 2012. An inventory and population-scale analysis of martian glacier-like forms. Icarus, 217(1). 243-255.

Spagnuolo, M.G., Rossi, A.P., Hauber, E., van Gasselt, S. 2011. Recent tectonics and subsidence on Mars: Hints from Aureum Chaos, Earth and Planetary Science Letters, 312 (1- 2). 13-21.

Squyres, S.W. 1978. Martian fretted terrain - Flow of erosional debris. Icarus, 34. 600-613. Squyres, S.W. 1979. The distribution of lobate debris aprons and similar flows on Mars. Journal of Geophysical Research, 84. 8087-8096.

Styszynska, A. 2004. The origin of coreless winters in the South Shetlands area (Antarctica). Polish Polar Research, 25. 45–66.

Suzuki, R., Fujita, K., and Ageta, Y. 2007. Spatial distribution of thermal properties on debris-covered glaciers in the Himalayas derived from ASTER data. Bulletin of Glaciological Research, 24. 13-22.

Svensson, H. 1959. Is the cross-section of a glacial valley a parabola? Journal of Glaciology, 3. 362–363.

Tanaka, K.L. 1986. The stratigraphy of Mars. Journal of Geophysical Research, 91. 139-158.

Tanaka, K.L. Skinner, J.A., Hare, T.M., Joyal, T., and Wenker, A. 2003. Resurfacing history of the northern plains of Mars based on geologic mapping of Mars Global Surveyor data. Journal of Geophysical Research, 108. 12.

Tanaka, K.L., Chapman, M.G., and Scott, D.H. 1992. Geologic map of the Elysium region of Mars (1:5,000,000). U.S. Geological Survey. Miscellanea Investigation Series, Map I-2147.

Tanaka, K.L., Rodriguez, J.A.P., Skinner, J.A., Bourke, M.C., Fortezzo, M.C., Herkenhoff, K.E., Kolb, E.J., and Okubo, C.H. 2008. North polar region of Mars: Advances in stratigraphy, structure, and erosional modification. Icarus, 196(2). 318-358.

Tanaka, K.L., Skilling, I. and Skinner, J. 2000. Mega-lahars of Elysium, Mars. Volcano/Ice Interaction on Earth and Mars Conference, University of Iceland, Reykjavik, Iceland. Abstract, 54.

Tanaka, K.L., Skinner, J.A. and Hare, T.M. 2005. Geologic map of the northern plains of Mars (1:15,000,000). U.S. Geological Survey Scientific Investigations Series, Map 2888.

Thomas, P.J., Squyres, S.W. and Carr, M.H. 1990. Flanks tectonics on Martian volcanoes. Journal of Geophysical Research, 95. 14345-14355.

Turner, J., Colwell, S.R., Marshall, G.J., Lachlan-Cope, T.A., Carleton, A.M., Jones, P.D.,Lagun, V., Reid, P.A., and Iagovkina, S. 2005. Antarctic climate change during the last 50 years. International Journal of Climatology, 25. 279–294.

Ulrich, M., Wagner, D., Hauber, E., de Vera, J.-P., and Schirrmeister, L. 2012. Habitable periglacial landscapes in Martian mid-latitudes. Icarus, 219(1). 345-357. doi: 10.1016/j.icarus.2012.03.019.

van der Veen, C. 1990. Crevasses on Glaciers. Polar Geography, 23(3). 213–245.

van Wyk de Vries, B. and Matela, R. 1998. Styles of volcano-induced deformation: Numerical models of substratum flexure, spreading, and extrusion. Journal of Volcanology and Geothermal Research, 81. 1–18.

Vanneste, M., Mienert, J. and Bünz, S. 2006. The Hinlopen Slide: A giant, submarine slope failure on the northern Svalbard margin, Arctic Ocean. Earth and Planetary Science Letters, 245. 373-388.

Vieira, G., López-Martínez, J., Serrano, E., Ramos, M., Gruber, S., Hauck, C., Blanco, J.J. 2008. Geomorphological observations of permafrost and ground-ice degradation on Deception and Livingston islands, maritime Antarctica. International Conference on Permafrost, 9. 1939-1844.

Vila, J., Marti, J., Ortiz, R., Garcia, A., Correig, A.M. 1992. Volcanic tremors at Deception Island (South Shetland Islands, Antarctica), Journal of Volcanology and Geothermal Research, 53. 89–102.

Walter T.R. and Troll V. 2001. Formation of caldera periphery faults: an experimental study. Bulletin of Volcanology, 63. 191-203.

Wang, J., Bennett, K.J., Scholes, D., Arvidson, R., Ward, J.G., Slavney, S., Guinness, E.A., Stein, T.C., and Heil-Chapdelaine, V. 2009. Planetary Data Access through the Orbital Data Explorer from the PDS Geosciences. Lunar and Planetary Science Conference, 40. Abstract #1193.

Wang, J., Bennett, K.J., Scholes, D.M., Slavney, S., Guinness, E.A., and Arvidson, R.E. 2011. Searchable Observation Data in PDS's Orbital Data Explorer. Lunar and Planetary Science Conference, 42. Abstract #1608.

Wang, J., Bennett, K.J., Scholes, D.M., Ward, J.G., Slavney, S., Guinness, E.A., and Arvidson, R.E. 2010. Updates to the Orbital Data Explorer from the PDS Geosciences. Lunar and Planetary Science Conference, 41. Abstract #1533.

Werner, S.C, and Tanaka, K.L. 2011. Redefinition of the crater-density and absolute-age boundaries for the chronostratigraphic system of Mars. Icarus, 215. 603–607.

Werner, S.C. 2009. The global Martian volcanic evolutionary history. Icarus, 201. 44-68.

Whalley, W.B., and Azizi, F. 2003. Rock glaciers and protalus landforms: analogous forms and ice sources on Earth and Mars. Journal of Geophysical Research, 108: E4. 8032.

Williams, D.A., Greeley, R., Hauber, E., Gwinner, K. and Neukum G. 2005. Erosion by flowing Martian lava: New insights for Hecates Tholus from Mars Express and MER data. Journal of Geophysical Research, 110.

Williams, R.S. 1978. Geomorphic processes in Iceland and on Mars: A comparative appraisal from orbital images. Geological Society of America Abstracts Programs, 10, 517.

Wilson, A.T. 2003. Life in perennially ice covered lakes on Mars — An antarctic analogue. Third International Conference on Mars Polar Science and Exploration. Abstract #8039.

Wilson, L., and Head, J.W. 2008. Tephra deposition on glaciers and ice sheets on Mars: Influence on ice survival, debris content and flow behaviour. Journal of Volcanology and Geothermal Research, 185, 290–297.

Woodworth-Lynas, C. and Guigné, J.Y. 2004. Extent of floating ice in an ancient Echus Chasma/Kasei Valles valley system, Mars. Lunar and Planetary Science Conference, XXXV. Abstract #1571.

Yokoyama, R., Shirasawa, M., and Pike, R.J. 2002. Visualizing topography by openness: A new application of image processing to digital elevation models. Photogrammetric Engineering and Remote Sensing, 68. 251-266.

Zanetti, M., Hiesinger, H., Reiss, D., Hauber, E., and Neukum, G. 2010. Distribution and evolution of scalloped terrain in the Southern Hemisphere, Mars. Icarus, 206(2). 691–706.

Zent, A.P. 1999. An open, snow-based, hydrologic system as an analogue for Noachian Mars. Lunar and Planetary Science Conference, XXX. Abstract #1803.

Zimbelman, J.R. 2001. Image resolution and evaluation of genetic hypothesis for planetary landscapes. Geomorphology, 37. 179-199.Aharonson, O., and Schorghofer, N. 2006. Subsurface ice on Mars with rough topography. Journal if Geophysical Research, 111. E11007.

Zimbelman, J.R., and Edgett, K.S. 1992. The Tharsis Montes, Mars: Comparison of volcanic and modified landforms [Abstract]. Lunar and Planetary Science Conference, XXXII, 31–34.

PhD thesis

Glacial geomorphology of the NW flank of the Hecates Tholus volcano, Mars

Appendixes

Miguel Ángel de Pablo Hernández

2015

Well, that's Mars. Enjoy it.

Don't ask it to be nothing else but what it is.

Ray Bradbury. *Martian Chronicles* (1950)